NORTHWESTERN UNIVERSITY

β-Biomaterials: Biomaterial Approaches for the Protection of Transplanted Beta Islets

A DISSERTATION

SUBMITTED TO THE GRADUATE SCHOOL
IN PARTIAL FULFILLMENT OF THE REQUIREMENTS

for the degree

DOCTOR OF PHILOSOPHY

Biomedical Engineering

By

Jacqueline Alexis Burke

EVANSTON, ILLINOIS

March 2022

ABSTRACT

β-Biomaterials: Biomaterial Approaches for the Protection of Transplanted Beta Islets

Islet transplantation is a therapy in which insulin-producing beta (β) islet cells are infused into the liver via the portal vein to restore glycemic control. This therapy is beneficial for patients suffering from chronic pancreatitis or type I diabetes. However, islet transplantation is not widely implemented due to the instant blood-mediated inflammatory reaction which kills about half of all transplanted cells and, in allogeneic cases, the need for lifelong immunosuppressive therapy, which is associated with a slew of side effects. Poly(ethylene glycol) (**PEG**) is an immune stealth polymer. PEG-based biocompatible materials known as "biomaterials" can be used to mitigate inflammatory immune responses. PEG-based biomaterials of focus include poly(poly ethylene glycol citrate-co-N-isopropylacrylamide) (**PPCN**) and poly(ethylene glycol)-*b*-poly(propylene sulfide)(**PEG-*b*-PPS**).

PPCN is a thermoresponsive, antioxidative hydrogel. PPCN can be used to transplant islets to the omentum (fat pad), instead of the hepatic vasculature. Omentum transplant prevents immediate islet contact with blood, thus avoiding complement activation and coagulation, mitigating oxidative stress, and enhancing islet viability and function. PPCN was found to be biocompatible when implanted in the omentum of nonhuman primates.

PEG-based biomaterials can also be used to improve the properties of transplant immunotherapies. PEG-*b*-PPS self-assembles into polymersome (**PS**) nanostructures and readily loads the mTOR inhibitor rapamycin. Loading rapamycin in PS overcomes issues associated with standard oral rapamycin (i.e. Rapamune®), such as poor bioavailability, broad biodistribution, hydrophobicity (preventing parenteral administration), and off-target side effects. While oral

rapamycin inhibits T cell proliferation directly, subcutaneously administered rapamycin-loaded polymersomes (**rPS**) modulate antigen-presenting cells instead of T cells significantly improving maintenance of normoglycemia in a murine allogeneic islet transplantation model. These results demonstrate the ability of a rationally designed nanocarrier to re-engineer the immunosuppressive mechanism of a drug for tolerance by controlling cellular biodistribution.

While generally PEG-based biomaterials are useful for a diverse array of applications. In patient populations with anti-PEG (**αPEG**) antibodies, PEG can have unintended effects. Enzyme-linked immunoassay (**ELISA**)-based methods are developed to assay for the presence of these abs. Two mouse models with αPEG ab are developed to provide a platform to screen PEG-based drugs for adverse effects in patients that possess these abs.

ACKNOWLEDGEMENTS

Guiding Forces

Professor Ameer, *The Vision, The Fuel*: During my early days in graduate school, Professor Ameer told me that the principles of Regenerative Engineering will be applied beyond the surface of the Earth. He said one day we will regenerate the atmosphere and stop global warming. With the bounds of exploration set beyond the sky, there were no limits for what could be achieved. Guillermo provided the vision and the funding to pursue research that defied the odds.

Professor Scott, *The Mechanism:* Professor Scott instilled in me that ambitions alone would not overcome gravity, but with methods and mechanisms our goals could be achieved. He pulled me back to earth with questions that challenged my aspirations with logic, but also propelled me forward to new areas of exploration. For Professor Scott, it was never enough to know how, but always essential to know why.

Dr. Xiaomin Zhang, *The Hands, The Heart:* Xiaomin took me under her wing, as if I was her daughter, and guided me into the realm of islet transplantation. She taught me the mother tongue of the field. She connected me with the leaders. She matched my pace, each step of the way, no matter how fast or how slow. She held my hand as I presented my work on the highest stage in the field, but also held my head when I had worked myself to exhaustion and sickness.

Most importantly, you all gave me the scientific freedom to explore my research interests without bounds (even if it meant covering the entire lab in a magenta mess of eosin Y).

To my committee members, Dr. Jason Wertheim, and Dr. Peter Rios, thank you for your thoughtful guidance. Dr. Wertheim thank you for providing the clinical expertise to shape my work for future translation. Peter, thank you for always being there to answer a quick text or take my phone, share a protocol or piece of advice. I am very excited to be your upstairs lab neighbor going forward.

Ground Control

To Team Burke Beta Biomaterials, Carolina Bohorquez Fuentes, and Helena Freire Haddad, thank you for putting up with my obsessive consumption of Café Bustelo. Thank you for helping me to learn to be a mentor. I know I pushed you very hard in the lab, but I hope you took a lot away from your research experience. Please know that I am very proud of all that you both have accomplished.

To the members of the Ameer lab, Dr. Bin Jiang, I am so sorry that you had to sit next to me and put up with me swearing at my laptop for the first 2 years of my PhD as I planned my first experiments. Thank you for always being on my side (my right side to be specific). You were always there to answer my novice research questions and share some witty humor. Chongwen Duan, thank you for being my brain when my brain was no longer functioning. You were always

the calm, cool, and collected shoulder to cry on when experiments or life did not go as planned. Thank you for training Nashi to become a lab manager. She loved sitting with you more than anything. Sherry, thank you for being the model of exemplar research and productivity. Samantha Huddleston and Nancy Rivera Bolaños, thank you for taking this graduate research journey with me. Like a diabetic's blood glucose, there were highs and lows. Thank you for taking these on with me. Sam, thank you for being my ally and role model for gender equality in Northwestern's graduate biomedical engineering department. Thank you to Huifeng for listening to my nonsense and being Nashi's best friend (maybe you just gave her the most treats). Dr. Simona Morochnik, the coolest PhD-almost MD in Chicago, thank you for being the exemplar of work-life balance in graduate school. Dr. Anthony Joseph Petty, thank you for being louder than me and having a worse Southeast Michigan accent than me. I greatly appreciated the company. Also, thank you for upgrading the Ameer lab glassware. To my other Ameer lab friends, Dr. Yonghui Ding, Dr. Xinlong Wang, Dr. Banu Akar, Dr. Jimmy Su, Joseph Song, Anamika Chatterjee, Cole Fuerste, Paul Puglisi, Shwetha Ramachandra, Baixue "Dorothy" Xiao, and Charlottle Marlinga, I have greatly appreciated the kindhearted support you have shown me over the years. Madeleine Goedegebuure and Maria Mendez-Santos thank you for supplying me with coffee so that I could continue to write this thesis. I am excited to see your future research.

To the members of the Scott lab: Dr. Sean David Allen, thank you for allowing me to call you at all hours with very random science questions and indulge my extravagant research proposals. Dr. Sharan Bobbola thank you for always telling me the truth, even if it was unpleasant. I will always be happy to drive out of my way to pick you up just so that I get to chat with you. Dr. Nick

Karabin, I miss showing up to lab on Saturday morning and seeing you there in your pajama pants. We would both just sip on our coffees and slightly nod, but never say a word. There was an unspoken understanding that working had to be done. Dr. Michael Vincent, thank you for getting "hyped" about experiments with me. I greatly appreciate your rigor and dedication. Thank you for answering all of my questions about "grown-up things," including car leases, investing in bitcoin, and startup compensation packages. Chamille Lescott, I always appreciate when we are team 7 am in the lab. I greatly appreciated your calm presence. Dr. Mallika Modak, Dr. Sophia, Li, and Dr. Molly Frey, thank you for taking on this journey with me, being my partner in the classroom, sharing insights, and making this journey more enjoyable. Clayton Rische, my fellow blue jay, and Dr. Trevor Stack, thank you for reminding me that there are things in life more important than that next data point. To the dream team, Dr. Simseok "Andrew" Yuk, Dr. Yuan Qian, Dr. Boaz Bishop, Sultan Almunif, Austeja Staneviciute, Natalie Klug, and Stephanie Zelentz, you truly have something special within yourselves and each other. Cherish that dynamic and you will do great things. Yu-gang "Bryan" Liu, thank you for always being up for driving through a blizzard to help me with a 16-hour, 100 animal mouse study. Dr. Fanfan Du, thank you for always being here on the weekends so that I never felt alone. I also always appreciated the rare occasion when you brought your kids. Their smiling faces made being in the lab on the weekend a bit brighter. Dr. Debora Scariot, Dr. Sijia Yi, and Dr. Sun-Young Kim thank you for being the archetype of hard work and superior science. I look up to all three of you.

George Harris and **Joe Girten** and all of the CCM staff, thank you for your can-do attitude and willingness to accommodate my extravagant experiments, especially when resources were slim during the pandemic. You never said no and always went out of your way to help me.

Home Base

Nathan Calzadilla, I must confess, at times during my graduate studies, I did love my mice more than you. Thank you for ensuring that I consume more than only peanut butter and espresso during the past 4.5 years. Thank you for reminding me to put my health before my science. Also, sorry for all of the nondisclosure agreements that I made you sign on bar napkins for the past years.

William & Kelly Burke, thank you to my parents for pushing me to always be ahead of the curve. While the other kids, were at Kumon and PSAT prep classes, my parents started my PhD training at the age of 9. Due to an unlucky diagnosis, my parents were forced to teach me blood glucose testing and insulin injecting. Due to their diligent guidance, this became second nature, as I could test my blood glucose and inject insulin under my elementary school desk without the other kids or teacher even noticing. These skills definitely came in handy when doing large diabetic mice experiments. They also taught me to accurately count carbs and calculate insulin dosing using ratios. As the accuracy of my math became avital for survival, I advanced to the top of my math classes. As I became older and began to understand the biological deficits of my own body, science also became a passion. My parents pushed me to advance these educational interests, pushing financial boundaries and their own knowledge comforts.

China Burke, thank you to my sister for making me laugh and reminding me not to take myself too seriously (or stare at reflective surfaces too much).

To my medical providers, thank you for all of the crazy things that you do to keep me functioning, like ordering blood work for me while in France at a conference or staying extra late, or coming in early for my appointments to accommodate my experimental schedule.

ABBREVIATIONS

αPEG	Anti-poly(ethylene glycol)
α-SMA	Alpha-smooth muscle actin
8-OHdG	8-oxo-2'-deoxyguanosine
ABC	Accelerated blood clearance
APC	Antigen-presenting cell
AUC	Area under the curve
AuNP	Gold nanoparticle
AX LN	Axillary lymph center (deep axillary/axillary/axial and superficial axillary/brachial lymph nodes)
BS	Biologic scaffold
BSA	Bovine serum albumin
BUN	Blood urea nitrogen
BW	Body weight
CA	Citric acid
cDC	Conventional dendritic cell
COVID-19	Coronavirus 2019
CP	Chronic pancreatitis
cryoTEM	Cryogenic transmission electron microscopy
DC	Dendritic cell
DCM	Dichloromethane
DLS	Dynamic light scattering
DP	Double positive
eNOS	Endothelial nitric oxide synthase
ELISA	Enzyme-linked immunoassay
FBS	Fetal bovine serum
FDA	Food and Drug Administration
FTIR	Fourier transform infrared spectroscopy

GDD	Glycerol 1,3-diglycerolate diacrylate
GPC	Gel permeation chromatography
HBPA	Heparin-binding peptide amphiphile
HD	Hydrodynamic diameter
H&E	Hematoxylin & eosin
H_2O_2	Hydrogen peroxide
HPLC	High-performance liquid chromatography
^{H}NMR	Proton nuclear magnetic resonance spectroscopy
IAT	Islet autologous transplantation
IBMIR	Instant blood mediated inflammatory reactions
ICG	Indocyanine green
IEQ	Islet equivalent
IgG	Immunoglobulin G
IgM	Immunoglobulin M
IN LN	Subiliac lymph center (subiliac/inguinal lymph nodes)
IPGTT	Intraperitoneal glucose tolerance test
IRB	Institutional review board
IV	Intravenous
IVIS	*In Vivo* Imaging System
KC	Kidney capsule
LC-MS-MS	Liquid chromatography with tandem mass spectrometry
LCST	Lower critical solution temperature
LPS	Lipopolysaccharide
M/M	Monocyte-and-macrophage-linage
MHC	Major histocompatibility complex
mPEG	Methoxy poly(ethylene glycol)
MPS	Mononuclear phagocyte system
MT	Masson's trichrome

mTOR	Mammalian target of rapamycin
NHP	Nonhuman primate
NIPAAm	N-isopropylacrylamide
NMR	Nuclear magnetic resonance spectroscopy
PBS	Phosphate buffered saline
pDC	Plasmacytoid dendritic cell
PEG	Poly(ethylene glycol)
PEG-OVA	PEGylated ovalbumin
PK	Pharmacokinetics
PLGA	Poly(lactic-co-glycolic acid)
pNIPAAm	Poly(N-isopropyl acrylamide)
PO	Per os (Latin for by mouth/oral)
POD	Post-operative day
PEG-*b*-PPS	Poly(ethylene glycol)-*b*-poly(propylene sulfide)
PPCN	Poly(poly ethylene glycol citrate-co-N-isopropylacrylamide)
PPGN	Poly(poly ethylene glycol glutarate-co-N-isopropylacrylamide)
PS	Polymersome
ROS	Reactive oxygen species
roGFP	Redox sensitive green fluorescent protein
rPS	Rapamycin-loaded polymersome
SAXS	Small angle x-ray scattering
SC	Subcutaneous
SD	Standard deviation
STZ	Streptozotocin
T1D	Type 1 diabetes
TD	T cell dependent
tDC	Tolerogenic dendritic cell
TI	T cell independent

TP	Total pancreatectomy
TP-IAT	Total pancreatectomy-islet autologous transplantation
Treg	Regulatory T cell
tSNE	T-distributed stochastic neighbor embedding
VEGF	Vascular endothelial growth factor

TABLE OF CONTENTS

ABSTRACT **3**

ACKNOWLEDGEMENTS **5**

ABBREVIATIONS **11**

LIST OF FIGURES **22**

LIST OF TABLES **25**

CHAPTER 1: OVERVIEW **26**

1.1 Motivation & Thesis Outline 26

1.2 Thesis Outline 27

CHAPTER 2: INTRODUCTION **30**

2.1 Chronic pancreatitis 30

2.2 Chronic pancreatitis and the promise of autologous islet transplantation 30

2.3 The need for an alternative autologous transplantation site 31

2.7 Mouse models to assess autologous islet transplantation 32

2.4 Type I diabetes 33

2.5 Type I diabetes and the promise of allogeneic islet transplantation 34

2.6 The need for tolerogenic immunotherapies for allogeneic transplantation 35

2.7 Nanomedicine-based approaches to immunotherapies for allogeneic transplantation 36

2.7 Mouse models to assess immunotherapies for allogeneic islet transplantation 38

2.4 Poly(ethylene glycol) 39

2.5 Anti-poly(ethylene glycol) antibodies 42

2.6 Immunological Mechanisms of αPEG Ab Induction 46

2.7 Pre-existing anti-poly(ethylene glycol) antibodies in the population **Error! Bookmark not defined.**

2.8 Anti-poly(ethylene glycol) antibodies and adverse reactions to PEGylated therapeutics .. 51

2.9 Anti-poly(ethylene glycol) antibodies and adverse reactions to PEGylated liposomes 54

2.10 Mitigating adverse reactions due to anti-poly(ethylene glycol) antibodies 57

2.11 Publication Information 60

CHAPTER 3: OMENTUM AUTOLOGOUS ISLET TRANSPLANTATION WITH AN ANTIOXIDATIVE CITRIC ACID-BASED THERMORESPONSIVE POLYMER 61

3.1 Abstract 61

3.2 Introduction 61

3.3 Results 65

3.3.1 PPCN is anti-inflammatory, maintains islet viability, and supports insulin secretion in culture 65

3.3.2 PPCN protects islets against induced oxidative stress, thereby preserving their function during culture 68

3.3.3 PPCN is a versatile islet delivery vehicle that preserves islet function *in vivo* 72

3.3.4 PPCN supports neovascularization, reduces inflammation, and mitigates DNA oxidative damage in transplanted islets 76

3.3.5 The omentum is not a viable site for allogeneic islet transplantation. 79

3.3.6 PPCN is well tolerated, does not elicit a deleterious foreign body response, and is resorbed when applied to the omentum of a non-human primate (NHP) 80

3.4 Discussion 83

3.5 Materials and Methods 87

3.5.1 Human Tissue 87

3.5.2 Animals 88

3.5.3 Materials 88

3.5.4 PPCN synthesis and solution preparation 88

3.5.5 Murine islet isolation 89

3.5.6 *In vitro* islet encapsulation, viability, and insulin secretion study 89

3.5.7 roGFP transduction and oxidation inhibition study 90

3.5.8 Murine islet transplantation procedure 91

3.5.9 Murine intraperitoneal glucose tolerance testing 92

3.5.10 Tissue collection and immunofluorescent staining 92

3.5.11 Biocompatibility and safety of PPCN in the omentum of nonhuman primates 92

3.5.12 Statistical analysis 93

3.6 Supplementary Information 94

CHAPTER 4: SUBCUTANEOUS NANOTHERAPY REPURPOSES THE IMMUNOSUPPRESSIVE MECHANISM OF RAPAMYCIN TO ENHANCE ALLOGENEIC ISLET GRAFT VIABILITY 100

4.1 Abstract 100

4.2 Introduction 100

4.3 Results 105

4.3.1 Rapamycin loading does not alter morphology, polydispersity 105

4.3.2 Polymersomes alter biodistribution, immunomodulation 106

4.3.3 Induction of CD4+ T cell deletion and anergy 109

4.3.4 Regulatory crosstalk between dendritic cells and T cells 109

4.3.4 Induction of suppressor monocytes & macrophages 111

4.3.5 Upregulation of suppressor $CD4^{bright}$ $CD8^{dim}$ T cells 111

4.3.6 Prevention of allogeneic islet graft rejection 112

4.3.7 Induction of antigen-specific tolerance 114

4.3.8 Mitigation of known rapamycin side effects 114

4.4 Discussion 118

4.5 Materials and Methods 124

4.5.1 Animals 124

4.5.2 Materials 124

4.5.3 Poly(ethylene glycol)-b-Poly(Propylene Sulfide) Synthesis 124

4.5.4 Nanocarrier Formulation 124

4.5.5 Nanocarrier Characterization 125

4.5..6 Quantification of Rapamycin Loading(50) 125

4.5.7 Rapamycin Stability in Nanocarrier 126

4.5.8 Indocyanine Green Biodistribution 126

4.5.9 Rapamycin Biodistribution 127

4.5.10 Immunomodulation Study 128

4.5.11Flow cytometry 128

4.5.12 tSNE 129

4.5.13 Allogeneic Islet Transplantation 130

4.5.14 Mixed Lymphocyte Reaction 131

4.5.15 Alopecia Assessment 132

4.5.16 T Cell RNA Sequencing 132

4.5.17 Albumin-Globulin Ratio 133

4.5.18 Statistical analysis 134

4.6 Supplementary Information 135

4.7 Publication Information 173

CHAPTER 5: ANTI-POLY(ETHYLENE GLYCOL) ANTIBODIES AND POLY(ETHYLENE GLYCOL)-BASED THERAPEUTIC STRATEGIES 174

5.1 Abstract 174

5.2 Introduction 174

5.3 Results 176

5.3.1 Development of αPEG IgG ELISA 176

5.3.2 Induction Mouse Model 181

5.3.3 Passive Transfer Mouse Model 186

5.4 Discussion 194

5.5 Materials and Methods 198

5.5.1 Animals 198

5.5.2 Enzyme-Linked Immunosorbent Assay 198

5.5.3 Induction Model 199

5.5.4 Passive Transfer Model 199

5.5.5 Data Analysis 199

CHAPTER 6: SUMMARY & RECOMMENDATIONS FOR FUTURE WORK 201

6.1 Summary of thesis work 201

6.2 Recommendations for future work 203

6.2.1 Omentum Autologous Islet Transplantation with an Antioxidative Citric Acid-Based Thermoresponsive Polymer in a Clinically Relevant Nonhuman Primate Model 203

6.2.2 Subcutaneous Nanotherapy Repurposes the Immunosuppressive Mechanism of Rapamycin to Enhance Allogeneic Kidney Graft Viability 205

REFERENCES 208

LIST OF FIGURES

Figure 1- 1. Thesis overview..... 28

Figure 2- 1. Chemical structures of PEG..... 40

Figure 2- 2. Properties of PEGylated therapeutics in the absence and presence of anti-poly(ethylene glycol) antibodies..... 41

Figure 3- 1. PPCN's thermoresponsive antioxidant property facilitates islet preservation. 64

Figure 3- 2. PPCN facilitates the preservation of both mouse and human islet viability and insulin secretion function *in vitro*. 67

Figure 3- 3. PPCN protects mouse and human islets against physiologic oxidative stress levels induced *in vitro*. 69

Figure 3- 4. PPCN localizes islets to fat pad transplantation site and preserves their function *in vivo*. 73

Figure 3- 5. PPCN protects transplanted islets against oxidation-induced DNA damage *in vivo*. 75

Figure 3- 6. The omentum is not a viable site for allogeneic islet transplantation. 78

Figure 3- 7. PPCN was well tolerated for 90 days with no signs of an inflammatory response when implanted in the omentum of female and male rhesus macaques. 81

Figure 4- 1. Subcutaneous rapamycin delivery via polymersomes (rPS) tolerizes intraportal islet grafts via direct modulation of APCs instead of T cells. 104

Figure 4- 2. Subcutaneous delivery via PS alters rapamycin's biodistribution and immunomodulation. 107

Figure 4- 3. rPS modulate APCs to induce T cell costimulation blockade. 110

Figure 4- 4. rPS treatment upregulates monocyte-and-macrophage-linage cells and induces a predominate suppressive phenotype. 113

Figure 4- 5. rPS treatment induces upregulation of double-positive $CD4^{bright}$ $CD8^{dim}$ T cells with suppressor functions. 115

Figure 4- 6. rPS reduce the effective drug dosage to achieve normoglycemia and mitigate side effects *in vivo* via antigen-specific tolerance. 117

Figure 5- 1. Schematic of ELISA for detection of αPEG IgG in mouse blood. 177

Figure 5- 2. ELISA optimization: Comparison of sample media. 179

Figure 5- 3. ELISA optimization: Comparison of poly(ethylene glycol) molecular weight. 180

Figure 5- 4. Schematic of timeline for induction of anti-poly(ethylene glycol antibodies. 182

Figure 5- 5. Following a single exposure, AuNPs induce a stronger αPEG antibody response; Steric presentation of PEG significantly alters antibody response against PEG MW 5 K. 183

Figure 5- 6. Two PEG MW 20 K exposures increase induction relative to other PEG MW; Steric presentation of PEG significantly alters Antibody response against PEG MW 20 K. 184

Figure 5- 7. Two doses of 20 K PEGylated AuNPs reliability induce αPEG antibodies. 185

Figure 5- 8. Passive transfer of anti-poly(ethylene glycol) immunoglobulin G via intravenous injection does not provide ideal pharmacokinetics for a sustained mouse model. 187

Figure 5- 9. Schematic overview of the passive transfer mouse model. 189

Figure 5- 10. Passive transfer model. Anti-poly(ethylene glycol) IgG concentration profile over time after subcutaneous administration..... 190

Figure 5- 11. Application of PT model to αPEG IgG concentration profile over time after subcutaneous administration of 35 and 50 µg/kg monoclonal αPEG IgG..... 192

Figure 5- 12. αPEG IgG concentration profile over time after subcutaneous administration of 20 µg/kg monoclonal αPEG IgG..... 193

LIST OF TABLES

Table 2- 1 PEGylated drugs approved by the FDA. 44

Table 2- 2. Comparison of T cell-independent and dependent mechanisms of αPEG Ab induction..... 48

CHAPTER 1: OVERVIEW

1.1 Motivation & Thesis Outline

Islet transplantation is a promising therapy for the restoration of glycemic control in patients that lack functional insulin-producing beta islet cells. Currently, islets are infused intraportally into the liver for engraftment.(1) Maintenance of normoglycemia is critical for overall health, as deviations in blood glucose are associated with both short-term and long-term complications.(2-4) Complications of hypoglycemia include dead in bed syndrome, seizure, tremors, and confusion. (2-4) Complications of hyperglycemia tend to occur in the long-term and include vascular disease, neuropathy, nephropathy, eye damage leading to blindness, foot damage leading to amputation, skin and mouth disorders.(2-4) The patient populations that can benefit the most from islet transplantation include those suffering from severe chronic pancreatitis (**CP**) and type I diabetes (**T1D**).

CP is a disease that involves prolonged inflammation of the pancreas. When cases are severe, a partial or total pancreatectomy may be performed. However, by removing the pancreas, insulin-producing islets are also removed. T1D is commonly recognized as an endocrine disorder that leads to the destruction of pancreatic β cells.(4) T1D patients are required to subcutaneously inject exogenous insulin for the duration of their life. In both patient populations, isolating insulin-producing islets and transplanting these cells to maintain glycemic control can greatly improve quality of life.

The human liver is currently the accepted islet transplantation site. However, clinical outcomes are not optimal. This finding is attributed to a significant loss of engrafted islets due to instant blood-mediated inflammatory reactions (**IBMIR**), thrombosis, inadequate vascularization, low oxygen tension in the liver parenchyma, and oxidative stress.(5-8) Therefore, the field is in

dire need of a clinically relevant alternative transplantation site. The omentum is being investigated as an extrahepatic islet transplantation site using autologous platelet-rich plasma and thrombin to form a biologic scaffold (**BS**) to localize the islets.(9, 10) Although promising, BS from diabetics is pro-inflammatory and the source of significant variability for patient outcomes.(11) Therefore, new materials that can reproducibly deliver and localize islets to the omentum in a minimally invasive manner and optimize their microenvironment to maintain viability and function are warranted.

In the case of T1D patients undergoing islet transplantations, islets are procured from cadaveric donors. Thus, immunosuppression is required to mitigate allogeneic and autoimmune responses from causing rejection. Although required to prevent rejection, immunosuppressive drugs can be cytotoxic to islets and increase the patient's risk for infections and malignancy.(12) Tolerogenic strategies that control innate and adaptive immune responses to maximize long-term islet function are desperately needed in order to make islet transplant the standard of care for all T1D patients.

While PEG-based biomaterials have immense potential to solve issues related to islet transplantation, it should be noted that the effectiveness of these biomaterials can be swayed by the presence of anti-PEG antibodies (**αPEG abs**) within the patient population.

1.2 Thesis Outline

Chapter 2 provides an overview of CP and T1D, followed by the potential application of islet transplantation in each patient population. The utilization of PEG-based biomaterials to enhance the protection of transplanted islets is highlighted. Specifically, the role of PEG-based

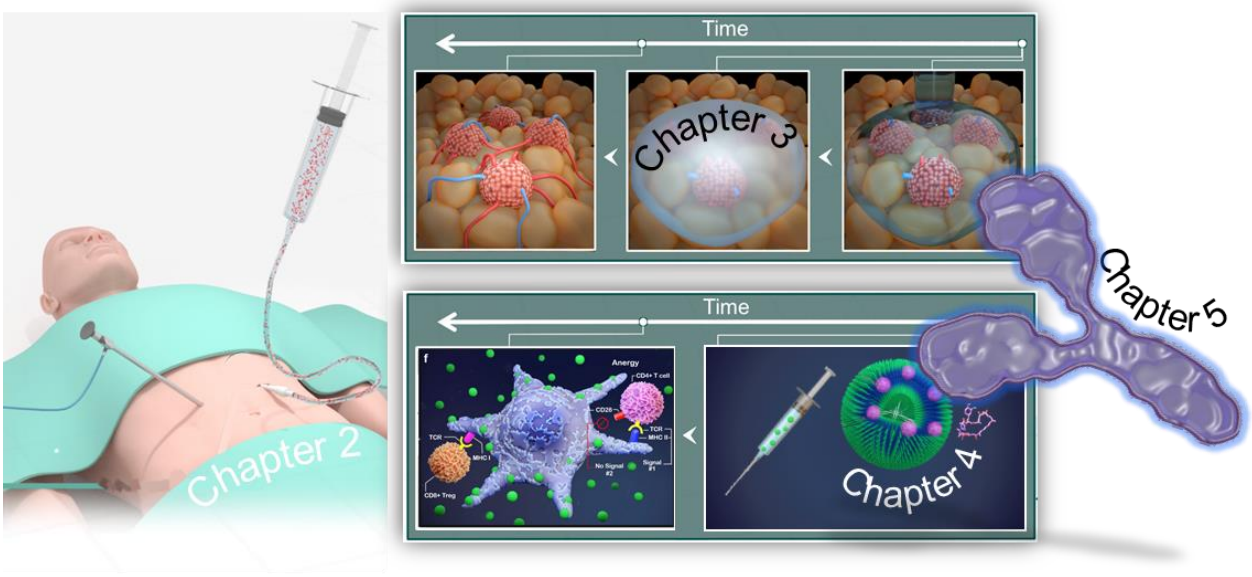

Figure 1- 1. Thesis overview.

biomaterials for enabling alternative transplantation sites and tolerogenic immunotherapies are discussed. Chapter 2 concludes with background on αPEG abs and discusses the need for assays to determine the concentrations of αPEG antibodies in the general population and for an animal model that possesses antibody concentrations that are representative of the patient population. In Chapter 3, a biodegradable, antioxidative, and thermoresponsive biomaterial termed poly(polyethylene glycol citrate-co-N-isopropylacrylamide) (**PPCN**) is assessed for omentum islet transplantation. Chapter 4 explores targeted delivery of an existing immunosuppressive drug using poly(ethylene glycol)-*b*-poly(propylene sulfide)(**PEG-*b*-PPS**)-based nanoparticles as a method to change the mechanism of the drug from immunosuppression to islet graft tolerance. Chapter 5 presents an assay and animals models for studying αPEG ab response. Chapter 6 provides a summary of this work's impact and discusses future directions.

CHAPTER 2: INTRODUCTION

2.1 Chronic pancreatitis

CP is a disease that involves a prolonged inflammation of the pancreas that severely compromises the patient's quality of life. Progression of the disease eventually leads to permanent loss of the endocrine and exocrine functions of the pancreas, resulting in digestive and metabolic problems. Morbidity is often due to the patient's inability to absorb essential nutrients, nutrition-related diseases, persistent pain that frequently requires hospitalization, and diabetes mellitus. Although pancreatitis does not affect a large percentage of the population (prevalence of 50 in 100,000 people with an annual incidence between 5 to 12 per 100,000 people), there is no cure and treatment is very costly with no adequate outcome.(13, 14) At least 50% of patients who suffer from CP will ultimately require some form of surgical intervention secondary to persistent refractory pain and complications of the disease.

2.2 Chronic pancreatitis and the promise of autologous islet transplantation

Unfortunately, 30% to 50% of patients that have undergone partial pancreatectomy will develop recurrent symptoms despite initially successful surgical interventions.(15) In instances where medical and standard surgical management have failed to provide relief, total pancreatectomy (**TP**) is the only way to relieve the pain. However, due to the resulting "brittle" diabetes, a particularly hard to control T1D with frequent, extreme swings in blood glucose levels, TP is rarely applied as the first line of treatment.(16, 17)

Islet autotransplantation (**IAT**) after near-total or total pancreatectomy (**TP-IAT**) may offer a solution to the aforementioned dilemma. With TP-IAT, in addition to alleviating the

intractable pain associated with severe CP, the endocrine function from the pancreatic islets could potentially be maintained, minimizing the risk of developing severe diabetes.

2.3 The need for an alternative autologous transplantation site

In contrast to allogeneic islet transplantation, which is done to treat T1D, patients undergoing TP-IAT receive their own islets eliminating the need for immunosuppression therapy and associated side effects. However, a significant challenge to the more common use and successful outcome of TP-IAT is the time constraint of 3 to 6 hours (vs. 3 to 7 days for allotransplantation) to perform the islet isolation procedure, limiting purity and resulting in larger islet tissue volumes that are not compatible with intraportal islet infusion due to rapid pressure increases.(18) In a study published in 2011 involving 409 patients that received TP-IAT from 1977 to 2011, only 25% of the cases were able to yield >5,000 IEQ/kg, which resulted in an unsatisfactory 31% insulin independence rate 3 years after the procedure.(17) Therefore, the limited number of islets that are available, compounded by the large cell death due to intraportal injection warrants new extrahepatic islet transplantation locations and a delivery vehicle that will maximize their function.

Extrahepatic sites that avoid direct contact with blood flow have traditionally been limited to organ capsules and surgical pouches, including kidney capsules (**KC**), and splenic, intramuscular, and subcutaneous pockets.(19-21) None of these locations have been able to replace intraportal injection either due to the inability to reproducibly scale-up and implement the associated surgical procedure in the clinical setting or failure to demonstrate maintenance of euglycemia post-transplantation.(19, 22) A potentially promising approach reported by Ricordi et al. uses the omentum as an alternative transplantation site.(9) However, the current procedure

relies on the surgeon using a 2-step procedure whereby islets, mixed with autologous platelet-rich plasma, are deposited on the tissue, followed by the addition of thrombin to create a fibrin gel, known as biologic scaffold (**BS**) to keep the transplanted islets in place. While the use of BS demonstrates the feasibility of this approach, the following challenges remain: 1) the procedure is highly variable due to reliance on a 2-step procedure impacting fibrin formation reaction kinetics and corresponding localization of the islets, 2) BS does not allow for optimization of the islets' environment to maximize function, and 3) BS is a source of significant variability due to inherently heterogeneous and pro-inflammatory characteristics of blood from patients with diabetes and pancreatitis.(11, 23) Therefore, the replacement of BS as the biomaterial to localize the islets to the omentum is warranted.

2.7 Mouse models to assess autologous islet transplantation

Given the small nature of mice and the difficulty of microsurgery, a syngeneic model of transplantation, in which islets are isolated from one mouse and transplanted to a mouse of the same strain, instead of autologous islet transplantation. A C57BL/6 to C57BL/6 syngeneic model is commonly used. A beta cell toxin known as streptozotocin (**STZ**) is used to render islets nonfunctional. To ensure there is virtually no islet function and thus severe hyperglycemia, the blood glucose of the mice must be over 400 mg/dl before transplantation(24). A KC mouse model is commonly used for islet transplant due to the facile procedure in the small mouse. Furthermore, the KC model allows for the transplanted islets to be removed without sacrificing the animal, as one kidney can simply be removed. At the end of an experiment, removing the transplanted islets allows for validation that the transplanted graft is responsible for changes in blood glucose, as opposed to residual islet function. However, the kidney capsule model is not possible in humans

and thus fails to capture the microenvironment that the islets are exposed to during transplantation and through engraftment(24). Unique to intraportal transplantation, infusion into the vasculature exposes islets to blood causing IBMIR and potential thrombosis(24). However, it is not possible to keep the mouse alive while removing the entire liver, as the islets may disperse throughout the entire organ, to validate the hyperglycemic state of the animal. Thus, it is best practice to utilize both models to ensure translation and rigor. Furthermore, the liver has a unique immune cell niche and it is a drain for potentially toxic drugs, thus exposing engrafting islets(24). Thus, intraportal transplantation provides islets with a greater challenge to survival. Given that isolated autologous islets are scarce in CP patients, it is necessary to have a mouse model that utilizes as few islets as possible. Utilizing excess islets can delay the graft rejection, giving a false sense of maintained normoglycemia and immunosuppression. While other models use up to 1000 IEQ (25, 26), our model uses a minimal islet mass of only ~200 murine islets (~175 IEQ) or ~100 murine islets (~88 IEQ).

2.4 Type I diabetes

T1D is commonly recognized as an endocrine disorder that leads to the destruction of pancreatic β cells.(4) Once at the terminal stage, it must be managed by lifetime exogenous insulin therapy. Since 2008, approximately 18,000 new cases of T1D have been diagnosed annually among people below the age of 20 across the United States.(27) By the year 2050, ~50 million Americans will be living with T1D, including approximately 600,000 juveniles.(28) In the United States, T1D costs the country approximately $14.4 billion annually.(29, 30) Complications of T1D are severe and can result from both hypoglycemia and hyperglycemia.(2-4) Adverse effects

include dead in bed syndrome, seizure, tremors, confusion, vascular disease, neuropathy, nephropathy, eye damage leading to blindness, foot damage leading to amputation, skin and mouth disorders. (2-4)

2.5 Type I diabetes and the promise of allogeneic islet transplantation

Islet transplantation is a promising treatment for T1D patients, which eliminates the need for exogenous insulin. In this method, pancreatic β cells are isolated from a cadaveric donor pancreas and transplanted via the portal vein to the liver of patients, where they can release insulin in direct response to changes in blood glucose(31, 32). Unlike whole pancreas transplantation, this procedure is minimally invasive and only requires local anesthesia. Islet transplantation reduces surgical risks and allows patients with significant cardiovascular risk to undergo the procedure(32). During the procedure, an interventional radiologist uses multiple imaging modalities to insert a catheter into the patient's portal vein, and islets are infused into the liver's vasculature(31, 32). To ensure euglycemia in patients that receive islets, 5000 IEQ/kg from 2 to 4 donors must be obtained, which is ten-fold higher than the theoretical number of islets needed to maintain euglycemia.[(1)]Several benefits to islet transplantation include enhanced glycemic control, improved quality of life, and reduction of diabetes-related complications such as amputation and blindness; however, this promising therapy is limited by the deleterious off-target effects of life-long immunosuppression, including islet toxicity, that ultimately leads to graft failure(31, 32). Currently, islets are infused intraportally into the liver for engraftment.[(1)] Approximately 60% of patients that underwent this procedure between 1990 and 2002 achieved insulin independence during the year following transplantation.[(33)] However, long-term insulin independence is difficult to maintain and within 5 years most patients must resume exogenous insulin therapy.[(33)]

2.6 The need for tolerogenic immunotherapies for allogeneic transplantation

Currently, islet transplantation therapy is limited to patients with potentially fatal hypoglycemia unawareness or those receiving patients already immunosuppressive therapy for kidney transplantation(31, 32). Improvements in immunosuppressive therapies would make islet transplantation the clinical standard of care for all T1D patients(31, 32).

Clinicians echo this need for targeted immunosuppressive therapies with enhanced efficacy and reduced off-target effects(34), as 64% of transplant recipients report that side effects significantly lower their quality of life(35), (36). Commonly prescribed immunosuppressive drugs tend to have nonspecific biodistributions—resulting in indiscriminate effects between target and non-target tissues(36-38). For example, rapamycin, a maintenance immunosuppressive drug, primarily partitions into red blood cells (95%) and then eventually accumulates in off-target organs, including the heart, kidneys, intestines, and testes(39-42). Furthermore, immunosuppressive drugs typically act on pathways that have many downstream effects(36). Rapamycin inhibits the mammalian target of rapamycin (**mTOR**) pathway, inhibiting T cell proliferation by arresting these cells in the G1 phase of the cell cycle and preventing IL-2 secretion(36, 37). However, mTOR is ubiquitously expressed and other unintended cell populations also experience cell cycle arrest (36, 37). Clinically, this leads to malignancy, enhanced susceptibility to infection, impaired wound healing, thrombopenia, alopecia, gastrointestinal distress gonadal dysfunction, hypertension, hyperlipidemia, nephrotoxicity, and peripheral edema(37, 43). In many cases, these off-target effects cause side effects that negatively impact the transplanted organ or tissue. For example, rapamycin, which is often given for pancreas and islet transplantation is diabetogenic(36, 37). Thus, a drug that is intended to protect the

transplanted graft from the host's immune system can actually be damaging the graft. Additionally, rapamycin is highly hydrophobic and has poor bioavailability. In some cases, toxic solubilizing agents, such as polyethoxylated castor oil, have been used to make this drug more bioavailable for parenteral administration, however, this is associated with hypersensitivity reactions, such as anaphylaxis(44, 45).

2.7 Nanomedicine-based approaches to immunotherapies for allogeneic transplantation

The field of nanomedicine has attempted to solve the issues associated with immunotherapeutics, such as rapamycin. Most notably, in 1999 the Food and Drug Administration (FDA) approved the drug Rapamune®, a nanocrystal formulation of rapamycin, intended to prevent activation and proliferation of T cells(46, 47). However, many issues persist with Rapamune®. Specifically, Rapamune®, which is given orally, has a bioavailability of only 14% in the solution form and 41% in tablet form(46). The low bioavailability is attributed to the first pass metabolism associated with the oral route of administration and transport by p-glycoprotein efflux pumps(47). Patients are burdened with frequent blood work to determine the whole blood concentration of rapamycin due to its small therapeutic window as even a fatty meal can alter its solubility and allow plasma concentration to reach dangerous levels(46). Rapamune®'s label warns that the most common side effects include peripheral edema, hypertriglyceridemia, hypertension, hypercholesterolemia, increased creatinine, abdominal pain, diarrhea, headache, fever, urinary tract infection, anemia, nausea, arthralgia, pain, and thrombocytopenia(46). More serve adverse effects include increased risk of injection, including tuberculosis, sepsis, and interstitial lung disease, and lymphoma or other malignancies, especially of the skin(46). More recent literature cites nanomedicine-based attempts to further enhance the bioavailability of

rapamycin, however, given the dose-dependent toxicity of the drug, these attempts have not been impactful in the area of immunosuppression, but instead have been deemed useful for cancer treatment(47). A logical approach to improve the efficacy of rapamycin while avoiding side effects is to use nanocarriers to target drug delivery to T cells. However, targeting T cells is challenging as they are not highly phagocytic. Ligand-based targeting approaches have been widely attempted throughout the field of nanomedicine, especially for cancer(48). However, ligand-targeted nanoparticles fail *in vivo* where other interactions in the environment outweigh the affinity of the ligand for the receptor or the receptor may be present at locations within the body that are not the intended target(48). For these reasons, to the best of our knowledge, there have been no reported attempts of T cell-targeted rapamycin-loaded nanoparticles for immunotherapy applications.

By changing the targeted cell population, we can use nanocarriers to alter the cell-mediated immunological mechanisms of rapamycin. We have previously demonstrated that PEG-*b*-PPS PSs are efficiently taken up by antigen-presenting immune cells (**APCs**) while avoiding T cells(49-51) via a passive nanostructure-dependent targeting mechanism. Therefore, to investigate how switching rapamycin's cellular target from T cells to APCs would modulate its immunological mechanism, we loaded rapamycin into PEG-*b*-PPS polymersomes (**rPS**) and assessed the impact on islet survival in a clinically relevant intraportal transplantation model. Fundamentally, a diabetic mouse model that effectively recapitulates the disease state and clinical islet transplantation procedure must be utilized to develop alternative immunosuppressive therapies(24). Herein, a severely diabetic, intraportal, limited islet mass murine model is utilized to mimic the milieu faced by human islets.

2.7 Mouse models to assess immunotherapies for allogeneic islet transplantation

Like with syngeneic transplantation, mimicking a true T1D disease state, in which there is virtually no insulin-producing beta islet function and thus severe hyperglycemia, is critical to determine the success of the applied therapy(24). We utilized STZ-induced diabetic mice with blood glucose concentrations over 400 mg/dl upon transplantation(24). Furthermore, it is critical to utilize a fully-MHC mismatched allogeneic mouse model with robust and rapid allogeneic reaction to ensure that a response can be detected and to ensure that a stout immunological challenge is provided for the test therapy(24). The Balb/c islet to C57BL/6 mouse model, utilized herein, is among the most vigorous murine models for allogeneic transplantation(24). While a kidney capsule mouse model is commonly used for islet transplant due to the facile procedure, the KC model fails to capture the microenvironment that the islets are exposed to during transplantation and through engraftment(24). Unique to intraportal transplantation, infusion into the vasculature exposes islets to blood causing IBMMIR and increased potential for thrombosis(24). Furthermore, an intraportal transplantation model must be used for immunotherapy development as the liver has a unique immune cell niche and it is a drain for potentially toxic immunosuppressive drugs, thus exposing engrafting islets(24). Thus, intraportal transplantation provides islets with a greater challenge to survival and allows for a rigorous assessment of potential immunotherapies. Given that cadaveric donor islets are scarce, it is necessary to have a mouse model that utilizes as few islets as possible. Utilizing excess islets can delay the graft rejection, giving a false sense of maintaining normoglycemia and immunosuppression. While other models use up to 1000 islet equivalents (**IEQ**)(25, 26), our model uses a minimal islet mass of only ~200 murine islets (~175 IEQ).

2.4 Poly(ethylene glycol)

PEG is a polymer composed of ethylene oxide monomers that have been engineered into a diverse range of chain conformations and structures. These architectures consist of both linear and branched polymer chains in molecular weight of ~550 to >8,000,000 Da (**Fig. 2-1**)(52-54). Over the past 40 years, PEG has shown great potential to overcome rapid clearance, low solubility, and high immunogenicity associated with controlled and therapeutic delivery of small molecules and biologics in both commercial and academic settings(55). PEG chains can be covalently attached to drugs or the surfaces of materials in a technique called PEGylation (**Fig. 2-1C**) (55, 56). PEG can also serve as an emulsifying agent in drug formulations (55, 56).

Following dense surface PEGylation, a steric shield of PEG chains can form wherein each PEG monomer subunit associates with two to three water molecules, inhibiting non-specific protein interactions to minimize immunogenic recognition by neutralizing antibodies and the degradative action of proteolytic enzymes(56, 57).

Moreover, PEGylation reduces non-specific clearance via the mononuclear phagocytic system by inhibiting receptor-mediated endocytosis and scavenging by phagocytic myeloid and endothelial cells(57, 58). In addition to reducing immunogenicity, PEGylation also increases the circulation time of small molecules by limiting clearance by the renal system and phagocytic innate immune cells of the mononuclear phagocyte system (**MPS**). Glomerular filtration depends heavily on the size and molecular weight of a particle due to the structure and permeability of the glomerulus(59, 60). PEGylation increases the hydrodynamic diameter (**HD**) and molecular weight of the PEGylated moiety, thereby limiting renal clearance and increasing circulation time (**Fig. 2-2**) (55, 61). Particles with an HD larger than 8 nm experience significantly reduced filtration and elimination by the kidneys(59).

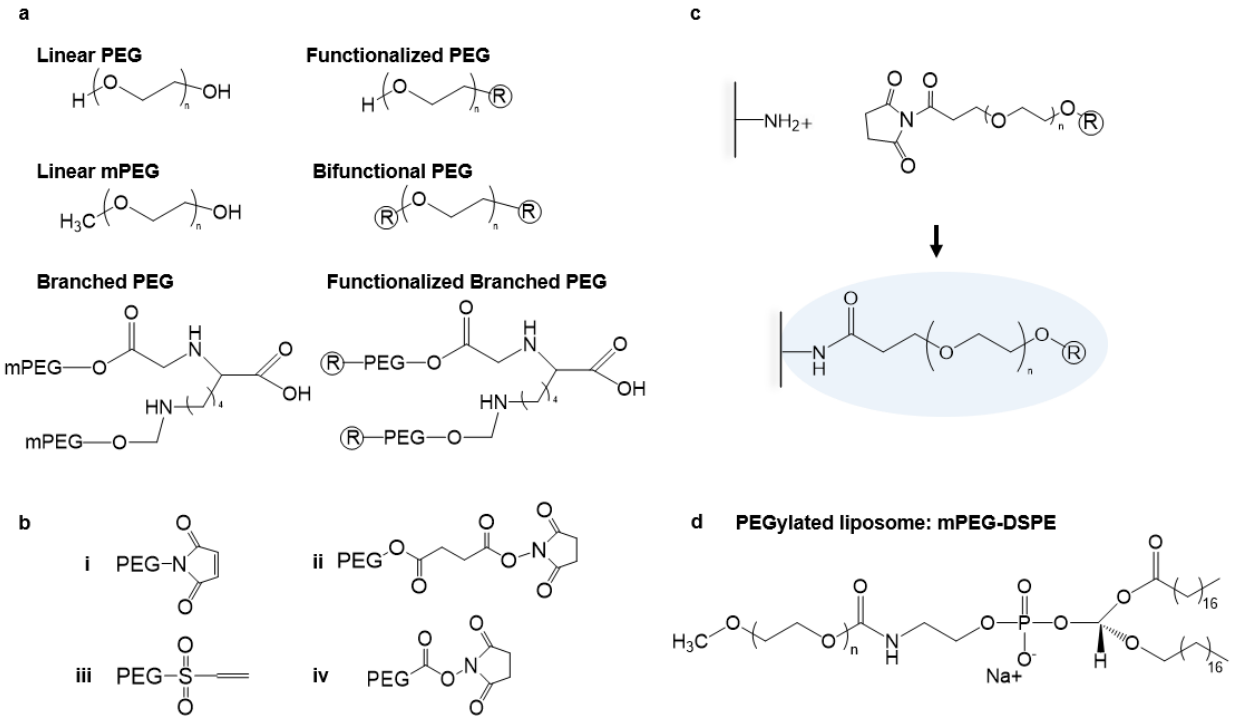

Figure 2- 1. Chemical structures of PEG.
a, Commonly used PEG architectures and functionalization. R represents a functional group. **b,** Common PEG R groups: **i** maleimide; **ii,** succinimidyl succinate; **iii,** vinyl sulfone; **iv,** N-Hydroxysuccinimide. **c** Click chemistry reaction between a bifunctional PEG chain and amine group on a protein-coated surface. **d,** PEGylated lipid, mPEG-DSPE, used in the formulation of PEGylated liposomal drugs such as Doxil®.

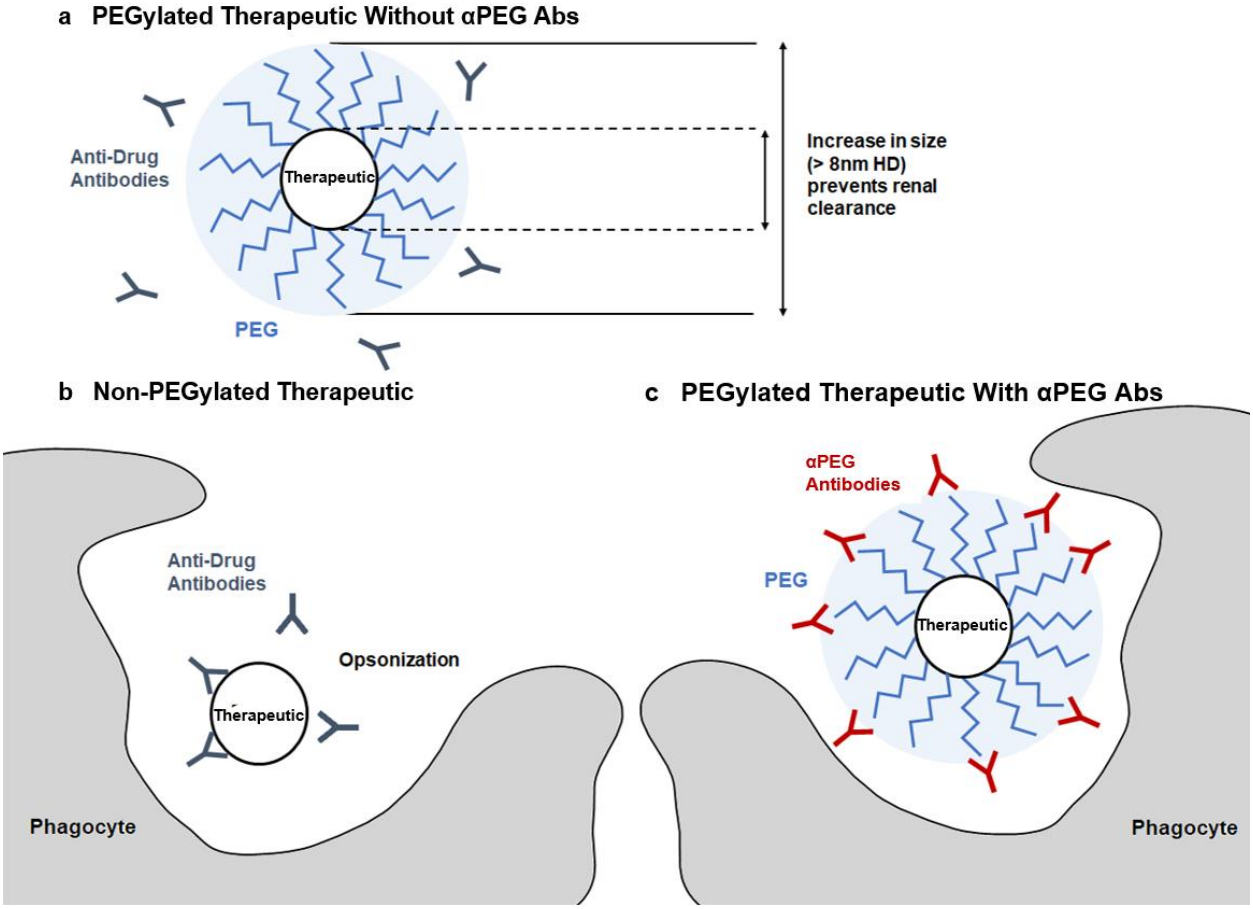

Figure 2- 2. Properties of PEGylated therapeutics in the absence and presence of anti-poly(ethylene glycol) antibodies
a, Poly(ethylene glycol) **(**PEG) associates with water molecules to create a shield around a PEGylated therapeutic, protecting the drug from immunogenic recognition by anti-therapeutic antibodies. Additionally, PEGylation increases the HD of a therapeutic, preventing renal clearance. **b,** The same therapeutic, if non-PEGylated, can be opsonized by anti-therapeutic antibodies, and later phagocytosed, in addition to being cleared by the kidneys. **c,** In the presence of αPEG antibodies, the PEGylated therapeutic can be opsonized by αPEG antibodies and phagocytosed.

Due to the unique properties conferred by PEG, PEGylation has become the go-to method of enhancing the delivery of therapeutic molecules(62). As of 2020, there were 21 PEGylated drugs approved by the FDA, and over 20 others in active clinical trials(63, 64). These drugs include PEGylated enzymes,

proteins, and liposomes, which are used in the treatment of numerous disorders such as infectious disease, cancer, autoimmune diseases, and genetic disorders(63) (64-67). Approved therapeutics currently contain PEG molecular weights ranging from less than1 kDa to 40 kDa (**Table 2-1**) (63) (64).

In addition to the extensive application of PEG in the pharmaceutical industry, the polymer is also used as a solvent and emulsifying agent in consumer products(68, 69). PEG can be found in everyday products such as shampoo, moisturizers, makeup, and soap(53, 68). In 1992, product formulation data reported to the FDA showed that 7 structures of PEG, varying in molecular weight, polymer architecture, and functionalization, could be found in 262 different commercially available cosmetic formulations(53). By 2015, the variations of PEG found in cosmetic products had increased drastically to over 340 structures(68). The prevalence of PEG in consumer products has increased in the past four decades, with a growing variety of chain sizes, structures, and functional groups, and this trend is likely to continue(53, 68).

2.5 Anti-poly(ethylene glycol) antibodies

PEG has been implemented so widely in the cosmetic and pharmaceutical industry partially due to its perceived inert nature(61). However, in 1983 it was first reported that αPEG Antibodies could be observed in rabbits following immunization with PEGylated ovalbumin (70). The antigen

was emulsified using Freund's complete adjuvant, which is known to amplify the antibody response(70). One year later, levels of pre-existing αPEG Antibodies were first detected in blood donors without previous exposure to PEGylated therapeutics(71). αPEG Antibodies detected in humans have been hypothesized to develop due to the repeated exposure to PEG-containing products(72). Both αPEG immunoglobulin M (**IgM**) and G (**IgG**) have been observed in healthy blood donors. IgM is associated with the primary immune response, appearing upon the first exposure to an antigen, while IgG is usually associated with a secondary antigen exposure(73). In the presence of pre-existing αPEG Antibodies, patients receiving treatment with a PEGylated drug can experience accelerated blood clearance, changes in pharmacokinetic after multiple doses, decreased receiving treatment with a PEGylated drug can experience accelerated blood clearance, changes in pharmacokinetic after multiple doses, decreased therapeutic function due to decreased therapeutic circulation time, and hypersensitivity reactions(74-76).

Since the 1990 approval of the first PEGylated drug Adagen®, an enzyme replacement therapy for the treatment of severe combined immunodeficiency disease, there has been a considerable increase in the pervasiveness of PEG in both the formulation of personal care products and FDA approved PEGylated therapeutics (**Fig.2-3**)(64). Physicians and researchers have been investigating how αPEG Antibodies emerge and interfere with therapeutics. Given the increasing prevalence of PEG in the clinic and on consumer's shelves, further investigation is required to fully assess the safety and efficacy of PEGylated drugs. Reactions to PEGylated drugs can cause life-threatening consequences to patients(74). Numerous reports of pre-existing and drug-induced αPEG Antibodies causing adverse reactions against PEGylated drugs in the lab and in the clinic have emerged in recent years(78, 79). Adverse reactions caused by αPEG Antibodies can lead to the early termination of clinical trials, posing a huge financial burden to drug

Table 2- 1 PEGylated drugs approved by the FDA.
Adapted from (63, 64).

Brand Name	Generic Name	Indication	PEGylated Molecule	PEG Size (77)	# PEG chains	Year Approved
Adagen	Pegademase bovine	Severe combined immunodeficiency disease	enzyme	5	11-17	1990
Oncaspar	Pegasparginase	Acute lymphoblastic leukemia	enzyme	5	69-82	1994
Doxil	Doxorubicin hydrochloride liposome	Ovarian cancer, AIDS-related Kaposi's Sarcoma, multiple myeloma	liposome	2	n/a	1995
Onivyde	Irinotecan liposome	Metastatic adenocarcinoma of the pancreas	liposome	2	n/a	1996
Pegasys	Peginterferon alfa-2a	Hepatitis B, C chronic	protein	40	1	2001
PegIntron	Peginterferon alfa-2b	Hepatitis C, chronic	protein	12	1	2001
Neulasta	Pegfilgrastim	Neutropenia, hematopoietic subsyndrome of acute radiation syndrome	protein	20	1	2002
Somavert	Pegvisomant	Acromegaly	protein	5	4-6	2003
Macugen	Pegaptanib	Neovascular age-related macular degeneration	aptamer	20	2	2004
Mircera	mPEG-epoetin beta	Anemia associated with chronic kidney disease	protein	30	1	2007
Cimzia	Certolizumab pegol	Crohn's disease, rheumatoid arthritis, psoriatic arthritis, ankylosing spondylitis	FAB fragment	40	1	2008

Table 2-1 (continued) PEGylated drugs approved by the FDA.
Adapted from (63, 64).

Brand Name	Generic Name	Indication	PEGylated Molecule	PEG Size (77)	# PEG chains	Year Approved
Krystexxa	Pegloticase	Gout	enzyme	10	36	2010
Sylatron	Peginterferon alfa-2b	Melanoma	protein	12	1	2011
Omontys	Peginesatide	Anemia associated with chronic kidney disease	peptide	40	1	2012
Movanik	Naloxegol	Opioid-induced constipation	small molecule	<1	1	2014
Plegridy	Peginterferon beta-1a	Multiple sclerosis	protein	20	1	2014
Adynovate	Antihemophilic factor, PEGylated	Hemophilia A	protein	20	1 or more	2015
Rebinyn	Coagulation factor IX, PEGylated	Hemophilia B	protein	40	1	2017
Asparlas	Calaspargase pegol	Acute lymphoblastic leukemia	enzyme	5	31-39	2018
Palynziq	Pegvaliase	Phenylketonuria	enzyme	20	9	2018
Revcovi	Elapegademase	Adenosine deaminase severe combined immunodeficiency	enzyme	5.6	13	2018

developers(78). It has been estimated that the cost per patient in a phase 3 clinical trial is approximately $42,000(80). Therefore, a failed clinical trial would result in the loss of millions, if not billions of dollars. This problem highlights a pressing need for testing PEGylated drugs in animal models with relevant blood concentrations of αPEG Antibodies before trials in human patients.

2.6 Immunological Mechanisms of αPEG Ab Induction

The immune mechanism that leads to the production of αPEG Antibodies must be understood. Both T-cell independent (**TI**) and T-cell dependent (**TD**) mechanisms have been proposed for the induction of αPEG Antibodies. TI αPEG Ab induction occurs when the antigen crosslinks with receptors on IgM (natural effector) memory B cells. These cells are commonly found in the marginal zone of the spleen in rodents(81). As a result, these cells secrete high concentrations of IgM. Low concentrations of IgG have also been observed in parallel with IgM. No class switching is observed. Antibodies produced via the TI pathway have a weaker affinity for PEG as compared to their TD counterparts. TI induction of αPEG Antibodies has been associated with injection of PEGylated nanoparticles, such as PEGylated liposomes (**Table 2-2**) (81-86).

Work by Ishida et *al.* has been transformative in the understanding of the TI mechanism (81-85). Ishida et *al.* demonstrated that the spleen plays a large role in the induction of αPEG IgM with PEGylated liposomes(87). Upon the first exposure to PEGylated liposomes, αPEG IgM are induced and secreted by the spleen. When a second injection is administered, IgM binds selectively to PEG, triggering the complement system. The liposomes are then opsonized and phagocytosed

by Kupffer cells in the liver. This leads to increased particle accumulation in the liver and a decrease in circulation time for the second dose of liposomes, associated with the accelerated blood clearance (**ABC**) phenomenon. Ishida et *al.* surgically removed the spleens of rats at different time points prior to a first injection with PEGylated liposomes. Animals that had been splenectomized showed reduced levels of αPEG IgM after the first exposure to PEGylated liposomes. After a second injection, the animals did not present the drastic decrease in circulation time nor an increase in liver accumulation of liposomes associated with the ABC phenomenon. Additionally, serum from splenectomized rats showed diminished complement activation upon exposure to PEGylated liposomes *in vitro.*

Ishida et *al.* employed immunodeficient athymic mice to verify TI αPEG Ab induction(84). These mice were injected with PEGylated liposomes, and 10 days after the injection αPEG IgM and IgG levels were assessed. A significant IgM titer was detected in the absence of T cells, and the depletion of marginal zone lymphocytes in the spleen, which are presumed to be B cells, significantly suppressed αPEG IgM induction. The authors propose that the induction of αPEG IgM occurs by a TI mechanism, in which PEG activates marginal B cells directly. The same mechanism has been observed in immune reactions against other highly repetitive structures, such as polysaccharides(88). The time course of αPEG Ab IgM and IgG titers induced by the TI mechanism have been assessed by Kozma et *al.* in a larger porcine animal model. Pigs injected intravenously with PEGylated liposomes showed a rise in IgM titers within 5 days, peaking around 10 days. IgG titers paralleled IgM titers in time course but were significantly lower in concentration. A secondary response did not occur with repeated injections(92).

In contrast, T cell-dependent (**TD**) mechanisms have been observed when the PEGylated moiety is an immunogenic protein(81, 93). The induction of Antibodies is triggered by the

Table 2- 2. Comparison of T cell-independent and dependent mechanisms of αPEG Ab induction(81, 86, 89-91).

	T-Cell Independent	T-Cell Dependent
Known Inducers	PEGylated Nanoparticles	PEGylated Proteins
Antigen Presentation	Antigen crosslinks with IgM (natural effector) memory B cells	Presentation of peptides to helper T cells by antigen-specific B cells
Primary Response	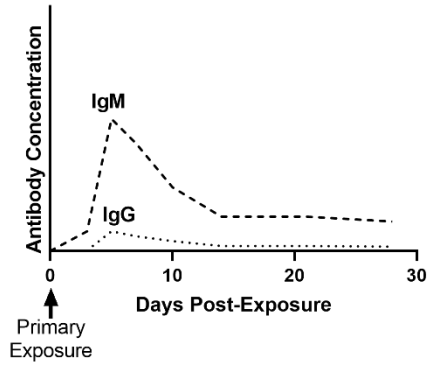	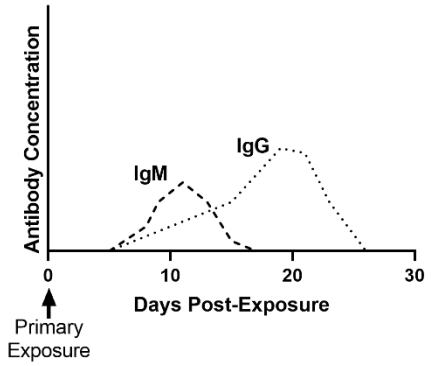
Secondary Response	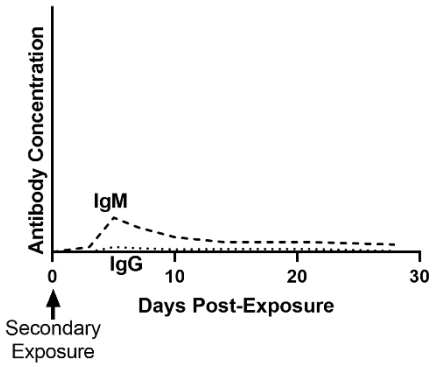	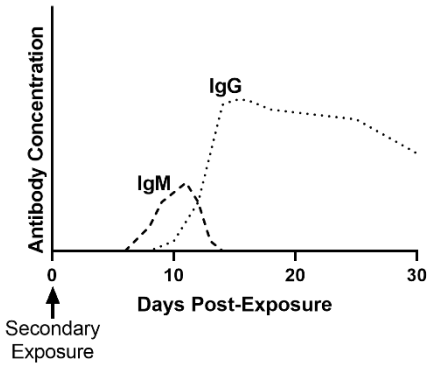
Avidity of Resulting αPEG Antibodies for PEG	Low	High

presentation of peptides to helper T cells by B cells. The resulting Antibodies have a high affinity for PEG. The Ab response is characterized by an initial peak in IgM, followed by class switching, and then a larger peak in IgG. The IgG peak is always greater in concentration than the IgG peak. Unlike TI mechanisms, TD mechanisms are characterized by a much stronger secondary response relative to the primary response (**Table 2-2**)(81, 86) (89-91). Sherman et *al.* and Saifer et *al.* demonstrated the TD mechanism in rabbits. Injection of PEGylated proteins given with or followed by Freund's adjuvant led to the production of IgG. These researchers showed that generally Ab production occurred despite variations in protein type (human interferon-alpha, porcine uricase, or human serum albumin), PEG functionalization (methoxy-, hydroxy-, t-BuO-), and molecular weight. Thus, validating the TD mechanism.

In a study by Mima et *al.* αPEG IgM were induced in a dose-dependent manner in mice injected with PEGylated ovalbumin (**PEG-OVA**)(81). However, immunodeficient mice did not develop αPEG IgM upon receiving the same PEG-OVA injection, indicating a TD mechanism. Another study investigated the αPEG IgM response upon administration of Pegfilgrastim, the PEGylated form of recombinant human granulocyte colony-stimulating factor(93). Splenectomized mice did not develop αPEG IgM, indicating that the spleen plays a role in Ab induction. This is consistent with previous observations of the Ab response to PEGylated liposomes(87). However, similar to PEG-OVA(81), the αPEG IgM response was significantly lower in immunodeficient mice(93). In animals treated with cyclophosphamide, which depletes mice of splenic B-cells, lower αPEG IgM levels were also observed(93).

2.7 Pre-existing anti-poly(ethylene glycol) antibodies in the population

In 1984, the first attempt to study the prevalence of αPEG Antibodies was made by Richter

et al. (71). Serum samples from 453 healthy volunteers were obtained from blood banks in Japan, Germany, and Italy, as well as from 92 patients allergic to ragweed and honey bee venom(71). Samples were analyzed using a passive hemagglutination assay, in which red blood cells (RBCs) coated with 6 kDa methoxy-PEG (**mPEG**) were incubated with serial dilutions of donor sera(71). If the blood agglutinated or clumped, the presence of Antibodies against PEG was confirmed. Due to the semi-quantitative nature of this assay, it is not possible to state the levels of detection in comparison to other quantitative methods. Positive αPEG Ab titers, predominantly IgM, were detected in 0.2% of healthy patients, and in 3.3% of patients with untreated allergies(71). The increased prevalence of pre-existing αPEG Ab in patients with allergies in comparison to healthy patients was not discussed, and the reason for this difference remains unknown(71). Patients with allergies were treated with PEGylated allergens for hyposensitization therapy for one year, and 50% of the patients had positive αPEG Ab titers at the end of the treatment(71). One year after the end of the treatment, positive titers were detected in only 28.5% of the patients. Despite the notable increase in detected αPEG Ab after treatment with PEGylated allergens and the persistence of αPEG Antibodies in over half of the patients, Richter *et al.* deemed the increased Ab response in patients with allergies to not be of clinical significance and claimed it would not affect treatment with PEGylated allergens. This conclusion ignored the risk of potentially anaphylaxis-inducing hyposensitization therapies and delayed research concerning αPEG Antibodies, as many doubted their importance in the clinic(94).

In 2016, Yang *et al.* analyzed 377 contemporary serum samples, as well as 79 historical serum samples from the 1970s to 1990s (72). Using a quantitative, competitive enzyme-linked immunosorbent assay (ELISA) with detection limits ranging from 2 to 15 ng/ml, 72% of

contemporary samples were found to have detectable levels of αPEG Antibodies. The geometric mean of αPEG Antibodies concentrations was calculated to be 52 ng/mL for IgG and 22 ng/mL for IgM. While race was not shown to influence αPEG Ab levels, both serum concentration and prevalence of αPEG IgG decreased with age, and females were more likely to have detectable αPEG IgM levels. Interestingly, analysis of historical samples showed a higher prevalence of αPEG Antibodies than previously reported (0.2% in 1984)(71). Approximately 56% of serum samples from the 1970s to 1990s presented detectable levels of αPEG IgG and/or IgM(72). The high percentage of historical samples that were positive for αPEG antibodies indicates that Richter *et al.* might have underestimated the prevalence of αPEG antibodies, likely due to the use of a less sensitive detection method(72).However, the increase in the presence of αPEG Ab from 56% in historical samples to 72% in contemporary samples supports the hypothesis that αPEG antibodies levels in the general population are increasing due to the increased prevalence of PEG in commonly used products.

2.8 Anti-poly(ethylene glycol) antibodies and adverse reactions to PEGylated therapeutics

Pegloticase is a recombinant uricase, PEGylated with approximately 36 chains of 10 kDa PEG, used in the treatment of patients with refractory gout(79). In the 2006 open-label phase I trial of Pegloticase, Ganson *et al.* detected anti-PEG IgG and IgM via ELISA in 5 out of 13 (38%) patients after a single subcutaneous injection of the drug(95). However, it should be noted that the ELISA was performed using a wash buffer containing 0.1% Tween-20, a polyoxyethylene surfactant that can have cross-reactivity with and alter the detection of αPEG antibodies(95).

Eight years later, Hershfield *et al.* investigated the efficacy of a less frequent dosing regimen of Pegloticase, as well as the presence of pre-existing and treatment-induced αPEG

antibody levels in a phase 2 clinical trial(79). Of the 30 participants, 13 (43%) developed αPEG Antibodies that led to accelerated drug clearance, relative to pharmacokinetics observed for patients without detectable antibodies(79). The percentage of patients who developed αPEG Ab is comparable to the 38% positive rate Ganson *et al.* had found in 2006(95). In addition to the ELISA developed by Ganson *et al.*, Hershfield *et al.* implemented a competition ELISA to determine the specificity of αPEG antibodies(79). Samples were incubated with PBS, 10 kDa PEG-diol (PEG without the methoxy terminal), or unmodified recombinant uricase(79). Incubation with 10 kDa PEG-diol, but not with the non-PEGylated uricase, caused inhibition in the αPEG Ab ELISA in all 13 αPEG Ab positive samples post-treatment(79). It was therefore concluded that the Antibodies recognized the PEG backbone, rather than the methoxy or the unmodified protein(79). In addition to treatment-induced antibodies, Hershfield *et al.* detected pre-existing αPEG antibodies in 19% of Pegloticase-naive patients, all of which were classified as non- or transient responders to the drug treatment(79). Given the correlation established between higher αPEG antibodies levels and decreased therapeutic efficacy, screening patients for pre-existing αPEG antibodies prior to the administration of PEGylated drugs can help to determine the probability of therapeutic success.

Pegnivacogin is an RNA aptamer that inhibits coagulation factor IXa, PEGylated with 40 kDa branched methoxy polyethylene glycol (mPEG)(78). A 2013 phase 2b clinical trial of the drug assessed the safety, efficacy, and pharmacokinetics of an anticoagulation system containing Pegnivacogin in patients with acute coronary syndrome(78). Minutes after the administration of the first dose, two patients developed an anaphylactic reaction, and one developed an isolated skin reaction(78). This caused the trial, involving 640 patients, to be terminated(74). The 3 patients that developed severe allergic reactions to the treatment with Pegnivacogin had the highest blood concentrations of pre-existing αPEG IgG among all study participants (within the top 2.3%). In

total, 36% of patients had positive titers of αPEG IgG. A competition ELISA showed that the Antibodies present in these samples were specific to Pegloticase, Pegnivacogin, Adagen®, 10 kDa PEG-diol, 10 kDa mPEG, and a hexylamino 40-kDa branched mPEG. Of note, the Antibodies did not bind to the un-PEGylated adapter, demonstrating the antibody's specificity to the PEG component of the drug. Serum samples from trial patients were tested using two ELISAs, one detecting IgG specific to the 40 kDa mPEG chains attached to Pegnivacogin, and the other IgG specific to Pegloticase. Similar to the ELISA developed by Hershfield *et al.*, the assay was not quantitative(79). The ELISAs read an absorbance relative to the αPEG Ab concentration of each sample, but without converting absorbance values to the actual αPEG Ab concentration through a standard curve, it is not possible to compare αPEG Ab levels between different studies(74, 79).

Pegasparaginase, commercially known as Oncaspar®, is an *E. coli*-produced asparaginase, PEGylated with 5 kDa mPEG through a succinimidyl succinate linker (SS-linker)(96). The drug is used to treat pediatric acute lymphoblastic leukemia (ALL)(96, 97). When PEGylated, the non-human epitopes present on the drug are less immunogenic, but in the presence of αPEG antibodies, neutralizing hypersensitivity reactions and accelerated drug clearance have occurred, compromising the efficacy of the treatment(98, 99).

After treatment with Pegasparaginase, in 2007 Armstrong *et al.* detected αPEG IgM in 9 out of 28 (32%) patients using a hemagglutination assay, and in 13 out of 28 (46%) patients by incubating samples with PEG beads and analyzing them via flow cytometry(100). Accelerated clearance of Pegasparaginase was linked to the presence of αPEG IgM in the study, as all patients with positive αPEG IgM titers exhibited low asparaginase activity. It was also reported that 13% of patients treated with unmodified asparaginase tested positive for αPEG Antibodies, although the antibodies did not interfere with the asparaginase serum activity. The Antibodies detected in

the control group are thought to be pre-existing αPEG Antibodies, rather than induced by the treatment, as the control drug did not contain PEG.

In 2020, Kloos *et al.* investigated neutralizing hypersensitivity reactions to Pegasparaginase in different stages of treatment(101). Patients received Pegasparaginase intravenously thrice over a 40-day induction phase. Following a 12-week interruption, patients received 14 doses of PEG-asparaginase in the intensification course(99, 102, 103). Out of 18 children, 12 developed neutralizing hypersensitivity reactions during the induction phase, and 6 during the intensification phase(101). In both phases, all patients presented αPEG IgG. αPEG IgM was detected in 75% of patients with hypersensitivity reaction during the induction phase, and in 50% of patients with the reaction during the intensification phase. In both groups, IgG titers were approximately 100 times higher than IgM titers. While both anti-asparaginase and anti-SS-linker antibodies have been detected, 39% of patients with hypersensitivity reactions had exclusively αPEG antibodies, indicating their capacity to provoke neutralizing reactions. The authors also observed pre-existing αPEG IgG and IgM in 58% and 21%, respectively, of patients with no adverse reactions to the treatment. Similar to observations made by Armstrong *et al.*, pre-existing αPEG antibodies did not have the same capacity to provoke neutralizing reactions as αPEG antibodies acquired from treatment(100, 101).

2.9 Anti-poly(ethylene glycol) antibodies and adverse reactions to PEGylated liposomes

PEGylated liposomes can be employed as drug carriers, with the benefits of altered pharmacokinetics and reduced drug toxicity(104). However, liposomes, as opposed to proteins, peptides, and enzymes, are known to act as potent adjuvants and can induce antibody responses against otherwise weakly immunogenic antigens(105, 106). In the early 2000s, it was observed

that αPEG IgG caused accelerated clearance after multiple injections of PEGylated liposomes(107-111). Sroda *et al.* injected rabbits intravenously with liposomes containing 20% of the PEG derivative of phosphatidylethanolamine (PE) (PEG-PE) weekly, for 6 weeks(112). The authors identified αPEG IgG in treated animals. In a 2005 study, Semple *et al.* detected liposome-reactive IgM one week after the first injection of PEGylated liposomes, with titer levels increasing over the course of four injections(113). Minimal IgM levels were observed in the plasma of mice injected with a PEG-free lipid, indicating the specificity of this antibody to PEG. It should be noted that 0.1% Tween was used in the detection ELISA(113). Cross-reactivity between Tween, which contains multiple PEG blocks within its structure, and αPEG antibodies may have altered results.

Doxil®, the PEGylated liposomal formulation of doxorubicin, was the first FDA-approved nano-drug, coming to the market in 1995(104, 114). The drug is currently used in the treatment of ovarian cancer, Kaposi's sarcoma, and melanoma(104), and has been shown to induce αPEG antibodies(76, 115). Approximately 10% of patients treated with Doxil® experienced acute infusion-related reactions that result in termination of treatment(114). Complement activation-related pseudo allergy (**CARPA**) is a major cause of these reactions(116-118). Neun *et al.* investigated the role of αPEG Antibodies in CARPA *in vitro(115)*. Well-characterized mouse αPEG IgG and IgM clones from commercial suppliers at a concentration of 10 µg/ml were incubated with Doxil®. A two-fold increase in complement component C3a plasma levels was observed after the drug was incubated with a PEG backbone-specific IgG clone. Additionally, all three of the assessed PEG backbone-specific IgM antibodies resulted in a more than a three-fold increase in C3a levels after incubation with Doxil®.

Kozma et *al.* assessed the time course of αPEG antibody titers CARPA pig model(92). Animals were immunized with PEGylated liposomes, which induced high titers of αPEG IgM.

Upon a bolus injection with Doxil®, a rapid decline of αPEG IgM titer was observed, as well as complement activation and pseudo-anaphylactic reactions in 4 out of 5 animals. The decrease in antibody titers can likely be attributed to the scavenging of the liposome-IgM complex by the MPS.

Neun *et al.* also investigated the relationship between complement activation by Doxil® and pre-existing αPEG Antibodies in healthy human donors(115). However, unlike in mice, a relationship between human αPEG Antibodies, Doxil®, and complement activation was not observed in this study. The authors hypothesized that the gap between mouse and human results occurs because mouse αPEG Antibodies are monoclonal, generated by a single parent B cell, and recognize the same epitope on an antigen. This results in high-affinity Antibodies, that were used in a high concentration in the *in vitro* study (10 μg/ml). In contrast, human αPEG Antibodies are polyclonal, produced by different B cell clones, and can bind to different epitopes in the same antigen. Antibodies present in human plasma have unknown characteristics and specificity, as they were generated from environmental exposure to PEG. This supports why pre-existing αPEG Antibodies do not possess the neutralizing capacity of treatment-induced αPEG Antibodies, as observed in earlier clinical studies(100, 101).

In parallel work by Hsieh *et al.*, pre-existing αPEG Antibodies were found to alter the pharmacokinetics, biodistribution, and therapeutic efficacy of Doxil® in murine models(76). However, the animals were injected intravenously with a commercially available antibody and had αPEG IgG serum concentration of approximately 15 μg/mL, similar to the 10 μg/mL concentration Neun *et al.* used when incubating mouse αPEG Antibodies with Doxil® *in vitro*(76, 115). The αPEG Antibodies concentrations used in these studies are too high compared to the 52 ng/ml mean

associated with the general population determined in Yang *et al.*, making the models clinically irrelevant for the majority of the population(72, 76).

Advances in the understanding and managing of αPEG Antibodies might be important in the context of the COVID-19 pandemic. Both the Pfizer-BioNTech and Moderna SARS-CoV-2 vaccines have been recently authorized by the FDA under an Emergency Use Authorization and contain messenger ribonucleic acid (mRNA) delivered within PEGylated lipid nanoparticles. These vaccines are the first approved mRNA vaccines, and the first to include the polymer in their compositions, containing PEG with a molecular weight of 2000 Da(65-67). Rare cases of anaphylaxis following vaccine administration have been reported by the Centers for Disease Control and Prevention (CDC)(119). It is suspected that αPEG Antibodies may be associated with anaphylactic reactions to the SARS-CoV-2 vaccine(120), and thus applying the methods outlined herein could be helpful in avoiding and managing these reactions.

Due to global efforts to combat COVID-19, there are over 90 vaccines against SARS-Cov-2 in active clinical trials(121). Many of them employ more traditional vaccine technology that does not contain PEG in their formulations. For example, the Oxford-AstraZeneca vaccine uses a chimpanzee adenovirus vector(122), while Sinovac's CoronaVac is an inactivated virus vaccine(123). As these and many others become approved and available to the public, PEG-free vaccines might offer a viable alternative for patients with known allergies to PEG or high concentrations of αPEG antibodies in order to avoid anaphylactic reactions.

2.10 Mitigating adverse reactions due to anti-poly(ethylene glycol) antibodies

There is a need for a standardized, sensitive, and quantitative method of αPEG Ab detection. Techniques such as hemagglutination, which were used for detection of αPEG Ab in

early studies can only detect Antibodies with a strong affinity or in large concentrations in a sample and are now outdated(70). Because of its higher sensitivity, ELISA is currently the gold-standard method to detect αPEG antibodies, however, multiple studies used polyoxyethylene-based surfactants such as Tween in blocking and wash buffers(95, 113). The addition of polyoxyethylene surfactants has been a target of critiques against αPEG Ab studies due to the ability of the surfactant to cross-react with αPEG Antibodies(124). While today the surfactants are no longer used in αPEG Antibodies ELISAs, most groups still develop their own detection assays(124). This makes it difficult to compare findings between studies, especially if the concentration of the Ab titer is not determined. A standardized protocol for αPEG Ab detection is necessary and would accelerate the advancement of the field.

Moreover, the induction of αPEG Antibodies has been investigated mostly with strong adjuvants administered alongside high quantities of a PEGylated entity(70, 76, 109, 111). As valuable as these studies can be in identifying the existence of αPEG Antibodies, there is no clinical relevance in the use of adjuvants to induce Antibodies against PEGylated therapeutics. An exception can be made in the case of PEGylated liposomes, where the nanocarrier itself can act as an adjuvant to enhance the immune response. Therefore, animal experiments that aim to induce αPEG Antibodies with therapeutic doses of PEGylated particles should be performed, considering the variety of molecular weights of PEG and polymer architectures found in FDA-approved treatments. As more studies are suggesting CARPA and accelerated drug clearance could be influenced by levels of pre-existing αPEG Antibodies(76, 115), there is a stronger need for animal models that accurately reflect the concentration of αPEG Antibodies found in the population. A model like this could be used to thoroughly understand how the blood concentration of αPEG Antibodies affects treatment with PEGylated therapeutics prior to a drug reaching clinical trials.

Finally, as the relationship between pre-existing αPEG Antibodies and adverse reactions to PEGylated drugs is better understood, preventative methods can be implemented in the clinic. For example, a standardized ELISA could be used to screen a patient's αPEG Antibodies blood concentration prior to starting treatment with PEGylated therapeutics. Therefore, patients with high blood concentrations of αPEG Antibodies that could potentially lead to anaphylaxis or decreased therapeutic efficacy could be directed to alternative therapeutics or receive additional monitoring in case adverse reactions occur after drug administration.

Initial misguided conclusions about the inert nature of PEG have delayed the scientific efforts to understand αPEG antibodies(71). Although some research groups have attempted to answer questions regarding the formation of both pre-existing and treatment-induced αPEG antibodies and reactivity with PEGylated drugs, there are still knowledge gaps yet to be explored. Recent discoveries in the structure of αPEG antibodies revealed an open ring structure that captures and stabilizes the flexible PEG chains(125). These findings may explain why free or crosslinked PEG chains do not elicit an αPEG antibody response, as the chains are not sterically presented in a way that allows them to interact with the open ring structure on αPEG antibodies. With the rising prevalence of PEG in consumer products and therapeutics, including novel COVID-19 vaccines, and consequently of αPEG antibodies, these gaps must no longer be ignored.

2.11 Publication Information

Sections of this chapter have been published with the following citation information:

Freire Haddad H, Burke JA, Scott EA, Ameer GA. Clinical Relevance of Pre-Existing and Treatment-Induced Anti-Poly(Ethylene Glycol) Antibodies. *Regen Eng Transl Med*. 2021 Mar 25:1-11. doi: 10.1007/s40883-021-00198-y. Epub ahead of print. PMID: 33786367; PMCID: PMC7993857.

CHAPTER 3: OMENTUM AUTOLOGOUS ISLET TRANSPLANTATION WITH AN ANTIOXIDATIVE CITRIC ACID-BASED THERMORESPONSIVE POLYMER

3.1 Abstract

Intrahepatic pancreatic islet transplantation is a therapy that is available to treat pancreatitis following total pancreatectomy. However, long-term efficacy is low because islet function deteriorates due to oxidative tissue damage during the isolation process and the harsh engraftment conditions in the liver's vasculature, which include ischemia-reperfusion injury, instant blood–mediated inflammatory reactions. Herein, we describe the use of the thermoresponsive, antioxidant macromolecule poly(polyethylene glycol citrate-co-N-isopropylacrylamide) (**PPCN**) to protect islet redox status and function *in vitro* and *in vivo* and to create a viable extrahepatic islet engraftment site in the abdomen. PPCN in aqueous media transitions from a liquid to an elastic hydrogel when exposed to body temperature via temperature-induced macromolecular self-assembly. Islets entrapped in the PPCN hydrogel and exposed to oxidative stress remain functional and support long-term euglycemia, in contrast to islets entrapped in BS. When applied to the omentum of non-human primates (**NHP**), PPCN is well-tolerated, safe, and mostly resorbed without fibrosis at 3 months post-implantation. These results support the use of PPCN as a scaffold for minimally invasive delivery of islets to the omentum and highlight the importance of scaffold antioxidant properties as a new mechanism to protect islet function and maximize long-term autologous graft performance.

3.2 Introduction

Cell and tissue transplantation can potentially treat a variety of diseases; however, the transplant's target location, microenvironment, and surgery side effects present significant

challenges to the success and availability of the procedure to patients.(126-128) This is the case for intrahepatic islet autologous transplantation (**IAT**) after total pancreatectomy (**TP**), a procedure referred to as **TP-IAT**, to treat patients with CP.(129-131),(132, 133) Although islet transplantation has been improved through the development of standardized islet isolation procedures, long-term outcomes remain sub-optimal. Deleterious conditions such as liver thrombosis, instant blood-mediated inflammatory reactions, and oxidative stress are reported to contribute to significant damage to the transplanted islets.(1, 130, 134) These findings highlight the importance of the transplant site given the fact that immunosuppression therapy is not required for TP-IAT.(132, 133) For example, patients that undergo TP-IAT have delayed alpha cell glucagon secretion response to systemic hypoglycemia, placing these patients at risk for severe hypoglycemia unawareness.(135) These issues reinforce the need for an alternate islet transplant engraftment site and new islet delivery methods that provide a microenvironment that supports islet function to improve the outcome of this cell therapy.

The successful engraftment of islets at an extrahepatic site requires a microenvironment that can provide adequate vascularization and protection against oxidative stress conditions.(6, 136, 137) Extrahepatic locations for islet transplantation have traditionally been limited to organ capsules, which have failed to be clinically adopted due to the invasive nature of the procedure.(138, 139) The omentum has recently been investigated as a transplantation site in animals and humans due to its easy access, high vascularity, and potential to localize islets using solid preformed scaffolds.(140) However, the use of solid scaffolds makes it difficult to implement minimally invasive techniques and can exacerbate inflammatory responses leading to fibrosis and limiting the widespread application of the procedure.(141, 142) To address this issue, a recent clinical trial investigated the feasibility of using autologous plasma and recombinant human

thrombin in a two-step endoscope-enabled procedure to deliver and secure allogeneic islets to the omentum for the treatment of T1D.(10) However, allogeneic grafts at this site functioned for less than 1 year, resulting in the termination of the trial.(143) It is hypothesized that tissue-resident macrophages in the omentum prime alloreactive T cells to destroy allogeneic islets. Furthermore, the complexity of the procedure and the enhanced inflammatory status, and elevated oxidative and carbonyl stress conditions that are innate to autologous plasma from T1D patients likely contributed to variable outcomes.(143) Given that alloreactive cell populations are not an issue for autologous transplantation, such as TP-IAT, we believe that the omentum could be a viable transplantation site given that an alternative anti-inflammatory gel could be used.

We hypothesized that body temperature-induced phase change of an antioxidant, water-soluble, degradable macromolecule would: 1) enable easy entrapment and delivery of islets to the omentum, 2) enable islet localization and engraftment on the target tissue upon delivery, and 3) significantly counter the negative effects of oxidative stress after islet isolation and transplantation (**Fig. 3-1a**). Poly(polyethylene glycol citrate-co-N-isopropylacrylamide) (**PPCN**) is a citrate-containing macromolecule with a lower critical solution temperature that allows the transition from a liquid to a gel at physiological body temperature and has intrinsic antioxidant properties that mitigate oxidative damage to tissues.(144-148) In this study, we report that PPCN protects mouse and human islets from oxidative stress-induced damage during the *in vitro* culture process as well as during engraftment in a mouse syngeneic transplantation model. In addition, we further demonstrate that the omentum is not a robust transplant site for allogeneic islets. We also show that the application of PPCN to the omentum of a nonhuman primate (**NHP**) is safe and does not induce a deleterious foreign body response as the material degrades.

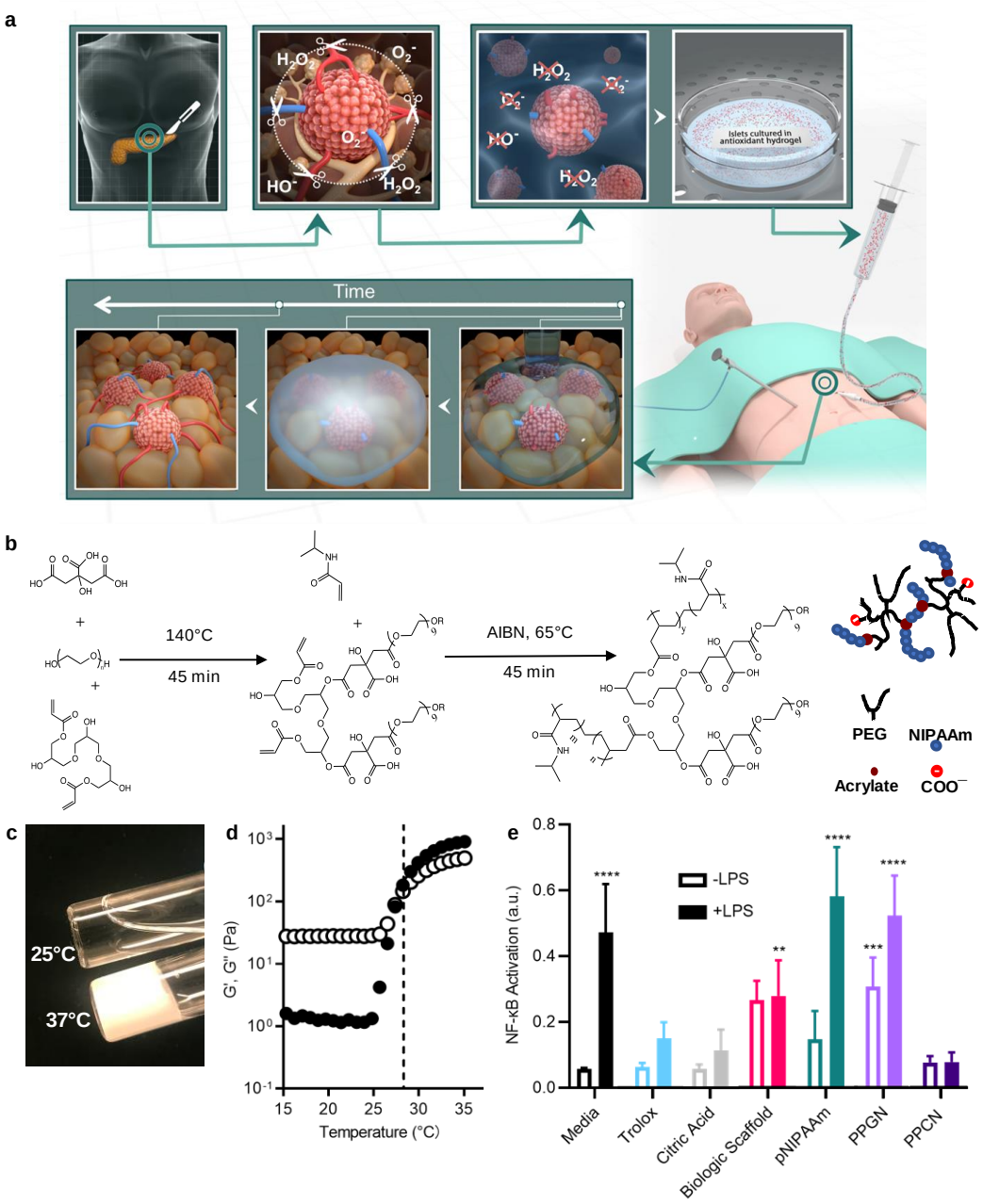

Figure 3- 1. PPCN's thermoresponsive antioxidant property facilitates islet preservation.
a, Schematic of PPCN-mediated islet protection against oxidative stress to preserve islet function throughout omentum transplantation. Top: Organ removal, islet tissue isolation, and transfer to a room temperature islet culture media containing the antioxidant thermoresponsive macromolecule PPCN that protects islets against oxidative damage during culture. Bottom: The thermoresponsive, phase-changing property of PPCN allows easy delivery of the islets in the liquid, localization through body temperature-induced gelation, and engraftment of islets into the omentum using laparoscopic surgery. **b,** Schematic illustrating the synthesis of PPCN. **c,** Digital photo showing the thermoresponsive transition of PPCN from a liquid (25°C) to a hydrogel (37°C). All samples were prepared in PBS at a concentration of 100 mg/mL and neutralized to pH 7.4. **d,** Rheological determination of the lower critical solution temperature of the PPCN. (black marker – storage modulus G'; white marker – loss modulus G"). **e,** Assessment of antioxidative properties for protection of RAW 264.7 macrophages cells against lipopolysaccharide (LPS)-induced NF-kB activation via Quanti-Blue cell-based assay. All data are presented as mean Nf-κB activation (a.u.) ± SD with *p<0.05; ** p<0.01; *** p<0.001; **** p<0.0001 relative to PPCN. Statistical significance was determined by two-way ANOVA with Tukey's multiple comparisons test. (n = 5).

3.3 Results

3.3.1 PPCN is anti-inflammatory, maintains islet viability, and supports insulin secretion in culture

PPCN was prepared via a two-step synthesis starting with a polycondensation reaction comprising citric acid, polyethylene glycol, and glycerol 1,3-diglycerolate diacrylate (**GDD**) followed by free-radical polymerization with N-Isopropylacrylamide (**NIPAAm**) (**Fig. 3-1b**). Successful synthesis was confirmed using **^{H}NMR**, **FTIR,** and rheology (**Fig. 3-1d, S3-1**). PPCN dissolved in phosphate saline buffer (**PBS**) exhibits a reversible liquid to solid phase transition at the lower critical solution temperature (**LCST**) of 28°C, which is lower than that of the homopolymer poly(N-isopropylacrylamide) (**pNIPAAm**) (32 °C) (**Fig. 3-1c,d**). At typical room temperatures, this LCST enables the easy addition of islets to the PPCN solution, their easy distribution to cell culture wells or delivery to target tissues in the body, and their entrapment at these locations via gelation at 37°C(149, 150) (**Fig. 3-1c,d**).

The anti-inflammatory properties of PPCN were confirmed *in vitro* as per the inhibition of NF-kB activation in the RAW-blue cell line (**Fig. 3-1e**). RAW-blue cells are engineered RAW264.7 macrophages that have been used to evaluate the intracellular antioxidant response due to lipopolysaccharide (**LPS**)-induced NF-kB expression.(151, 152) Antioxidants are known to suppress NF-κB activation as well as the subsequent transcription of inflammation-related genes.(10, 153, 154) Cells exposed to LPS in the presence of the antioxidant Trolox, an analog of vitamin E, reduced NF-kB expression by 68% relative to cells exposed to LPS in cell culture media. PPCN exhibited an 84% reduction in NF-kB expression (**Fig. 3-1e**). Cells exposed to a hydrogel formed from BS, a clinically used hydrogel for islet transplantation to the omentum in humans(10), effected a 41% inhibition of NF-kB expression, respectively (**Fig. 3-1e**). A non-

antioxidative version of PPCN made with glutaric acid, instead of citric acid (**Fig. S3-2**). This version is known as poly(polyethylene glycol glutarate-co-N-isopropylacrylamide) (**PPGN**).

To assess the impact of PPCN on islet function, the viability and insulin secretion function of mouse and human islets in standard suspension culture, and after entrapment in BS, PPCN, or pNIPAAm were evaluated *in vitro*. Freshly isolated islets were either cultured on tissue culture plastic or mixed with autologous BS, PPCN, or pNIPAAm solutions at room temperature. Islets were successfully entrapped in each hydrogel by adding thrombin to the BS or incubating the islet-PPCN or islet-pNIPAAm mixtures at 37°C. The viability of the entrapped islets was monitored over time with the resazurin assay (**Fig. 3-2**). When compared to freshly isolated islets, except for the pNIPAAm group, the viability of islets was maintained at 48 hours of *in vitro* culture. Islets entrapped in pNIPAAm experienced a viability loss of 40% at 24 hours and 60% at 48 hours (**Fig. 3-2a**). Live/Dead staining of the islets at 24 hours of culture confirmed the presence of many dead cells in the pNIPAAm group whereas islets in suspension culture, in PPCN, or in BS exhibited similarly high viabilities (**Fig. 3-2e**). Insulin secretion was evaluated using the *in vitro* glucose stimulation/insulin secretion (**GSIS**) test, which reports a stimulation index (the GSIS index) (**Fig. 3-2c**). A GSIS index of 1 or below indicates the complete loss of glucose response.(155) During *in vitro* culture, at day 0, islets in all four groups have an average GSIS index of 7.15±1.23 (**Fig. 3-2c**). The GSIS index of the pNIPAAm group drops by 65% at 24 hours of culture, which is consistent with the loss of islet viability observed in this group (**Fig. 3-2c**). A relatively smaller drop in the GSIS index was measured for the other three groups (26% for suspension culture, 17.5% for BS, and 14.8% for PPCN) (**Fig. 3-2c**). Islets cultured in BS for 48 hours also lost their glucose responsiveness as their GSIS index dropped from 6.45±0.72 to

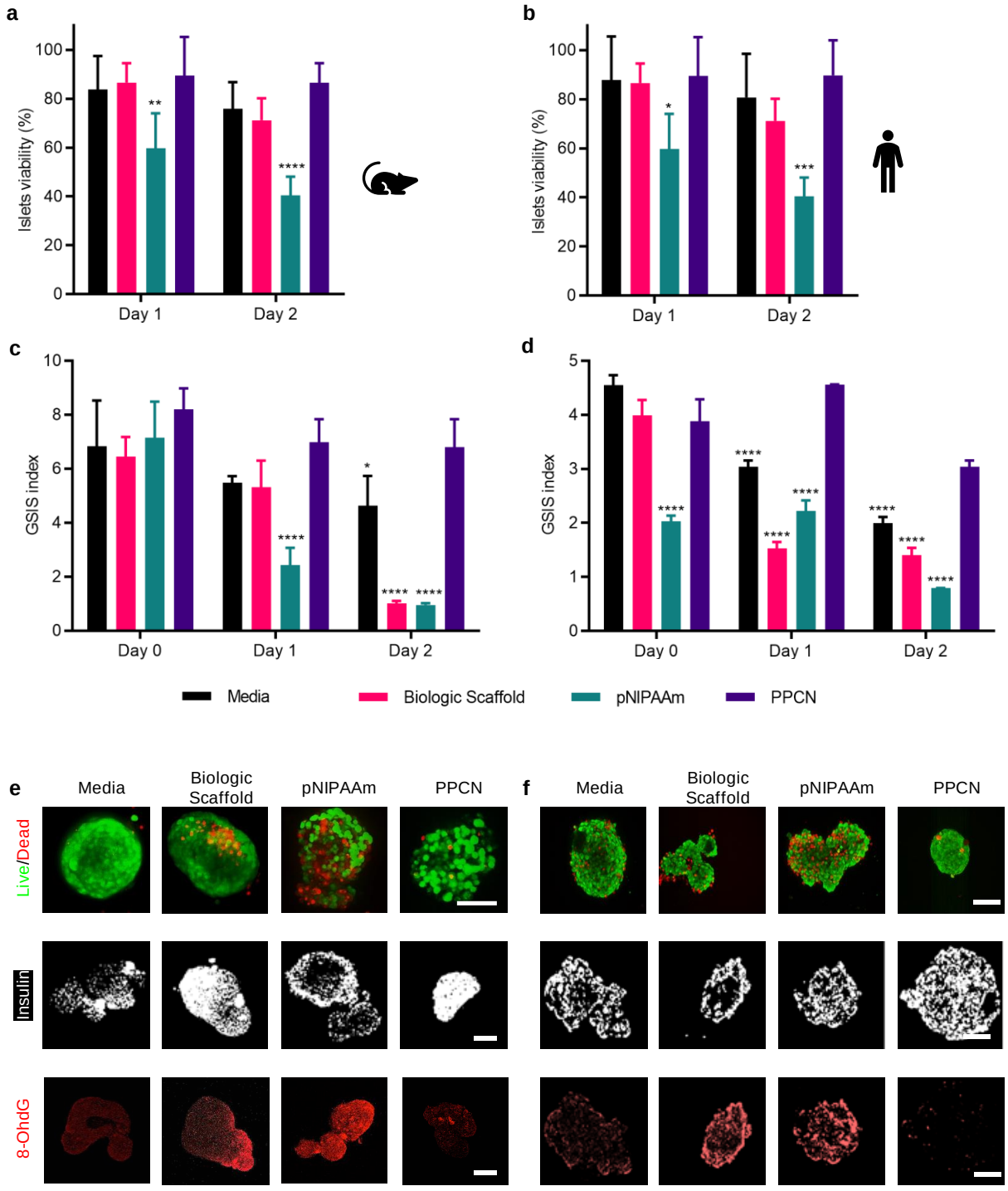

Figure 3- 2. PPCN facilitates the preservation of both mouse and human islet viability and insulin secretion function *in vitro*.

a,b, Mouse and human islet viability as measured fluorescently by resazurin reduction via after prolonged culture under various conditions. **c,d,** Corresponding glucose-stimulated insulin secretion (GSIS) index of the cultured islets. All data are presented as mean ± SD with *p<0.05; ** p<0.01; *** p<0.001; **** p<0.0001 relative to PPCN. Statistical significance was determined by two-way ANOVA with Tukey's multiple comparisons test. (n = 5). **e,f** Live/dead and immunostaining of mouse islets for insulin and 8-OHdG after 2 days of *ex vivo* culture under various conditions. (scale bar: 100 um).

1.01±0.09 with partial disassembly of the islets also observed (**Fig. 3-2c**). Within 24 to 48 hours of culture, a 25% and 7.3% decrease in GSIS index was observed for islets in suspension culture and islets in PPCN, respectively, confirming the protective role of PPCN (**Fig. 3-2c**). Similar results were observed for human islets (**Fig. 3-2b,d**).

Intracellular insulin staining also revealed that islets cultured in pNIPAAm showed signs of an insulin-deficient core, whereas islets cultured in the other three conditions showed uniform insulin expression across the entire islet structure. To assess whether the protective effects of PPCN may be due to its antioxidant properties, we probed for the nuclear DNA oxidation marker 8-oxo-2'-deoxyguanosine (**8-OHdG**) on both mouse and human islets after 48 hours in culture. Staining for 8-OHdG revealed significantly more oxidized residues in cells cultured in pNIPAAm and BS relative to PPCN (**Fig. 3-2e,f**). This finding could potentially explain the observed islet function preservation as per the GSIS indices. In conclusion, culturing islets in PPCN better preserves their insulin secretion function.

3.3.2 PPCN protects islets against induced oxidative stress, thereby preserving their function during culture

To further understand whether the antioxidant property of PPCN would preserve islets viability and function, redox-sensitive islets were created by expressing the transgene for the redox-sensitive green fluorescent protein (roGFP) gene in the cytosol of freshly harvested islets via a lentiviral vector. The incorporation of one disulfide bond between cysteine A147 and A204 in the protein structure of roGFP enables its use as a redox reporter that can indicate the oxidation status through the quantification of the relative fluorescence intensity at two excitation

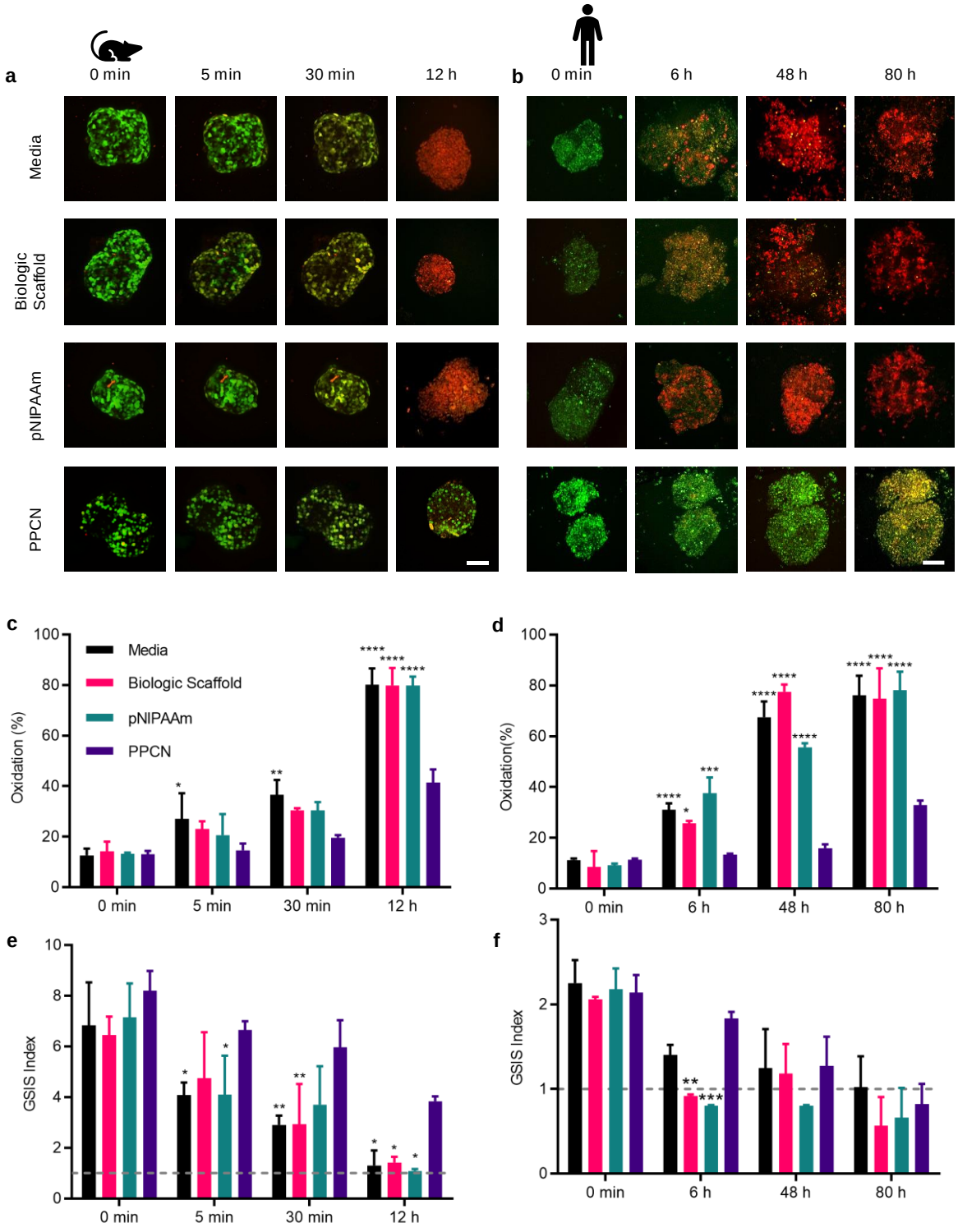

Figure 3- 3. PPCN protects mouse and human islets against physiologic oxidative stress levels induced *in vitro*.
a,b, Oxidation rate of mouse and human islets, respectively, overexpressing roGFP under various culture conditions. 10 uM H_2O_2 was used to induce oxidative damage. (Green–488 nm excitation signal, reduced status; Red–405 nm excitation signal, oxidized status. (scale bars: 100 um). **c,d,** Quantification of oxidation (%) in roGFP-overexpressing islets. **e,f,** Glucose-stimulated insulin secretion (GSIS) index of islets stressed with H_2O_2. All data are presented as mean ± SD with *p<0.05; ** p<0.01; *** p<0.001; **** p<0.0001 relative to PPCN. Statistical significance was determined by two-way ANOVA with Tukey's multiple comparisons test. (n = 5).

wavelengths 405 and 488 nm (**Fig. S3-3a,b**).(156, 157) Under normal reduced conditions, the protein is excited at 488 nm; however, upon exposure to an oxidizing environment, the formation of the disulfide bond leads to a shift in the excitation wavelength that peaks at 405 nm (**Fig. 3a**). This shift provides a signal difference that can be used to monitor and quantify the islet's redox status within scaffolds by measuring the ratio between the fluorescence intensity emission after excitation at 405 or 488 nm. Transgene expression of roGFP in the cytosol did not affect the normal viability and insulin secretion function of both human and mouse islets (**Fig. S3-3c-f**).

To accelerate the rate of oxidative damage *in vitro*, 10 μM hydrogen peroxide (**H_2O_2**) was added to each of the islet culture environments described in the aforementioned paragraph. This H_2O_2 concentration was chosen to mimic *in vivo* H_2O_2 concentrations produced by host inflammatory cells that expose transplanted islets to oxidative damage.(158-160) Confocal microscopy imaging was used to monitor the progression of oxidative damage in both mouse and human islets. (**Fig. 3-3a,b**) At time 0, before the introduction of the H_2O_2, a dominant signal at 488 nm (reduced form shown as green) was observed in islets from all four groups with a baseline average oxidation percentage of 13% for mouse islets and 10% for human islets (**Fig. 3-3a-d**). Five minutes after introducing H_2O_2, an increase in oxidation of 27.0%, 23.1%, 20.6 %, and 14.6% was measured for mouse islets in the control media suspension culture, BS, pNIPAAm, and PPCN, respectively. At 30 minutes, the oxidation was significantly increased for islets cultured in media suspension (36.5%), BS (30.4%), and pNIPAAm (30.4%), whereas oxidation of islets entrapped in PPCN increased to 19.7%. At 12 hours, 44% oxidation was observed in the PPCN group, whereas 80% oxidation was observed in the remaining groups. A similar trend was also observed for human islets (**Fig. 3-3 b,d**); however, human islets overall appeared more resistant to the oxidation damage when compared to mouse islets. Starting with a 10% baseline oxidation for all

the testing groups, 6 hours after introducing the H_2O_2, an increase in oxidation to 31.1%, 25.8%, 37.6 %, and 13.5% was measured for human islets in control media suspension culture, BS, pNIPAAm, and PPCN, respectively (**Fig. 3-3b,d**). PPCN's protective effect is extremely evident at the 80-hour time point, as 76.3% of the islets cultured in the other three environments showed signs of oxidation compared to 34.0% of those cultured in PPCN (**Fig. 3-3d**). Significant islet disaggregation was observed in the control media suspension culture, BS, and pNIPAAm groups, whereas the morphology of the islets entrapped in PPCN remained intact.

To study the correlation between the progression of oxidative damage and loss of islet function, the GSIS index of both mouse and human islet was measured on similar time scales (**Fig. 3-3 e,f**). For the mouse islets, a decrease in GSIS index was observed as early as 5 minutes after introducing the H_2O_2. Relative to t=0, at 5 minutes the GSIS index for islets suspended in cell culture media, BS, pNIPAAm, and PPCN decreased by 40.2%, 26.5%, 42.7%, and 18.9% to 4.08, 4.74, 4.09 and 6.64, respectively. At 30 minutes, the GSIS index for islets in media, BS, pNIPAAm, and PPCN decreased to 2.90, 2.93, 3.70, and 5.97, respectively. At 12 hours, islets in media, BS, and pNIPAAm lost their glucose responsiveness as per GSIS indices close to 1, meaning the islets became completely leaky and cannot distinguish the difference between low and high glucose concentrations. In contrast, at 12 hours, islets in PPCN were able to maintain a GSIS stimulation index of 3.84, confirming the protective properties of PPCN (**Fig. 3-3e**). To assess whether the results obtained with murine cells would also translate to human cells, human islets were evaluated using the same experimental set-up (**Fig. 3-3f**). The results demonstrated a significant loss of function at the 6-hour time point, as the GSIS index dropped from 2.15 to 1.40, 0.91, 0.80, and

1.83 for islets in media suspension culture, BS, pNIPAAm, and PPCN, respectively. At 12 hours, islets in media suspension culture, BS, and pNIPAAm completely lost insulin secretion response to glucose. In contrast, the GSIS of islets entrapped in PPCN was similar to the value obtained at 6 hours (**Fig. 3-3f**).

3.3.3 PPCN is a versatile islet delivery vehicle that preserves islet function *in vivo*

To evaluate whether PPCN could be used to deliver islets to an extrahepatic site, the abdominal fat pad of the mouse was used to mimic islet transplantation to the omentum in humans. This model was selected because both structures are well-vascularized fat tissue located in the intraperitoneal cavity.(161) The key steps for the islet transplantation procedure are summarized in **Fig. 3-4a**. Upon application to the fat pad, complete gelation of the PPCN occurred within seconds of contact with the tissue, securing all the islets on the fat pad. No suturing or tissue glue was required for this step due to the tissue adhesive nature of PPCN. The entire procedure was accomplished within 5 min. In contrast, BS required longer times to solidify via the thrombin crosslinking reaction, making it difficult to control the final location of the islets. Additional control groups were included in the study. Islet transplantation to the KC was included as a positive control as it is widely used as an extrahepatic islet transplantation location in small animals. However, KC transplantation is not performed in humans due to anatomical differences.(138) Furthermore, intraportal islet transplantation was used as an additional positive control, as this is the clinically used site of transplantation in humans. However, with this site, it is not possible to retrieve the transplanted islets while keeping the animal alive to ensure that any changes in blood glucose are a result of the transplanted islets and not residual pancreatic function.

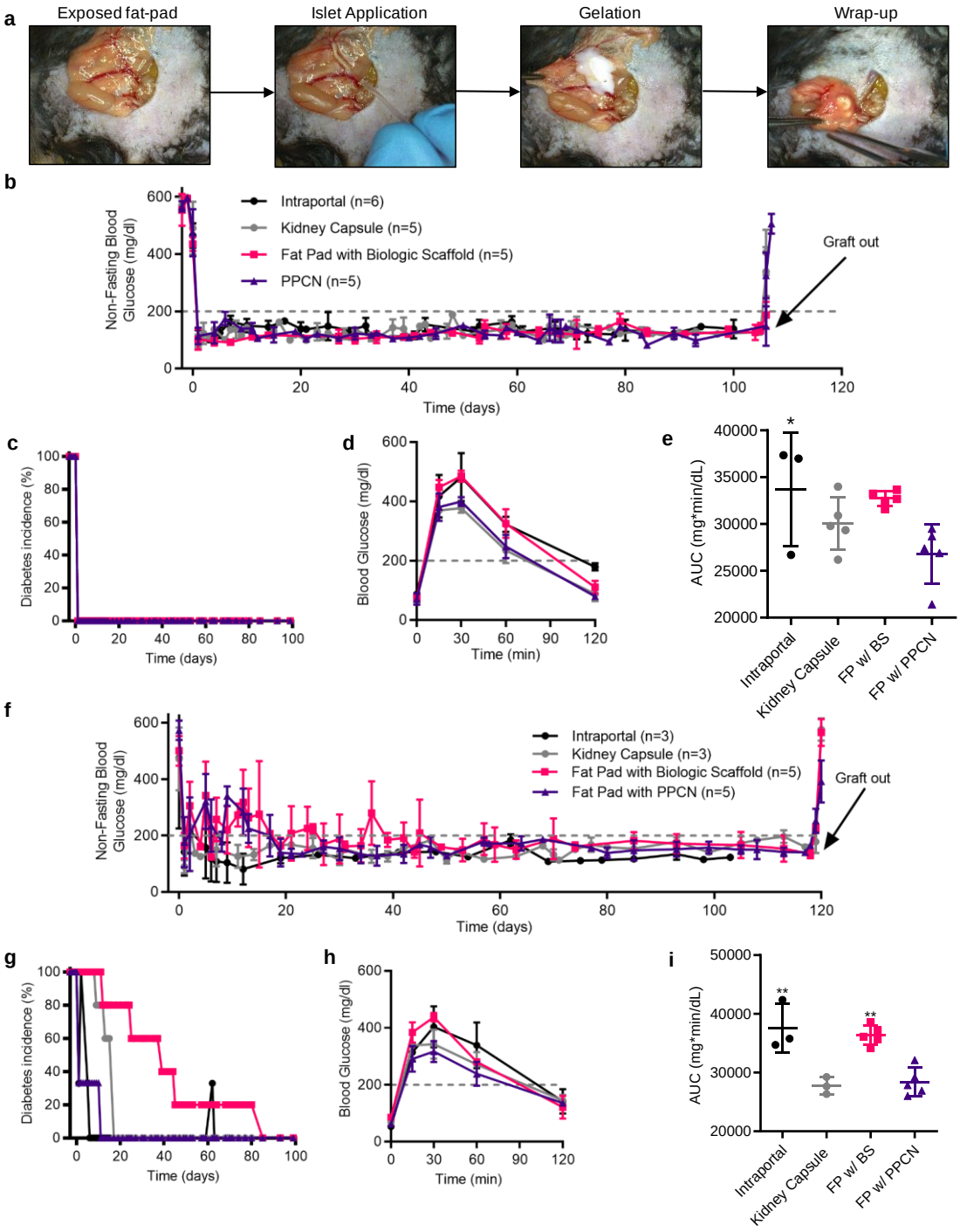

Figure 3- 4. PPCN localizes islets to fat pad transplantation site and preserves their function *in vivo*.
a, PPCN facilitates islet transplantation to the mouse fat pad. **b,** Non-fasting blood glucose concentration (mg/dl) of mice transplanted with approximately 8,200 IEQ/kg body weight of islets to the liver (intraportal), kidney capsule, or on the fat pad with biologic scaffold or PPCN. **c,** Diabetes incidence (%) (blood glucose concentration greater than 200 mg/dl) by treatment group. **d,e,** Glycemic profile (**d**) and area under the curve of the profile (AUC, mg * min * dL^{-1}) (**e**) during the IPGTT study performed at 1 month after the transplantation. **f,** Non-fasting blood glucose measurements of mice transplanted with a marginal islet mass (approximately 4,100 IEQ/kg body weight). **g,** Diabetes incidence (%) (blood glucose concentration greater than 200 mg/dl) by treatment group. **h,i,** Glycemic profile (**h**) and AUC (**i**) of the profile during the IPGTT study performed 1 month after the transplantation. All data are presented as mean ± SD with *** $p<0.001$ relative to PPCN. Statistical significance was determined by two-way ANOVA with Tukey's multiple comparisons test. ($n \geq 3$).

When transplanting 8,200 islets equivalent (**IEQ**) per kilogram body weight (162), animals in all three groups achieved euglycemia the day following the transplantation procedure. (**Fig. 3-4b**) Euglycemia was maintained in all four groups until day 104 post-transplantation, at which point a second survival surgery was performed to remove the transplanted islet graft to confirm the source of insulin production (with the exception of the intraportal group). After recovering from the surgery, hyperglycemia was detected in all animals, confirming that the islets contained within the fat pad (or KC) were responsible for maintaining euglycemia (100% converted to euglycemia, n=5) (**Fig. 3-4b**).

Intraperitoneal glucose tolerance tests (**IPGTT**) were performed at day 30 post-transplantation. The quantified area under the curve (**AUC**) for the PPCN group was slightly lower than those for the KC and BS groups, but no significant difference was observed using 8,200 IEQ islets for transplantation (**Fig. 3-4d,e**).

To further investigate the ability of PPCN to maintain islet function after transplantation, a marginal number of islets was used for a subsequent transplantation study. When 4,100 IEQ/kg BW was used (less than one donor per animal),(163) animals that received islets in the liver (intraportal), KC, abdominal fat pad via BS, and abdominal fat pad via PPCN achieved euglycemia within 5.3±0.6, 4.3±3.7, 25.3±13.5, and 13±4 days, respectively (**Fig. 3-4f,g**). IPGTT performed at one-month post-transplant shows that animals transplanted with BS had higher blood glucose at 15-, 30- and 60-minute time points, while blood glucose values for the PPCN group were comparable to those of the KC control (**Fig. 3-4h**). The AUC in the BS group is significantly larger than those of the PPCN and kidney control groups ($p<0.01$) (**Fig. 3-4i**). The islet graft was explanted at 120 days post-transplantation. Upon graft removal, euglycemic

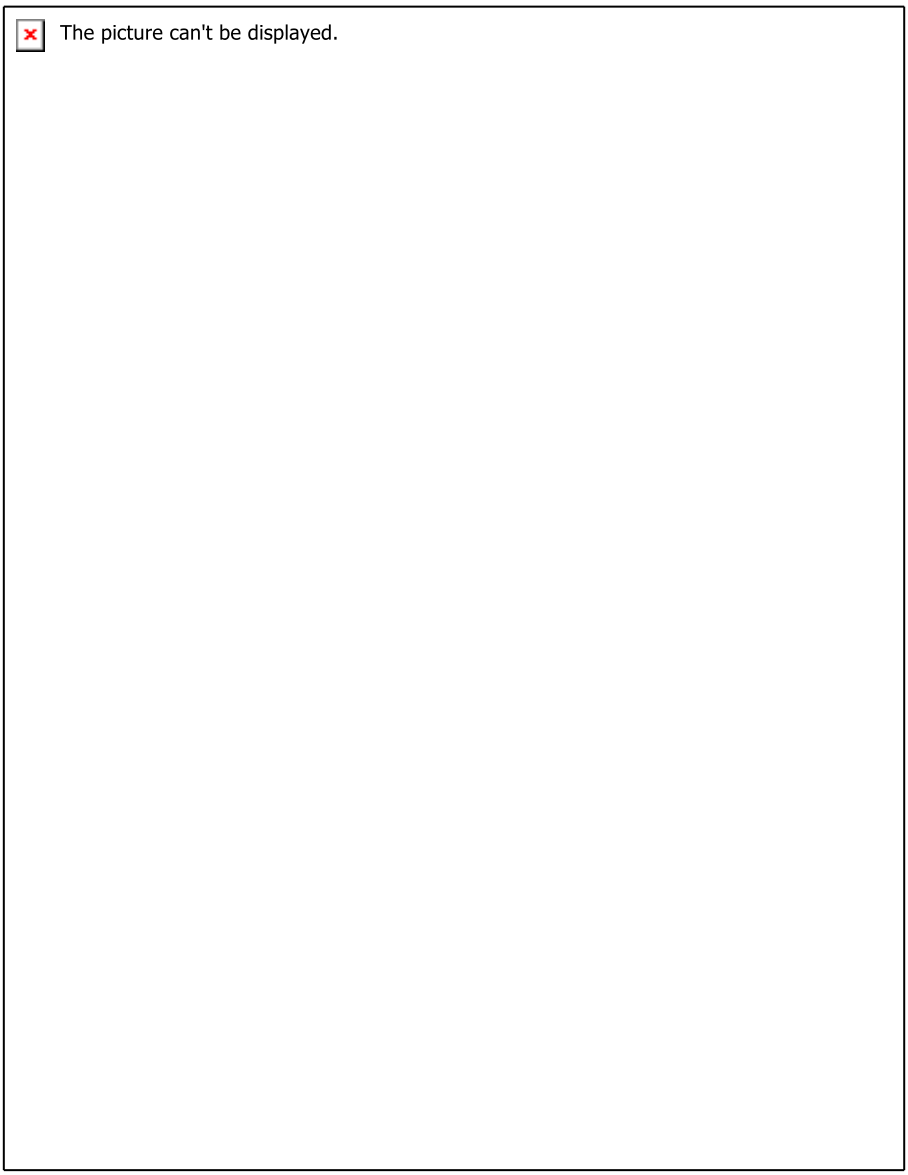

Figure 3- 5. **PPCN protects transplanted islets against oxidation-induced DNA damage *in vivo.***
a, Representative histology, and immunofluorescence images of islets transplanted to the kidney capsule (KC), fat pad with biologic scaffold (FP w/ BS) or fat pad with PPCN (FP w/ PPCN), including, from left to right: Masson's trichrome, hematoxylin and eosin (H&E), anti-α-SMA (red) and anti-8-OHdG (red) with anti-insulin (green) and nuclear dye DAPI (blue) counterstain. For H&E staining, arrows indicate the presence of blood vessels. (Scale bars: 100 um). **b,** Quantification of intra-islet vascular density using α-SMA positive structures in immunofluorescence images. **c,** Quantification of nuclear oxidation based on 8-OHdG positive cells in immunofluorescence images. **e,** Quantification of islet size by area in FP groups (w/ BS or PPCN). **f,g,** Quantification (**f**) and digital images (**g**) of reactive oxidative and nitrogen species *in vivo* 24 hours post-transplantation as measured via IVIS by the total flux of L-012 activity. **h, i,j,** To evaluate protective antioxidative effects *ex vivo*, islets were pre-stressed with 10 μM H_2O_2 for 5 min *in vitro* before the transplantation. **h,** Non-fasting blood glucose concentration (mg/dl) of mice transplanted with approximately 8,200 IEQ/kg body weight of pre-stressed islets to the FP w/ BS or PPCN. **i,** Body weight of mice transplanted with approximately 8,200 IEQ/kg body weight of pre-stressed islets to the FP w/ BS or PPCN. Mice in the FP w/ BS group were euthanized on day 18 post-transplantation due to severe weight loss. **j,** Digital images (top) and H&E histology (bottom) of the fat pad explanted at 18 days for the BS group or 100 days for the PPCN group. All data are presented as mean ± SD ($n \geq 3$; ** $p<0.01$). All data are presented as mean ± SD with *$p<0.05$; ** $p<0.01$; *** $p<0.001$ relative to PPCN. Statistical significance was determined by T-test, one-way or two-way ANOVA with Tukey's multiple comparisons test. ($n \geq 3$).

animals that had received islets via PPCN to the fat pad or in suspension to the KC all reverted to the hyperglycemia states within 48 hours (100 % converted, n=5). In the case of BS, one animal failed to regain hyperglycemia with an average non-fasting blood glucose of 300 mg/dL 48 hours post graft explant, while the rest of the group reverted to the hyperglycemia (80% converted to euglycemia, n=5).

3.3.4 PPCN supports neovascularization, reduces inflammation, and mitigates DNA oxidative damage in transplanted islets

Histological and immunofluorescence staining was performed on the explanted islet grafts (fat pad and kidney). Masson's trichrome (**MT**) and hematoxylin & eosin (**H&E**) staining were performed to assess collagen production and the morphology of the islet grafts (**Fig. 3-5a left**). Antibody probes against insulin, alpha-smooth muscle actin (**α-SMA**) confirmed the production of insulin, the presence of healthy islet structures, and intra-islets neovascularization in the transplanted islets (**Fig. 3-5a right**). Both, BS and PPCN were completely absorbed, leaving islets surrounded by native adipose tissue. Few collagen fibrils and inflammatory cells were observed in the MT-stained sections at the transplant area, suggesting the absence of a chronic foreign body response due to BS or PPCN. Because increased oxidative stress has previously been reported to be closely associated with the diabetic condition and islet damage in several experimental and clinical settings,(6) co-staining of the 8-OHdG marker was conducted to evaluate oxidation-induced DNA damage in the islet grafts (**Fig. 3-5b**). The expression of 8-OHdG was significantly higher in islets engrafted in the fat pad with BS whereas no signal was observed from islets engrafted with PPCN. Although a large amount of 8-OHdG positive cells were also observed in the kidney control group, unlike the BS group, the majority of the 8-OHdG positive cells in the

KC group were present in the native kidney tissue and not in the grafted islets. There was significantly more vascularization throughout the islets engrafted via PPCN relative to BS according to H&E and α-SMA staining, suggesting a more favorable engraftment of the islet's microvasculature with the recipient's native vasculature ($p<0.05$). (**Fig. 3-5c**) The favorable islet engraftment due to PPCN is further confirmed by the larger size of the islets relative to islets transplanted using BS (**Fig. 3-5d)**.

Given that it has been reported that initial oxidative stress on the islets has been shown to negatively impact engraftment, we assessed reactive oxidative and nitrogen species at 24 hours post-transplantation, in real-time, using a L-012 probe. Analysis by IVIS revealed that islet transplantation with BS cause a significant ($p<0.05$) increase in reactive species at the site of transplantation, whereas reactive species in the PPCN treatment group resembled the sham condition (**Fig. 3-5e,f**). Data including treatment with the non-antioxidative version of PPCN, PP**G**N is shown in the supplement (**Fig. S3-4**).

To further evaluate the use of PPCN to protect islets against oxidative tissue damage, freshly isolated islets were first entrapped in BS or PPCN and subsequently exposed to 10 μM H_2O_2 in cell culture medium, a physiologically relevant concentration, for 5 minutes. After exposure to H_2O_2, the hydrogen peroxide-containing medium was removed, and the islets were transplanted into the fat pad of syngeneic recipient mice. Non-fasting blood glucose levels of these graft recipients were closely monitored before and after the transplantation. Although no significant morphological changes and oxidation damage were observed after 5 minutes of exposure to H_2O_2 according to *in vitro* culture studies, the *in vivo* performance of these H_2O_2 exposed islets is significantly different (**Fig. 3-5g**). Euglycemia was established in the recipients that received islets via PPCN within 24 hours post-transplantation, similar to the mice that received

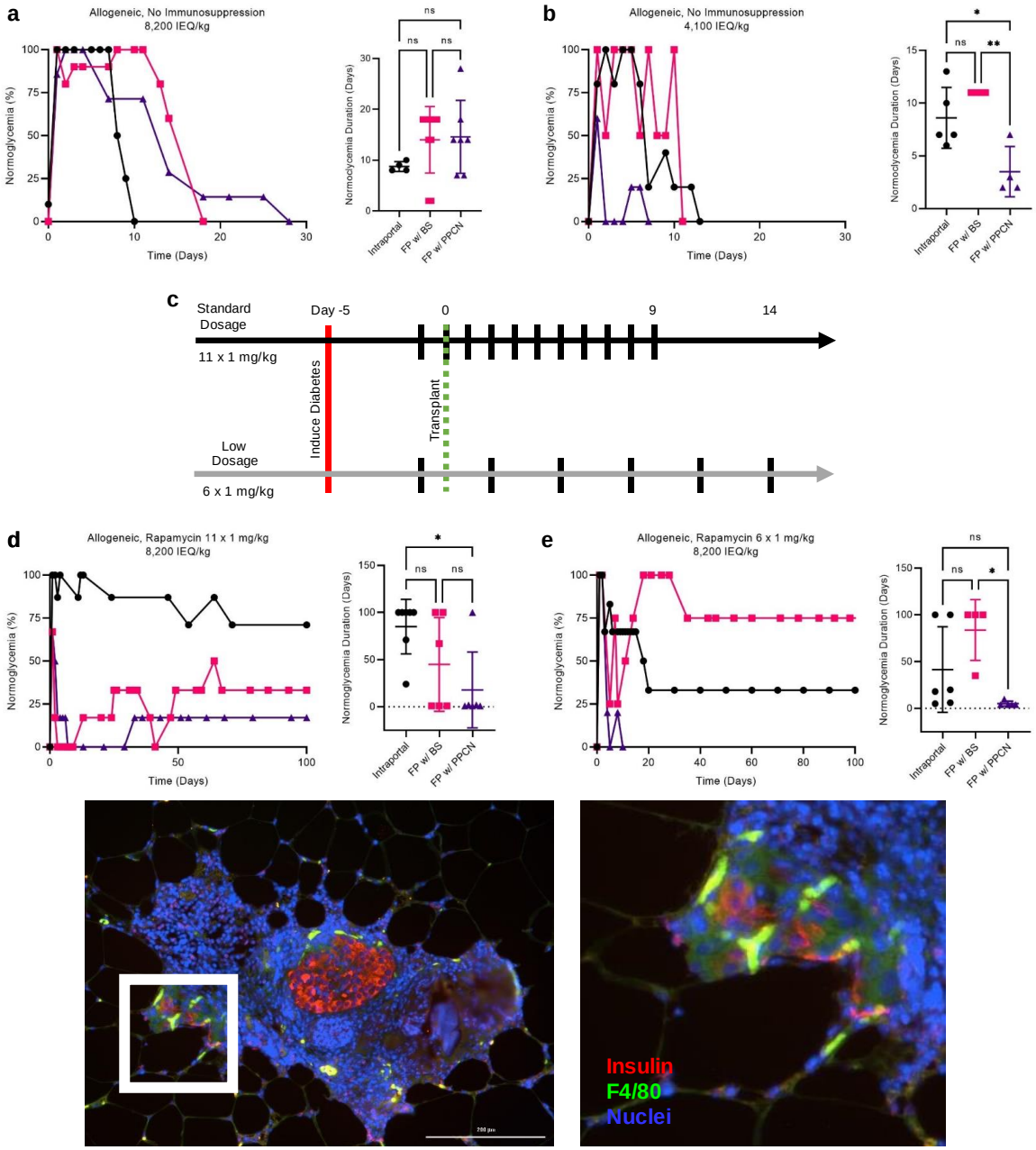

Figure 3- 6. **The omentum is not a viable site for allogeneic islet transplantation.**
Fully major histocompatibility complex (MHC)-mismatched islet transplantation was performed using Balb/c donors and C57BL/6 recipients. Islets were transplanted intraportally to the liver (Intraportal; black circle), to the fat pad with biologic scaffold (FP w/ BS; pink square), or to the fat pad with PPCN (FP w/ PPCN; purple triangle). **a,b,d,e** Left: Percentage of mice experiencing normoglycemia (%) (Blood glucose concentration < 200 mg/dl) as a function of time post-transplantation. Right: Duration of normoglycemia (Days). Mice were treated with **a,** 8,200 islet equivalents (IEQ)/kg body weight (162), no immunosuppression, **b,** 4,100 IEQ/kg BW, no immunosuppression), **c,** Schematic showing dosage protocols for subcutaneous rapamycin. The standard dosage protocol consisted of 11 x 1 mg/kg BW doses on postoperative days (POD) -1 to 9. The low dosage protocol consisted of 6 x 1 mg/kg BW dosage on POD -1, 2, 5, 8, 11, and 14. Mice treated with **d,** 8,200 IEQ/kg body weight, standard dosage rapamycin protocol subcutaneous rapamycin 1 mg/kg day -1 to 9, or **e,** 8,200 IEQ/kg BW, low dosage rapamycin protocol 1 mg/kg day. All data are presented as mean ± SD with *p<0.05; ** p<0.01; *** p<0.001 relative to PPCN. Statistical significance was determined by one-way ANOVA with Tukey's multiple comparisons test. ($n \geq 3$). f, Immunohistochemistry of fat pad excised from a mouse after failed PPCN transplantation: anti-insulin (red) and anti-F4/80 (green) and nuclear dye DAPI (blue) counterstain (scale bar: 200 μm).

8,200 IEQ/kg BW (**Fig. 3A**). In contrast, all BS islets grafts exposed to H_2O_2 *in vitro* remained hyperglycemic and animals had to be euthanized 15 days post-transplantation due to significant weight loss (**Fig. 3-5g,h**). A dramatic difference in the tissue volume at the transplant site was also observed at the time of graft removal. Islet grafted using PPCN were approximately 10 times the size of the islets grafted using BS (**Fig. 3-5i**). These results highlight the destructive effects of oxidative stress on the *in vivo* function of islets post-transplantation and PPCN's capacity to protect islets against oxidative damage and loss of function.

3.3.5 The omentum is not a viable site for allogeneic islet transplantation.

Despite the success of PPCN to preserve islet function for syngeneic transplantation, the omentum (fat pad), regardless of material, is not a viable site for allogeneic islet transplantation. Fully major histocompatibility complex (**MHC**)-mismatched islet transplantation was performed using Balb/c donors and C57BL/6 recipients. Islets were transplanted intraportally to the liver, to the fat pad with BS, or to the fat pad with PPCN. To exclude variability in transplant protection due to immunosuppressive drugs, in the first experiments, no immunosuppressive therapy was given. When a standard islet mass of 8,200 IEQ/kg is transplanted, BS and PPCN do not show advantageous outcomes in terms of graft survival, as indicated by normoglycemia relative to the intraportal control (**Fig. 3-6a**). A more challenging assessment of the transplantation site was performed by transplanting a marginal mass of 4,100 IEQ/kg. Marginal transplant showed that the fat pad site with PPCN performed significantly worse than intraportal transplant ($p<0.05$) or fat pad transplant with BS ($p<0.01$) (**Fig. 3-6b**). To assess a more clinically relevant situation, the immunosuppressant rapamycin was given subcutaneously (**SC**) at either a standard dosage protocol (11 x 1 mg/kg, postoperative day (**POD**) -1 to 9) or low dosage protocol (6 x 1 mg/kg,

POD -1, 2, 5, 8, 11, 14) (**Fig. 3-6c**). Mice treated with the standard dosage protocols and transplanted to the fat pad with PPCN had significantly worse normoglycemia duration than mice that were transplanted via the intraportal site ($p<0.05$) (**Fig. 3-6d**). There was no significant difference between the intraportal site and fat pad with BS or fat pad with BS and fat pad with PPCN (**Fig. 3-6d**). In regard to the low dosage protocol, there was no significant difference between intraportal and fat pad with BS or PPCN. Fat pad with BS transplant had a significantly longer normoglycemia duration than fat pad with PPCN. Other dosing schedules, and formulations, including a nanoparticle formulation of rapamycin known as rPS, which will be discussed in Chapter 4, where also tried for the PPCN condition, however, none were successful (**Fig. S3-5**). Allogeneic islet transplantation to the fat pad with PP**G**N, the non-antioxidative formulation of PPCN, was performed without immunosuppression (**Fig. S3-6**). While PPCN did extend normoglycemia beyond that achieved with PPGN, the results with PPCN were still not on par with standard methods of transplantation. When the fat pad graft was excised and immunohistochemistry was performed for islets (insulin; red) and macrophages (F4/80; green) with nuclei counter stain, there is colocalization of the macrophages with degraded islets. In conclusion, fat pad transplantation in a fully MHC mismatched model was not beneficial as compared to intraportal transplantation.

3.3.6 PPCN is well tolerated, does not elicit a deleterious foreign body response, and is resorbed when applied to the omentum of a non-human primate (NHP)

Unlike the abdominal fat pad found in small rodents, the omentum in large animals such as NHPs and humans is a natural defense mechanism for the pathophysiology of intra-abdominal diseases due to its well-vascularized structure and angiogenic properties.(165) The pro-inflammatory environment of the omentum in a human could impact islet function; hence, the

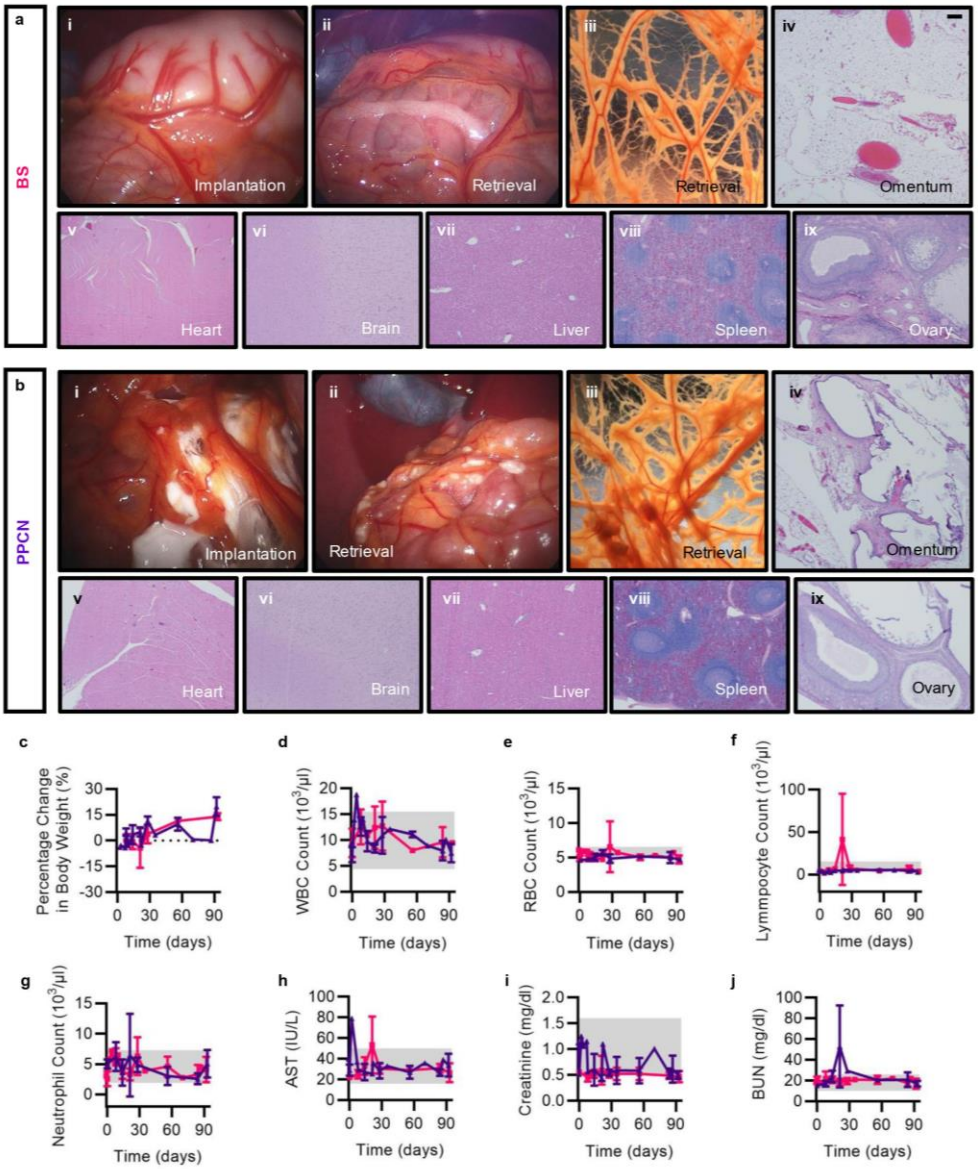

Figure 3- 7. PPCN was well tolerated for 90 days with no signs of an inflammatory response when implanted in the omentum of female and male rhesus macaques.

a(i-iii),b(i-iii), Digital images showing the laparoscopic application (**i**), laparoscopic retrieval (**ii**), and extended omentum upon necroscopy (**iii**) ~90 days after implantation for biologic scaffold (**BS**) (**a**) or poly(polyethylene glycol citrate-co-N-isopropylacrylamide) (**PPCN**) (**b**), respectively. **a(iv-ix),b(iv-ix),** Representative images of histology with hematoxylin and eosin (H&E) staining from various tissues after necropsy for BRS (**a**) or PPCN (**b**) treatment, respectively, including omentum (**iv**), heart (**v**), brain (**vi**), liver (164), spleen (**viii**), and ovary (**ix**). Representative images for gallbladder, kidney, stomach, jejunum, colon, mesenteric lymph node, lung, skeletal muscle, mandibular lymph node, and testis are included in the supplementary information. Scale bar = 200 µm. Representative tissues were taken from female macaques. **c-j,** Body weight, complete blood cell counts, and blood chemistry panels before and after implantation for BS (pink square) and PPCN (purple triangle), including percentage change in body weight (**c**), white blood cell (**WBC**) count (**d**), red blood cell (**RBC**) count (**e**), lymphocyte count (**f**), neutrophil count (**g**), aspartate transaminase (**AST**) concentration (**h**), creatinine concertation (**i**), and blood urea nitrogen (**BUN**) concentration (**j**). A grey box indicates the normal range for each parameter. All data are presented as mean ± SD. (n = 2 for BRS group: 1 female, 1 male; n = 5 for PPCN group: 2 females, 3 males).

compatibility of the scaffold with this tissue is of utmost importance.(165) The similarity in islet architecture, islets functions, as well as the size and anatomy of the omentum between humans and NHPs motivated us to investigate the tissue response to PPCN in NHPs, specifically, the rhesus macaque.(166) BS was used as a control (**Fig. 3-7a**). PPCN application to the omentum is shown in **Fig. 3-7bi**. PPCN can easily be applied as a liquid through syringes and rapidly transitions into an opaque hydrogel within seconds upon contact with the tissue at body temperature. The graft was secured and covered with surrounding fat pad tissue without the need for sutures or staples. Over the course of the 3-month study, the health of the animals, including disposition, body weight, complete blood count, and chemistry, was carefully monitored. Body weight was maintained or increased for both groups (**Fig. 3-7c**). Analysis of blood chemistry, complete blood count, and white blood cell differentials from blood samples drawn weekly revealed normal values for the duration of the 3-month study (**Fig. 3-7d-j**). Kidney health, as assessed by creatinine and blood urea nitrogen (**BUN**) concentrations showed no impairment in function (**Fig. 3-7i,j**). Drug and toxin metabolism by the liver showed a transient spike immediately after the surgery presumably due to the use of systemic pain management and antibiotics. Once such treatments were over, AST levels returned to normal and were maintained throughout the entire length of the study (**Fig. 3-7h**). At 3 months post-surgery, the implantation site was surgically accessed and inspected for any signs of inflammation or a foreign body response to the BS or PPCN and to retrieve a biopsy of the implantation site. For the PPCN treated animals, except for a small amount of white matter that appeared to be remaining PPCN (~20% of originally applied material), gross inspection of the surrounding tissue was normal. The histopathology report confirmed the absence of inflammation, fibrosis, or tissue abnormalities, except for a few areas that showed signs of remaining PPCN. Tissue composition, including vascularization, also appeared normal. (**Fig. 3-7b**). In all, PPCN

applied to the omentum was well tolerated by large NHPs, as the animals maintained their baseline health throughout the study with no changes in behavior, blood parameters, and the omentum.

3.4 Discussion

Intraportal hepatic transplantation of healthy islets has been considered a last resort therapy for chronic pancreatitis for the past 30 years.(167) Despite improvements in islets isolation techniques, long-term graft survival, and sustained insulin independence remain challenges with this procedure.(130) Furthermore, severe hypoglycemia unawareness due to the delayed glucagon secretion response by the alpha cells in the transplanted islets at the hepatic location has motivated the exploration of alternative extrahepatic transplantation sites.(135) We have developed a temperature-responsive, phase-changing, easy-to-use, liquid biomaterial with anti-inflammatory and antioxidant properties that we hypothesized would protect islets against oxidative stress and prolong their function *in vitro* and during extrahepatic islet transplantation. The great omentum is a location that is ideal from the clinical perspective due to its large, well-vascularized area, and accessibility via minimally invasive procedures.(130, 163) However, since its physiological role involves protecting the peritoneal cavity from invading infectious diseases, the pro-inflammatory environment at the omentum site may result in unexpected severe inflammatory responses towards the transplanted islets and the biomaterial used to deliver them. (165)

To date, several natural and synthetic biomaterials have been investigated as vehicles to facilitate the engraftment of islets in the omentum.(168-170) Pedraza et al., used a polydimethylsiloxane (**PDMS**) porous scaffold in a STZ-induced diabetic rat model to restore euglycemia with 10,000 IEQ/kg BW (1800 IEQ/rat). However, a fibrous capsule developed around the graft area according to the histology data, due to the foreign body response elicited by the use

of PDMS.(171) Modifications to the PDMS with the angiogenic growth factor platelet-derived growth factor (**PDGF-BB**) or fibrin gel were able to slightly reduce the number of islets to 8,333 IEQ/kg body weight (250 IEQ per mice); however, it took 19 days for the recipient to achieve euglycemia. (172) Berman et al., demonstrated the use of a porous polyglactin and poly-P-dioxanone scaffold (Codman Ethisorb^{TM} Duan Patch) to achieve minimum exogenous insulin requirements (0.3 to 0.4 IU/kg/day) with 5093 IEQ/kg autologous islets transplanted to the omentum of cynomolgus macaques.(173) Immunofluorescence and histological staining of the explanted islet graft demonstrated elevated host cell infiltration around the graft area. Stendahl *et al.* investigated the use of vascular endothelial growth factor (**VEGF**) and fibroblast growth factor-2 (**FGF-2**) with heparin-binding peptide amphiphile (**HBPAs**) nanofibers in a poly (L-lactic acid) scaffold. In their study, only 78% of the mice receiving the VEGF/FGF-1-releasing scaffold achieved euglycemia within 54 days after transplantation.(174) Furthermore, bi-layered PEG and PEG-VEGF islet encapsulation systems have recently been described. However, islet transplantation with 17,391 IEQ/Kg (4,000 IEQ/rat) did not resolve hyperglycemia, indicating insufficient insulin secretion.(175) Berman et al., evaluated autologous BS hydrogel as a vehicle to deliver human islets to the omentum with a clinically relevant number of islets (8,200 IEQ/kg BW (1,300 IEQ/rat)). Euglycemia was achieved the day after the transplantation.(10) However, the pro-inflammatory and pro-oxidative environment of autologous plasma from T1D patients likely contributed to graft failures during the first clinical trial of islet transplantation to the omentum in humans.(176, 177) Therefore, to develop a clinically useful material for extrahepatic transplantation of pancreatic islets, BS and PPCN were both evaluated in the study. We evaluated two islet doses: 8,200 IEQ/kg BW and 4,100 IEQ/kg BW per recipient. These islet masses represent 50% and 25% of the total islets found in healthy mouse pancreas, the latter being a

substantial reduction in islet dose when compared to previous reports.(141, 178-180) Using 8,200 IEQ/kg BW, euglycemia was achieved in both the PPCN and BS groups confirming non-inferiority of PPCN to BS. However, in the marginal islet study, PPCN was a superior delivery vehicle as euglycemia was achieved 13±4 days after the transplantation in contrast to the 25±13 days in the BS group. Delayed insulin response was also observed in the BS group when the transplanted islets were exposed to sudden blood glucose changes via the IPGTT test, indicating insufficient glucose control. Furthermore, unlike scaffolds reported by others, PPCN was completely resorbed by the time of explantation. No cell infiltration or fibrosis was observed around the graft area and islets were incorporated into the surrounding adipose tissue with enhanced intra-islets vasculature.

The islet isolation process and *in vitro* cell culture have been shown to expose islets to oxidative stress, both by facilitating the generation of reactive oxygen species (**ROS**) and by hindering the adaptive upregulation of cellular antioxidants.(6, 181),(182) Furthermore, insulin-producing beta cells have significantly lower levels of antioxidant enzymes catalase, superoxide dismutase, and glutathione peroxidase, which make them particularly vulnerable to oxidative damage especially during ischemia-reperfusion injury.(183),(182, 184, 185) These findings have therefore prompted studies that use antioxidant peptides and oxygen generating strategies to improve islet function. An example is the addition of the peptide carnosine during *ex vivo* islet culture and oxygen-generating PDMS-CaO_2 scaffolds for islet encapsulation.(159, 186) Although intriguing *in vitro* results have been reported, antioxidant scaffold approaches have not been evaluated *in vivo* for islet transplantation.(187) One potential explanation for the observed superior performance of PPCN may be its intrinsic antioxidant property, which is due to the polyethylene oxide citrate moieties present within the polymer backbone. Reduced DNA oxidative damage was consistently observed in islets engrafted with PPCN as per the 8-OHdG staining.

In order to determine whether there is a link between reducing oxidative stress and the preservation of islet viability and insulin secretion function, oxidative stress reporter islets were created using roGFP overexpression. Intracellularly expressed roGFP has been used in several studies as an effective reporter protein to allow real-time non-destructive monitoring of the cellular redox state.(188, 189) We hereby report for the first time the use of this redox probe technology to evaluate the protective properties of an antioxidant biomaterial. When exposed to H_2O_2 induced oxidative stress, both human and mouse islets entrapped in PPCN experienced a significant delay in the progression of oxidation, thereby better preserving viability and glucose-stimulated insulin secretion response. To further demonstrate the impact of oxidation damage during the *ex vivo* culture period on islet performance post-transplantation, oxidative stress was induced for 5 minutes in the same way as the *in vitro* studies through low dose H_2O_2 treatment before the transplantation. After the transplantation, no sign of islet damage was observed in the PPCN group as euglycemia was achieved the next day after transplantation similar to the original 8,200 IEQ/kg study. However, in the case of the BS group, hyperglycemia persisted after the transplantation, indicating the complete loss of insulin secretion function in those islets. Our results provide strong evidence regarding the link between oxidative stress *in vitro* and islets insulin secretion function *in vivo* and that an antioxidant microenvironment is able to preserve the insulin secretion function of the isolated islets.

An advantage of the hepatic intraportal transplantation procedure is its minimally invasive nature. Therefore, many of the procedures that involve extra-hepatic islets transplantation sites that worked well in animal studies face difficulties when applied to humans because they require open surgery or significant tissue disruption. Other methods that use enzyme- or light-activated *in situ* polymerized scaffolds result in insufficient encapsulation due to the uneven polymerization or

additional damage to the encapsulated islets as well as the surrounding native tissue.(190) Procedures that involve long gelation times risk allowing islets to leak into the IP cavity as we found in this study. Unlike methods used to date, encapsulation and delivery of the islets using PPCN can be easily achieved via an endoscope-enabled procedure by suspending the isolated islets in the PPCN solution at room temperature and applying the material to the omentum as a liquid. The thermoresponsive nature of the PPCN enables uniform gelation within seconds after exposure to body temperature and secures the islets in a defined engraftment location. The demonstrated safety of PPCN when applied to the greater omentum of a large NHP further confirms its realistic use as an alternative to autologous platelet-rich plasma and thrombin.

In conclusion, these observed differences strongly indicated the impact of accumulated oxidative damage on the islets' function post-transplantation, and the advantages of adopting an antioxidant scaffold, like PPCN, for achieving the optimal results for the islets transplantation procedure.

3.5 Materials and Methods

All chemicals used in the study including citric acid, poly(ethylene glycol), glycerol 1,3-diglycerolate diacrylate, poly-N-isopropylacrylamide, collagenase (type XI), dextran, and Thrombin from murine plasma were purchased from Sigma-Aldrich (St Louis, MO).

3.5.1 Human Tissue

Human islets were obtained from Northwestern University Human Islet Transplant Program (Institutional Review Board (**IRB**) exemption: STU00207825).

3.5.2 Animals

8 to 12-week-old, male C57BL/6 and Balb/c mice were purchased from Jackson Labs. Mice were housed in the Center for Comparative Medicine at Northwestern University. All animal protocols were approved by Northwestern University's Institutional Animal Care and Use Committee (**IACUC**).

4 to 10 kg rhesus macaques were purchased from PrimGen (or similar). Animals were negative for Herpes B, tuberculosis (**TB**), simian immunodeficiency virus (**SIV**), simian retrovirus (**SRV**), Simian T-lymphotropic virus (**STLV**). All animal protocols were approved by the University of Wisconsin at Madison or the University of Illinois at Chicago and Northwestern University's IACUC.

3.5.3 Materials

All chemicals used in the study including citric acid, poly(ethylene glycol), glycerol 1,3-diglycerolate diacrylate, poly-N-isopropylacrylamide, collagenase (type XI), dextran, and Thrombin from murine plasma were purchased from Sigma-Aldrich (St Louis, MO).

3.5.4 PPCN synthesis and solution preparation

Poly(polyethylene glycol citrate-co-N-isopropylacrylamide) (PPCN) was synthesized from citric acid, poly(ethylene glycol), glycerol 1,3-diglycerolate diacrylate, and poly-N-isopropylacrylamide following the previously published method.(146) The resulting PPCN were then neutralized with sodium hydroxide, sterilized with ethylene oxide gas sterilization, and properly vented before use. To encapsulate islets, a 100 mg/ml PPCN solution was made by dissolving lyophilized PPCN in sterile PBS.

3.5.5 Murine islet isolation

Mice were first anesthetized with an intraperitoneal injection of ketamine and xylene. After a midline abdominal incision, cold collagenase solution was injected into the pancreas via the cannulated bile duct. The collagenase-infused pancreas was then dissected and incubated at 37 °C for 15 min. After the digestion, the large undigested connective tissue was removed by passing the digested pancreas through a mesh screen. The filtrate was then applied to a discontinuous dextran gradient to separate islets from the remaining connective tissue fragments. After two gradient washes, the purified islets were hand-picked and counted under the microscope.

3.5.6 *In vitro* islet encapsulation, viability, and insulin secretion study

The encapsulation of islets within PPCN and pNIPAAm was achieved utilizing their thermoresponsive nature. Islets were purified and counted before mixing into the PPCN or pNIPAAm room temperature solution. For in vitro study, the islets loaded PPCN solution is then added into the non-tissue culture coated plates and incubated under 37 °C for 5 mins to solidify the PPCN. After the hydrogel formed inside the well, warm islets culture medium was added to the well to support the islet's growth before returning the plate into the incubator. The encapsulation of islets within BS gel was done in a similar fashion, except a thrombin calcium solution was added into an initial mixture of plasma and islets to solidify the BS gel before the addition of growth media.

The viability of the encapsulated islets was assessed after 24 days of incubation using two different methods: the resazurin assay for quantification (Sigma) and the Live/Dead assay for visualization

(Life Technologies, Carlsbad, CA). Both assays were performed following the manufacturer's protocol.

Low (2.8 mM) and high (28 mM) glucose solutions were prepared in Kreb's buffer for the glucose-stimulated insulin secretion test. The concentrations were determined based on the NIH human islets standard operating procedure. Briefly, after the removal of growth media from the encapsulated islets, the islets were first washed with the low glucose solution then sequentially incubated in a) low glucose equilibration solution, b) low glucose solution, and c) high glucose solution for 1 hour each. After the incubation, the solution from b) and c) were collected and measured using an insulin ELISA kit (Thermo Fisher for mouse islets, and Mercodia, Uppsala, Sweden for human islets). The stimulation index was defined as the ratio of stimulated (high glucose) to baseline (low glucose) insulin secretion.

The test was done by comparing the different amounts of insulin secreted by the islets when subject to low (2.8 mM) and high (28 mM) glucose concentrations. The results were reported as stimulation index (SI), which is acquired by dividing the amount of insulin produced by the islets in the high glucose solution by the insulin amount produced in the low glucose solution. (**Fig. 1c**) Since the low glucose concentration is a representation of the blood glucose level under normal fasting conditions, d enhanced insulin secretion is expected when the islets are transferred from the low glucose solution to the high glucose solution. Therefore, the higher the stimulation index, the more sensitive the islets are.

3.5.7 roGFP transduction and oxidation inhibition study

To access the oxidation status of the islets under varied culture conditions, freshly isolated islets were treated with engineered lentivirus encoding the roGFP gene. roGFP expression was monitored using a fluorescent microscope after the transduction. The expression level of the roGFP

protein was monitored for 96 hours after the transduction of the roGFP viral vector. The reduced protein signal (488 nm) was observed to be gradually increasing and reached a maximum at 72 hours, while the oxidized protein signal remained at a minimum level at that point. Once the roGFP protein expression reached its maximum in the viral vector treated islets, these roGFP-islets were either cultured in standard media suspension, platelet-rich plasma (BS) gel, pNIPAAm homopolymer, or PPCN.

The oxidation inhibition study was carried out in ibidi 15 well glass bottom slides. roGFP-islets were split into each well before treatment with various conditions (PPCN, pNIPAAm, or BS). Baseline (0 minute) confocal images of the islets under each condition were taken with two excitation wavelengths (405 nm and 475 nm) and one fixed emission wavelength of 509 nm. Hydrogen peroxide was then added into the islets culture with a final concentration of 10 μM. The oxidation status of the islets was monitored under confocal microscopy at each time point. The oxidation percentage was quantified based on the fluorescent intensity under the two wavelengths using ImageJ.

3.5.8 Murine islet transplantation procedure

STZ-induced diabetes For *in vivo* islets transplantation, donor animals were pre-treated with STZ to induce diabetes one week before the transplantation. Three different transplant locations were applied in the study. The abdominal fat pad transplantation is used for PPGN, BS and PPCN, and islet transplantation. Intraportal transplantation to the liver and the KC transplantation were used as the positive control. Both procedures were conducted following previously published procedures. For the abdominal fat pad model, A small incision was first created on the abdominal part of the animal to expose the abdominal fat pad, followed by the application of room

temperature islets-PPCN suspension. Purified islets were transplanted with 40 μl of PPGN, BS, or PPCN. After the gel solidified on the fat pad, all the islets got secured in place before returning back into the intraperitoneal cavity. After the transplantation surgery, the non-fasting blood glucose of the animals was monitored on daily basis for the first two weeks post-surgery, and then once a week afterward. By the end of the study, graft explant was conducted via a survival surgery. Animals were allowed to recover from the surgery, and their blood glucose levels were monitored for another 48 hours, after which time the mice were sacrificed.

3.5.9 Murine intraperitoneal glucose tolerance testing

Intraperitoneal glucose tolerance tests (**IPGTTs**) were performed one-month post-transplantation. The animals were fasted for 16 hours before receiving an intraperitoneal injection of 2g/kg body weight of 50% dextrose (Abbott Labs, North Chicago, IL) solution. Blood glucose was measured at 0, 15, 30, 60, and 120 minutes after the glucose injection.

3.5.10 Tissue collection and immunofluorescent staining

Islets containing fat pad and kidney were harvested and processed for paraffin sectioning. Immunofluorescent staining for blood vessel, insulin, cell death(191), and oxidation marker (8-OHdG) was performed following the manufacture's protocol. Digital images were acquired with a Nikon fluorescent microscope. Images were then processed with ImageJ.

3.5.11 Biocompatibility and safety of PPCN in the omentum of nonhuman primates

The day before implantation, blood was drawn from all animals and collected in sodium citrate

tubes. The blood was spun down at 1500 g for 10 minutes and the plasma fraction was collected for use in the BS group. A thrombin solution was made by dissolving 1000 IU/ml PBS supplemented with calcium and magnesium. Rhesus macaques were placed under general anesthesia. BS (2 ml plasma, 2 ml thrombin solution) or PPCN (4 ml) was applied onto the greater omentum via laparotomy. Body temperature and weight, complete blood cell counts, white blood cell differential, and blood chemistry were measured before and at several intervals, after the surgery, until euthanasia to assess for infection, liver function, kidney function, and blood composition. At approximately 90 post implantations, the animals were euthanized. A full necropsy was performed. Histology was performed by the Veterinary Diagnostic Laboratory at the College of Veterinary Medicine at the University of Illinois Chicago. A full histopathology report was provided.

3.5.12 Statistical analysis

Statistical analyses were performed using Prism 6, Two-way ANOVA was used to measure differences for experiments with multiple data sets with a Tukey test performed between groups with significant differences to correct for the multiple pair-wise comparisons. A value of $p \leq 0.05$ was considered to be statistically significant. Values are reported as the mean±SD.

3.6 Supplementary Information

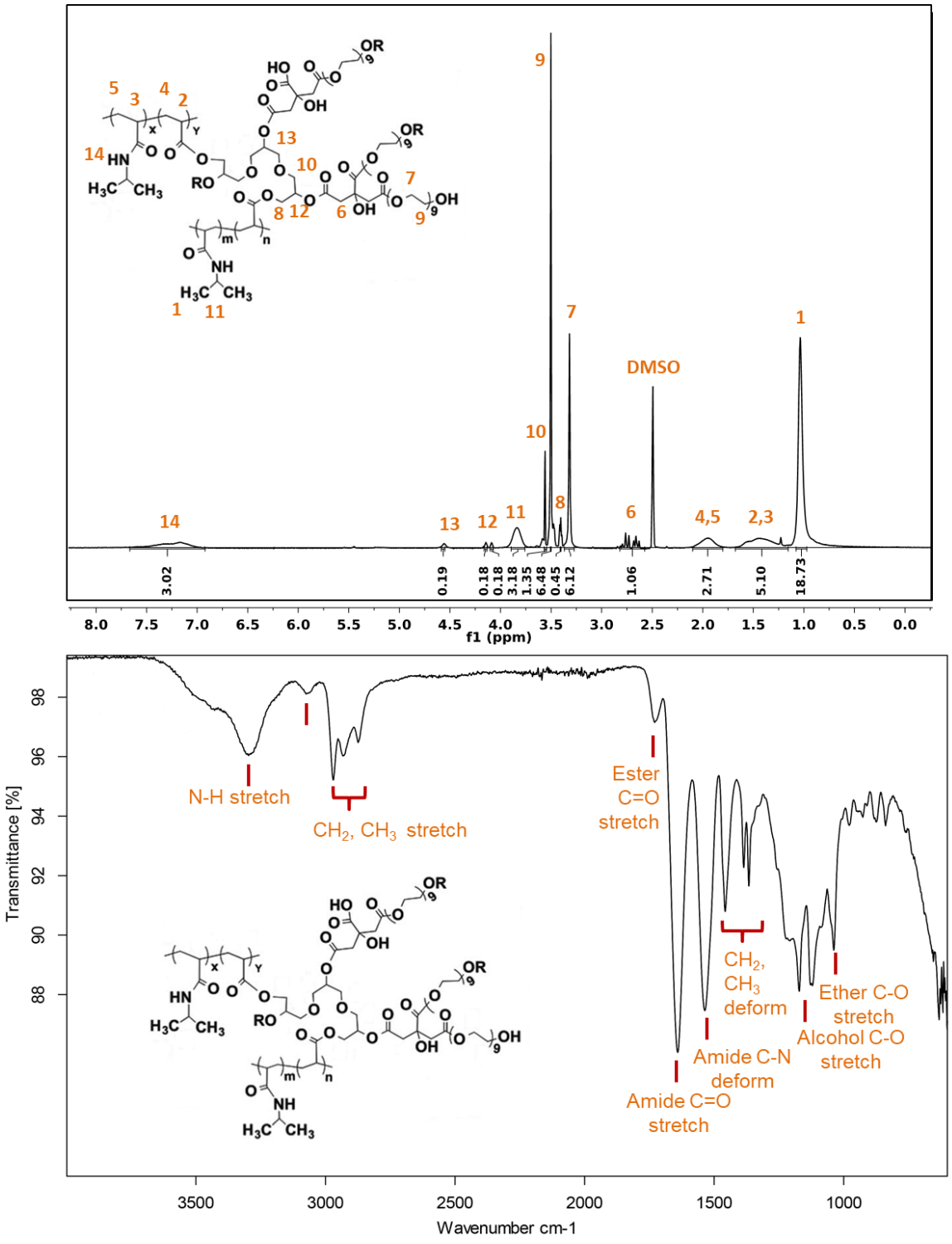

Supplementary Figure S3-1 | ^{1}H-NMR and ATR-FTIR spectra confirm the formation of poly(polyethylene glycol citrate-co-N-isopropylacrylamide) (PPCN). proton nuclear magnetic resonance spectroscopy (**^{1}H-NMR**); attenuated total reflection Fourier transform inferred spectroscopy (**ATF-FTIR**).

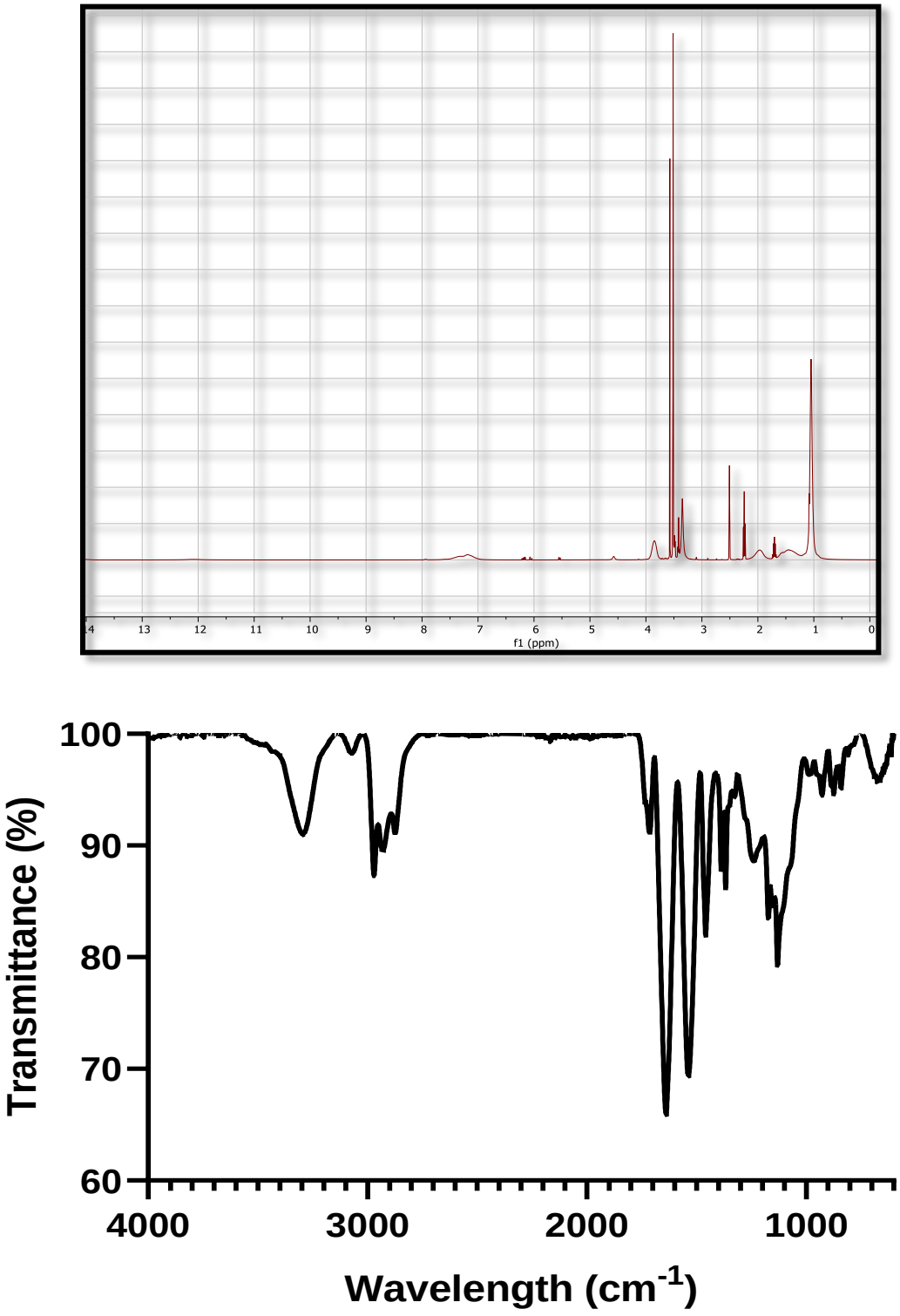

Supplementary Figure S3-2 | ^{1}H-NMR and ATR-FTIR spectra confirm the formation of poly(polyethylene glycol glutarate-co-N-isopropylacrylamide) (PPGN). proton nuclear magnetic resonance spectroscopy (**^{1}H-NMR**); attenuated total reflection Fourier transform inferred spectroscopy (**ATF-FTIR**).

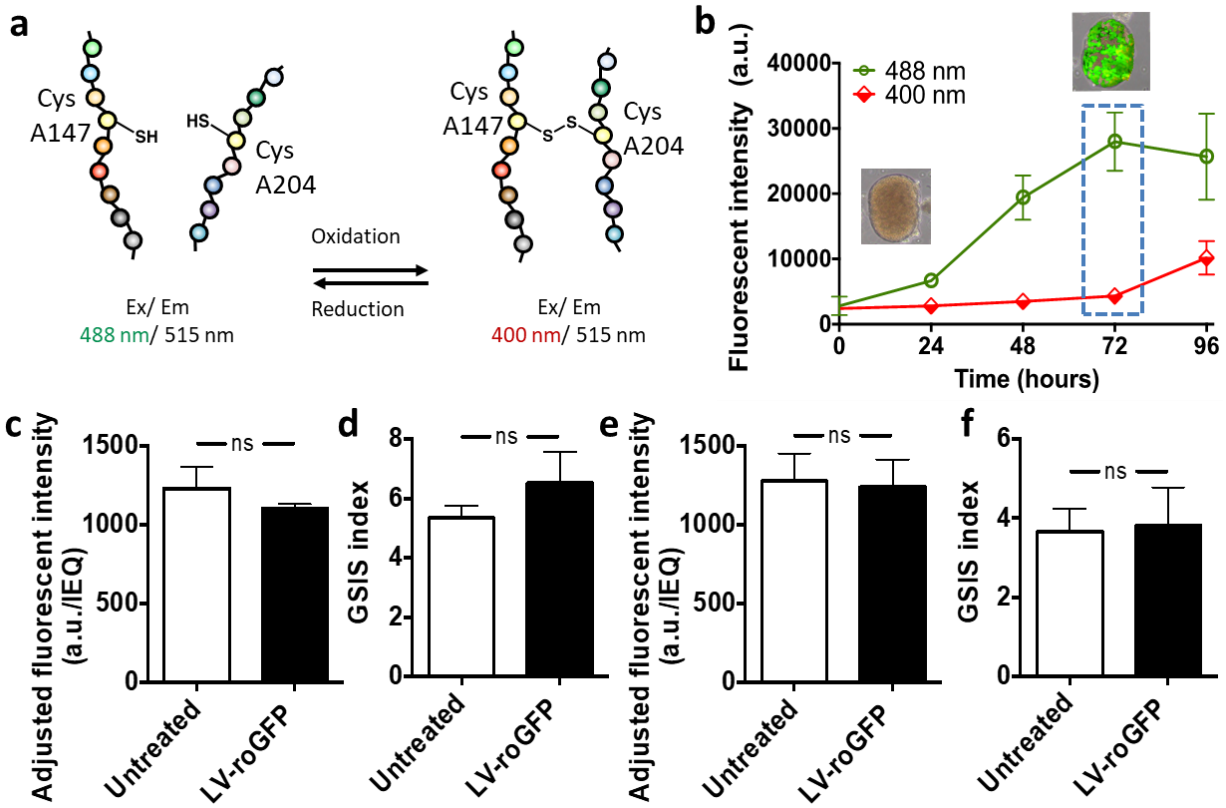

Supplementary Figure S3-3 | Overexpression of roGFP does not affect islet viability and insulin secretion function. a, Schematic of the transition between the reduced and oxidized forms of roGFP. **b,** The fluorescence intensity of reduced and oxidized RoGFP signals over time (insert: RoGFP overexpressing islets at time 0 and time 72 hours after the addition of the viral vector). **c-f,** Viability and islet insulin secretion function were preserved after roGFP overexpression for both mouse (**c, d**) and human (**e, f**) islets. All data are presented as mean ± SD ($n \geq 3$; ns: $p>0.05$).

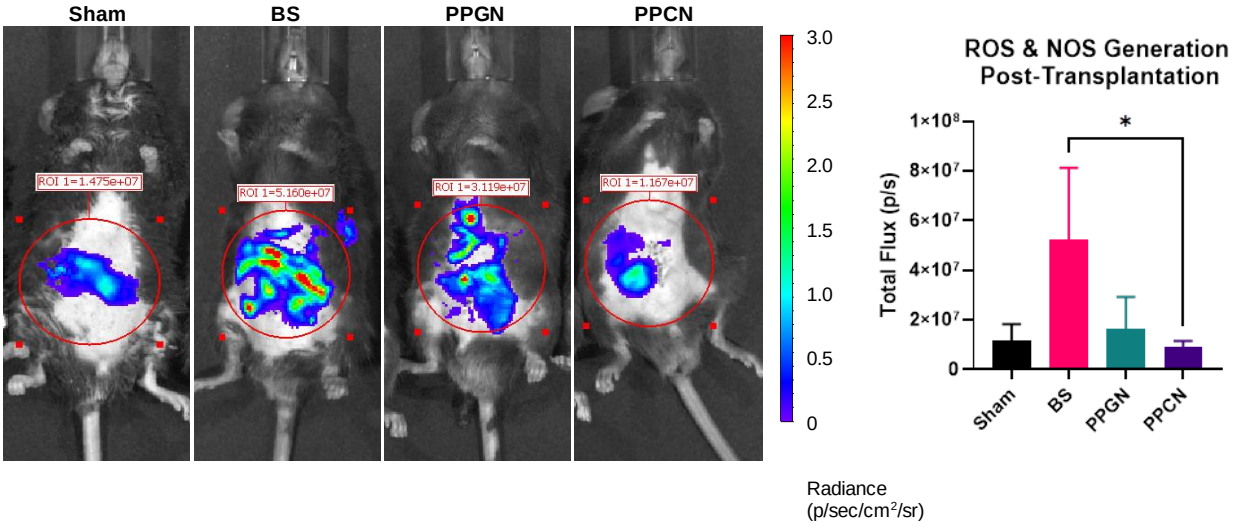

Supplementary Figure S3-4 | Assessment of reactive oxidative species (ROS) and islet transplantation without immunosuppression, including fat pad transplantation with PPGN. IVIS images (**left**) and quantification (**right**) of reactive oxidative and nitrogen species *in vivo* 24 hours post-transplantation as measured via IVIS by the total flux of L-012 activity. All data are presented as mean ± SD with *p<0.05. Statistical significance was determined by one-way ANOVA with Tukey's multiple comparisons test. (n = 3).

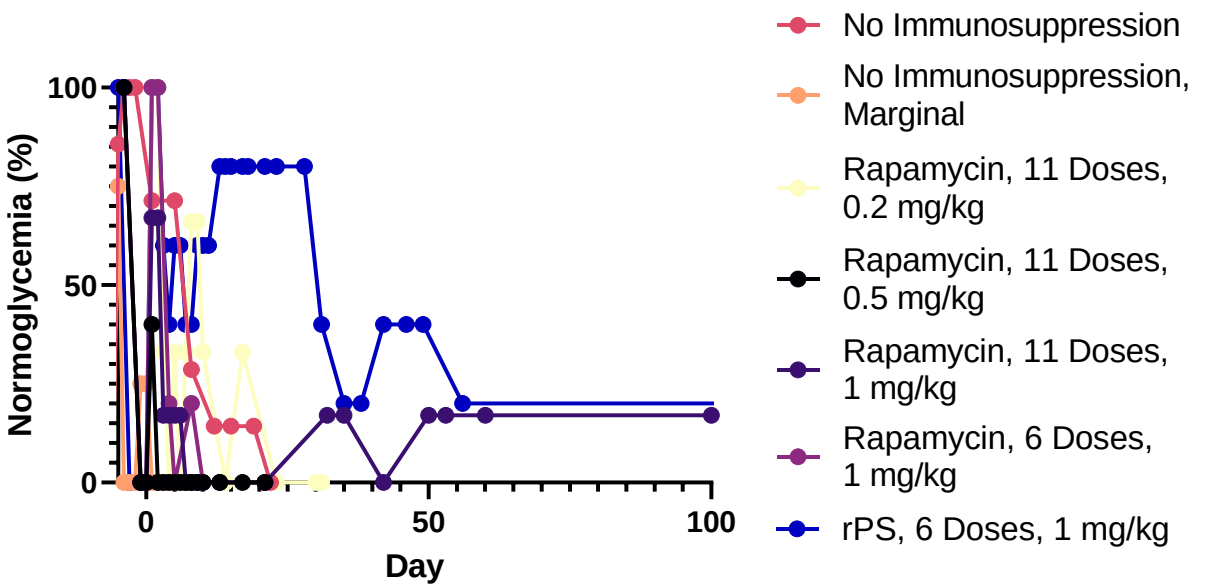

Supplementary Figure S3-4 | Allogeneic islet transplantation to the fat pad with PPCN using various immunosuppressive regimens. Fully major histocompatibility complex (MHC)-mismatched islet transplantation was performed using Balb/c donors and C57BL/6 recipients. Islets were transplanted to the fat pad with PPCN. All transplants utilized 8,200 IEQ/kg, unless marginal is indicated, in which 4,100 IEQ/kg were transplanted. Various immunosuppressive protocols were utilized, as indicated by the key within the figure.

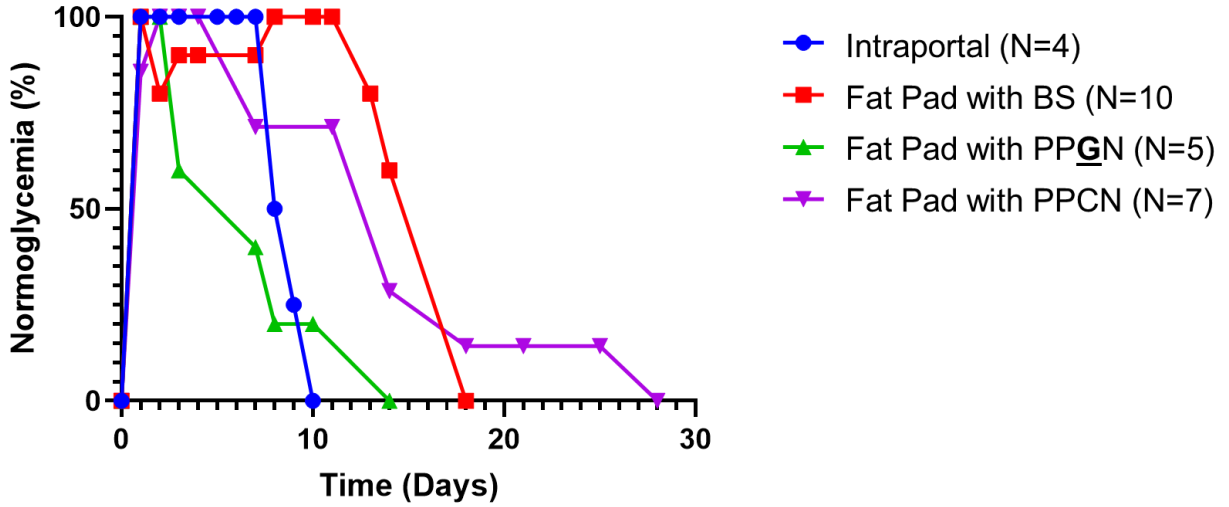

Supplementary Figure S3-6 | Allogeneic islet transplantation without immunosuppression, including fat pad transplantation with PPGN. Fully major histocompatibility complex (MHC)-mismatched islet transplantation was performed using Balb/c donors and C57BL/6 recipients. 8,200 IEQ/kg islets were transplanted intraportally to the liver or to the fat pad with BS, PPGN or PPCN. The percentage of normoglycemic mice was recorded. Mice were considered normoglycemic if blood glucose was < 200 mg/dl.

.

CHAPTER 4: SUBCUTANEOUS NANOTHERAPY REPURPOSES THE IMMUNOSUPPRESSIVE MECHANISM OF RAPAMYCIN TO ENHANCE ALLOGENEIC ISLET GRAFT VIABILITY

4.1 Abstract

Standard oral rapamycin (i.e. Rapamune®) administration is plagued by poor bioavailability and broad biodistribution. Thus, this pleiotropic mTOR inhibitor has a narrow therapeutic window, numerous side effects, and provides inadequate protection to transplanted cells and tissues. Furthermore, the hydrophobicity of rapamycin limits its use in parenteral formulations. Here, we demonstrate that subcutaneous delivery via PEG-*b*-PPS PS nanocarriers significantly alters rapamycin's cellular biodistribution to repurpose its mechanism of action for enhanced immunosuppression while minimizing side effects. While oral rapamycin inhibits naïve T cell proliferation directly, subcutaneously administered rPS modulate antigen-presenting cells in lieu of T cells significantly improving maintenance of normoglycemia in a clinically relevant, MHC-mismatched, allogeneic, intraportal (liver) islet transplantation model. These results demonstrate the ability of a rationally designed nanocarrier to re-engineer the immunosuppressive mechanism of a drug by controlling cellular biodistribution.

4.2 Introduction

T1D is an endocrine disorder that leads to pancreatic β cell destruction and requires management with lifelong exogenous insulin therapy(31). Islet transplantation has emerged as a promising treatment for T1D by eliminating the need for exogenous insulin(31). This protocol involves three key components: acquisition of viable insulin-producing cells, the surgical transplantation of these cells into a suitable physiological location to maintain glucose sensitivity

and responsiveness, and an immunosuppressive regimen to maintain islet viability and protection from the host's immune system(31). While all three components remain active areas of research, the need for immunosuppression remains the key limitation preventing islet transplantation from becoming the clinical standard of care for all T1D patients(31, 192). A critical advancement in this regard was the advent of orally administered (**PO**) nanocrystal rapamycin, i.e. Rapamune®. This drug was used in the first non-steroidal immunosuppressive protocol for islet transplantation, known as the Edmonton protocol(193). Rapamycin inhibits the mammalian target of rapamycin (**mTOR**) pathway to directly inhibit T cell proliferation by arresting these cells in the G1 phase of the cell cycle and preventing IL-2 secretion(194). Although more effective than prior immunosuppressive protocols including steroids, patients undergoing transplantation procedures are still plagued by frequent graft rejection and an unpleasant array of side effects(34, 194).

Side effects related to oral rapamycin administration stem primarily from poor and inconsistent bioavailability and the wide cellular biodistribution. Rapamune® has a bioavailability of only 14% in the solution form and 41% in tablet form(194). The low bioavailability is attributed primarily to the first pass metabolism associated with the oral route of administration, cytochrome P450 elimination, and transport by p-glycoprotein efflux pumps. For example, absorption of Rapamune® is significantly affected by fat content in food, and cytochrome P450 isoenzyme CYP3A4 metabolism can cause serious drug-drug interactions(194). With regards to biodistribution, lipophilic Rapamune® primarily partitions into red blood cells (95%) and then eventually accumulates in off-target organs, including the heart, kidneys, intestines, and testes(39, 41, 42), leading to side effects. These side effects occur due to the ubiquitous expression of mTOR in diverse cell types, resulting in unintended cell populations also experiencing cell cycle arrest(192, 194). Adverse effects stated on Rapamune® package insert include malignancy,

enhanced susceptibility to infection, impaired wound healing, thrombopenia, alopecia, gastrointestinal distress, gonadal dysfunction, hypertension, hyperlipidemia, nephrotoxicity, and peripheral edema(43, 194). To balance the need to maintain immunosuppression with the avoidance of side effects, patients must undergo frequent blood work to ensure that the rapamycin concentration is within the small therapeutic window of 5 to 15 ng/mL in whole blood(39, 194). Of note, mTOR inhibition can have distinct responses depending on the cell type. For example, rapamycin maintains dendritic cells (**DCs**) in an immature tolerogenic state that resists coreceptor expression in response to inflammatory stimuli, a process known as costimulation blockade(195).

Given the plethora of problems associated with oral Rapamune®, an alternative therapy that bypasses the oral route of administration reduces adverse effects and improves transplantation outcomes is needed. Subcutaneous administration (**SC**) would avoid bioavailability issues that plague oral Rapamune® including first-pass metabolism, elimination by intestinal cytochrome CYP3A4 and p-glycoprotein, and variability associated with food composition(194). Importantly, SC administration provides the advantage of targeting lymphatic drainage(196). Unlike intravenous administration, the SC route would allow patients to take their medication from their own homes. The T1D patient population is well versed in the SC method of injection due to the need to inject insulin. Furthermore, the SC route provides access to antigen-presenting cells (**APCs**), including the aforementioned DCs that can elicit potent tolerogenic responses upon modulation by rapamycin. Tolerogenic DCs (**tDCs**) constitutively generate regulatory T cells (**Tregs**) as well as express anti-inflammatory cytokines, both of which have been linked to enhanced survival of transplanted islets(196).

However, due to the lipophilic nature of rapamycin, it is poorly soluble and therefore very difficult to formulate into a parenteral drug for SC administration(197). Others have attempted to

solve the formulation issues associated with rapamycin by using nanotechnology(47). Previous studies have fabricated rapamycin nanocarriers from a variety of materials, including lipids, protein, poly(lactic-co-glycolic acid) (**PLGA**), and other polymers(47). Due to the ubiquitous nature of rapamycin's mTOR inhibition, these nanocarriers have been researched for a wide array of applications, such as immunomodulation, cancer, cardiovascular diseases, and neurodegenerative diseases(47, 198, 199). Of note, literature cites the need for investigation into the use of rapamycin nanocarriers for the treatment of diabetes(47). To this end, we hypothesized that focusing rapamycin's mTOR inhibition on APCs instead of T cells using engineered nanocarriers could achieve sustained immunosuppression and survival of transplanted islets via the SC route with lower dosage and minimal side effects (**Fig. 4-1**). Sustained tolerance to transplanted islet grafts would allow for real-time sensing of glucose and insulin release to modulate blood glucose for the treatment of T1D. To control the biodistribution of rapamycin specifically to target APCs, we generated rPS. The PEG-*b*-PPS PS platform allows for efficient loading of lipophilic drugs within the PPS membrane(50), has been validated to be nontoxic in both mice and nonhuman primates,(49, 200-203) and undergoes uptake by DC and monocyte populations(203), which are critically responsible for directing T cell activation during immune responses(202, 204, 205). Importantly, PEG-*b*-PPS is non-immunomodulatory relative to other common nanomaterials, with an immunostimulatory profile that is determined almost exclusively by the loaded therapeutic(203). For example, unloaded blank PEG-*b*-PPS PS elicit minimal immunomodulatory activity, whereas comparable PLGA nanocarriers cause an extensive coreceptor expression (e.g. CD80, CD86), and modification of the inflammatory status of the immunomodulatory response, including alteration of immune cell populations, changes in coreceptor expression (e.g. CD80, CD86), and modification of the inflammatory status of

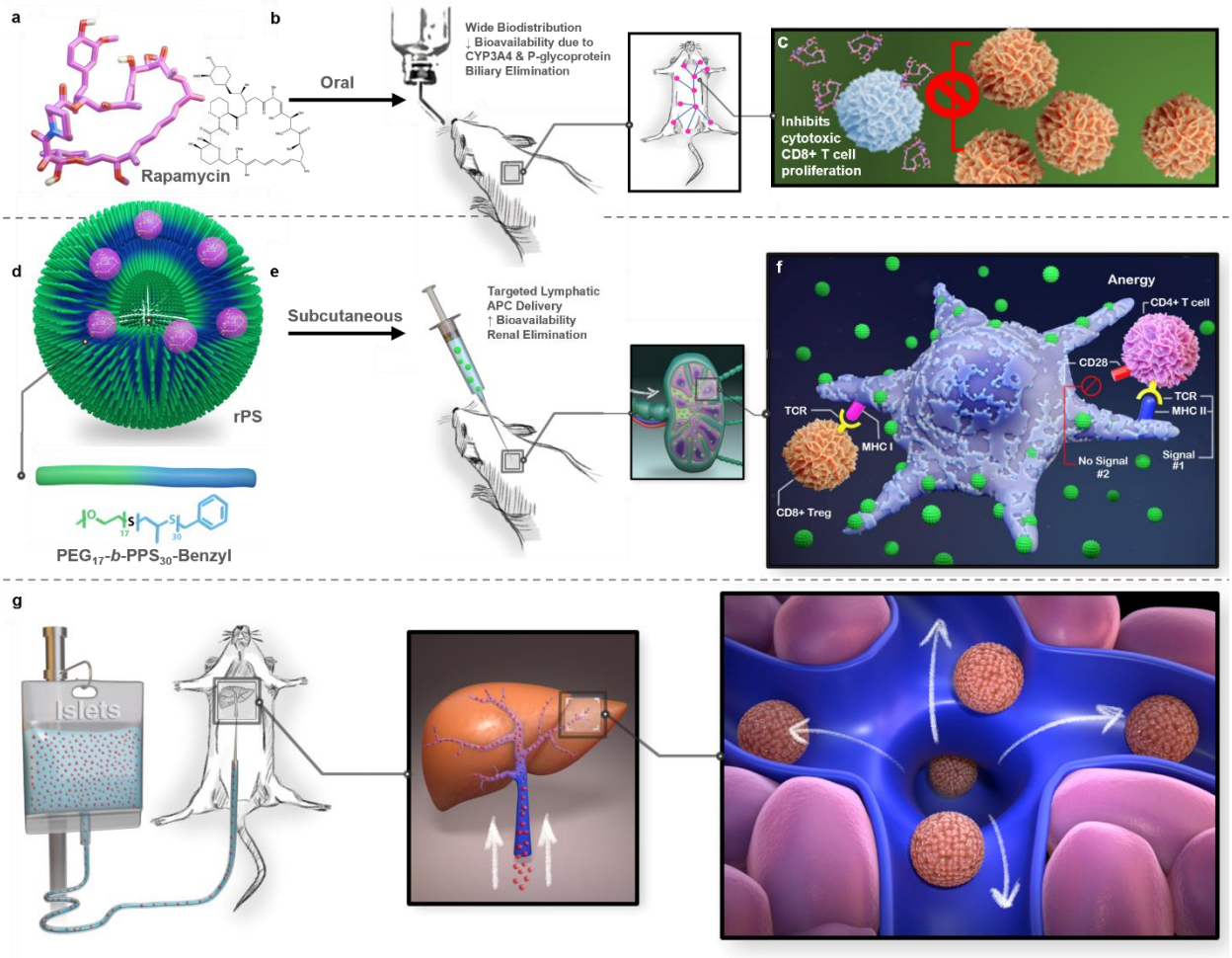

Figure 4- 1. Subcutaneous rapamycin delivery via polymersomes (rPS) tolerizes intraportal islet grafts via direct modulation of APCs instead of T cells.

a, Rapamycin is a hydrophobic mTOR inhibitor that is used as an immunosuppressive drug. **b,** Clinically, rapamycin is given orally. Oral administration (i.e. Rapamune®) results in a wide biodistribution and low bioavailability, as it is a substrate for CYP3A4, and p-glycoprotein and s cleared via biliary elimination. **c,** Oral rapamycin primarily acts on T cells to prevent cytotoxic CD8+ T cell proliferation. **d,** Alternately, rapamycin can be easily loaded into the hydrophobic membrane of polymersomes (**PS**) to form rapamycin-loaded polymersomes (**rPS**). **e,** When injected subcutaneously (**SC**) into mice, rPS drain into the brachial lymph nodes where they are uptaken by antigen-presenting cells (**APCs**). As a result, APCs develop an anti-inflammatory, semi-mature phenotype, in which they express high levels of MHC II to present to CD4+ T cell receptors, but they do not express costimulatory molecules. Without activation from costimulation, CD4+ T cells go into a state of anergy or become tolerogenic CD8+ regulatory T cells (Tregs). **g,** To assess the ability of SC rPS to provide a tolerogenic state that allows for fully major histocompatibility complex (MHC) mismatched allogeneic graft survival, islet transplantation was performed in diabetic mice at the clinically relevant intraportal (liver) transplantation site and graft viability was assessed by the restoration and maintenance of normoglycemia.

numerous immune cell subsets(206). Thus, our mechanistic assessment of inflammatory status of numerous immune cell subsets(206). Thus, our mechanistic assessment of rPS-mediated immunosuppression avoids interference from background immunomodulation due to the drug delivery vehicle.

Herein, we present the first application of SC rapamycin nanotherapy for islet transplantation, as well as the first example of reorchestrating the mechanism of an immunosuppressant by rationally controlling its cellular biodistribution. Liquid chromatography with tandem mass spectrometry (**LC-MS-MS**) was used to assess the biodistribution of the small molecule drug rapamycin delivered within PEG-*b*-PPS PS at nanogram resolution (ng/mg or ng/mL). Efficacy of this strategy is assessed by high parameter spectral flow cytometry with analysis via T-distributed stochastic neighbor embedding (**tSNE**), RNA sequencing, and a clinically relevant intraportal fully major histocompatibility complex (**MHC**) mismatched allogeneic islet transplantation model. Our results provide insight into how nanocarrier-mediated modulation of cellular biodistribution can significantly change the metabolism and therapeutic window, reduce adverse events, and enhance the anti-inflammatory efficacy of an immunosuppressant by rationally repurposing its therapeutic mechanism of action.

4.3 Results

4.3.1 Rapamycin loading does not alter morphology, polydispersity

PEG-*b*-PPS PS were characterized to assess encapsulation efficiency and retention of their vesicular nanostructure following the loading of rapamycin to form rPS. Rapamycin encapsulation efficiency was found to be greater than 55% for rPS following self-assembly and therapeutic

loading via thin-film hydration of desiccated PEG-*b*-PPS films. Neither the PS vesicular nanostructure nor the polydispersity was significantly modulated by rapamycin loading as assessed by dynamic light scattering (**DLS**), cryogenic transmission electron micrograph (**cryoTEM**), and small-angle x-ray scattering (**SAXS**) (**Fig. 4-2a-c**). The stability of rapamycin loading was assessed in 1X phosphate-buffered saline (**PBS**) at 4 °C, finding approximately 94% of the drug was retained over the course of 1 month (**Fig. S4-1**). Rapamycin is relatively lipophilic with a logP of 4.3(197), and thus these results were consistent with past attempts to load molecules of low water solubility into PEG-*b*-PPS nanostructures.

4.3.2 Polymersomes alter biodistribution, immunomodulation

To demonstrate that PEG-*b*-PPS PS can alter the biodistribution of a small molecule following SC administration, indocyanine green dye (**ICG-PS**) was loaded into PS to serve as a traceable model payload. C57BL/6 mice were administered ICG via oral gavage, ICG via SC injection, or ICG-PS via SC, sacrificed animals at 2, 24, and 48 h post-administration, and analyzed organs via IVIS (**Fig. S4-2**). We show that SC of ICG-PS allowed for sustained residence within the superficial axillary/brachial lymph nodes at 24 and 48 h post-injection, whereas free form ICG dye had been cleared at these later time points (**Fig. 4-2d**). To confirm that this effect holds true for rapamycin, a single dose (1 mg per kg body weight, 0.125 mg rapamycin per mL) of Rapamune® PO, rapamycin (in 0.2% carboxymethyl cellulose) SC or rPS (6.7 mg polymer per mL) SC was administered to C57BL/6 mice. Animals were sacrificed at 0.5, 2, 8, 18, 24, and 48 h post-injection to assess rapamycin content in blood and various organs. We found that delivery of rapamycin via rPS increases rapamycin concentration in immune cell-rich tissues, such as the blood, liver, axillary lymph center (deep axillary/axillary/axial and superficial axillary/brachial

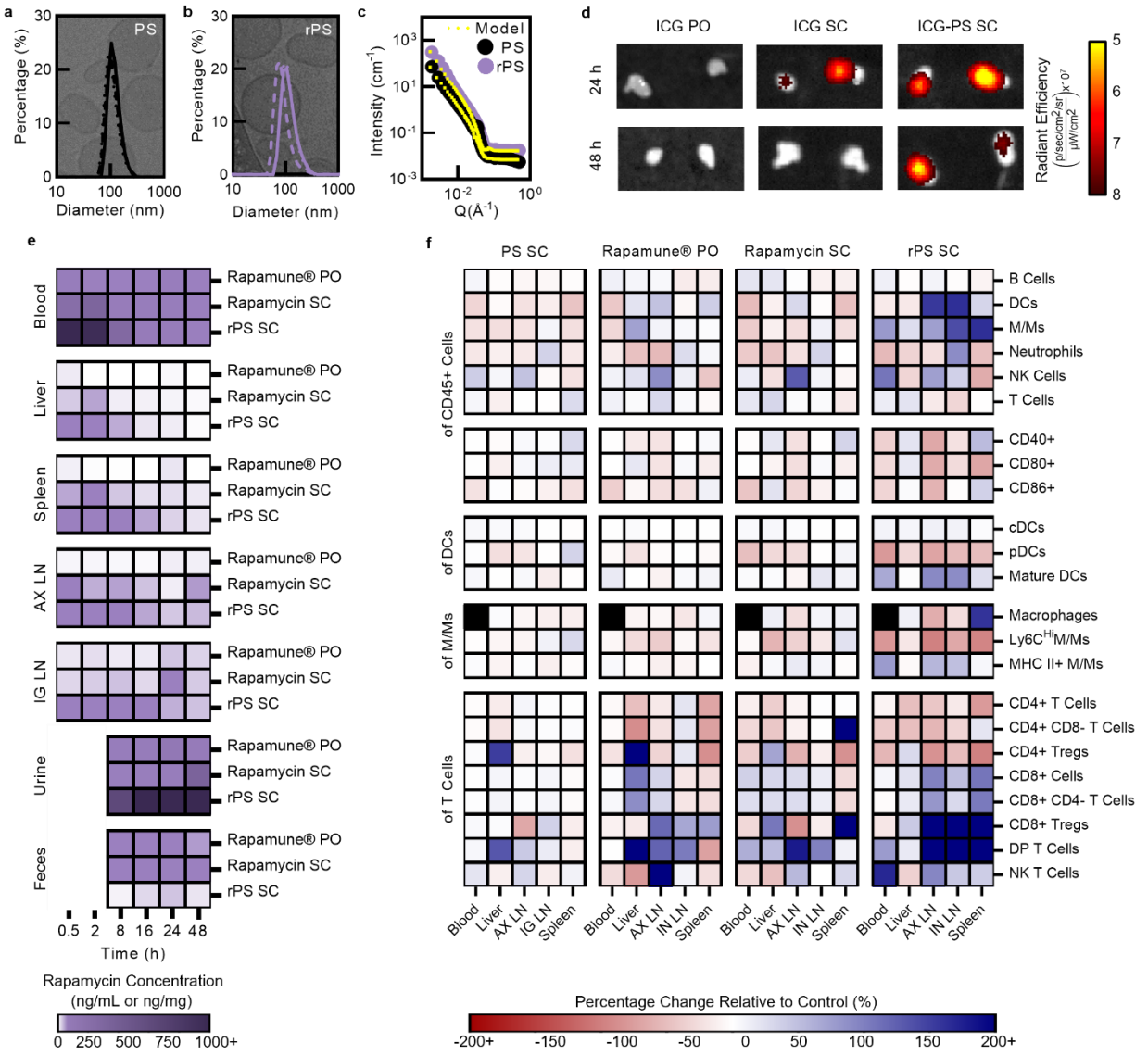

Figure 4- 2. Subcutaneous delivery via PS alters rapamycin's biodistribution and immunomodulation.
a,b, Cryogenic transmission electron micrograph (cryoTEM) of polymersomes (PS) (**a**) and rapamycin-loaded polymersomes (rPS) (**b**) with overlay of size distribution by dynamic light scattering (DLS) (n = 3). Scale bars represent 100 nm. (n = 3). **c,** Small-angle x-ray scattering (SAXS) transformed data of PS (●) and rPS (●) with polymer vesicular model fit (--). (n = 3-5). **d,** Biodistribution of indocyanine green (ICG) dye in the superficial axillary/brachial LN (of the axillary lymphocenter (AX LN)) 24 and 48 hours after oral gavage of ICG or subcutaneous injection (SC) with ICG or ICG-loaded polymersomes (ICG-PS) (n = 5 mice/group). **e,** Biodistribution of rapamycin after a single 1 mg rapamycin per kg body weight dose (Table S4-1) of Rapamune® via oral gavage (PO), rapamycin (in 0.2% carboxymethyl cellulose) via SC or rapamycin-loaded polymersomes (rPS) via SC. All formulations were at a concentration of 0.125 mg/mL rapamycin. rPS formulations contained 6.7 mg polymer per mL. Rapamycin concentration (ng/mL or ng mg) in various tissues over time (0.5 h, 2 h, 8 h, 16 h, 24 h, and 48 h) as assessed by liquid chromatography-tandem mass spectrometry (LC-MS/MS). Assessed tissues included blood, liver, axillary lymphocenter (deep axillary/axillary/axial and superficial axillary/brachial lymph nodes; AX LN), subiliac ly mphocenter (subiliac/inguinal lymph nodes; IN LN), spleen, urine, and feces. (n = 6 mice/group). **f,** Flow cytometry analysis of CD45+ cell populations from mice administered with PS SC, Rapamune® PO, rapamycin SC or rPS SC, using the standard dosage protocol (11 doses, over 11 days, 1 mg rapamycin per kg body weight per dose or equivalent volume (Table S4-1), formulated at 0.125 mg rapamycin per mL, PS and rPS formulations contained 6.7 mg polymer per mL). A cohort of mice was left untreated as a control. Macrophages were not assessed in blood as indicated by a black box" All data are presented as mean percentage change relative to the untreated control cohort. (n = 6 mice/group).

lymph nodes; **AX LN**), subiliac lymph center (subiliac/inguinal lymph nodes; **IN LN**), and spleen (**Fig. 4-2e, S4-3**). Regarding elimination, as expected, oral Rapamune® was found in the feces due to the established route of biliary elimination. SC rapamycin also resulted in fecal elimination. Surprisingly, when SC rPS was administered, rapamycin was primarily found in the urine relative to the feces, indicating renal elimination (**Fig. 4-2e, S4-3**).

To assess both the organ and cellular effects of rapamycin delivery via PEG-*b*-PPS PS, immune cell populations from various tissues were isolated after repeated doses (11 doses, over 11 days, 1 mg rapamycin per kg body weight per dose or equivalent volume (**Table S4-1**), formulated at 0.125 mg rapamycin per mL) of unloaded PS SC, Rapamune® PO, rapamycin SC or rPS SC (PS and rPS formulations contained 6.7 mg polymer per mL). This "standard dosage" immunosuppressive protocol is accepted to provide similar immunosuppressive effects in mice as compared to clinical immunosuppressive protocols, such as the Edmonton protocol, used in humans(207, 208). When unloaded PS were injected, very little immunomodulation was observed via flow cytometry (**Fig. 4-2f, S4-4, Tables S4-2-26**). However, when rapamycin was loaded within PS, potent immunomodulation occurred (**Fig. 4-2f, Tables S4-2-26**). The relative immunologically inert status of the unloaded PS allowed for the majority of the effects of rPS to be attributed to the altered biodistribution of the drug, as opposed to the nanocarrier itself. A significant change in immunomodulation is observed for PS-mediated rapamycin delivery (**Fig. 4-2f, S4-4, Tables S4-2-26**). Taken in combination with the inert nature of PEG-*b*-PPS, our results demonstrate that rapamycin's organ and cellular biodistribution have a strong influence on the resulting immunological effect.

4.3.3 Induction of CD4+ T cell deletion and anergy

To characterize changes more deeply in immune cell populations in response to rPS delivery, we dosed healthy mice with unloaded blank PS SC, Rapamune® PO, rapamycin SC, or rPS SC (11 doses, over 11 days, 1 mg rapamycin per kg body weight equivalent, formulated at 0.125 mg rapamycin per mL, polymersome formulations contained 6.7 mg polymer per mL). Subsequently, organs (blood, liver, AX LN, IN LN, and spleen) were extracted for assessment via high-parameter spectral flow cytometry. To further understand the changes in immune cell populations as a result of rPS treatment, the inflammatory state of APC populations was assessed via receptor expression. Specifically, CD40, CD80 and CD86 coreceptor presentation on DCs (**Fig. 4-3a-c,g**) and monocyte-and-macrophage-linage (**M/Ms**)(209) (**Fig. 4-3d-f,h**) was analyzed. MHC II presentation was assessed on DCs and M/Ms (**Fig. 4-3g,h, S4**). With rPS, costimulation blockade is observed as indicated by the significant downregulation of CD40, CD80, and CD86 (**Fig. 4-3a-f**)(210) in AX LN. Furthermore, rPS enhances MHC II+ APCs (**Fig. 4-3g,h**). Opposing expression by MHC and coreceptors causes depletion of the CD4+ T cell population (**Fig. 4-3i, S4-4**). Any remaining CD4+ T cells are left in a state of anergy as indicated by the significant decrease in CD4 expression (**Fig. 4-3j**). These effects are most potent in the AX LN near the site of SC injection, but also occur to various lesser extents in blood, liver, IN LN, and spleen (**Tables S4-2-26**).

4.3.4 Regulatory crosstalk between dendritic cells and T cells

rPS treatment causes a significant increase in DCs within AX LN and IN LN (**Fig. 4-3k**). More specifically, an increase in novel CD8+ CD11b+ double-positive (**DP**) conventional DCs (**cDCs**) is observed (**Fig. 4-3l**). Despite the overall increase in the DC population, plasmacytoid

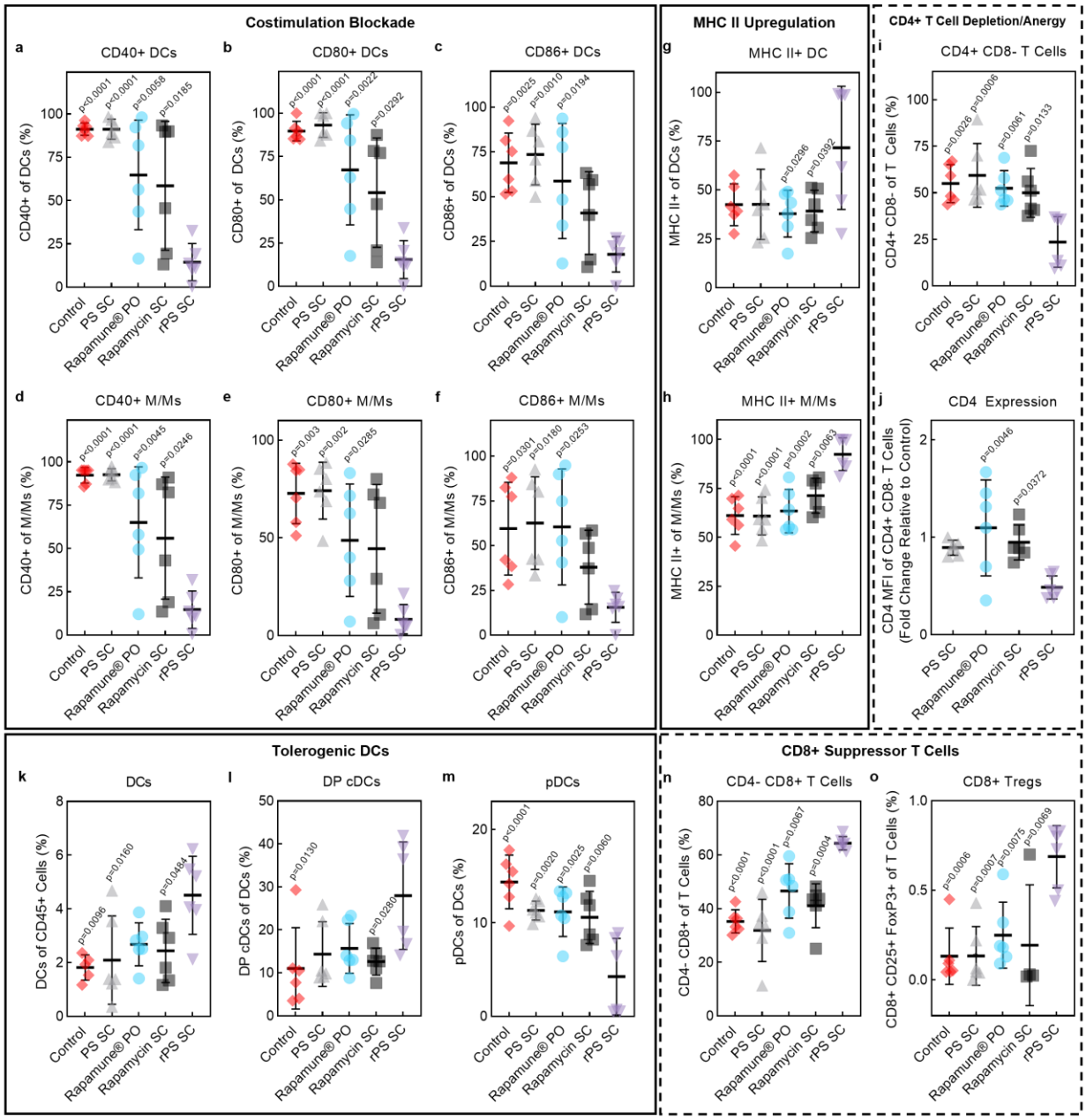

Figure 4- 3. rPS modulate APCs to induce T cell costimulation blockade.

Mice were treated with: polymersomes (PS; ▲) subcutaneous injection (SC), Rapamune® (●) oral gavage (PO), rapamycin (in 0.2% carboxymethyl cellulose; ■) SC, or rapamycin-loaded polymersomes (rPS; ▼) SC, using the standard dosage protocol (11 doses, over 11 days, 1 mg rapamycin per kg body weight per dose or equivalent volume (Table S1), formulated at 0.125 mg rapamycin per mL, PS and rPS formulations contained 6.7 mg polymer per mL). A cohort of mice was left as an untreated control (♦). Cell populations were analyzed by flow cytometry. **a-h)** Analysis of costimulation and major-histocompatibility complex (MHC) II: percentage of CD40+ (**a,d**), CD80+ (**b,e**), CD86+ (**c,f**) and MHC II+ (**g,h**) dendritic cells (DCs) (**a-c,g**) and monocyte-and-macrophage-linage cells (M/Ms) (**d-f,h**). **I,j)** Analysis of CD4+ T cells: percentage of CD4+ CD8- T cells (of T cells) (**i**) and CD4 expression by CD4+ CD8- T cells (fold change of MFI relative to control) (**j**). **k-m**) Analysis of DCs: percentage of DCs (**k**) of CD45+ cells, percentage of DP cDCs of DCs (**l**), percentage of pDCs of DCs (**m**). **n,o**) Analysis of CD8+ T cell populations: percentage of CD4- CD8+ T cells of T cells (**n**) and percentage of CD8+ Tregs of T cells (**o**). Data are from the axillary lymphocenter (deep axillary/axillary/axial and superficial axillary/brachial lymph nodes; AX LN). All data are presented as a mean percentage or median fluorescent intensity (211) ± SD. Significant p-values relative to the rPS treatment are displayed on the graphs. Statistical significance was determined by one-way ANOVA with Tukey's multiple comparisons test. (n = 6 mice/group).

DCs (**pDCs**) are significantly reduced (**Fig. 4-3m**). A significant decrease in the overall T cell population was observed due to a significant decrease in CD4+ T cells (**Fig. 4-3i**). As a result, CD8+ T cells take over a larger portion of the T cell population (**Fig. 4-3n**), accompanied by a significant upregulation of CD8+ Tregs (**Fig. 4-3o**).

4.3.4 Induction of suppressor monocytes & macrophages

rPS treatment causes a significant upregulation of M/Ms in the AX LN (**Fig. 4-4a**). These M/Ms are predominantly Ly-6C^{Lo} monocytes (**Fig. 4-4b,c**). To further understand the specific nature of M/M immunomodulation with rPS treatment, phenotypic analysis of the M/M population was performed on each tissue. Consideration for CD40, CD80, CD86, MHC II, Ly-6C, and macrophage markers (F4/80 and/or CD169) was used to assign cells to one of 32 phenotypes for blood (no macrophage markers) or 64 phenotypes for AX LN and spleen Phenotypic analysis reveals that rPS treatment promotes the dominance of a single suppressor M/M phenotype for each tissue, while rapamycin and control treatments present a diverse range of M/M phenotypes with often contradicting inflammatory statuses. In blood, control treatments result in a majority of CD40+ CD80+ CD86- Ly6-C^{Hi} MHC II- monocytes, while rPS treatment pushes M/Ms towards a CD40- CD80+ CD86- Ly6-C^{Lo} MHC II+ phenotype (**Fig. 4-4d**). rPS treated LNs are predominantly CD40- CD80- CD86- Ly6-C^{Lo} MHC II+ monocytes (**Fig. 4-4d**). rPS treated spleens are predominantly CD40+ CD80- CD86+ Ly6-C^{Lo} MHC II+ macrophages (**Fig. 4-4d**).

4.3.5 Upregulation of suppressor CD4^{bright} CD8^{dim} T cells

Interestingly, with rPS treatment, DP CD4+ CD8+ T cells have a significantly larger population in the AX LN (**Fig. 5e,g**). tSNE with Barnes-Hut approximations was used to visualize the data

after gating, downsampling, and concatenation of treatment groups. From, tSNE visualization, it is observed that DP T cells cluster within the CD4+ CD8- T cell group, rather than within the CD4- CD8+ T cells (**Fig. 5e**). Using expression level analysis, CD4 expression by DP T cells in the rPS treatment group is similar to that of CD4+ CD8- T cells, whereas CD8 expression by DP T cells is significantly reduced as compared to CD4- CD8+ T cells (**Fig. 5f,h**). The relationship between the expression of the DP and single-positive (**SP**) T cells can be quantified as a DP: SP expression ratio. Thus, the rPS treated DP T cell population is deemed $CD4^{bright}CD8^{dim}$.

4.3.6 Prevention of allogeneic islet graft rejection

In vivo assessment of rapamycin redistribution via rPS was conducted using a clinically relevant intraportal (liver) fully-MHC mismatched allogeneic islet transplantation model. Diabetes was induced in C57BL/6 mice via STZ injection. To ensure the most stringent and severe model of T1D, diabetes was defined by blood glucose over 400 mg/dl(24). A standard dosage protocol known to allow for fully-MHC mismatched allogeneic islet graft viability for more than 100 days was compared to a low dosage protocol (**Fig. 4-6a**). The standard dosage protocol consisted of 11 injections given daily. The low-dosage protocol consisted of 6 doses given every 3 days (**Fig. 4-6a**). Each dose, regardless of protocol, consists of 1 mg rapamycin per kg body weight, formulated at 0.125 mg rapamycin per mL. rPS formulations contained 6.7 mg polymer per mL. Diabetic C57BL/6 mice received approximately 200 islets from fully MHC mismatched Balb/c mice in the liver via the portal vein (175 IEQ). Efficacy of the dosing regimen was confirmed by the restoration and maintenance of normoglycemia (blood glucose concentration < 200 mg/dL), confirming survival of the islet graft. As expected, mice that did not receive treatment all experienced graft

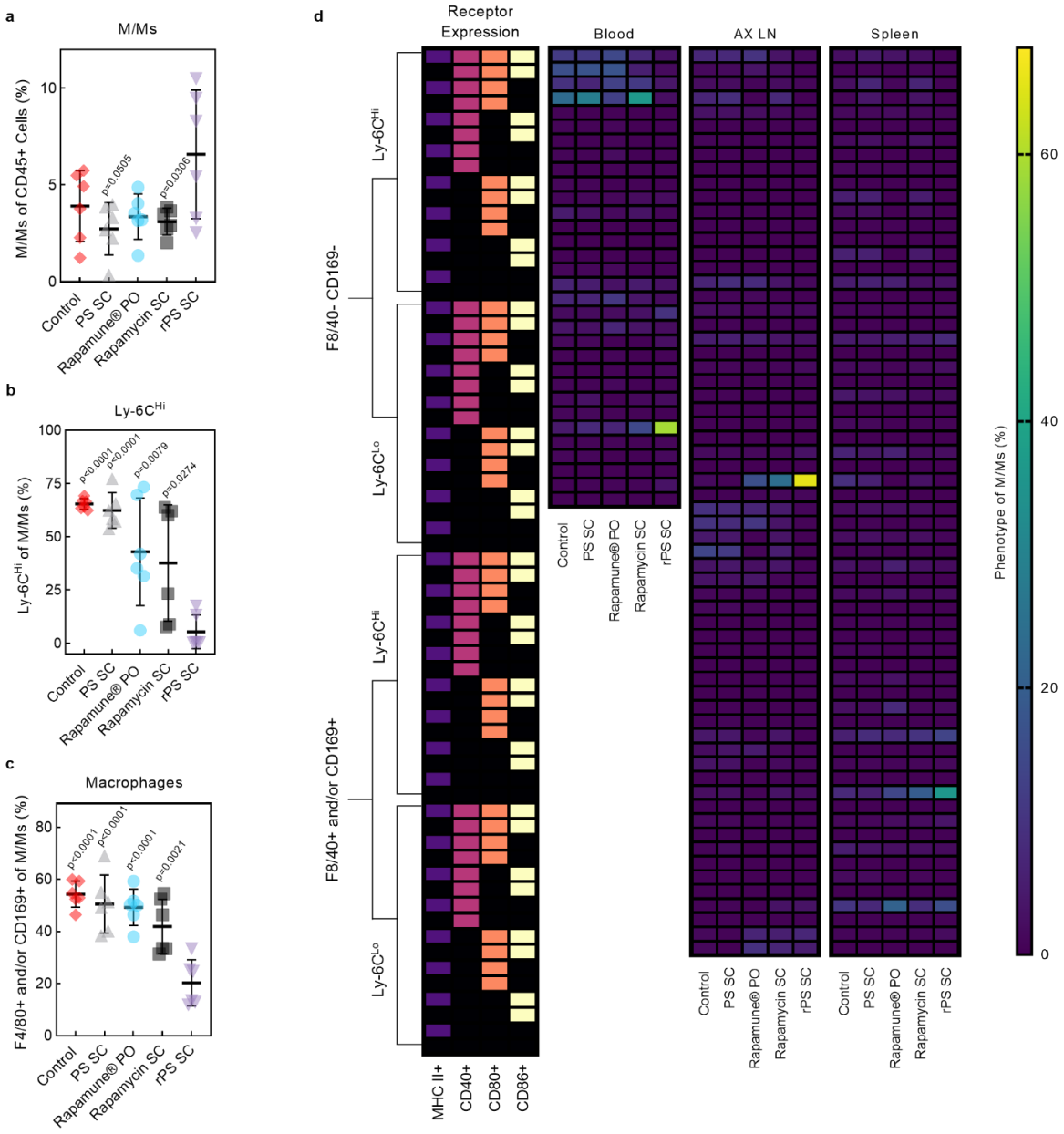

Figure 4- 4. rPS treatment upregulates monocyte-and-macrophage-linage cells and induces a predominate suppressive phenotype.

Mice were treated with: polymersomes (PS; ▲) subcutaneous injection (SC), Rapamune® (●) oral gavage (PO), rapamycin (in 0.2% carboxymethyl cellulose; ■) SC, or rapamycin-loaded polymersomes (rPS; ▼) SC, using the standard dosage protocol (11 doses, over 11 days, 1 mg rapamycin per kg body weight per dose or equivalent volume (Table S1), formulated at 0.125 mg rapamycin per mL, PS and rPS formulations contained 6.7 mg polymer per mL). A cohort of mice was left as an untreated control (♦). A cohort of mice was left as an untreated control (♦). Cell populations were analyzed by flow cytometry. **a-c**) Analysis of monocyte-and-macrophage-linage (M/M) populations from the axillary lymphocenter (deep axillary/axillary/axial and superficial axillary/brachial lymph no des; AX LN): percentage of M/Ms of CD45+ cells (**a**), percentage of Ly-6C^{Hi} M/Ms of M/Ms (**b**), percentage of macrophages (F4/80+ and/or CD169+) of M/Ms (**c**). All data are presented as mean percentage ± SD. Significant p-values relative to the rPS treatment are displayed on graphs. Statistical significance was determined by one-way ANOVA with Tukey's multiple comparisons test. (n = 6 mice/group). **d**) Analysis of M/M populations by phenotype with consideration for Ly-6C, macrophage markers (F4/80 and/or CD169; except for blood where macrophages were not considered), CD40, CD80, and CD86, MHC II. Data from blood, AX LN, and spleen are shown in heatmap form. (n = 6 mice/group).

rejection within 10 days of transplantation (**Fig. 4-6b, S4-5-7**). 67% of mice treated with the the standard SC rapamycin protocol and only 8% of the mice treated with Rapamune® remained normoglycemic 100 days post-transplantation (**Fig. S4-5-7**). When the low-dosage protocol was used, only 25% of the mice treated with Rapamune® and 58% of the mice treated with SC rapamycin remained normoglycemic 100 days post-transplantation, whereas 83% of mice treated with low-dosage rPS had normal blood glucose concentrations (**Fig. 4-6b, S4-5-7**). Furthermore, intraperitoneal glucose tolerance test (**IPGTT**), conducted at 30 days post-transplantation showed no difference in islet responsiveness with low dosage rPS treatment as compared to standard dosage rapamycin (**Fig. S4-5,6**).

4.3.7 Induction of antigen-specific tolerance

A MLR was performed to assess antigen-specific tolerance induction. At 100 days post-transplantation, normoglycemic mice were sacrificed and splenic T cells were isolated. Recipient B6 T cells were cultured with donor, T cell-depleted, mitomycin-c-treated, Balb/c splenocytes (**Fig. 4-6d**). T cells from recipients treated with low dosage rPS showed significantly less proliferation relative to those that achieved normoglycemia with low dosage rapamycin treatment (**Fig. 4-6d**).

4.3.8 Mitigation of known rapamycin side effects

RNA sequencing analysis of splenic T cells demonstrated that rPS mitigated the expression of genes associated with rapamycin-induced adverse effects (**Fig. 4-6d, Table S4-27,28**). Malignancy is a known side effect associated with oral Rapamune® and SC rapamycin, in general. Oral Rapamune® treatment was associated with the downregulation of tumor suppressor genes,

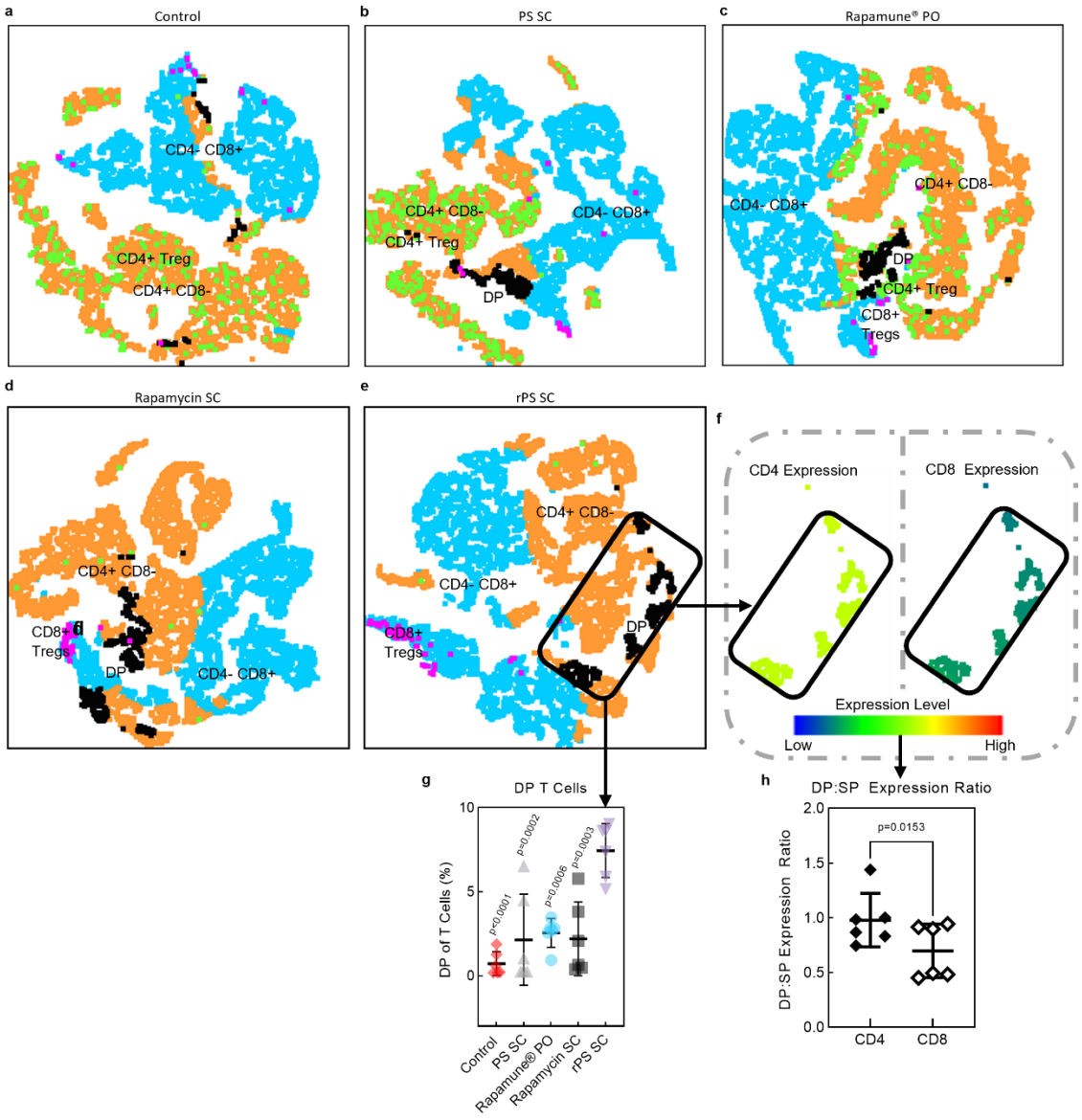

Figure 4- 5. rPS treatment induces upregulation of double-positive CD4^{bright} CD8^{dim} T cells with suppressor functions. Mice were treated with: polymersomes (PS; ▲) subcutaneous injection (SC), Rapamune® (●) oral gavage (PO), rapamycin (in 0.2% carboxymethyl cellulose; ■) SC, or rapamycin-loaded polymersomes (rPS; ▼) SC, using the standard dosage protocol (11 doses, over 11 days, 1 mg rapamycin per kg body weight per dose or equivalent volume (Table S1), formulated at 0.125 mg rapamycin per mL, PS and rPS formulations contained 6.7 mg polymer per mL). A cohort of mice was left as an untreated control (♦). Cell populations were analyzed by flow cytometry. **a-e,** tSNE visualization of CD3+ immune cell populations from the axillary lymphocenter (deep axillary/axillary/axial and superficial axillary/brachial lymph nodes; AX LN) with color-coded gated overlays of the previously described cell populations: CD4+ CD8- (orange), CD4- CD8+ (blue), CD4+ CD8+ double-positive (DP; black), CD4+ regulatory (CD4+ Treg; green) and CD8+ regulatory (CD8+ Treg; magenta). Solid line outlines DP T cell populations for rPS treated cohort (**e**). **f,** tSNE heatmap statistic of CD4 (left) and CD8 (right) expression from rPS treated group. **g,** Percentage of DP T cells in AX LN. All data are presented as mean percentage (of T cells) ± SD. Significant p-values relative to the rPS treatment are displayed on graphs. Statistical significance was determined by one-way ANOVA with Tukey's multiple comparisons test. **h,** Ratio of DP:SP (single positive CD4+ CD8- or CD4- CD8+) T cell CD4 and CD8 expression in the AX LN for rPS treated mice. The significant p-value is displayed on the graph. Statistical significance was determined by paired two-tailed t-test. (n = 6 mice/group).

specifically interferon-induced protein with tetratricopeptide repeats 2 (*Ifit2*) and mitoferrin-1/ solute carrier family 25 member 37 (*Slc25a37*) (**Fig. 4-6d, Table S4-27,28**) the former of which was also upregulated by SC rapamycin (**Fig. 4-6d, Table S4-27,28**). Furthermore, SC rapamycin was associated with the upregulation oncogenes: PDZ domain protein kidney 1-interacting protein (*Pdzk1ip1*/*MAP17*), solute carrier family 43 member 1 (*Slc43a1*), T cell acute lymphocytic leukemia protein 1 (*Tal1*) and exportin 7 (*Xpo7*) (**Fig. 4-6d, Table S27,28**). Dysregulation of these cancer-associated genes was not observed with rPS treatment (**Fig. 4-6d, Table S4-27,28**). In regard to metabolic regulation, rPS caused less inhibition of *Ier3*, which is associated with decreasing inflammation and hypertension (**Fig. 4-6d, Table S4-27,28**). rPS also limited inhibition of *Trib1*, of which downregulation is associated with long-term differentiation of CD8+ T cells and chronic infection (**Fig. 4-6d, Table S4-27,28**).

We observed that mice treated with SC free form rapamycin controls experienced injection site alopecia (**Fig. 4-6e**). Alopecia is a known side effect of rapamycin, impacting approximately 10% of patients(212). While alopecia was reduced in the low dosage SC rapamycin group (**Fig. 4-6e, S8**), no alopecia was observed in the low dosage rPS group (**Fig. 4-6e, S8**). Histological analysis confirms our gross observations (**Fig. 4-6e**). Only immature follicles were identified in the standard SC rapamycin group (**Fig. 4-6e**), with some mature follicles present in the low dosage SC rapamycin group (**Fig. 4-6e**). Organized mature follicles were identified in the low dosage rPS group (**Fig. 4-6e**).

Additionally, mice treated with standard dosage rPS had no significant alteration in albumin:globulin ratio (**A/G**) relative to control and PS treated mice. Both Rapamune® PO and rapamycin SC treated mice showed elevation in A/G (**Fig. S4-9**).

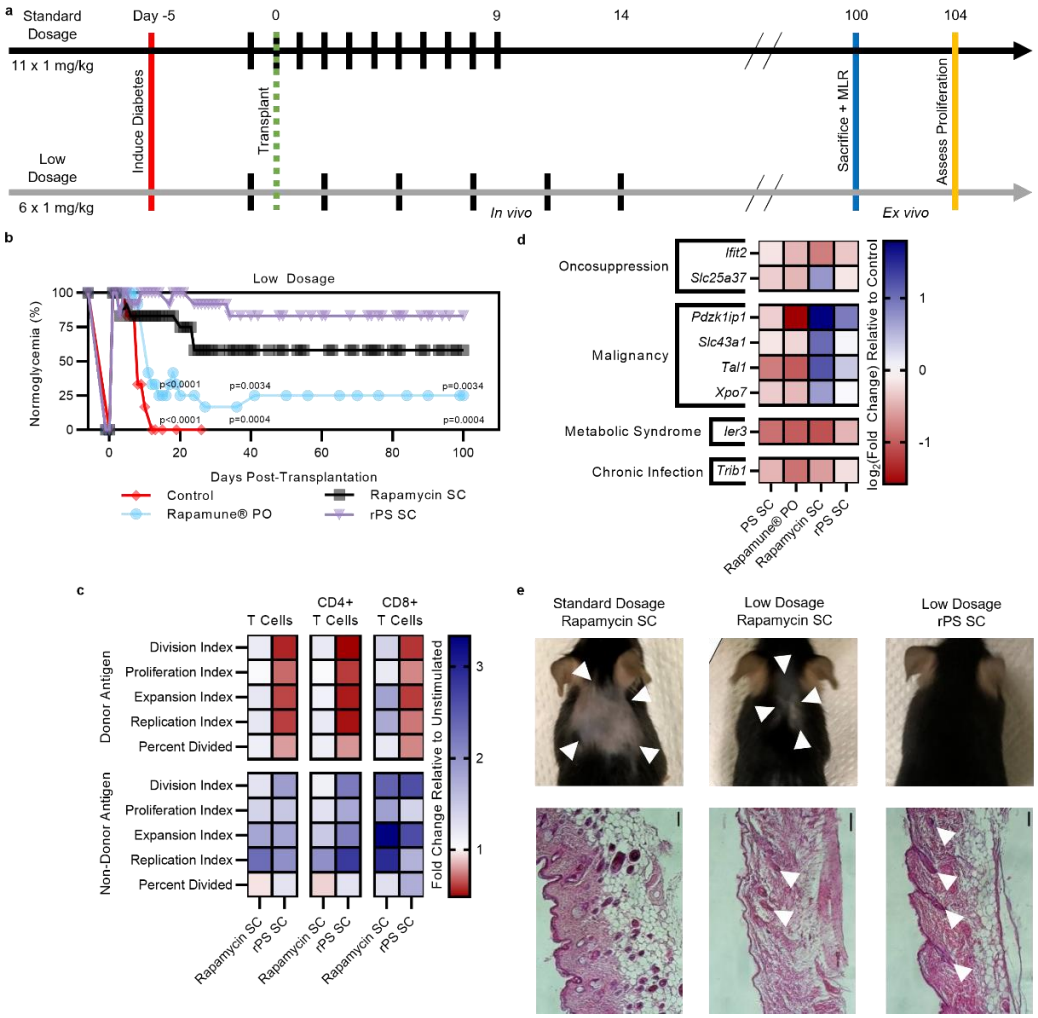

Figure 4- 6. rPS reduce the effective drug dosage to achieve normoglycemia and mitigate side effects *in vivo* via antigen-specific tolerance.

a, Standard dosage and low dosage schemes for rapamycin during fully major histocompatibility complex (MHC) mismatched allogeneic islet transplantation (day 0) experiment. Diabetes was induced (day -5) via streptozotocin (STZ) injection. The standard dosage protocol consists of 11 doses, given daily starting at day -1. The low dosage protocol consists of 6 doses, given every 3 days, starting at day -1. Mice were treated with: Rapamune® oral gavage (PO), rapamycin (in 0.2% carboxymethyl cellulose) subcutaneous injection (SC), or rapamycin-loaded polymersomes (rPS) SC. Regardless of protocol, each dose consisted of 1 mg rapamycin per kg body weight per dose, formulated at a concentration of 0.125 mg rapamycin per mL (Table S1). PS formulations contained 6.7 mg polymer per mL. A cohort of mice was left as an untreated control. **b,** Post-transplantation normoglycemia (%) (blood glucose < 200 mg/dl) following islet transplantation for low dosage protocol. No treatment (♦); Rapamune® PO (●); rapamycin SC (■); rPS SC ($n \geq 12$ mice/group). **c,** A mixed lymphocyte reaction (MLR) was performed between splenic T cells from low dosage protocol recipients (C57BL/6) 100 days post-transplantation and T cell-depleted, mitomycin-c treated donor (Balb/c) or non-donor (C3H) splenocytes. Prior to reaction, recipient T cells were treated with CellTrace Violet proliferation dye. Cells were cultured for 4 days. The assessment was performed using flow cytometry. Results are shown as mean fold change relative to unstimulated (cultured alone) recipient T cells. Division index: # of divisions / # of cells (start of culture); proliferation index: # of divisions / # of cells that divided; expansion index: # of cells (end of culture) / # of cells (start of culture); replication index: # of divided cells / # of cells that divided; percent divided: # divided cells / # of cells (end of culture) x 100. (n = 6 mice/group; n = 3 reactions/mouse). **d,** RNA sequencing analysis of splenic T cells for genes associated with rapamycin side effects. ($n \geq 6$ mice/group). All data are presented as mean $\log_2$(fold change) relative to control. **e,** Top: Digital photos of SC injection site on mouse dorsal showing alopecia 30 days after allogeneic islet transplantation by treatment group. Bottom: Hematoxylin and eosin histology of skin taking from mice 100 days post-transplantation with. White arrows show mature hair follicles. Scale bars represent 100 µm. (n = 5-7 mice/group).

4.4 Discussion

A grand challenge of pharmaceutical development is to harness the rational engineering of nanoscale drug carriers (i.e. nanocarriers) to selectively modify target cells while minimizing uptake by cells and organs responsible for side effects(44). By controlling delivery kinetics and target specificity, nanocarriers can alter the interconnected network of cells contributing to observed therapeutic effects, thus significantly changing the therapeutic window and reducing both the dosage and adverse events of a drug during treatment(44). Effects of changing the network of targeted cells are particularly evident during immunotherapy, where small subsets of immune cells can elicit potent cytokine and T cell responses that can propagate into unique systemic responses. With these concepts in mind, we investigated whether SC delivery and nanocarrier-directed changes in the cellular biodistribution of rapamycin, a common therapeutic that elicits diverse cell-specific effects, can repurpose its mechanism of action at the cellular level to decrease side effects and enhance efficacy.

The targeted cell population and the amount of delivered drug are critical considerations for targeted therapies. Rapamycin achieves immunosuppression by directly acting on T cells(194). However, when given clinically via standard oral administration, the resulting broad biodistribution of rapamycin influences numerous off-target cells and reduces the dose that reaches T cells for desired effects(39, 47, 194). Lack of specificity cannot be overcome with increased dosage given that rapamycin is associated with dose-dependent toxicity(39, 47). We have previously shown that giving drugs, including rapamycin, via PS, allows for selective uptake by APCs while avoiding T cells(50, 203). We hypothesized that switching the target cell population from T cells to APCs would change the immunosuppressive mechanism of rapamycin to reduce both dosage and side effects.

Route of administration is another tool that is employed to impact biodistribution and overcome drug-specific barriers to delivery. For example, SC injection could avoid diet-dependent bioavailability and variable metabolism via CYP3A4 and P-glycoprotein that are associated with orally administered rapamycin(194). Using these tools—cellular targeting and route of administration—the temporal and both organ and cellular biodistribution of a drug can be precisely manipulated for the desired effect. Herein, we show that SC delivery of rapamycin via PS creates a rapamycin biodistribution that perturbs the network of inflammatory cells in a manner that supports the survival of transplanted allogeneic islets. While others have attempted to use nanocarriers for the delivery of rapamycin(47), to the best of our knowledge, we showcase the first use of SC rapamycin nanotherapy for a transplantation application.

Although drug-loaded PS primarily target APCs within lymphoid organs, as we have previously shown(203), the downstream effects of SC rPS modulate a diverse network of immune cells. The most profound cellular effects of rPS were observed in the draining AX LN and included an upregulation of APCs and a downregulation of CD4+ T cells. These rPS-induced modulations of immune cells provide a foundation for an inflammatory environment that is amenable to allogeneic islet transplantation. Importantly, we show the downregulation of T cells in immunomodulatory organs and at the site of intraportal islet transplantation—the liver—a key objective of immunosuppressive rapamycin therapy(194). This was achieved without directly targeting T cells, and instead via enhanced targeting of APCs that dictate T cell function during inflammatory responses(210). Thus, redistribution of our cellular network via rPS treatment establishes a foundation for cellular immunomodulation.

While direct donor antigen recognition by both CD4+ or CD8+ T cells and indirect presentation of donor antigen to CD8+ T cells contribute to a rejection response, only indirect

donor antigen presentation to CD4+ T cells is required for rejection(213). Therefore, rPS cause deletion and/or anergy in CD4+ T cells as indicated by the significant reduction in the CD4+ T cell population and reduction in expression of CD3 and CD4(210, 214). The unique combination of costimulation blockade as evidenced by reduced CD40/80/86 expression and enhanced MHC II presentation by APCs may account for the observed CD4+ T cell demise.

In the lymph nodes, rPS induces phenotypic changes in the DC population which are amenable to islet transplantation tolerance. Phenotypic changes are enhanced by symbiotic relationships between these DCs and CD8+ T cells to promote a quiescent environment. Along with the overall significant increase in DCs, a significant increase in novel DP CD8+ CD11b+ cDCs was observed. CD11b+ cDCs cross-present antigens to CD4+ T cells and CD8+ cDCs cross-present antigens to CD8+ T cells to induce tolerogenic behavior(195). The presence of DP cDCs suggests that these cells may have the ability to cross-present donor antigens to both CD4+ and CD8+ T cells or DP CD4+ CD8+ T cells, which are also significantly upregulated in the lymph nodes. Furthermore, tolerogenic tDCs can cause CD8+ T cells to become CD8+ CD25+ FoxP3+ Tregs. CD8+ Tregs have enhanced suppressor capabilities relative to their CD4+ counterparts(215). The tolerogenic properties of CD8+ Tregs have been shown to prevent graft-versus-host disease and autoimmune diseases(215). Despite their tolerized state, CD8+ Tregs confer immunoprotection against pathogens(215). In addition, rPS causes a significant downregulation of pDCs, which are known to secrete interferon-gamma and activate cytotoxic CD8+ T cells(216). Both interferon-gamma secretion and cytotoxic CD8+ T cells are known to damage islet grafts, thus pDC-mediated reduction boosts the potential for graft survival(217).

In addition to DCs, rPS treatment induces suppressor phenotypes in M/Ms. Suppressor M/Ms are notable in blood lymph nodes and spleen. While other treatments confer a M/M

population that is dividing between activator and suppressor phenotypes, rPS treatment promotes a single phenotype characterized by its MHC II+ Ly-6C^{Lo} status. Mature MHC II+ Ly-6C^{Lo} M/Ms are a type of patrolling cell that is able to penetrate tissue during steady-state conditions. Ly-6C^{Lo} monocytes have the ability to phagocytose both nanoparticles and apoptotic debris(205). This non-classical monocyte population has a dual-fold advantage for transplantation applications, in which it supports an anti-inflammatory phenotype amenable to graft tolerance(218) and it has been shown to aid in the prevention of viral infections(219). These monocytes have the ability to cross-present the apoptotic debris to CD8+ T cells and tolerize the CD8+ T cell, suppressing antigen-specific responses(205), in a similar manner to that of CD8+ cDCs(195).

The tolerogenic effects of rPS-treated APCs go beyond CD4+ and CD8+ T cells to create a hospitable environment for the islet graft. Niche T cell populations also make an important contribution to the congenial environment observed with rPS immunomodulatory therapy. For example, the upregulation of DP CD4+ CD8+ T cells in the lymph nodes is observed. Controversy has surrounded DP T cells as both suppressive and cytotoxic functions have been demonstrated(220, 221). This is because while CD4^{dim} CD8^{bright} cells are cytotoxic(220), CD4^{bright} CD8^{dim} DP T cells are anti-inflammatory(221, 222). tSNE visualization in combination with CD4 and CD8 expression level analysis helped to reveal that rPS confer CD4^{bright} CD8^{dim} DP T cells with known suppressor function, such as secreting anti-inflammatory cytokines(222). Interestingly, these cells also show enhanced responsiveness during infection, for example activating effector cells in the case of the human immunodeficiency virus(222).

rPS treatment confers antigen-specific tolerance. At 100 days after successful transplantation, T cells from low dosage rPS treated mice show restraint in ex vivo proliferation in response to a donor antigen challenge. However, these T cells still respond to a foreign (non-

donor) antigen with proliferation. Achieving antigen-specific tolerance as opposed to immunosuppression may allow patients to only take a short course of immunomodulatory therapy to maintain the viability of their grafts for the long term. Short course therapy may be particularly advantageous for the transplant field, a common cause of graft rejection (36 patients per 100 patients per year for kidney transplant) is patient nonadherence with long-term immunosuppressive therapy(223). Furthermore, side effects, including progressive cancers and infections, common to drugs that induce nonspecific tolerance, such as Nulojix® (224), can be avoided(224). In addition to its responsiveness to foreign antigens, rPS treatment demonstrates maintenance of immune function as indicated by unaltered A/G.

Our use of the liver transplantation site is critical for the translation of murine studies as the commonly used KC is not a feasible site for human islet transplantation(24). KC transplantation fails to expose the islets to the immune environment of the liver(24). For example, islets transplanted to the KC are not exposed to blood to induce the IBMIR(24). Additionally, the exposure of the islets to immunosuppressive drugs differs between the liver and KC transplantation sites. When islets are infused into the vasculature of the liver, they first encounter neutrophils. Furthermore, rPS treatment significantly reduces the neutrophil population in blood and liver and downregulates the expression of CD11b (**Fig. S4-10**). CD11b is critical for neutrophil migration(225). Graft infiltrating neutrophils have been shown to cause transplant failure(226), thus reduction in this cell type and reduced mobility may contribute to enhanced graft survival. With reduced CD11b expression, neutrophils may show decreased ability to reach islets and infiltrate the graft. Furthermore, MHC molecules are the most significant alloantigens involved in graft rejection, thus using a fully MHC-mismatched model is critical for rigorous assessment of allogeneic transplantation. It is important to note that all combinations of fully mismatched mouse

models confer the same potency and kinetics of alloimmune response. We utilized the combination of Balb/c islets transplanted into C57BL/6 recipient mice, which provides the greatest challenge to islet survival and normoglycemia restoration(24). Utilizing excess islets can delay the graft rejection, giving a false sense of maintained normoglycemia and immunosuppression. While other models use up to 1000 islet equivalents (**IEQ**)(25, 192), our model uses a minimal islet mass of only ~200 murine islets (~175 IEQ).

Subcutaneous rPS injection engages lymphatic drainage, simplifies therapeutic administration,(196) and changes the method of elimination from biliary to renal. Changing the routes of administration and elimination overcomes several challenges that have historically plagued oral rapamycin regimens. The SC route of administration avoids interactions in the intestine as well as variability due to food intake. Furthermore, rPS formulation favors renal over biliary elimination of rapamycin, thus reducing interaction with the liver. Specifically, SC rapamycin delivery via rPS may improve bioavailability over oral delivery by circumventing first-pass metabolism and p-glycoprotein efflux(47). Many murine studies involving rapamycin use intraperitoneal injection(192), however, this route is not easily translatable to humans. Finally, SC injection is advantageous over infusion as patients can perform the injection themselves, as opposed to requiring the services of a health care professional. In summary, this study demonstrates how the rational delivery of engineered nanoparticles can repurpose the biochemical mechanism of action of a drug by targeting specific immune cell types, laying the foundation for methods of rationally enhancing therapeutic efficacy while mitigating adverse effects.

4.5 Materials and Methods

4.5.1 Animals

8 to 12-week-old, male C57BL/6, Balb/c, and C3H mice were purchased from Jackson Labs. Mice were housed in the Center for Comparative Medicine at Northwestern University. All animal protocols were approved by Northwestern University's Institutional Animal Care and Use Committee (**IACUC**).

4.5.2 Materials

Unless explicitly stated below, all reagents and chemicals were purchased from Sigma-Aldrich.

4.5.3 Poly(ethylene glycol)-b-Poly(Propylene Sulfide) Synthesis

PEG-*b*-PPS was synthesized as previously described by us(50). In brief, methyl ether PEG (MW 750) was functionalized with mesylate. The mesylate was reacted with thioacetic acid to form PEG-thioacetate and then base activating the thioacetate to form a thiolate anion and initiate ring-opening polymerization of propylene sulfide. Benzyl bromide was used as an end-capping agent to form PEG_{17}-*b*-PPS_{30}-Bz or the thiolate anion was protonated to form PEG_{17}-*b*-PPS_{30}-SH. The polymer was characterized by ^{H}NMR and gel permeation chromatography (**GPC**).

4.5.4 Nanocarrier Formulation

PS were formed via thin-film hydration, as previously described(50, 203). In brief, 20 mg of PEG_{17}-*b*-PPS_{30}-Bz was weighted in a sterilized 1.8 mL glass high-performance liquid chromatography (**HPLC**) vial. 750 ul of dichloromethane (**DCM**) was added to the vial. To form, rPS 0.5 mg of rapamycin (Selleckchem), dissolved at 25 mg/mL in ethanol, was also added. The

vial was desiccated to remove the DCM. Next, 1 mL of PBS was added to the vial. The vials were shaken at 1500 rpm overnight. PS were extruded multiple times first via 0.2 um and then 0.1 um syringe filters. Excess rapamycin was removed via size exclusion chromatography using a Sephadex LH-20 column with PBS.

4.5.5 Nanocarrier Characterization

DLS: DLS measurements were performed on a Nano 300 ZS Zetasizer (Malvern) and were used to determine nanocarrier diameter distribution and corresponding polydispersity index.

cryoTEM: 200-mesh lacey carbon grids were glow-discharged for 30 seconds in a Pelco easiGlow glow-discharger at 15mA with a chamber pressure of 0.24 mBar. 4 µL of the sample was then pipetted onto the grid and plunge-frozen into liquid ethane in an FEI Vitrobot Mark III cryo plunge freezing device for 5 seconds with a blot offset of 0.5mm. Grids were then loaded into a Gatan 626.5 cryo transfer holder, imaged at –172 °C in a JEOL JEM1230 LaB6 emission TEM at 100kV, and the data was collected on a Gatan Orius 2k x 2k camera.

SAXS: SAXS was performed at Argonne National Laboratory's Advanced Photon Source with collimated X-rays (10 keV; 1.24 Å). Data reduction was performed using Primus software and modeling was performed using SASView.

4.5..6 Quantification of Rapamycin Loading(50)

rPS nanocarriers (50 ul) were lyophilized and re-dissolved in HPLC grade dimethylformamide (**DMF**). Salts were removed via centrifugation at 17,000 g for 10 minutes. Rapamycin content of the nanocarriers was characterized via HPLC (Thermo Fisher Dionex UltiMate 3000) using an Agilent Polypore 7.5 x 300 mm column and an Agilent Polypore 7.5 x 50 mm guard column. The

system was housed at 60°C. DMF (0.5 mL/minute) was used as the mobile phase. Rapamycin was detected at 270 nm. Thermo Scientific Chromeleon software was used for analysis. The concentration of rapamycin was characterized via the AUC in comparison to a standard curve of rapamycin concentrations.

4.5.7 Rapamycin Stability in Nanocarrier

rPS formulations were fabricated as previously described. Formulations were stored at 4°C in glass scintillation vials. At various time points, the formulations were vortexed, 1 mL samples were transferred to Millipore Amicon Ultra Centrifuge 10,000 NMWL Tubes and centrifuged at 4000 g in a swinging bucket rotor to remove the unloaded drug. The retentate was brought back up to its original volume using PBS. Quantification of rapamycin was performed as previously described.

4.5.8 Indocyanine Green Biodistribution

ICG PS were formed using thin-film rehydration, as previously described(203). In brief, 20 mg of PEG_{17}-*b*-PPS_{30}-Bz was weighted in a sterilized 1.8 mL glass HPLC vial. 750 ul of DCM was added to the vial. The vial was desiccated to remove the DCM. Next, 1 mL of 0.258 mM ICG in PBS was added to the vial. The vials were shaken at 1500 rpm overnight. PS were extruded multiple times first via 0.2 um and then 0.1 um syringe filters. Float-A Lyzer G2 Dialysis devices (Fisher) were used to remove unloaded ICG. ICG loading was quantified relative to standards composed of known amounts of polymer and ICG in a 1:33 molar ratio using absorbance at 820 nm as previously described by our group(203). ICG concentration was matched at 50 ug/mL. C57BL/6

mice received ICG PO, ICG SC, or ICG-PS SC. The injection volume was 150 ul. At 2, 24- and 48-h post-injection, the mice were sacrificed, blood was collected via cardiac puncture, and perfusion was performed using heparinized PBS. The liver, spleen, kidneys, heart, and lung were harvested and imaged via IVIS Lumina with an excitation wavelength of 745 nm, an emission wavelength of 810 nm, an exposure time of 2 seconds, and a f/stop of 2.

4.5.9 Rapamycin Biodistribution

Healthy C57BL/6 mice were administered a single 1 mg per KG body weight dose of Rapamune® oral solution (Pfizer) or generic equivalent (VistaPharm) PO, rapamycin (in 0.2% CMC) via SC or rPS SC. All formulations were at a concentration of 0.125 mg rapamycin per mL or equivalent volume; polymersome formulations contained 6.7 mg polymer per mL (**Table S1**). Mice were sacrificed at the following time points: 0.5, 2, 8, 16, 24, and 48 h. Urine and feces were collected via metabolic cages during the duration between injection and sacrifice for the 8, 16, 24, and 48-h timepoints. The following tissues and/or organs were collected: blood, brain, fat pad, heart, kidneys, liver, lungs, AX LN, IN LN, spleen. Rapamycin was extracted from blood and urine using a solution of methanol and acetonitrile (50:50 v/v) doped with rapamycin-D3 (Cambridge Isotope Laboratories) as an internal standard. Tissue samples were homogenized in homogenization tubes prefilled with stainless steel ball bearings (Sigma) using a solution of phosphoric acid (8%), acetonitrile, and acetic acid (30:67.2:2.8 v/v/v). After homogenization, tissue samples were also doped with rapamycin-D3. All samples were precipitated via incubation at -20 °C, followed by centrifugation. The supernatant was collected and LC-MS/MS (Shimadzu LC-30AD pumps; SIL-30ACMP autosampler; CBM-20A oven; Sciex Qtrap 6500) was used to determine rapamycin

concentration. Rapamycin had a retention time of 2.7 minutes. Rapamycin-D3 had a retention time of 3.0 minutes.

4.5.10 Immunomodulation Study

Healthy C57BL/6 mice were subjected to a "standard dosage regime." Animals were administered with blank PS SC, Rapamune® oral solution (Pfizer) or generic equivalent (VistaPharm) PO, rapamycin (in 0.2% CMC) via SC or rPS via SC at a dose of 1 mg/kg (**Table S1**). All formulations were at a concentration of 0.125 mg rapamycin per mL or equivalent volume; polymersome formulations contained 6.7 mg polymer per mL (**Table S1**). A cohort of mice was left as an untreated control. After 11 days, the mice were sacrificed. Blood, liver, AX LN, IN LN, and spleen were collected and processed for flow cytometry.

4.5.11Flow cytometry

Blood was spun down at 3000 g for 25 minutes to separate the plasma and blood cells. The blood cells were treated with 1X red blood cell lysis buffer (Fisher) for 5 minutes on ice, washed with PBS, and spun down, thrice. The liver was minced, treated with collagenase for 45 minutes at 37 °C, processed through a 70 nm filter, and then treated with 1X red blood cell lysis buffer (Fisher) for 5 minutes on ice, washed with PBS, and spun down. The spleen was processed through a 70 nm filter and treated with 1X red blood cell lysis buffer (Fisher) for 5 minutes on ice, washed with PBS, and spun down. Lymph nodes were passed through a 70 nm filter, washed with PBS, and spun down. All cells were resuspended in a cocktail of Zombie Near Infrared (BioLegend) for viability and anti-mouse CD16/CD32 (TruStain FcX; BioLegend) for FcR blocking with BD

Brilliant Violet cell staining buffer and incubated at 4 °C for 15 minutes. Next, an antibody cocktail consisting of Pacific Blue anti-mouse CD11c (BioLegend), BV480 anti-mouse NK1.1 (BD), BV510 anti-mouse CD19 (BioLegend), BV570 anti-mouse CD3 (BioLegend), BV605 anti-mouse F4/80 (BioLegend), BV650 anti-mouse MHC II (IA-IE) (BioLegend), BV711 anti-mouse Ly-6C (BioLegend), BV750 anti-mouse CD45R/B220 (BioLegend), BV785 anti-mouse CD11b (BioLegend), AF532 anti-mouse CD8a (Invitrogen), PerCP-Cy5.5 anti-mouse CD45 (BioLegend), PerCp-eFluor711 anti-mouse CD80 (Invitrogen), PE-Dazzle 594 anti-mouse CD25 (BioLegend), PE-Cy5 anti-mouse CD4 (BioLegend), PE-Cy7 anti-mouse CD169 (BioLegend), APC anti-mouse FoxP3 (Invitrogen), AF647 anti-mouse CD40 (BioLegend), APC-R700 anti-mouse Ly-6G (BioLegend), and APC/Fire 750 anti-mouse CD86 (BioLegend) was added to the cells and incubated for 20 minutes at 4 °C. The cells were washed with PBS, fixed, and permeabilized using a FoxP3 Fix/Perm Kit (BioLegend), according to the manufacturer's protocol. Next, APC anti-mouse FoxP3 (BioLegend) was added and incubated for 30 minutes in the dark at room temperature. Finally, cells were washed twice with PBS and resuspended in cell buffer. The cells were analyzed on an Aurora flow cytometer (CyTek). Spectral unmixing was performed using SpectroFlo (CyTek) and analysis was performed using FlowJo software. Gating was performed as outlined in **Fig. S4**(227, 228).

4.5.12 tSNE

For each analysis, FlowJo's DownSample plugin was used to randomly select an equal number of events from the T cell population for every sample. The purpose of DownSample was to both normalize the contribution of each mouse replicate and reduce the computational burden. Next, samples from mice that underwent the same treatment, and the same cell population were

concatenated. The tSNE plugin was run on concatenated samples using the Auto opt-SNE learning configuration with 3000 iterations, a perplexity of 50, and a learning rate equivalent to 7% of the number of events(229). The KNN algorithm was set to exact (vantage point tree), and the Barnes-Hut gradient algorithm was employed.

4.5.13 Allogeneic Islet Transplantation

Diabetes was induced via STZ (**IP**; 190 mg/kg) injection five days prior to transplantation and confirmed via hyperglycemia (blood glucose > 400 mg/dl). Starting the day prior to transplantation, mice were treated with: PS SC, Rapamune® PO, rapamycin (in 0.2% carboxymethyl cellulose) SC, or rPS SC at 1 mg rapamycin per kg body weight (**Table S1**) in accordance with a standard dosage (11 doses, given daily) or a low dosage (6 doses, given every 3rd day). All drugs were formulated at 0.125 mg rapamycin per mL. rPS formulations contained 6.7 mg polymer per mL. On the day of transplantation, islets were isolated from Balb/c mice via common bile duct cannulation and pancreas distension with collagenase. Islets isolated from two donors (~200 mouse islets, ~175 IEQ) were transplanted to C57BL/6 recipients via the portal vein. Body weight and blood glucose concentration were monitored closely for 100 days post-transplantation. Intraperitoneal glucose tolerance test (**IPGTT**) was performed one-month post-transplantation. The animals were fasted for 16 h before being injected intraperitoneally with 2 g dextrose (200 g/L; Gibco) per kg body weight. Blood glucose concentrations were measured at 0, 15, 30, 60- and 120-minutes post-injection.

4.5.14 Mixed Lymphocyte Reaction

At 100 days post-transplantation, recipient (C57BL/6) mice were sacrificed, and spleens were excised. The organs were processed as was done for flow cytometry. T cells were isolated via nanobead incubation and magnetic sorting (BioLegend). T cells were stained with CellTrace Violet proliferation dye (Invitrogen). Spleens were also excised from donor mice Balb/c, in addition to C3H and C57BL/6 controls. Donor splenocytes were depleted of T cells via treatment with anti-mouse CD90.2 antibody (BioLegend) and rabbit complement for 45 minutes at 37° C. Following T cell depletion, donor splenocytes underwent mitomycin C treatment for 45 minutes at 37° C. CellTrace labeled recipient T cells and T cell-depleted, mitomycin C treated splenocytes were counted and brought to a concentration of $2x10^6$ cells per mL in RPMI 1640 media (Gibco) containing 10% fetal bovine serum (**FBS**), 1% penicillin-streptomycin (Gibco), 1% L-glutamine (Gibco) and 10% 2-mercaptoethanol. Cells were cultured in V-bottom 96 well plates (Cellstar), a ratio of 1:2 (recipient T cells : donor splenocytes) for 4 days. Controls consisted of recipient T cells alone, anti-CD3 2C11 clone (BioLegend) treated recipient T cells, recipient T cells, and C57BL/6 splenocytes, recipient T cells and C3H splenocytes, donor Balb/c splenocytes alone, C57BL/6 splenocytes alone, and C3H splenocytes alone. Cells were processed for flow cytometry as described above. Extracellular antibodies included: FITC anti-mouse CD3 (BD), AF700 anti-mouse CD4 (eBiosciences), PerCP anti-mouse CD8 (BD), PE-CF594 anti-mouse CD44 (BD), PE anti-mouse CD62L (BD), PE-Cy7 anti-mouse CD25 (BioLegend) and BV711 H-2kb (BD). Intracellular antibodies included AF647 anti-mouse Granzyme B (BD). The cells were analyzed on a Northern Lights flow cytometer (CyTek). Spectral unmixing was performed using SpectroFlo (CyTek) and analysis was performed using FlowJo software. Gating was performed as outlined in

Fig. S4(227, 228). Proliferation analysis was performed using the Proliferation Platform in FlowJo.

4.5.15 Alopecia Assessment

Dorsal photos were taken weekly to assess for alopecia. At 100-days post-transplantation, the mice were euthanized, and skin samples were excised in the dorsal region at the SC injection site. Skin samples were placed in cassettes, fixed in 4% paraformaldehyde, and embedded in paraffin. Tissue blocks were sectioned at a thickness of 5 nm and stained with hematoxylin and eosin (**H&E**). Digital images were taken on a Nikon microscope.

4.5.16 T Cell RNA Sequencing

Healthy C57BL/6 mice were treated with: PS SC, Rapamune® PO, rapamycin (in 0.2% carboxymethyl cellulose) SC, or rPS SC, using the standard dosage protocol (11 doses, over 11 days, 1 mg rapamycin per kg body weight per dose or equivalent volume (Table S1), formulated at 0.125 mg rapamycin per mL, PS and rPS formulations contained 6.7 mg polymer per mL). A cohort of mice was left as an untreated control. After 11 days, the mice were sacrificed, and the spleen was excised. The organs were processed as was done for flow cytometry. T cells were isolated via nanobead incubation and magnetic sorting (BioLegend). RNA was isolated from T cells using RNeasy Mini Kit with DNase digestion (Qiagen). RNA-seq was conducted at the Northwestern University NUSeq Core Facility. Total RNA will be quantified with Qubit and quality assessed with Agilent Bioanalyzer. The NEBNext Ultra II RNA Library Prep Kit for Illumina (New England Biolabs, Ipswich, MA) was used for library prep following the

manufacturer's protocol using the NEBNext rRNA depletion option. Briefly, rRNA was first depleted from the total RNA samples. Then after fragmentation, reverse transcription was performed to convert RNA to cDNA, followed by end repair, adaptor ligation, and PCR amplification of libraries. Prior to sequencing, the prepared libraries were checked for fragment sizing on a Bioanalyzer using a High Sensitivity DNA chip and quantified with Qubit. The sequencing of the libraries was conducted on an Illumina NovaSeq 6000 NGS System, using an SP flow cell to generate paired-end 150 bp reads. Sequencing quality was analyzed with FastQC v0.11.5(230) and reads were trimmed and filtered with Trimmomatic v0.39(231)**.** One sample from each treatment group was discarded due to low sequencing and/or alignment quality. Reads were aligned with STAR v2.7.6a (232) to the GENCODE M27 GRCm39 mouse reference genome primary assembly using the GRCm39 mouse reference primary comprehensive gene annotation (https://www.gencodegenes.org/mouse/). Quantification and differential expression were performed with Cuffdiff from Cufflinks v2.2.1(233-235), again using the GENCODE GRCm39 mouse reference primary comprehensive gene annotation and a 0.05 FDR. Detailed settings for each software are included in **Table S27**. The raw data is displayed in **Table S28**.

4.5.17 Albumin-Globulin Ratio

Healthy C57BL/6 mice were treated with: PS SC, Rapamune® PO, rapamycin (in 0.2% carboxymethyl cellulose) SC, or rPS SC, using the standard dosage protocol (11 doses, over 11 days, 1 mg rapamycin per kg body weight per dose or equivalent volume (Table S1), formulated at 0.125 mg rapamycin per mL, PS and rPS formulations contained 6.7 mg polymer per mL). A cohort of mice was left as an untreated control. After 11 days, the mice were sacrificed, and cardiac puncture was used for blood collection. Blood samples were allowed to clot and then spun down at 2000 g for 10 minutes to obtain serum. Pierce 660 nm Protein Assay (ThermoFisher) was used

to quantify serum protein concentration. Samples were diluted to fall within the range of the mouse albumin ELISA kit (Abcam) using 1X PBS. Albumin concentration was analyzed using the ELISA assay. Globulin concertation was determined by subtracting the albumin concentration from the total protein concentration in each sample.

4.5.18 Statistical analysis

Statistical analysis was performed using one- or two-way ANOVA with Tukey's multiple comparisons test or paired two-tailed t-test. Significant P-values relative to the rPS treatment are displayed in the figures. Non-diabetic survival data was assessed using the Mantel-Cox Log-rank test. All statistical analyses were performed using GraphPad Prism software.

4.6 Supplementary Information

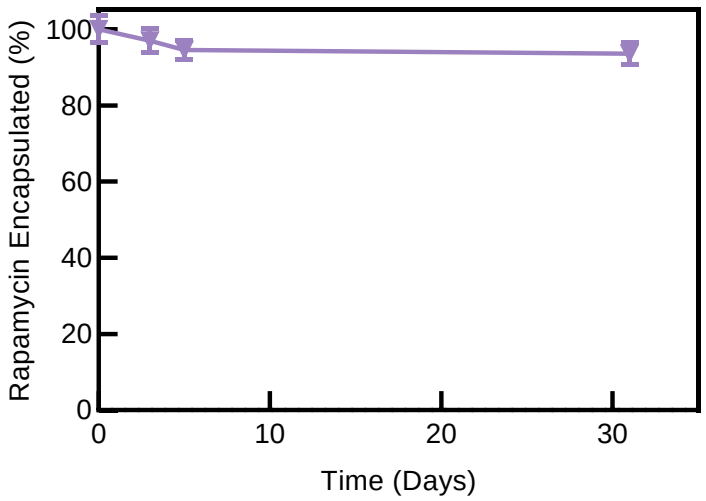

Figure S4-1 | Characterization of rapamycin-loaded polymersomes (rPS) encapsulation stability. rPS were fabricated, unencapsulated rapamycin was removed and rPS samples were stored at 4 °C in phosphate-buffered saline (PBS) at a concentration of 0.125 mg rapamycin/mL. At various time points, released rapamycin was removed and loaded rapamycin concentration was assessed via HPLC. (n = 3-5).

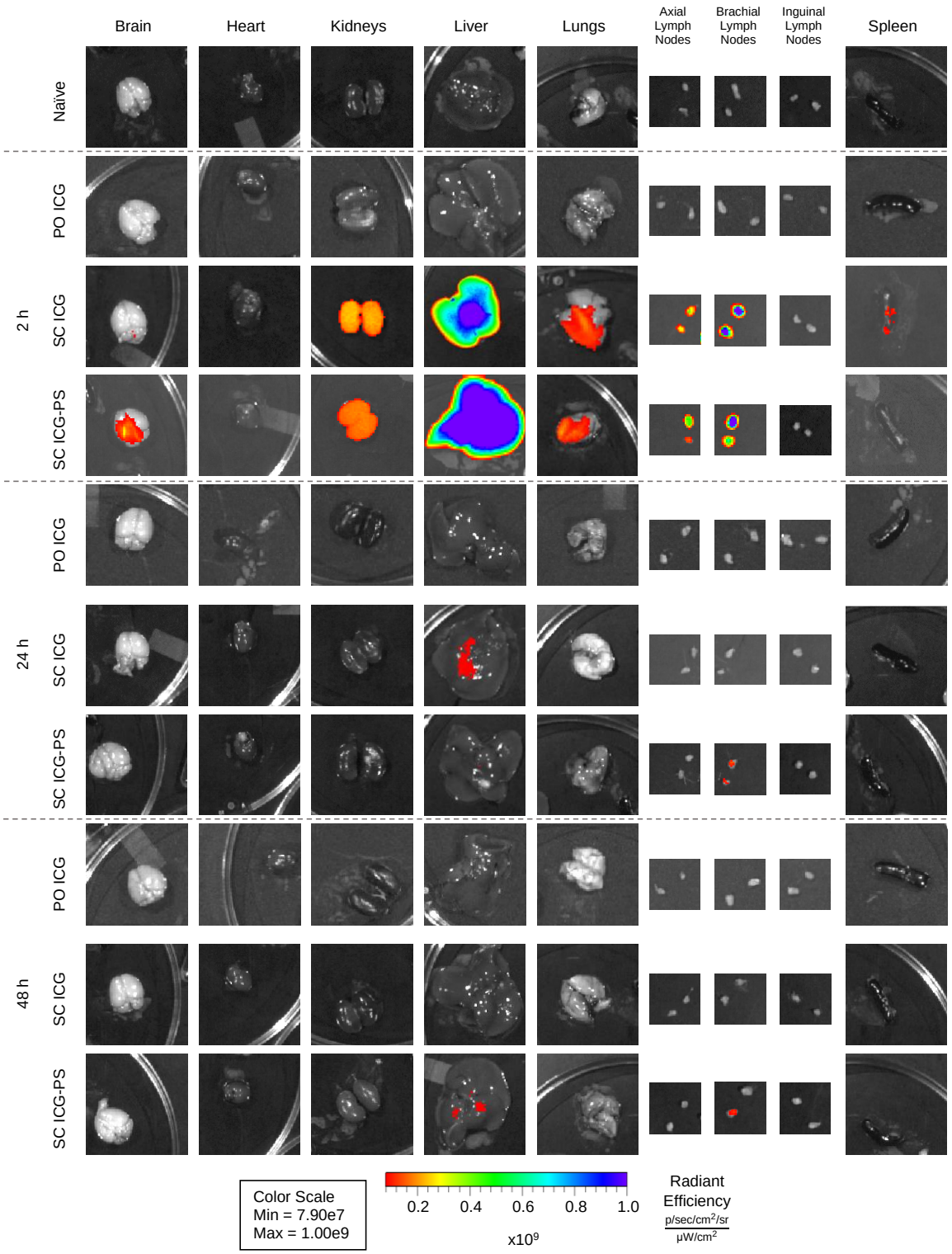

Figure S4-2 | Biodistribution of indocyanine green (ICG) dye and ICG loaded into polymersomes (ICG-PS). Mice were administered with an oral gavage (PO) of ICG, subcutaneous injection (SC) of ICG or SC of ICG-PS, and sacrificed at 2, 24, and 48 hours after injection (n = 5 mice/group). IVIS was performed on extracted organs to quantify ICG dye.

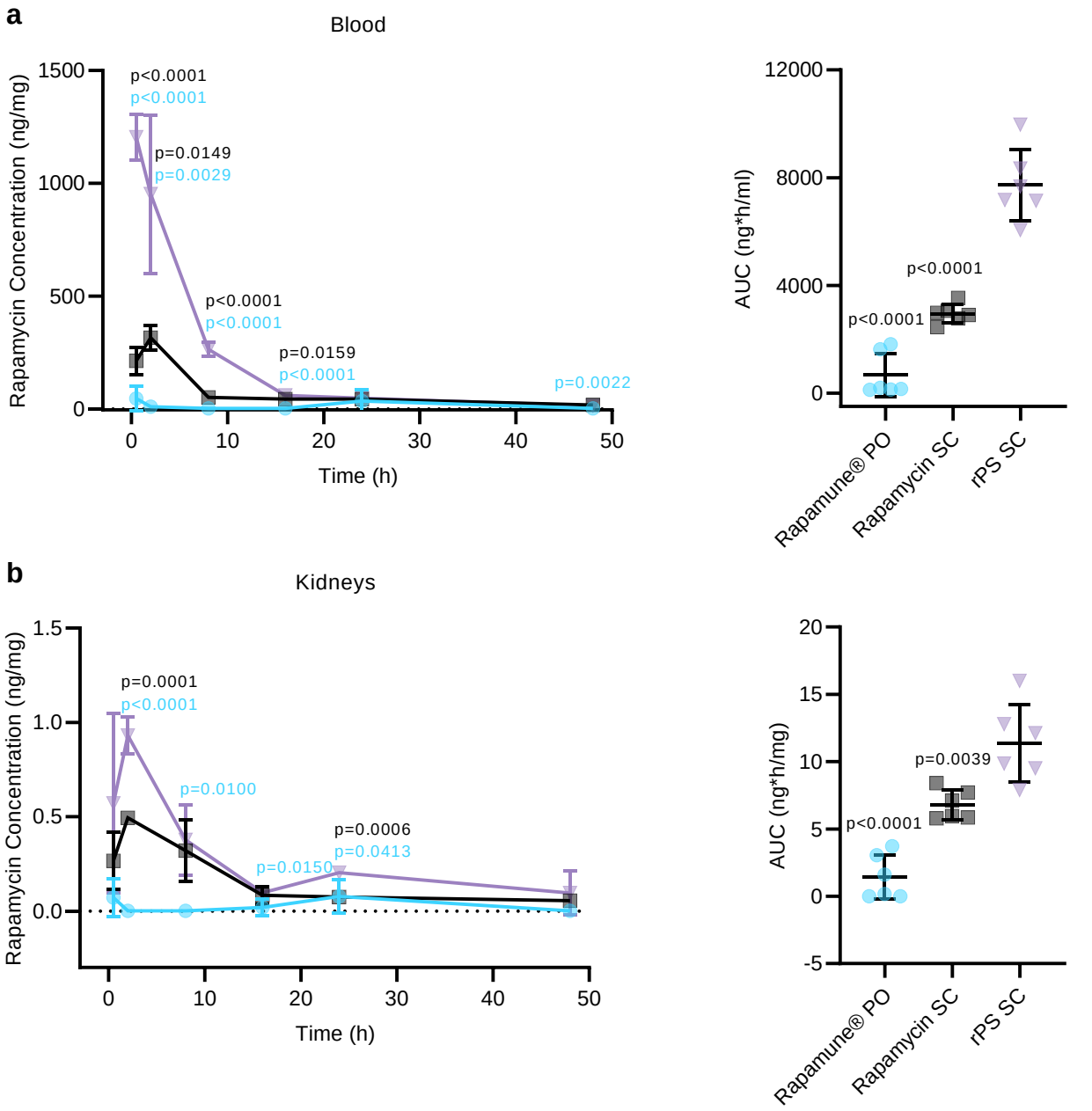

Figure S4-3 | Biodistribution of rapamycin by formulation. Rapamycin concentration in the **a,** blood, **b,** kidneys, **c,** liver, **d,** axillary lymphocenter (deep axillary/axillary/axial and superficial axillary/brachial lymph nodes; AX LN), **e,** subiliac lymphocenter (subiliac/inguinal lymph nodes; IN LN) **f,** spleen, **g,** urine, and **h,** feces, 0.5 h, 2 h, 8 h, 16 h, 24 h, and 48 h after a single 1 mg rapamycin per kg body weight dose. Doses were formulated at a concentration of 0.125 mg rapamycin per mL. Polymersome formulations contained 6.7 mg polymer per mL. Specific formulations include: Rapamune® (●) via oral gavage (PO), rapamycin (in 0.2% carboxymethyl cellulose); ■) via subcutaneous injection (SC) or rapamycin-loaded polymersomes (rPS; ▼) via SC. Rapamycin concentration was also analyzed in the lungs, brain, heart, and fat; concentrations were below 1 ng/mg for all treatment groups at all timepoints. Analysis was performed using liquid chromatography-tandem mass spectrometry (LC-MS/MS). Statistical significance was determined by one-way (**right**) or two-way (**left**) ANOVA with Tukey's multiple comparisons test. Significant p-values relative to the rPS treatment are displayed on the graphs. (n = 6 mice/group).

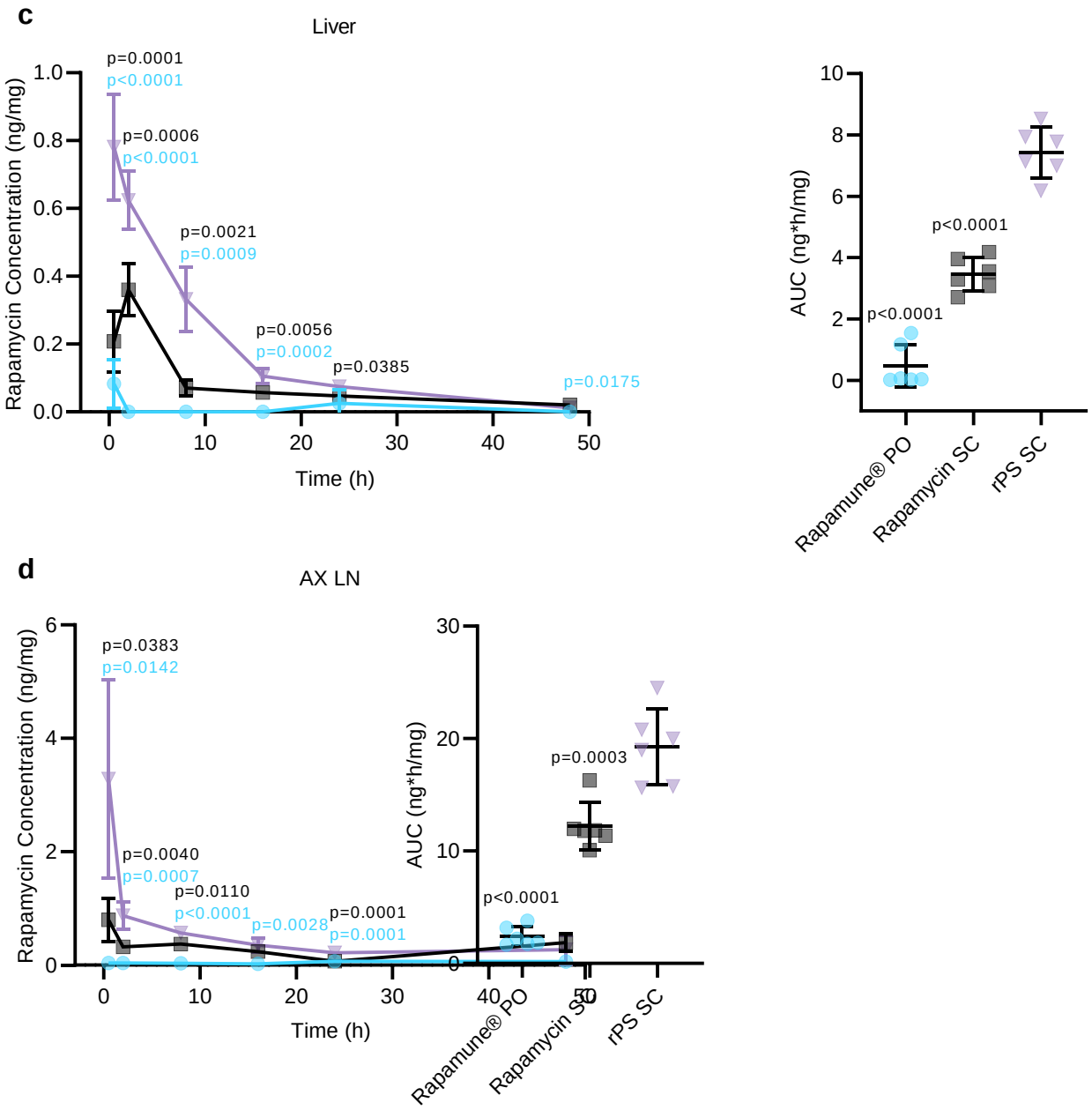

Figure S4-3 | Biodistribution of rapamycin by formulation (continued).

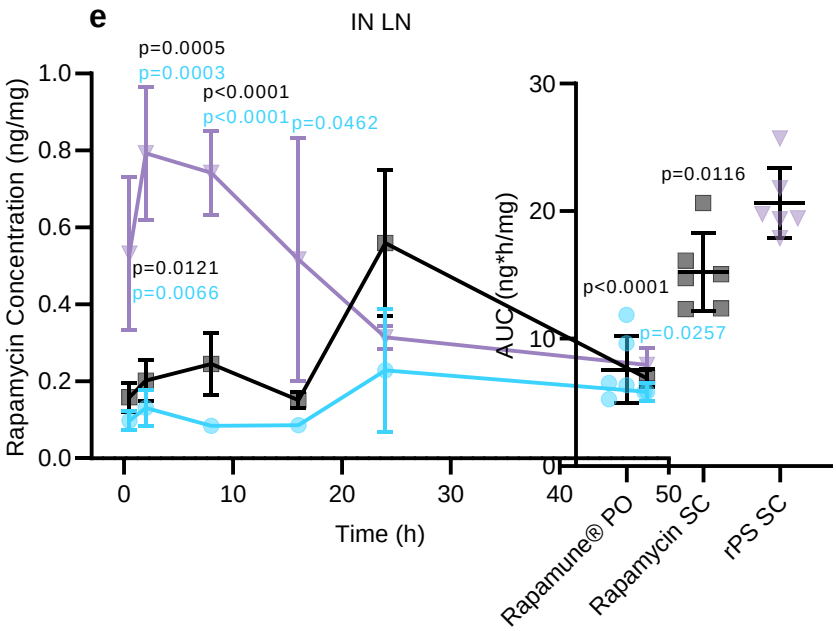

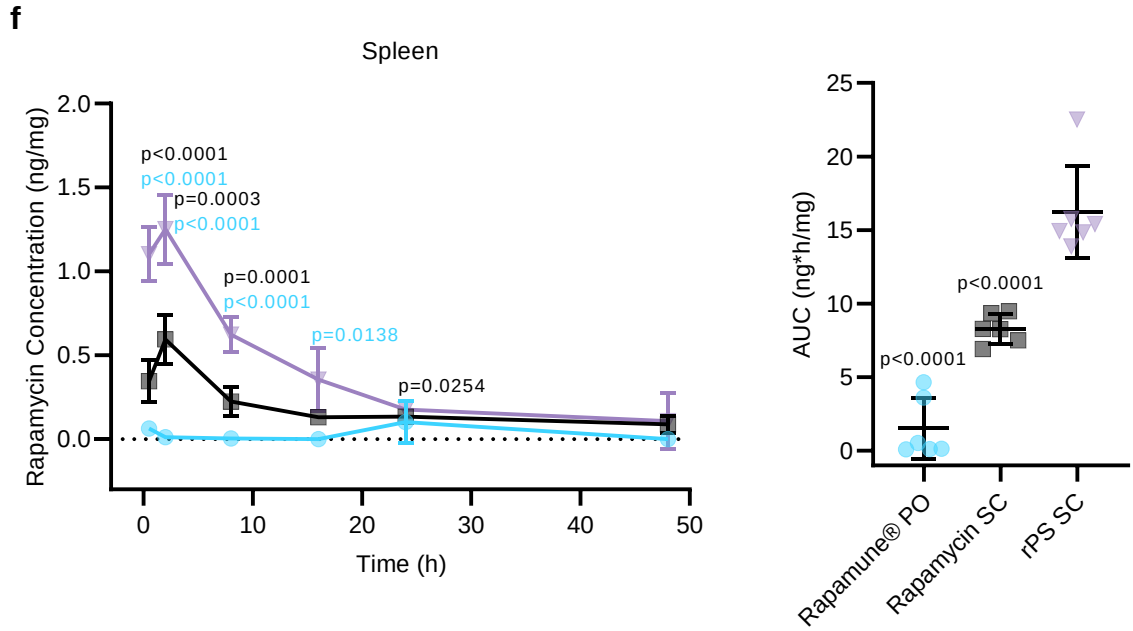

Figure S4-3 | Biodistribution of rapamycin by formulation (continued).

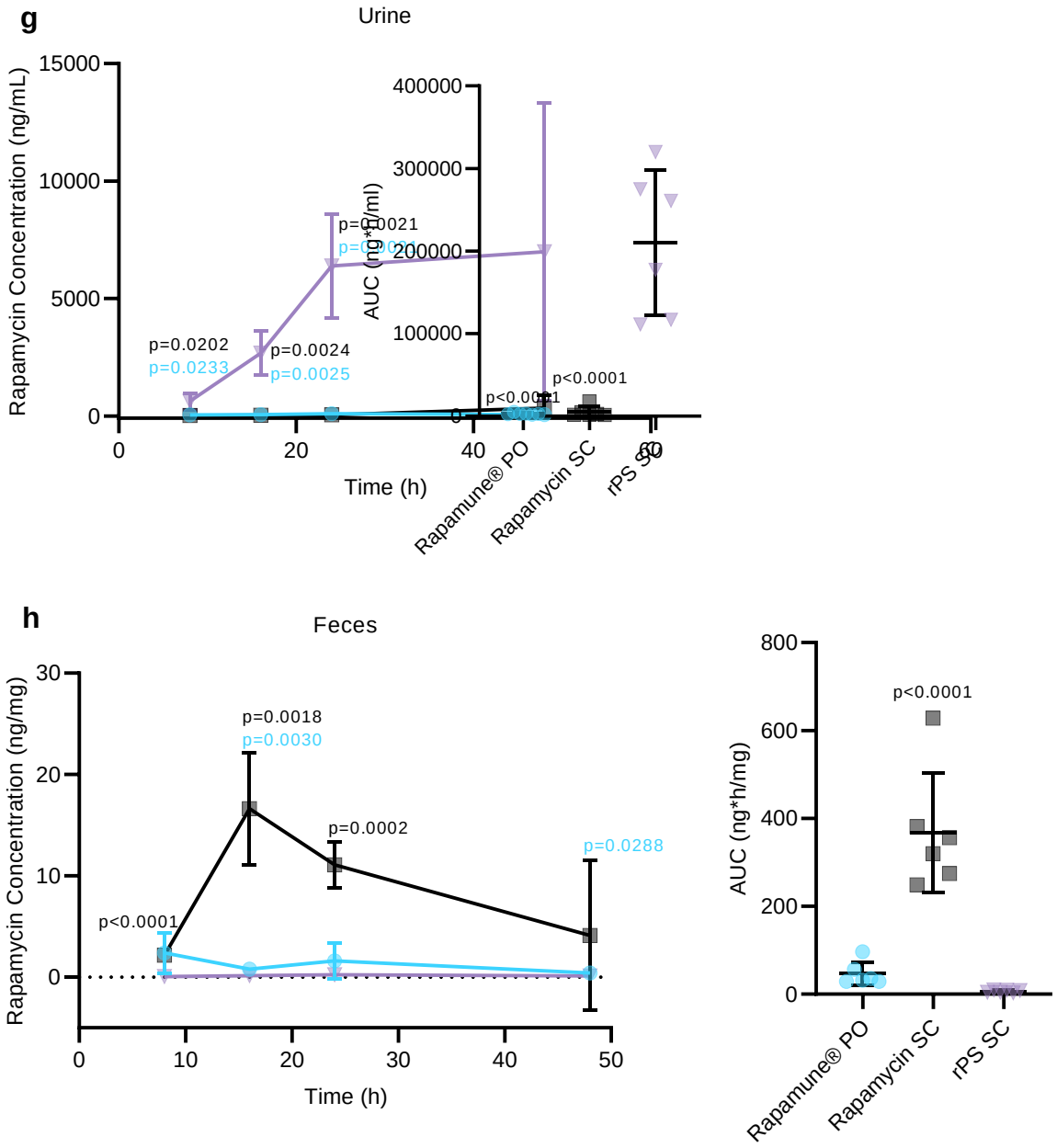

Figure S4-3 | Biodistribution of rapamycin by formulation (continued).

Table S4-1 | Formulation dosing. Dosing information for blank polymersomes (PS) SC, Rapamune® PO, rapamycin (in 0.2% carboxymethyl cellulose) SC, and rapamycin-loaded polymersomes (rPS) SC. All rapamycin-containing formulations are made at a rapamycin concentration of 0.125 mg/mL and dosed at 1 mg rapamycin per kg body weight according to the weight of the animal using the following chart. There is 6.7 mg of PEG-*b*-PPS polymer per mL in the PS and rPS formulations. Before each dose, mice are weighed, and their body weight is rounded to the nearest half gram. The table below is used to determine the volume of the required dose.

Body Weight (g)	Injection Volume (ul)
25.0	200
25.5	204
26.0	208
26.5	212
27.0	216
27.5	220
28.0	224
28.5	228
29.0	232
29.5	236
30.0	240
30.5	244
31.0	248
31.5	252
32.0	256
32.5	260
33.0	264

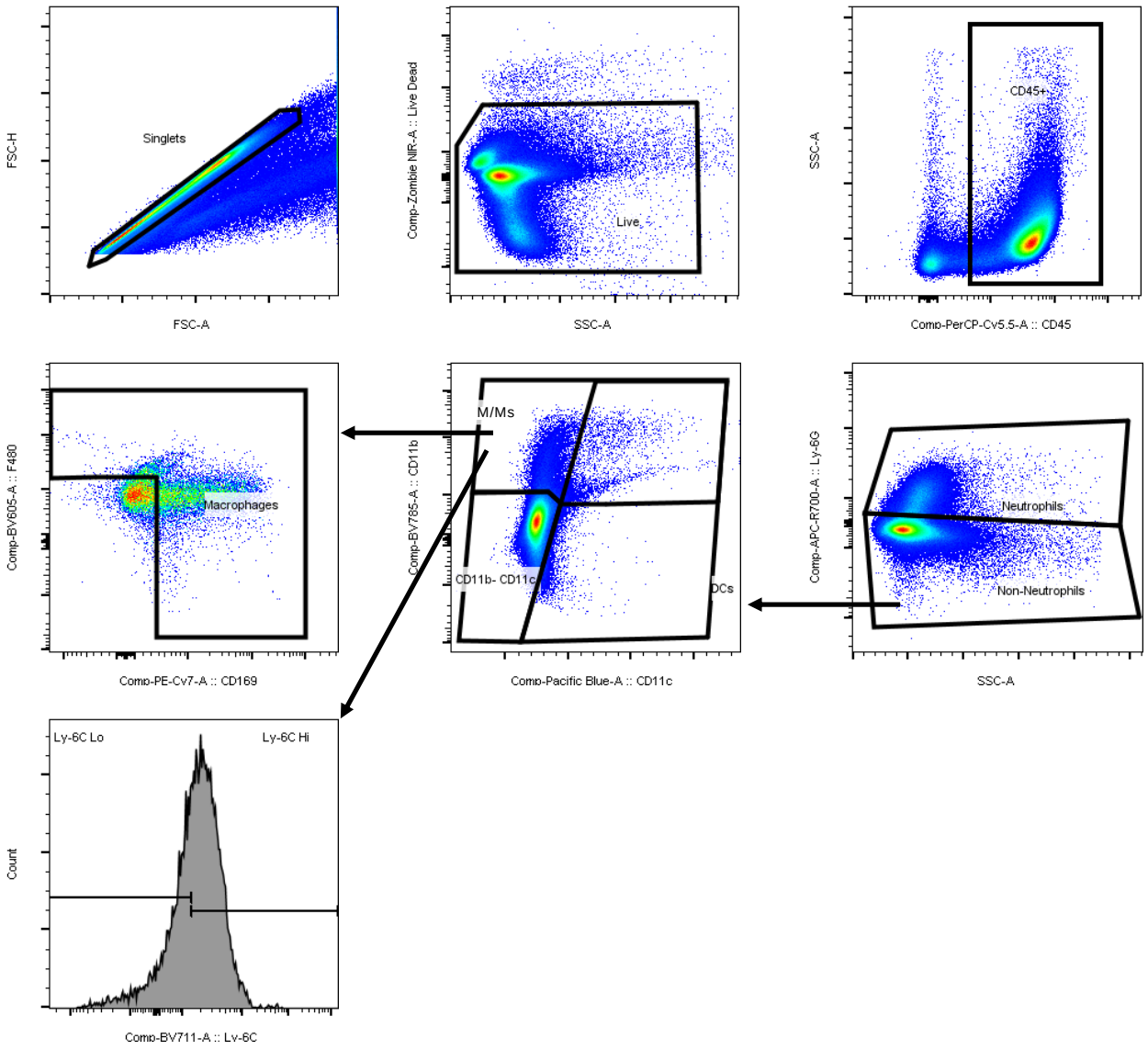

Figure S4-4 | Gating strategy for cell populations in flow cytometry studies. Representative pseudocolor plots and histograms are displayed from an example mouse lymph node. Dendritic cells (DCs); monocyte-and-macrophage-linage cells (M/Ms).

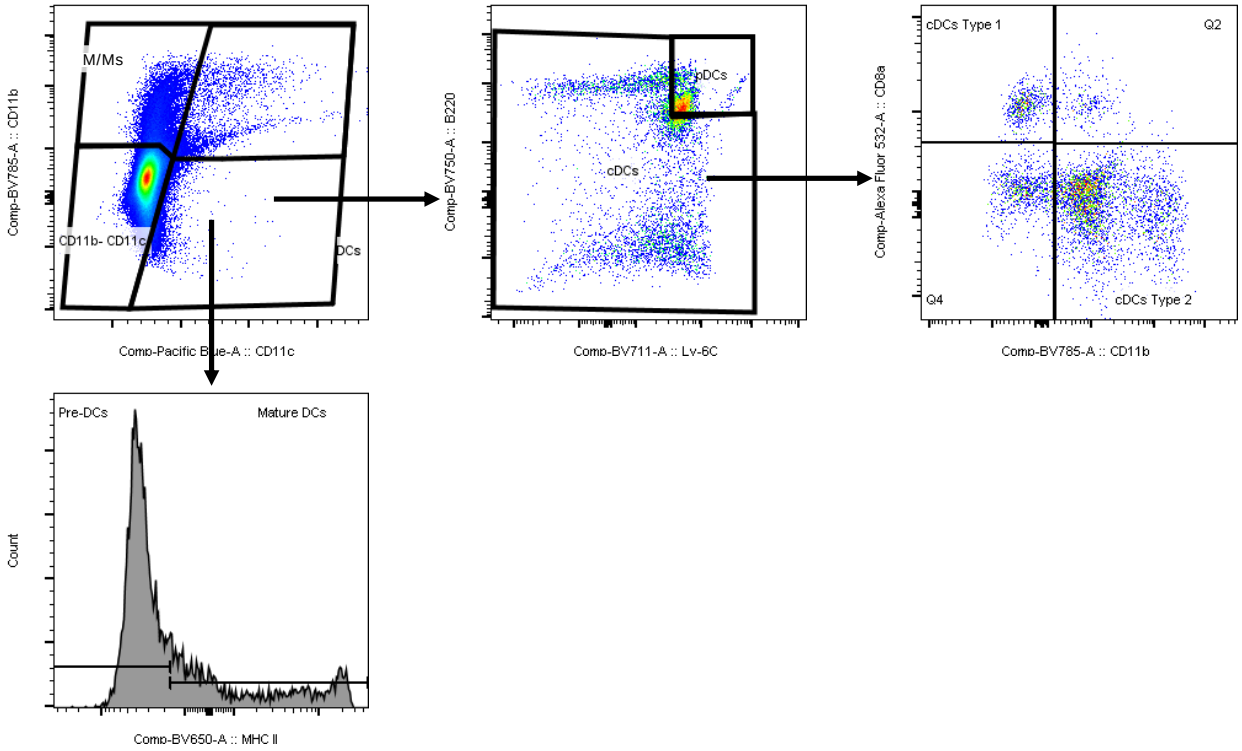

Figure S4-4 (continued) | Gating strategy for cell populations in flow cytometry studies. Representative pseudocolor plots and histograms are displayed from an example mouse lymph node. Dendritic cells (DCs); monocyte-and-macrophage-linage cells (M/Ms); conventional dendritic cells (cDCs); plasmacytoid dendritic cells (pDCs).

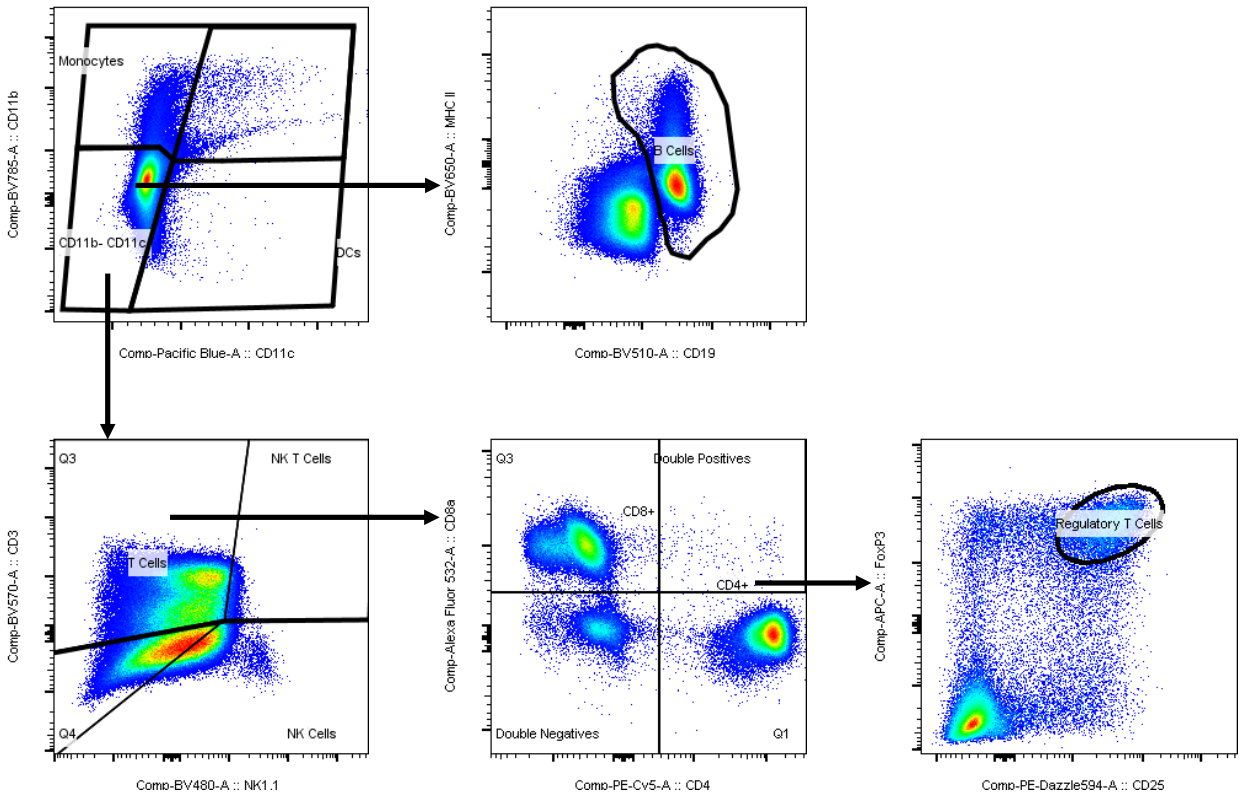

Figure S4-4 (continued) | Gating strategy for cell populations in flow cytometry studies. Representative pseudocolor plots and histograms are displayed from an example mouse lymph node.

Table S4-2 | Cell type overview in blood.

Cell Type	Treatment	Mean Percentage Cell Type+ Cells of CD45+ Cells	Standard Deviation of Percentage Cell Type+ Cells of CD45+ Cells	Mean Number of Cell Type+ Cells	Standard Deviation of Number of Cell Type+ Cells	Mean Number of CD45+ Cells	Standard Deviation of Number of CD45+ Cells
B Cells	Control	41.37	11.83	38413.33	139326.17	85932.00	523489.56
	PS SC	26.80	11.12	26762.33	130621.33	958000.00	450150.51
	Rapamune® PO	27.93	5.75	392271.67	123079.55	858000.00	371634.83
	Rapamycin SC	51.43	12.19	43845.33	256209.86	94823.67	826594.92
	rPS SC	49.50	16.82	14753.67	130724.73	34752.67	450513.92
DCs	Control	1.76	0.86	1440.67	7126.41	85932.00	523489.56
	PS SC	1.59	0.79	1232.67	2630.35	958000.00	450150.51
	Rapamune® PO	0.70	0.33	10264.67	2165.97	858000.00	371634.83
	Rapamycin SC	1.65	0.82	1423.67	1526.12	94823.67	826594.92
	rPS SC	1.96	0.76	710.67	6661.58	34752.67	450513.92
M/Ms	Control	4.42	2.33	2581.33	24765.29	85932.00	523489.56
	PS SC	5.11	1.19	1952.33	15517.57	958000.00	450150.51
	Rapamune® PO	3.59	1.00	45049.33	12992.77	858000.00	371634.83
	Rapamycin SC	4.03	1.63	3281.33	18349.79	94823.67	826594.92
	rPS SC	18.67	10.65	7495.67	22116.83	34752.67	450513.92
Neutrophils	Control	38.07	10.25	31338.33	194440.74	85932.00	523489.56
	PS SC	37.73	8.96	17700.00	145603.02	958000.00	450150.51
	Rapamune® PO	33.97	9.13	432976.33	143024.63	858000.00	371634.83
	Rapamycin SC	24.30	5.74	27780.00	167731.33	94823.67	826594.92
	rPS SC	5.91	1.62	2068.67	20997.23	34752.67	450513.92
NK Cells	Control	2.18	0.78	2245.67	16456.92	85932.00	523489.56
	PS SC	3.09	1.55	1825.33	27808.79	958000.00	450150.51
	Rapamune® PO	4.44	1.60	47199.33	17094.01	858000.00	371634.83
	Rapamycin SC	3.07	1.13	3352.00	28694.84	94823.67	826594.92
	rPS SC	5.91	1.62	2068.67	20997.23	34752.67	450513.92
T Cells	Control	23.07	6.53	15608.33	85998.26	85932.00	523489.56
	PS SC	14.53	7.25	13464.67	56834.12	958000.00	450150.51
	Rapamune® PO	13.60	3.68	201953.00	62181.06	858000.00	371634.83
	Rapamycin SC	25.33	4.52	21580.00	177012.81	94823.67	826594.92
	rPS SC	24.90	5.99	8095.33	73820.89	34752.67	450513.92

Table S4-3 | Costimulation in blood.

Marker	Treatment	Mean Percentage Marker+ Cells of CD45+ Cells	Standard Deviation of Percentage Marker+ Cells of CD45+ Cells	Mean Number of Marker+ Cells	Standard Deviation of Number of Marker+ Cells	Mean Number of CD45+ Cells	Standard Deviation of Number of CD45+ Cells
CD40+	Control	93.00	1.74	36814.33	497751.88	85932.00	523489.56
	PS SC	91.40	27.14	25028.67	417054.92	958000.00	450150.51
	Rapamune® PO	89.57	19.12	1219666.67	377299.17	858000.00	371634.83
	Rapamycin SC	95.77	8.74	42958.33	674020.70	94823.67	826594.92
	rPS SC	42.00	16.62	6686.33	311448.17	34752.67	450513.92
CD80+	Control	89.03	4.86	33404.67	491227.44	85932.00	523489.56
	PS SC	88.37	25.38	23289.67	393460.05	958000.00	450150.51
	Rapamune® PO	85.67	19.37	1196333.33	390669.38	858000.00	371634.83
	Rapamycin SC	92.77	7.25	39593.33	683853.14	94823.67	826594.92
	rPS SC	42.77	16.20	1152.67	303010.31	34752.67	450513.92
CD86+	Control	12.64	4.74	10771.33	51327.98	85932.00	523489.56
	PS SC	11.65	3.21	2763.00	47646.09	958000.00	450150.51
	Rapamune® PO	10.38	2.62	102541.00	35949.02	858000.00	371634.83
	Rapamycin SC	9.86	3.35	6488.00	37002.77	94823.67	826594.92
	rPS SC	8.28	2.95	1840.67	42595.50	34752.67	450513.92

Table S4 | DC subsets in blood.

DC Subsets	Treatment	Mean Percentage Subset+ Cells of DCs	Standard Deviation of Percentage Subset+ Cells of DCs	Mean Number of Subset+ Cells	Standard Deviation of Number of Subset+ Cells	Mean Number of DCs	Standard Deviation of Number DCs
cDCs	Control	84.00	9.74	1259.33	7154.05	1440.67	7126.41
	PS SC	98.93	26.13	1151.33	2566.31	1232.67	2630.35
	Rapamune® PO	96.83	21.82	10197.33	2161.05	10264.67	2165.97
	Rapamycin SC	92.61	3.58	1306.67	1526.38	1423.67	1526.12
	rPS SC	99.24	0.75	683.67	6646.94	710.67	6661.58
pDCs	Control	16.00	9.75	179.67	54.97	1440.67	7126.41
	PS SC	1.04	4.61	75.33	90.33	1232.67	2630.35
	Rapamune® PO	3.19	1.54	67.67	31.10	10264.67	2165.97
	Rapamycin SC	7.39	3.59	114.33	85.31	1423.67	1526.12
	rPS SC	0.76	0.74	8.67	41.84	710.67	6661.58
Mature DCs	Control	49.00	21.06	803.00	5826.28	1440.67	7126.41
	PS SC	67.03	20.45	436.00	2023.92	1232.67	2630.35
	Rapamune® PO	68.40	20.83	8307.33	3043.98	10264.67	2165.97
	Rapamycin SC	40.93	22.43	519.00	1445.91	1423.67	1526.12
	rPS SC	97.63	7.97	689.00	6028.88	710.67	6661.58

Table S4-5 | M/Ms subsets in blood.

M/M Subsets	Treatment	Mean Percentage Subset+ Cells of M/Ms	Standard Deviation of Percentage Subset+ Cells of M/Ms	Mean Number of Subset+ Cells	Standard Deviation of Number of Subset+ Cells	Mean Number of M/Ms	Standard Deviation of Number M/Ms
Ly6C^{Hi}M/Ms	Control	72.93	7.68	1920.00	18948.07	2581.33	24765.29
	PS SC	77.17	21.44	1336.67	11575.41	1952.33	15517.57
	Rapamune® PO	73.37	16.31	34061.33	11795.64	45049.33	12992.77
	Rapamycin SC	84.00	14.25	2718.00	10454.99	3281.33	18349.79
	rPS SC	7.32	15.08	523.00	7642.39	7495.67	22116.83
MHC II+ M/Ms	Control	44.83	21.36	1050.00	16179.23	2581.33	24765.29
	PS SC	62.50	17.08	669.33	10888.42	1952.33	15517.57
	Rapamune® PO	67.37	15.70	29337.67	8232.08	45049.33	12992.77
	Rapamycin SC	16.10	38.56	581.33	17165.09	3281.33	18349.79
	rPS SC	96.33	7.07	7254.00	19283.91	7495.67	22116.83

Table S4-6 | T cell subsets in blood.

T Cell Subsets	Treatment	Mean Percentage Subset+ Cells of T Cells	Standard Deviation of Percentage Subset+ Cells of T Cells	Mean Number of Subset+ Cells	Standard Deviation of Number of Subset+ Cells	Mean Number of T Cells	Standard Deviation of Number T Cells
CD4+ T Cells	Control	35.57	5.45	5639.67	23515.00	15608.33	85998.26
	PS SC	32.90	12.11	4322.67	22675.55	13464.67	56834.12
	Rapamune® PO	40.13	11.92	66687.67	17068.51	201953.00	62181.06
	Rapamycin SC	30.30	3.55	6665.00	46354.16	21580.00	177012.81
	rPS SC	28.00	8.94	2114.33	27185.36	8095.33	73820.89
CD4+ CD8- T Cells	Control	26.70	9.10	4835.33	20094.28	15608.33	85998.26
	PS SC	28.53	11.62	3069.67	21411.43	13464.67	56834.12
	Rapamune® PO	36.43	11.97	58813.33	16667.21	201953.00	62181.06
	Rapamycin SC	18.67	6.45	4757.67	32786.91	21580.00	177012.81
	rPS SC	13.37	13.09	1127.00	22348.40	8095.33	73820.89
CD4+ Tregs	Control	2.22	0.81	311.33	743.69	15608.33	85998.26
	PS SC	0.94	0.70	310.00	706.38	13464.67	56834.12
	Rapamune® PO	1.32	0.51	1471.33	677.55	201953.00	62181.06
	Rapamycin SC	1.50	0.67	268.67	1177.81	21580.00	177012.81
	rPS SC	0.86	0.37	66.00	646.76	8095.33	73820.89
CD8+ Cells	Control	31.43	14.52	3642.67	33601.54	15608.33	85998.26
	PS SC	30.40	11.09	4814.33	17329.75	13464.67	56834.12
	Rapamune® PO	20.75	12.13	59197.00	27719.10	201953.00	62181.06
	Rapamycin SC	39.60	11.57	7834.67	104564.96	21580.00	177012.81
	rPS SC	36.83	15.31	2778.00	38903.55	8095.33	73820.89
CD8+ CD4- T Cells	Control	22.53	9.96	2833.33	31486.70	15608.33	85998.26
	PS SC	27.70	9.51	3557.33	16000.50	13464.67	56834.12
	Rapamune® PO	18.78	11.19	54724.67	26160.05	201953.00	62181.06
	Rapamycin SC	27.93	10.75	5919.00	88497.49	21580.00	177012.81
	rPS SC	22.20	11.54	1788.00	31108.98	8095.33	73820.89
CD8+ Tregs	Control	0.62	0.70	45.00	1444.56	15608.33	85998.26
	PS SC	1.04	0.48	61.67	860.95	13464.67	56834.12
	Rapamune® PO	1.08	0.41	1443.33	857.70	201953.00	62181.06
	Rapamycin SC	0.38	0.59	52.67	2110.74	21580.00	177012.81
	rPS SC	0.52	0.29	43.67	557.39	8095.33	73820.89
DP T Cells	Control	8.91	6.74	810.67	2314.56	15608.33	85998.26
	PS SC	2.85	3.76	1257.00	1529.95	13464.67	56834.12
	Rapamune® PO	2.08	1.19	4746.33	2017.82	201953.00	62181.06
	Rapamycin SC	11.68	4.58	1916.00	16502.79	21580.00	177012.81
	rPS SC	14.71	7.45	992.00	7942.93	8095.33	73820.89
NK T Cells	Control	3.20	1.67	565.67	3766.60	15608.33	85998.26
	PS SC	4.81	1.79	538.00	3651.42	13464.67	56834.12
	Rapamune® PO	6.31	1.93	7538.00	1621.03	201953.00	62181.06
	Rapamycin SC	2.82	1.06	684.33	4437.08	21580.00	177012.81
	rPS SC	15.73	7.03	1320.00	3332.25	8095.33	73820.89

Table S4-7 | Cell type overview in the liver.

Cell Type	Treatment	Mean Percentage Cell Type+ Cells of CD45+ Cells	Standard Deviation of Percentage Cell Type+ Cells of CD45+ Cells	Mean Number of Cell Type+ Cells	Standard Deviation of Number of Cell Type+ Cells	Mean Number of CD45+ Cells	Standard Deviation of Number of CD45+ Cells
B Cells	Control	38.17	6.72	46768.67	194035.03	129997.00	545053.97
	PS SC	60.40	13.62	79924.33	143340.01	131463.00	434741.45
	Rapamune® PO	40.00	11.93	227868.33	102167.42	554606.67	207841.93
	Rapamycin SC	39.17	5.55	56810.00	88483.69	143517.67	299411.17
	rPS SC	77.33	27.92	333732.33	122550.29	432908.00	316211.11
DCs	Control	7.11	2.58	9590.67	13721.25	129997.00	545053.97
	PS SC	3.91	2.08	5107.33	22347.34	131463.00	434741.45
	Rapamune® PO	6.79	4.48	29436.00	13926.27	554606.67	207841.93
	Rapamycin SC	5.08	2.47	7064.33	30618.44	143517.67	299411.17
	rPS SC	17.04	9.55	73920.67	39605.01	432908.00	316211.11
M/Ms	Control	7.17	4.37	9934.67	52602.34	129997.00	545053.97
	PS SC	5.02	3.67	6528.67	31318.45	131463.00	434741.45
	Rapamune® PO	13.64	5.86	67590.00	23936.21	554606.67	207841.93
	Rapamycin SC	11.10	3.26	15430.33	25416.28	143517.67	299411.17
	rPS SC	3.45	10.16	15535.67	84646.45	432908.00	316211.11
Neutrophils	Control	13.37	4.32	18518.33	36928.64	129997.00	545053.97
	PS SC	5.20	2.20	6608.67	21713.02	131463.00	434741.45
	Rapamune® PO	3.53	1.22	21758.00	13360.68	554606.67	207841.93
	Rapamycin SC	8.59	2.14	12299.00	14796.76	143517.67	299411.17
	rPS SC	3.12	4.59	13331.33	28301.54	432908.00	316211.11
NK Cells	Control	5.04	2.11	7296.67	42805.94	129997.00	545053.97
	PS SC	0.83	3.94	1115.67	40282.48	131463.00	434741.45
	Rapamune® PO	9.61	3.83	61151.00	36484.69	554606.67	207841.93
	Rapamycin SC	2.74	6.26	3633.00	43683.89	143517.67	299411.17
	rPS SC	3.12	4.59	13331.33	28301.54	432908.00	316211.11
T Cells	Control	40.07	7.74	51241.00	164575.21	129997.00	545053.97
	PS SC	66.13	25.30	87195.00	51388.63	131463.00	434741.45
	Rapamune® PO	34.57	12.76	191635.67	86726.40	554606.67	207841.93
	Rapamycin SC	47.10	14.24	69080.33	78596.36	143517.67	299411.17
	rPS SC	10.28	13.69	46039.33	121680.46	432908.00	316211.11

Table S4-8 | Costimulation in the liver.

Marker	Treatment	Mean Percentage Marker+ Cells of CD45+ Cells	Standard Deviation of Percentage Marker+ Cells of CD45+ Cells	Mean Number of Marker+ Cells	Standard Deviation of Number of Marker+ Cells	Mean Number of Marker+ Cells	Standard Deviation of Number of CD45+ Cells
CD40+	Control	46.60	6.22	61494.33	234351.25	129997.00	545053.97
	PS SC	60.80	9.86	79788.33	174751.11	131463.00	434741.45
	Rapamune® PO	37.23	6.78	200514.67	87244.61	554606.67	207841.93
	Rapamycin SC	60.87	9.75	87418.00	115833.61	143517.67	299411.17
	rPS SC	59.20	20.85	261440.67	121124.41	432908.00	316211.11
CD80+	Control	43.47	7.24	57007.67	218924.83	129997.00	545053.97
	PS SC	34.83	5.36	45451.33	137575.82	131463.00	434741.45
	Rapamune® PO	58.63	19.43	322120.33	141615.06	554606.67	207841.93
	Rapamycin SC	53.47	7.35	76058.67	115193.67	143517.67	299411.17
	rPS SC	13.70	16.75	59794.00	189778.54	432908.00	316211.11
CD86+	Control	48.40	7.11	59844.33	284132.43	129997.00	545053.97
	PS SC	61.67	5.79	81138.67	233255.04	131463.00	434741.45
	Rapamune® PO	35.93	17.54	206848.00	127257.23	554606.67	207841.93
	Rapamycin SC	53.70	6.15	76356.00	176014.51	143517.67	299411.17
	rPS SC	85.97	21.09	371576.00	143225.18	432908.00	316211.11

Table S4-9 | DC subsets in the liver.

DC Subsets	Treatment	Mean Percentage Subset+ Cells of DCs	Standard Deviation of Percentage Subset+ Cells of DCs	Mean Number of Subset+ Cells	Standard Deviation of Number of Subset+ Cells	Mean Number of DCs	Standard Deviation of Number DCs
cDCs	Control	73.53	12.31	7385.00	3742.91	9590.67	13721.25
	PS SC	78.27	6.53	3986.33	1102.63	5107.33	22347.34
	Rapamune® PO	89.90	4.23	2448.33	1091.08	29436.00	13926.27
	Rapamycin SC	80.47	7.25	5689.33	1808.80	7064.33	30618.44
	rPS SC	93.80	5.04	70117.33	47562.73	73920.67	39605.01
pDCs	Control	26.47	12.42	2207.00	14577.22	9590.67	13721.25
	PS SC	21.73	6.68	1120.00	21869.19	5107.33	22347.34
	Rapamune® PO	9.98	4.20	26950.00	13549.72	29436.00	13926.27
	Rapamycin SC	19.53	7.36	1375.00	31515.99	7064.33	30618.44
	rPS SC	6.20	4.92	3793.33	24861.87	73920.67	39605.01
Mature DCs	Control	95.90	3.30	9035.67	13672.02	9590.67	13721.25
	PS SC	99.63	0.21	5089.33	22214.42	5107.33	22347.34
	Rapamune® PO	98.07	0.87	28941.00	13795.25	29436.00	13926.27
	Rapamycin SC	98.63	0.68	6968.00	30618.40	7064.33	30618.44
	rPS SC	99.83	0.48	73818.00	39520.15	73920.67	39605.01

Table S4-10 | M/Ms subsets in the liver.

M/M Subsets	Treatment	Mean Percentage Subset+ Cells of M/Ms	Standard Deviation of Percentage Subset+ Cells of M/Ms	Mean Number of Subset+ Cells	Standard Deviation of Number of Subset+ Cells	Mean Number of M/Ms	Standard Deviation of Number M/Ms
Macrophages	Control	64.53	20.68	5648.67	50066.58	9934.67	52602.34
	PS SC	83.13	8.26	5475.00	31547.39	6528.67	31318.45
	Rapamune® PO	78.47	9.16	53263.33	19535.49	67590.00	23936.21
	Rapamycin SC	85.10	8.18	13262.67	25949.90	15430.33	25416.28
	rPS SC	98.60	3.23	15352.00	76252.75	15535.67	84646.45
Ly6C^{Hi}M/Ms	Control	11.43	5.46	1337.33	2220.17	9934.67	52602.34
	PS SC	2.58	2.23	142.33	1623.80	6528.67	31318.45
	Rapamune® PO	3.31	0.61	2232.00	807.62	67590.00	23936.21
	Rapamycin SC	7.76	4.72	1179.67	4716.01	15430.33	25416.28
	rPS SC	0.18	3.64	24.67	8238.36	15535.67	84646.45
MHC II+ M/Ms	Control	89.90	9.20	8762.33	39818.30	9934.67	52602.34
	PS SC	97.47	19.32	6372.67	16122.11	6528.67	31318.45
	Rapamune® PO	74.87	10.26	51049.67	20117.57	67590.00	23936.21
	Rapamycin SC	92.53	14.79	14265.00	14875.77	15430.33	25416.28
	rPS SC	99.77	20.80	15510.67	47949.01	15535.67	84646.45

Table S4-11 | T cell subsets in the liver.

T Cell Subsets	Treatment	Mean Percentage Subset+ Cells of T Cells	Standard Deviation of Percentage Subset+ Cells of T Cells	Mean Number of Subset+ Cells	Standard Deviation of Number of Subset+ Cells	Mean Number of T Cells	Standard Deviation of Number T Cells
CD4+ T Cells	Control	22.07	11.54	11604.67	53181.32	51241.00	164575.21
	PS SC	6.25	21.13	5537.67	34699.10	87195.00	51388.63
	Rapamune® PO	10.65	5.15	17375.67	8764.35	191635.67	86726.40
	Rapamycin SC	9.44	9.83	6945.33	27571.67	69080.33	78596.36
	rPS SC	7.55	20.08	3200.00	34004.79	46039.33	121680.46
CD4+ CD8- T Cells	Control	17.03	11.34	8448.00	53613.11	51241.00	164575.21
	PS SC	4.04	21.18	3142.33	34458.36	87195.00	51388.63
	Rapamune® PO	2.89	4.23	4541.00	6084.59	191635.67	86726.40
	Rapamycin SC	7.20	10.11	4753.67	27118.49	69080.33	78596.36
	rPS SC	6.85	18.45	2319.67	29590.91	46039.33	121680.46
CD4+ Tregs	Control	0.77	0.44	381.67	305.66	51241.00	164575.21
	PS SC	0.28	0.40	245.00	806.63	87195.00	51388.63
	Rapamune® PO	3.14	1.58	5261.67	2953.24	191635.67	86726.40
	Rapamycin SC	0.30	0.57	220.67	1702.40	69080.33	78596.36
	rPS SC	0.22	1.04	105.33	2513.45	46039.33	121680.46
CD8+ Cells	Control	65.43	23.25	32786.00	47661.55	51241.00	164575.21
	PS SC	91.77	29.43	79877.00	32849.59	87195.00	51388.63
	Rapamune® PO	75.27	15.00	144491.33	67538.43	191635.67	86726.40
	Rapamycin SC	79.50	22.77	54450.67	25280.17	69080.33	78596.36
	rPS SC	42.43	10.54	17283.33	61147.11	46039.33	121680.46
CD8+ CD4- T Cells	Control	61.00	21.89	30646.67	48015.92	51241.00	164575.21
	PS SC	86.23	27.93	77933.00	32782.16	87195.00	51388.63
	Rapamune® PO	67.47	14.20	131656.67	62948.03	191635.67	86726.40
	Rapamycin SC	53.33	26.29	52874.33	24645.45	69080.33	78596.36
	rPS SC	41.80	10.90	17039.67	57248.63	46039.33	121680.46
CD8+ Tregs	Control	7.73	2.60	3928.33	8499.92	51241.00	164575.21
	PS SC	17.70	6.94	15236.33	6231.04	87195.00	51388.63
	Rapamune® PO	9.46	5.54	19535.00	16232.60	191635.67	86726.40
	Rapamycin SC	12.63	5.30	8659.33	6490.10	69080.33	78596.36
	rPS SC	0.95	3.05	371.67	10014.45	46039.33	121680.46
DP T Cells	Control	4.51	2.81	2133.67	766.32	51241.00	164575.21
	PS SC	2.21	0.45	1923.33	668.01	87195.00	51388.63
	Rapamune® PO	7.75	4.26	12847.00	7252.00	191635.67	86726.40
	Rapamycin SC	2.22	0.53	1567.00	847.69	69080.33	78596.36
	rPS SC	0.75	2.63	270.33	7053.32	46039.33	121680.46
NK T Cells	Control	26.47	11.46	14172.00	52350.72	51241.00	164575.21
	PS SC	11.86	17.15	10152.67	28984.04	87195.00	51388.63
	Rapamune® PO	9.60	7.39	13478.33	7535.29	191635.67	86726.40
	Rapamycin SC	17.70	7.62	12249.33	30014.19	69080.33	78596.36
	rPS SC	50.67	27.14	25037.67	34420.67	46039.33	121680.46

Table S4-12 | Cell type overview in AX LN.

Cell Type	Treatment	Mean Percentage Cell Type+ Cells of CD45+ Cells	Standard Deviation of Percentage Cell Type+ Cells of CD45+ Cells	Mean Number of Cell Type+ Cells	Standard Deviation of Number of Cell Type+ Cells	Mean Number of CD45+ Cells	Standard Deviation of Number of CD45+ Cells
B Cells	Control	38.00	11.11	57161.20	34908.49	647333.33	233897.99
	PS SC	36.40	13.12	46486.67	73129.72	694000.00	276126.26
	Rapamune® PO	35.47	11.21	35263.67	24659.09	139162.33	121880.55
	Rapamycin SC	33.03	5.79	40744.72	33887.27	413951.33	129698.52
	rPS SC	39.50	8.35	15530.86	100691.43	163020.33	166868.55
DCs	Control	1.82	0.47	245677.67	133559.24	647333.33	233897.99
	PS SC	1.33	1.65	259737.33	150361.73	694000.00	276126.26
	Rapamune® PO	2.25	0.80	2067.00	2049.54	139162.33	121880.55
	Rapamycin SC	1.81	1.18	135307.58	72790.82	413951.33	129698.52
	rPS SC	5.22	1.46	64596.37	39394.87	163020.33	166868.55
M/Ms	Control	4.74	1.83	5636.67	1311.28	647333.33	233897.99
	PS SC	3.18	1.35	8869.00	6850.30	694000.00	276126.26
	Rapamune® PO	2.98	1.17	22946.33	11262.35	139162.33	121880.55
	Rapamycin SC	3.17	0.69	3737.97	1703.86	413951.33	129698.52
	rPS SC	9.43	3.33	2452.78	1942.88	163020.33	166868.55
Neutrophils	Control	8.60	10.30	329268.33	157141.70	647333.33	233897.99
	PS SC	6.72	10.17	371417.33	175233.08	694000.00	276126.26
	Rapamune® PO	6.41	2.14	10897.00	11135.30	139162.33	121880.55
	Rapamycin SC	9.74	1.50	229831.99	122767.83	413951.33	129698.52
	rPS SC	1.61	0.30	8657.43	4963.67	163020.33	166868.55
NK Cells	Control	0.91	0.35	12279.43	6662.44	647333.33	233897.99
	PS SC	1.25	0.90	9345.73	5115.35	694000.00	276126.26
	Rapamune® PO	1.46	2.01	2894.00	5212.91	139162.33	121880.55
	Rapamycin SC	0.90	1.21	7475.20	2795.68	413951.33	129698.52
	rPS SC	1.61	0.30	8657.43	4963.67	163020.33	166868.55
T Cells	Control	51.13	7.87	31402.67	102063.35	647333.33	233897.99
	PS SC	54.50	14.70	23053.93	95352.70	694000.00	276126.26
	Rapamune® PO	65.43	8.47	89959.00	75939.71	139162.33	121880.55
	Rapamycin SC	55.30	9.40	13158.87	44745.82	413951.33	129698.52
	rPS SC	41.67	9.15	15415.10	75461.78	163020.33	166868.55

Table S4-13 | Costimulation in AX LN.

Marker	Treatment	Mean Percentage Marker+ Cells of CD45+ Cells	Standard Deviation of Percentage Marker+ Cells of CD45+ Cells	Mean Number of Marker+ Cells	Standard Deviation of Number of Marker+ Cells	Mean Number of CD45+ Cells	Standard Deviation of Number of CD45+ Cells
CD40+	Control	91.90	4.79	594173.33	223298.01	647333.33	233897.99
	PS SC	90.30	5.55	631292.00	255649.91	694000.00	276126.26
	Rapamune® PO	90.73	31.23	114088.67	94095.39	139162.33	121880.55
	Rapamycin SC	92.87	38.19	384303.33	192469.37	413951.33	129698.52
	rPS SC	33.43	13.45	51265.54	24196.62	163020.33	166868.55
CD80+	Control	79.80	8.16	515093.33	194066.38	647333.33	233897.99
	PS SC	79.70	11.03	556884.67	226535.69	694000.00	276126.26
	Rapamune® PO	90.87	31.27	114260.33	94205.23	139162.33	121880.55
	Rapamycin SC	79.03	31.14	326848.44	159586.77	413951.33	129698.52
	rPS SC	28.97	11.51	46968.12	25053.06	163020.33	166868.55
CD86+	Control	6.20	45.36	41648.03	219468.30	647333.33	233897.99
	PS SC	5.42	49.48	37337.20	226087.53	694000.00	276126.26
	Rapamune® PO	88.07	32.06	109079.67	89843.97	139162.33	121880.55
	Rapamycin SC	6.22	14.18	25712.46	20234.55	413951.33	129698.52
	rPS SC	4.21	9.66	7610.05	12847.87	163020.33	166868.55

Table S4-14 | DC subsets in AX LN.

DC Subsets	Treatment	Mean Percentage Subset+ Cells of DCs	Standard Deviation of Percentage Subset+ Cells of DCs	Mean Number of Subset+ Cells	Standard Deviation of Number of Subset+ Cells	Mean Number of DCs	Standard Deviation of Number DCs
cDCs	Control	83.47	4.31	204908.21	110621.41	245677.67	133559.24
	PS SC	88.00	2.28	229006.17	132247.02	259737.33	150361.73
	Rapamune® PO	90.43	2.06	2067.00	2049.54	2067.00	2049.54
	Rapamycin SC	87.00	3.51	117841.74	63103.45	135307.58	72790.82
	rPS SC	99.43	3.30	64249.36	39191.13	64596.37	39394.87
pDCs	Control	16.53	2.88	40769.46	22462.48	245677.67	133559.24
	PS SC	12.00	1.01	30731.16	17447.93	259737.33	150361.73
	Rapamune® PO	13.13	2.64	299.33	197.93	2067.00	2049.54
	Rapamycin SC	13.00	2.79	17465.83	9457.03	135307.58	72790.82
	rPS SC	0.57	4.11	347.01	648.54	64596.37	39394.87
Mature DCs	Control	39.33	10.69	96238.71	51641.95	245677.67	133559.24
	PS SC	45.07	18.01	119440.53	72285.61	259737.33	150361.73
	Rapamune® PO	40.90	12.01	815.67	443.89	2067.00	2049.54
	Rapamycin SC	48.13	10.69	65316.83	36146.06	135307.58	72790.82
	rPS SC	98.57	31.53	63672.28	40478.69	64596.37	39394.87

Table S4-15 | M/Ms subsets in AX LN.

M/M Subsets	Treatment	Mean Percentage Subset+ Cells of M/Ms	Standard Deviation of Percentage Subset+ Cells of M/Ms	Mean Number of Subset+ Cells	Standard Deviation of Number of Subset+ Cells	Mean Number of M/Ms	Standard Deviation of Number M/Ms
Macrophages	Control	54.87	5.02	3116.92	877.07	5636.67	1311.28
	PS SC	51.80	11.10	4600.32	2766.87	8869.00	6850.30
	Rapamune® PO	53.17	6.98	10976.67	5088.99	22946.33	11262.35
	Rapamycin SC	51.03	10.40	1935.01	984.29	3737.97	1703.86
	rPS SC	12.67	8.87	311.45	1017.00	2452.78	1942.88
Ly6C^{Hi}M/Ms	Control	66.40	2.56	3760.41	889.98	5636.67	1311.28
	PS SC	62.20	8.39	5508.41	3857.79	8869.00	6850.30
	Rapamune® PO	61.67	25.26	10365.67	5479.93	22946.33	11262.35
	Rapamycin SC	62.00	27.27	2324.27	919.77	3737.97	1703.86
	rPS SC	0.34	7.92	8.95	637.74	2452.78	1942.88
MHC II+ M/Ms	Control	53.70	9.62	2980.01	1221.61	5636.67	1311.28
	PS SC	54.00	9.71	4789.69	5213.16	8869.00	6850.30
	Rapamune® PO	54.53	11.09	17219.00	8858.44	22946.33	11262.35
	Rapamycin SC	63.53	8.87	2413.72	1139.34	3737.97	1703.86
	rPS SC	99.87	8.39	2449.14	1360.76	2452.78	1942.88

Table S4-16 | T cell subsets in AX LN

T Cell Subsets	Treatment	Mean Percentage Subset+ Cells of T Cells	Standard Deviation of Percentage Subset+ Cells of T Cells	Mean Number of Subset+ Cells	Standard Deviation of Number of Subset+ Cells	Mean Number of T Cells	Standard Deviation of Number T Cells
CD4+ T Cells	Control	46.23	11.32	14638.06	20743.71	31402.67	102063.35
	PS SC	48.50	17.55	10922.19	25782.33	23053.93	95352.70
	Rapamune® PO	53.63	9.63	14122.33	11056.03	89959.00	75939.71
	Rapamycin SC	40.50	15.63	5227.05	7098.23	13158.87	44745.82
	rPS SC	18.70	13.65	1652.04	16060.45	15415.10	75461.78
CD4+ CD8- T Cells	Control	46.07	10.36	1583.62	23678.31	31402.67	102063.35
	PS SC	48.27	17.08	1078.21	26697.26	23053.93	95352.70
	Rapamune® PO	47.93	9.50	13440.00	10576.85	89959.00	75939.71
	Rapamycin SC	40.00	13.07	505.24	8866.40	13158.87	44745.82
	rPS SC	11.28	13.59	125.73	13783.80	15415.10	75461.78
CD4+ Tregs	Control	4.98	1.82	10281.77	5408.11	31402.67	102063.35
	PS SC	4.63	1.85	8119.50	4551.24	23053.93	95352.70
	Rapamune® PO	3.79	3.00	442.00	291.11	89959.00	75939.71
	Rapamycin SC	3.98	2.09	5809.22	3367.94	13158.87	44745.82
	rPS SC	0.87	0.36	11378.07	7574.11	15415.10	75461.78
CD8+ Cells	Control	33.23	4.67	10218.96	11392.90	31402.67	102063.35
	PS SC	35.23	12.50	8069.78	18256.24	23053.93	95352.70
	Rapamune® PO	52.70	9.95	13902.33	9597.56	89959.00	75939.71
	Rapamycin SC	43.80	7.80	5745.70	4609.56	13158.87	44745.82
	rPS SC	73.40	3.28	10306.27	21469.93	15415.10	75461.78
CD8+ CD4- T Cells	Control	33.03	4.34	71.78	13901.59	31402.67	102063.35
	PS SC	35.00	11.59	11.79	19746.55	23053.93	95352.70
	Rapamune® PO	50.07	10.13	13646.00	9464.58	89959.00	75939.71
	Rapamycin SC	43.30	8.19	3.15	6813.40	13158.87	44745.82
	rPS SC	65.97	2.51	83.31	24227.84	15415.10	75461.78
CD8+ Tregs	Control	0.18	0.16	58.10	32.44	31402.67	102063.35
	PS SC	0.05	0.16	57.50	154.35	23053.93	95352.70
	Rapamune® PO	0.20	0.18	72.00	90.23	89959.00	75939.71
	Rapamycin SC	0.03	0.34	62.60	171.56	13158.87	44745.82
	rPS SC	0.58	0.17	1069.95	504.81	15415.10	75461.78
DP T Cells	Control	0.19	0.70	751.48	699.04	31402.67	102063.35
	PS SC	0.26	2.71	928.11	2494.73	23053.93	95352.70
	Rapamune® PO	2.15	0.86	759.00	552.63	89959.00	75939.71
	Rapamycin SC	0.50	2.20	324.61	634.49	13158.87	44745.82
	rPS SC	7.42	1.61	1057.23	2561.14	15415.10	75461.78
NK T Cells	Control	2.63	1.74	5050461.04	3555755.95	31402.67	102063.35
	PS SC	3.79	2.30	2866257.02	2050627.34	23053.93	95352.70
	Rapamune® PO	13.94	7.04	6882.33	2766.34	89959.00	75939.71
	Rapamycin SC	2.56	3.27	725499.04	455627.28	13158.87	44745.82
	rPS SC	7.04	1.64	299322.00	246994.89	15415.10	75461.78

Table S4-17 | Cell type overview in IG LN.

Cell Type	Treatment	Mean Percentage Cell Type+ Cells of CD45+ Cells	Standard Deviation of Percentage Cell Type+ Cells of CD45+ Cells	Mean Number of Cell Type+ Cells	Standard Deviation of Number of Cell Type+ Cells	Mean Number of CD45+ Cells	Standard Deviation of Number of CD45+ Cells
B Cells	Control	41.83	8.48	233047.33	72754.70	550666.67	160973.50
	PS SC	41.07	12.49	166358.33	102232.28	587000.00	242078.78
	Rapamune® PO	30.47	11.79	122404.67	82420.65	174205.67	202708.43
	Rapamycin SC	35.90	8.20	76695.63	30486.32	213818.00	59034.91
	rPS SC	39.80	4.49	46388.86	74134.13	81818.00	171878.11
DCs	Control	1.09	2.11	5796.73	10991.88	550666.67	160973.50
	PS SC	1.17	1.11	20241.00	8773.17	587000.00	242078.78
	Rapamune® PO	4.12	1.87	10413.00	9568.99	174205.67	202708.43
	Rapamycin SC	1.41	0.81	3056.00	2223.59	213818.00	59034.91
	rPS SC	5.36	1.29	4456.07	3642.81	81818.00	171878.11
M/Ms	Control	3.04	1.74	16120.07	3779.42	550666.67	160973.50
	PS SC	2.83	1.76	21727.67	9022.05	587000.00	242078.78
	Rapamune® PO	5.67	0.93	18541.67	10556.13	174205.67	202708.43
	Rapamycin SC	2.23	2.79	4613.98	5881.94	213818.00	59034.91
	rPS SC	10.28	1.68	8585.00	15900.79	81818.00	171878.11
Neutrophils	Control	4.13	3.31	22324.00	21155.23	550666.67	160973.50
	PS SC	5.89	6.13	43089.33	15872.99	587000.00	242078.78
	Rapamune® PO	12.23	4.56	27802.00	13705.20	174205.67	202708.43
	Rapamycin SC	7.72	2.12	16285.83	3864.42	213818.00	59034.91
	rPS SC	1.61	0.38	1343.79	2330.57	81818.00	171878.11
NK Cells	Control	1.22	0.30	6803.40	2461.39	550666.67	160973.50
	PS SC	1.09	0.28	3449.33	2559.90	587000.00	242078.78
	Rapamune® PO	1.40	0.83	2829.33	1796.20	174205.67	202708.43
	Rapamycin SC	1.01	0.21	2225.06	897.27	213818.00	59034.91
	rPS SC	1.61	0.38	1343.79	2330.57	81818.00	171878.11
T Cells	Control	51.87	10.33	289044.33	116447.72	550666.67	160973.50
	PS SC	51.50	12.07	204755.00	109870.50	587000.00	242078.78
	Rapamune® PO	39.63	10.38	105533.33	68482.31	174205.67	202708.43
	Rapamycin SC	55.97	11.63	120726.52	38272.54	213818.00	59034.91
	rPS SC	32.37	5.68	25613.48	44870.74	81818.00	171878.11

Table S4-18 | Costimulation in IG LN.

Marker	Treatment	Mean Percentage Marker+ Cells of CD45+ Cells	Standard Deviation of Percentage Marker+ Cells of CD45+ Cells	Mean Number of Marker+ Cells	Standard Deviation of Number of Marker+ Cells	Mean Number of CD45+ Cells	Standard Deviation of Number of CD45+ Cells
CD40+	Control	93.77	6.85	514154.67	154549.23	160973.50	160973.50
	PS SC	96.27	10.56	407775.33	204606.43	242078.78	242078.78
	Rapamune® PO	85.17	8.48	237573.67	149156.69	202708.43	202708.43
	Rapamycin SC	93.73	9.91	199647.69	53453.09	59034.91	59034.91
	rPS SC	63.87	8.25	51720.37	117374.14	171878.11	171878.11
CD80+	Control	77.27	12.50	415228.33	133035.87	160973.50	160973.50
	PS SC	86.13	11.08	325658.33	182050.10	242078.78	242078.78
	Rapamune® PO	67.87	11.82	209405.33	121159.31	202708.43	202708.43
	Rapamycin SC	79.50	8.42	168955.93	40686.90	59034.91	59034.91
	rPS SC	43.20	12.70	34601.65	115767.19	171878.11	171878.11
CD86+	Control	3.83	1.93	19126.03	7213.08	160973.50	160973.50
	PS SC	4.27	1.27	25139.00	10524.18	242078.78	242078.78
	Rapamune® PO	10.08	8.03	13199.67	11771.04	202708.43	202708.43
	Rapamycin SC	4.74	1.10	10066.01	3430.85	59034.91	59034.91
	rPS SC	4.98	1.30	4214.69	4592.02	171878.11	171878.11

Table S4-19 | DC subsets in IG LN.

DC Subsets	Treatment	Mean Percentage Subset+ Cells of DCs	Standard Deviation of Percentage Subset+ Cells of DCs	Mean Number of Subset+ Cells	Standard Deviation of Number of Subset+ Cells	Mean Number of DCs	Standard Deviation of Number DCs
cDCs	Control	82.77	7.00	4819.98	10720.96	5796.73	10991.88
	PS SC	86.53	4.09	19147.33	8439.45	20241.00	8773.17
	Rapamune® PO	94.77	2.82	9667.33	9026.94	10413.00	9568.99
	Rapamycin SC	84.80	5.50	2612.58	2154.25	3056.00	2223.59
	rPS SC	99.30	2.35	4425.11	3394.05	4456.07	3642.81
pDCs	Control	17.23	7.07	976.75	348.81	5796.73	10991.88
	PS SC	13.47	4.15	1070.67	474.47	20241.00	8773.17
	Rapamune® PO	5.16	2.68	731.00	544.47	10413.00	9568.99
	Rapamycin SC	15.20	5.55	443.42	141.82	3056.00	2223.59
	rPS SC	0.70	2.30	30.96	262.56	4456.07	3642.81
Mature DCs	Control	40.27	12.24	2365.44	5527.18	5796.73	10991.88
	PS SC	35.17	12.49	10723.00	4605.24	20241.00	8773.17
	Rapamune® PO	57.30	12.52	5683.33	5429.74	10413.00	9568.99
	Rapamycin SC	40.87	19.10	1276.22	1883.69	3056.00	2223.59
	rPS SC	98.30	15.36	4385.78	2348.47	4456.07	3642.81

Table S4-20 | M/Ms subsets in IG LN.

M/M Subsets	Treatment	Mean Percentage Subset+ Cells of M/Ms	Standard Deviation of Percentage Subset+ Cells of M/Ms	Mean Number of Subset+ Cells	Standard Deviation of Number of Subset+ Cells	Mean Number of M/Ms	Standard Deviation of Number M/Ms
Macrophages	Control	50.17	8.49	8044.19	2399.881159	16120.07	3779.42
	PS SC	41.93	10.43	11625.67	4724.903142	21727.67	9022.05
	Rapamune® PO	39.53	12.39	9164.67	5371.711359	18541.67	10556.13
	Rapamycin SC	54.57	3.77	2514.19	3520.687766	4613.98	5881.94
	rPS SC	26.27	14.72	2279.63	9419.812106	8585.00	15900.79
Ly6C^{Hi}M/Ms	Control	69.37	11.27	11105.21	1442.21	16120.07	3779.42
	PS SC	76.93	12.75	11251.67	5375.56	21727.67	9022.05
	Rapamune® PO	47.17	8.95	9950.00	5456.61	18541.67	10556.13
	Rapamycin SC	65.77	16.24	3036.62	1703.42	4613.98	5881.94
	rPS SC	0.84	21.54	66.07	6087.07	8585.00	15900.79
MHC II+ M/Ms	Control	51.43	15.89	8363.66	4871.36	16120.07	3779.42
	PS SC	42.43	17.47	16641.00	7150.23	21727.67	9022.05
	Rapamune® PO	66.70	7.61	13846.33	7894.57	18541.67	10556.13
	Rapamycin SC	60.50	10.05	2795.32	4988.71	4613.98	5881.94
	rPS SC	99.63	13.14	8557.30	12151.83	8585.00	15900.79

Table S4-21 | T cell subsets in IG LN.

T Cell Subsets	Treatment	Mean Percentage Subset+ Cells of T Cells	Standard Deviation of Percentage Subset+ Cells of T Cells	Mean Number of Subset+ Cells	Standard Deviation of Number of Subset+ Cells	Mean Number of T Cells	Standard Deviation of Number T Cells
CD4+ T Cells	Control	45.67	8.65	132322.98	47863.06	289044.33	116447.72
	PS SC	46.10	7.14	104618.33	45781.39	204755.00	109870.50
	Rapamune® PO	58.07	8.46	61414.33	42299.13	105533.33	68482.31
	Rapamycin SC	39.37	14.39	46274.44	8486.20	120726.52	38272.54
	rPS SC	23.33	21.94	2825.47	33575.49	25613.48	44870.74
CD4+ CD8- T Cells	Control	45.40	8.66	17969.05	56222.08	289044.33	116447.72
	PS SC	45.83	7.53	104245.00	47076.70	289044.33	116447.72
	Rapamune® PO	56.17	8.35	61013.67	42282.34	204755.00	109870.50
	Rapamycin SC	38.60	14.66	5253.41	20227.28	105533.33	68482.31
	rPS SC	10.97	28.58	257.56	34775.83	120726.52	38272.54
CD4+ Tregs	Control	6.17	1.69	92909.26	51873.48	25613.48	44870.74
	PS SC	5.58	2.60	6393.67	46554.04	289044.33	116447.72
	Rapamune® PO	5.96	3.23	4359.33	12921.71	204755.00	109870.50
	Rapamycin SC	4.46	0.98	50839.05	28671.81	105533.33	68482.31
	rPS SC	0.97	1.28	16888.56	7786.85	120726.52	38272.54
CD8+ Cells	Control	32.07	4.87	91975.50	38562.24	25613.48	44870.74
	PS SC	34.37	6.98	51788.33	36480.41	289044.33	116447.72
	Rapamune® PO	28.50	8.06	29745.67	16194.11	204755.00	109870.50
	Rapamycin SC	42.03	12.34	49956.23	22477.04	105533.33	68482.31
	rPS SC	66.67	24.35	13664.29	9302.63	120726.52	38272.54
CD8+ CD4- T Cells	Control	31.77	4.80	156.82	36883.53	289044.33	116447.72
	PS SC	34.13	6.19	51415.00	28753.48	204755.00	109870.50
	Rapamune® PO	26.57	8.12	29345.00	16124.90	105533.33	68482.31
	Rapamycin SC	41.30	12.08	35.90	8673.38	120726.52	38272.54
	rPS SC	54.27	18.01	210.32	14539.47	25613.48	44870.74
CD8+ Tregs	Control	0.06	0.02	831.92	501.62	289044.33	116447.72
	PS SC	0.06	3.26	88.67	475.96	204755.00	109870.50
	Rapamune® PO	2.17	2.56	784.00	530.74	105533.33	68482.31
	Rapamycin SC	0.03	0.04	893.39	483.18	120726.52	38272.54
	rPS SC	0.78	0.43	3217.15	1835.22	25613.48	44870.74
DP T Cells	Control	0.28	0.10	9411.70	5264.24	289044.33	116447.72
	PS SC	0.28	1.01	462.67	3900.35	204755.00	109870.50
	Rapamune® PO	2.10	1.49	474.33	1116.21	105533.33	68482.31
	Rapamycin SC	0.74	0.26	2993.29	1819.89	120726.52	38272.54
	rPS SC	12.37	6.74	1224.31	647.13	25613.48	44870.74
NK T Cells	Control	3.29	0.67	418481798.61	302962489.20	289044.33	116447.72
	PS SC	2.44	2.50	4775.33	207043573.78	204755.00	109870.50
	Rapamune® PO	6.96	3.83	3930.33	62424848.97	105533.33	68482.31
	Rapamycin SC	2.39	1.20	58749218.06	37946612.20	120726.52	38272.54
	rPS SC	4.67	1.17	747665.84	461104.60	25613.48	44870.74

Table S4-22 | Cell type overview in the spleen.

Cell Type	Treatment	Mean Percentage Cell Type+ Cells of CD45+ Cells	Standard Deviation of Percentage Cell Type+ Cells of CD45+ Cells	Mean Number of Cell Type+ Cells	Standard Deviation of Number of Cell Type+ Cells	Mean Number of CD45+ Cells	Standard Deviation of Number of CD45+ Cells
B Cells	Control	54.43	11.09	65659.67	45382.27	645070.67	329724.69
	PS SC	54.53	9.61	37886.00	54898.61	718000.00	324786.78
	Rapamune® PO	40.77	3.24	24953.00	169524.76	56639.33	408233.32
	Rapamycin SC	54.33	11.65	29099.00	56053.78	687333.33	312143.67
	rPS SC	48.00	5.99	5083.00	111546.23	32851.00	237932.38
DCs	Control	10.58	7.22	329097.33	188360.08	645070.67	329724.69
	PS SC	5.28	2.83	391735.33	208108.26	718000.00	324786.78
	Rapamune® PO	5.80	3.67	3445.00	41941.23	56639.33	408233.32
	Rapamycin SC	4.42	3.63	357498.33	199089.25	687333.33	312143.67
	rPS SC	19.13	9.62	14995.00	17631.79	32851.00	237932.38
M/Ms	Control	6.29	2.77	38670.00	25221.35	645070.67	329724.69
	PS SC	3.37	0.79	24188.67	10546.17	718000.00	324786.78
	Rapamune® PO	5.63	1.73	3021.33	19012.60	56639.33	408233.32
	Rapamycin SC	3.71	0.90	24737.67	10931.85	687333.33	312143.67
	rPS SC	18.27	7.26	5857.00	11810.98	32851.00	237932.38
Neutrophils	Control	12.23	3.14	77884.00	41701.45	645070.67	329724.69
	PS SC	10.17	1.76	73023.67	34975.20	718000.00	324786.78
	Rapamune® PO	9.61	3.44	5048.33	41129.87	56639.33	408233.32
	Rapamycin SC	11.36	6.64	76977.00	43632.63	687333.33	312143.67
	rPS SC	1.15	0.82	624.00	893.88	32851.00	237932.38
NK Cells	Control	1.57	1.13	10189.00	4850.41	645070.67	329724.69
	PS SC	1.74	0.29	12535.00	6136.78	718000.00	324786.78
	Rapamune® PO	1.62	0.61	1356.33	1191.59	56639.33	408233.32
	Rapamycin SC	2.53	0.98	17188.33	8936.87	687333.33	312143.67
	rPS SC	1.15	0.82	624.00	893.88	32851.00	237932.38
T Cells	Control	21.30	4.95	137928.33	71386.06	645070.67	329724.69
	PS SC	26.03	6.83	186784.33	84242.12	718000.00	324786.78
	Rapamune® PO	30.63	10.66	17687.67	37875.63	56639.33	408233.32
	Rapamycin SC	21.93	8.88	154654.00	86632.37	687333.33	312143.67
	rPS SC	24.97	12.44	6026.00	17287.68	32851.00	237932.38

Table S4-23 | Costimulation in the spleen.

Marker	Treatment	Mean Percentage Marker+ Cells of CD45+ Cells	Standard Deviation of Percentage Marker+ Cells of CD45+ Cells	Mean Number of Marker+ Cells	Standard Deviation of Number of Marker+ Cells	Mean Number of CD45+ Cells	Standard Deviation of Number of CD45+ Cells
CD40+	Control	43.20	4.93	279502.67	145669.40	645070.67	329724.69
	PS SC	56.50	14.44	405457.67	185760.19	718000.00	324786.78
	Rapamune® PO	45.43	18.68	25718.33	287087.75	56639.33	408233.32
	Rapamycin SC	56.07	15.43	380779.67	182124.92	687333.33	312143.67
	rPS SC	73.57	20.52	27710.67	118337.10	32851.00	237932.38
CD80+	Control	28.00	10.63	179108.00	90468.40	645070.67	329724.69
	PS SC	32.13	8.12	230656.67	98251.95	718000.00	324786.78
	Rapamune® PO	45.13	19.87	26373.00	63616.46	56639.33	408233.32
	Rapamycin SC	24.57	7.57	170064.33	82917.17	687333.33	312143.67
	rPS SC	9.32	16.44	4595.67	100231.79	32851.00	237932.38
CD86+	Control	22.13	10.80	138730.33	91987.97	645070.67	329724.69
	PS SC	11.91	10.62	85617.00	36457.62	718000.00	324786.78
	Rapamune® PO	27.93	6.67	15363.33	120268.01	56639.33	408233.32
	Rapamycin SC	14.18	11.30	92044.00	56169.93	687333.33	312143.67
	rPS SC	47.03	16.89	11505.00	55079.18	32851.00	237932.38

TableS24 | DC subsets in the spleen.

DC Subsets	Treatment	Mean Percentage Subset+ Cells of DCs	Standard Deviation of Percentage Subset+ Cells of DCs	Mean Number of Subset+ Cells	Standard Deviation of Number of Subset+ Cells	Mean Number of DCs	Standard Deviation of Number DCs
cDCs	Control	95.30	2.02	63030.00	50019.07	329097.33	188360.08
	PS SC	93.53	2.80	35588.00	16810.90	391735.33	208108.26
	Rapamune® PO	99.17	3.23	3421.33	41207.26	3445.00	41941.23
	Rapamycin SC	95.44	1.38	27862.33	18666.23	357498.33	199089.25
	rPS SC	98.83	0.94	5021.00	16342.97	14995.00	17631.79
pDCs	Control	4.70	2.07	2499.33	1619.72	329097.33	188360.08
	PS SC	6.47	2.84	2459.33	1318.67	391735.33	208108.26
	Rapamune® PO	0.78	3.23	22.67	723.04	3445.00	41941.23
	Rapamycin SC	4.56	1.42	1316.00	639.44	357498.33	199089.25
	rPS SC	1.17	0.90	51.00	316.12	14995.00	17631.79
Mature DCs	Control	77.10	6.07	52178.33	42295.69	329097.33	188360.08
	PS SC	71.37	11.22	27055.00	13012.30	391735.33	208108.26
	Rapamune® PO	91.53	3.51	3185.67	38229.17	3445.00	41941.23
	Rapamycin SC	85.63	4.72	24960.00	18131.59	357498.33	199089.25
	rPS SC	98.20	3.48	4994.67	15388.09	14995.00	17631.79

Table S4-25 | M/Ms subsets in liver.

M/M Subsets	Treatment	Mean Percentage Subset+ Cells of M/Ms	Standard Deviation of Percentage Subset+ Cells of M/Ms	Mean Number of Subset+ Cells	Standard Deviation of Number of Subset+ Cells	Mean Number of M/Ms	Standard Deviation of Number M/Ms
Macrophages	Control	28.80	23.13	14002.00	12503.00	38670.00	25221.35
	PS SC	21.43	19.91	5213.67	3138.05	24188.67	10546.17
	Rapamune® PO	58.33	15.92	1819.00	15108.23	3021.33	19012.60
	Rapamycin SC	33.57	23.28	8379.00	4519.09	24737.67	10931.85
	rPS SC	79.93	10.37	4877.00	8979.77	5857.00	11810.98
Ly6C^{Hi}M/Ms	Control	40.60	14.57	12341.33	6448.84	38670.00	25221.35
	PS SC	64.83	21.58	15635.00	7776.33	24188.67	10546.17
	Rapamune® PO	32.67	15.08	962.67	3515.43	3021.33	19012.60
	Rapamycin SC	59.70	23.63	14556.67	7586.83	24737.67	10931.85
	rPS SC	1.00	8.13	87.33	1935.23	5857.00	11810.98
MHC II+ M/Ms	Control	93.40	3.45	36341.00	23834.14	38670.00	25221.35
	PS SC	85.33	7.63	20652.67	8947.65	24188.67	10546.17
	Rapamune® PO	99.23	0.47	2998.00	18687.92	3021.33	19012.60
	Rapamycin SC	88.23	5.61	21823.33	9501.53	24737.67	10931.85
	rPS SC	99.43	0.40	5815.67	11700.44	5857.00	11810.98

Table S4-26 | T cell subsets in spleen.

T Cell Subsets	Treatment	Mean Percentage Subset+ Cells of T Cells	Standard Deviation of Percentage Subset+ Cells of T Cells	Mean Number of Subset+ Cells	Standard Deviation of Number of Subset+ Cells	Mean Number of T Cells	Standard Deviation of Number T Cells
CD4+ T Cells	Control	52.40	27.27	72980.67	41515.76	137928.33	71386.06
	PS SC	53.27	28.20	99608.33	54369.30	186784.33	84242.12
	Rapamune® PO	0.69	1.98	126.33	1939.20	17687.67	37875.63
	Rapamycin SC	49.73	24.72	78707.00	47905.98	154654.00	86632.37
	rPS SC	6.90	3.60	525.67	1417.90	6026.00	17287.68
CD4+ CD8- T Cells	Control	4.18	2.10	72686.33	41463.31	137928.33	71386.06
	PS SC	5.04	2.62	99254.67	54697.79	186784.33	84242.12
	Rapamune® PO	0.18	0.08	33.33	50.77	17687.67	37875.63
	Rapamycin SC	49.23	27.11	78015.00	48004.31	154654.00	86632.37
	rPS SC	4.51	3.24	376.00	805.44	6026.00	17287.68
CD4+ Tregs	Control	52.23	27.95	5913.00	3461.56	137928.33	71386.06
	PS SC	53.07	28.93	9389.00	5048.76	186784.33	84242.12
	Rapamune® PO	0.16	0.23	24.67	230.45	17687.67	37875.63
	Rapamycin SC	2.30	0.99	3461.67	1981.65	154654.00	86632.37
	rPS SC	0.26	0.14	14.00	29.27	6026.00	17287.68
CD8+ Cells	Control	36.43	7.77	49571.00	25044.13	137928.33	71386.06
	PS SC	34.63	8.16	64538.00	28707.59	186784.33	84242.12
	Rapamune® PO	38.27	16.03	6844.00	4784.38	17687.67	37875.63
	Rapamycin SC	31.23	13.04	48548.67	28726.69	154654.00	86632.37
	rPS SC	80.83	29.89	4226.33	5086.62	6026.00	17287.68
CD8+ CD4- T Cells	Control	36.20	7.89	49264.33	24901.99	137928.33	71386.06
	PS SC	34.43	8.01	64164.33	28560.80	186784.33	84242.12
	Rapamune® PO	38.10	15.98	6810.67	4738.45	17687.67	37875.63
	Rapamycin SC	30.70	12.90	47813.67	28368.55	154654.00	86632.37
	rPS SC	78.43	29.34	4073.67	4465.12	6026.00	17287.68
CD8+ Tregs	Control	0.13	0.35	166.33	84.34	137928.33	71386.06
	PS SC	0.10	0.71	185.67	92.40	186784.33	84242.12
	Rapamune® PO	0.74	1.70	51.67	85.55	17687.67	37875.63
	Rapamycin SC	0.48	5.46	443.00	279.66	154654.00	86632.37
	rPS SC	0.43	1.05	22.33	670.57	6026.00	17287.68
DP T Cells	Control	0.23	0.26	306.67	146.37	137928.33	71386.06
	PS SC	0.20	0.16	373.67	153.50	186784.33	84242.12
	Rapamune® PO	0.18	0.08	33.33	50.77	17687.67	37875.63
	Rapamycin SC	0.53	0.24	735.00	391.83	154654.00	86632.37
	rPS SC	2.44	1.12	152.67	777.84	6026.00	17287.68
NK T Cells	Control	8.05	4.47	11048.33	6388.92	137928.33	71386.06
	PS SC	9.92	9.85	17355.00	9074.11	186784.33	84242.12
	Rapamune® PO	12.82	13.46	497.33	351.49	17687.67	37875.63
	Rapamycin SC	11.57	9.57	18372.00	11360.73	154654.00	86632.37
	rPS SC	14.60	7.26	1086.00	993.40	6026.00	17287.68

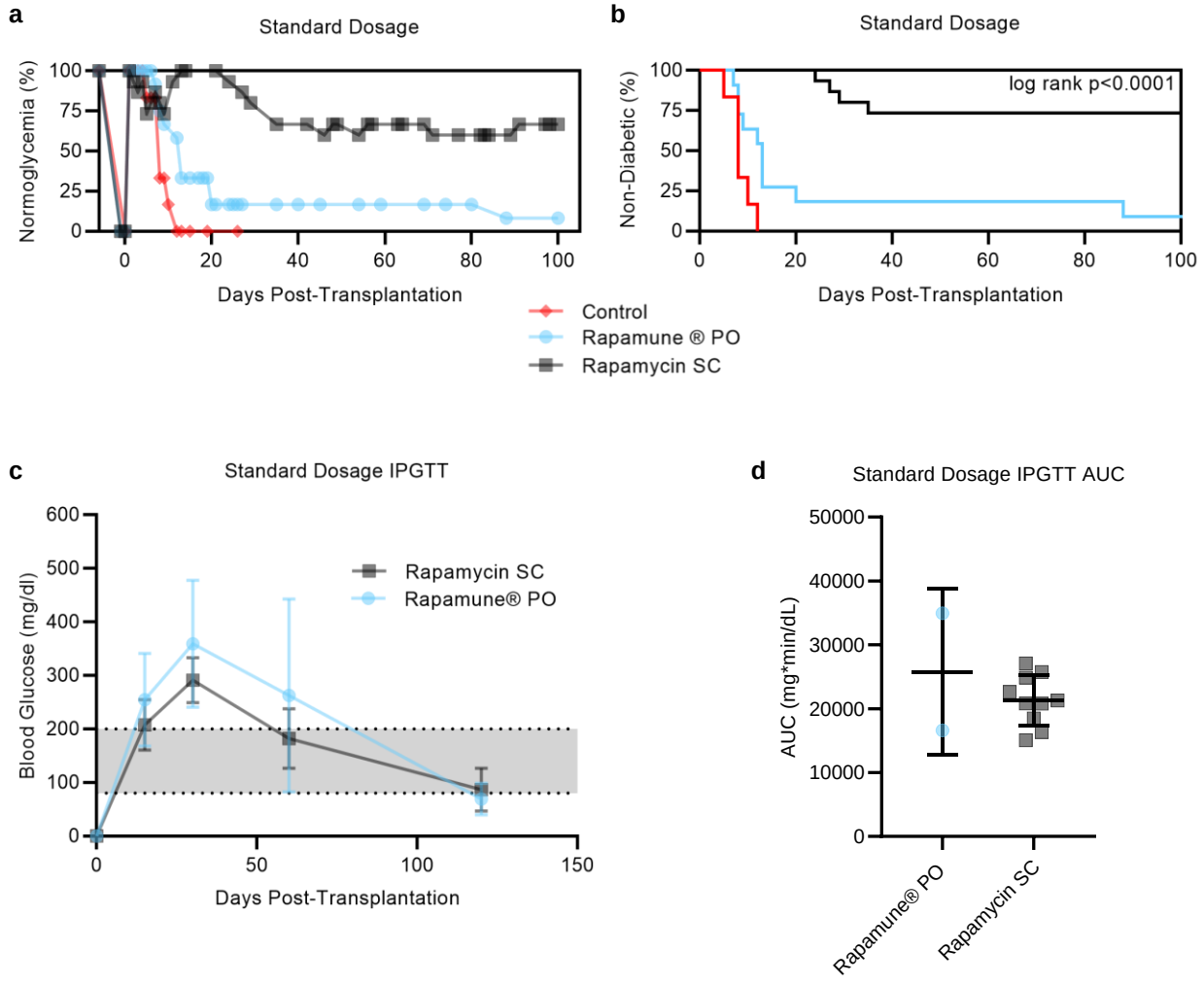

Figure S4-5 | Islet Transplantation: Standard dosage protocol normoglycemia and Intraperitoneal glucose tolerance test (IPGTT). Diabetes was induced (day -5) via streptozotocin (STZ) injection. Rapamycin was given in accordance with the standard dosage protocol, consisting of 11 doses, given daily starting at day -1. Mice were treated with: Rapamune® oral gavage (PO) or rapamycin (in 0.2% carboxymethyl cellulose) subcutaneous injection (SC). Regardless of protocol, each dose consisted of 1 mg rapamycin per kg body weight per dose, formulated at a concentration of 0.125 mg rapamycin per mL. Polymersome formulations contained 6.7 mg polymer per mL. A cohort of mice was left as an untreated control. **a,** Post-transplantation normoglycemia (%) (blood glucose < 200 mg/dl) following islet transplantation for low dosage protocol. No treatment (♦); Rapamune® PO (●); rapamycin SC (■) ($n \geq 12$ mice/group). **b,** Kaplan-Meier analysis of non-diabetic survival. Diabetes was defined as two consecutive blood glucose measurements < 400 mg/dl. ($n \geq 12$ mice/group). Statistical analysis was performed using the Mantel-Cox Log-rank test. **c,d,** If mice were normoglycemic at 30 days post-transplantation, an intraperitoneal glucose tolerance test (IPGTT) was performed. Mice were fasted for 16 h. The animals were fasted for 16 h before being injected intraperitoneally with 2 g dextrose (in 200 g/L solution) per kg body weight. Blood glucose concentrations were measured at 0, 15, 30, 60- and 120-minutes post-injection. Blood glucose curves were plotted (**c**) and the area under the curve was analyzed (**d**). All data are presented as mean percentage ± SD. Significant p-values relative to the rPS treatment are displayed on graphs. Statistical significance was determined by one-way (**d**) or two-way (**c**) ANOVA with Tukey's multiple comparisons test. (n = 2 mice for Rapamune® PO group and n = 10 mice for the rapamycin SC group).

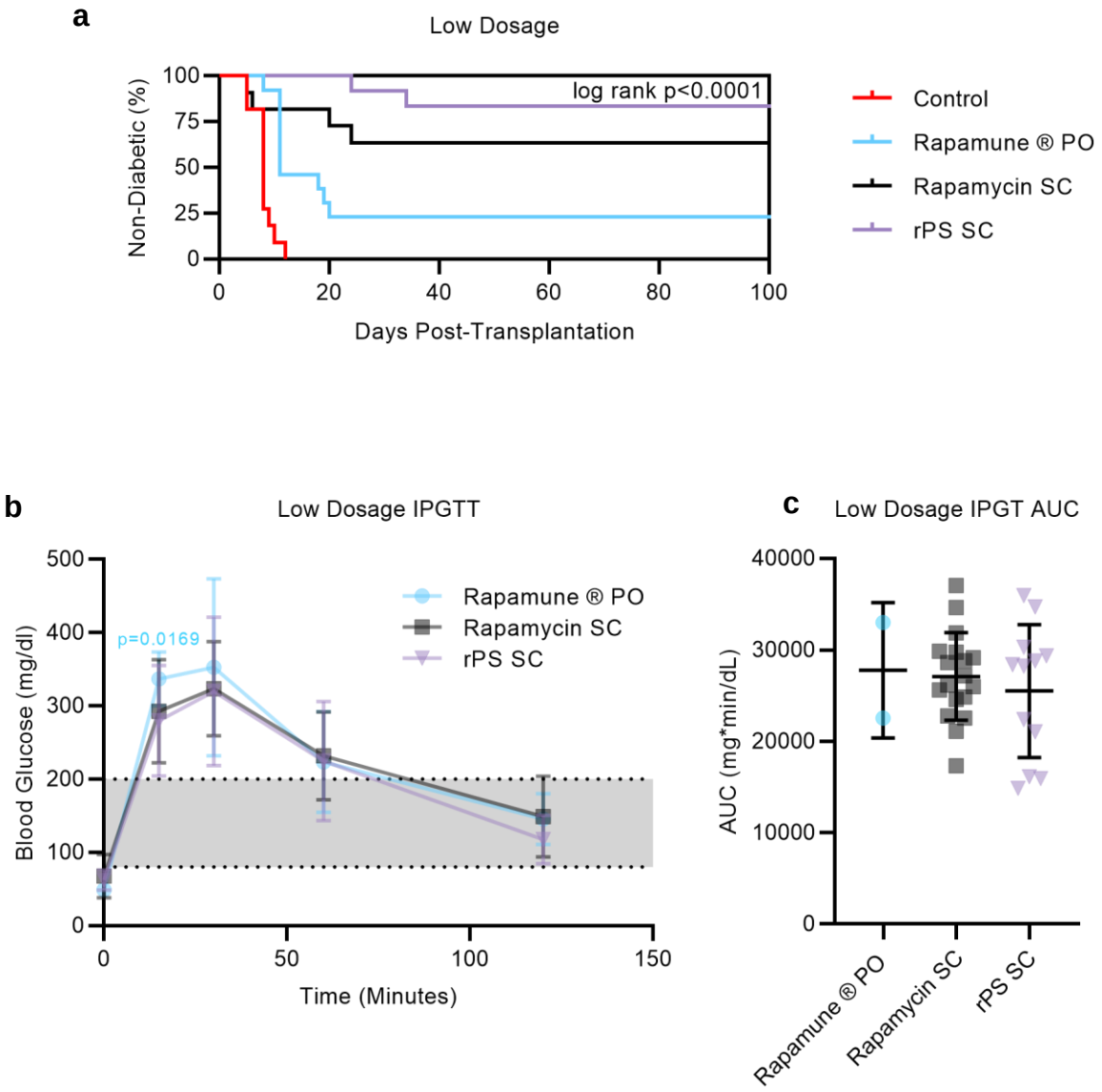

Figure S4-6 | Islet Transplantation: Low dosage protocol normoglycemia and Intraperitoneal glucose tolerance test (IPGTT). Diabetes was induced (day -5) via streptozotocin (STZ) injection. Rapamycin was given in accordance with the standard dosage protocol, consisting of 11 doses, given daily starting at day -1. Mice were treated with: Rapamune® oral gavage (PO), rapamycin (in 0.2% carboxymethyl cellulose) subcutaneous injection (SC), or rapamycin-loaded polymersomes (rPS) SC. Regardless of protocol, each dose consisted of 1 mg rapamycin per kg body weight per dose, formulated at a concentration of 0.125 mg rapamycin per mL. Polymersome formulations contained 6.7 mg polymer per mL. A cohort of mice was left as an untreated control. **a,** Kaplan-Meier analysis of non-diabetic survival. Diabetes was defined as two consecutive blood glucose measurements < 400 mg/dl. ($n \geq 12$ mice/group). Statistical analysis was performed using the Mantel-Cox Log-rank test. ($n \geq 12$ mice/group). **b,c,** If mice were normoglycemic at 30 days post-transplantation, an intraperitoneal glucose tolerance test (IPGTT) was performed. Mice were fasted for 16 h. The animals were fasted for 16 h before being injected intraperitoneally with 2 g dextrose (in 200 g/L solution) per kg body weight. Blood glucose concentrations were measured at 0, 15, 30, 60- and 120-minutes post-injection. Blood glucose curves were plotted (**b**) and the area under the curve was analyzed (**c**). All data are presented as mean percentage ± SD. Significant p-values relative to the rPS treatment are displayed on graphs. Statistical significance was determined by one-way (**c**) or two-way (**b**) ANOVA with Tukey's multiple comparisons test. (n = 2 mice for Rapamune® PO group, n = 18 mice for the rapamycin SC group, n = 12 mice for the rPS SC group).

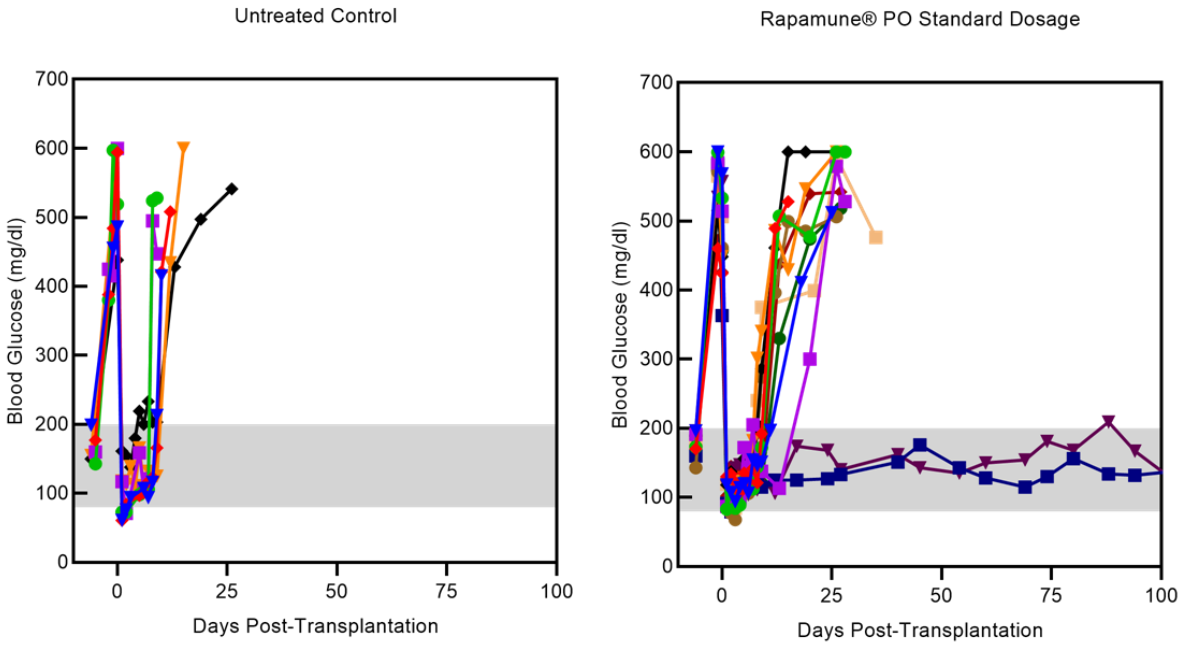

Figure S4-7 | |Islet Transplantation: Blood glucose data by treatment. Diabetes was induced (day -5) via streptozotocin (STZ) injection. The standard dosage protocol consists of 11 doses, given daily starting at day -1. The low dosage protocol consists of 6 doses, given every 3 days, starting at day -1. Mice were treated with: Rapamune® oral gavage (PO), rapamycin (in 0.2% carboxymethyl cellulose) subcutaneous injection (SC), or rapamycin-loaded polymersomes (rPS) SC. Regardless of protocol, each dose consisted of 1 mg rapamycin per kg body weight per dose, formulated at a concentration of 0.125 mg rapamycin per mL. PS formulations contained 6.7 mg polymer per mL. A cohort of mice was left as an untreated control. Normoglycemic range (blood glucose < 200 mg/dl) is indicated by gray shading. Each colored line represents an individual mouse ($n \geq 12$ mice/group).

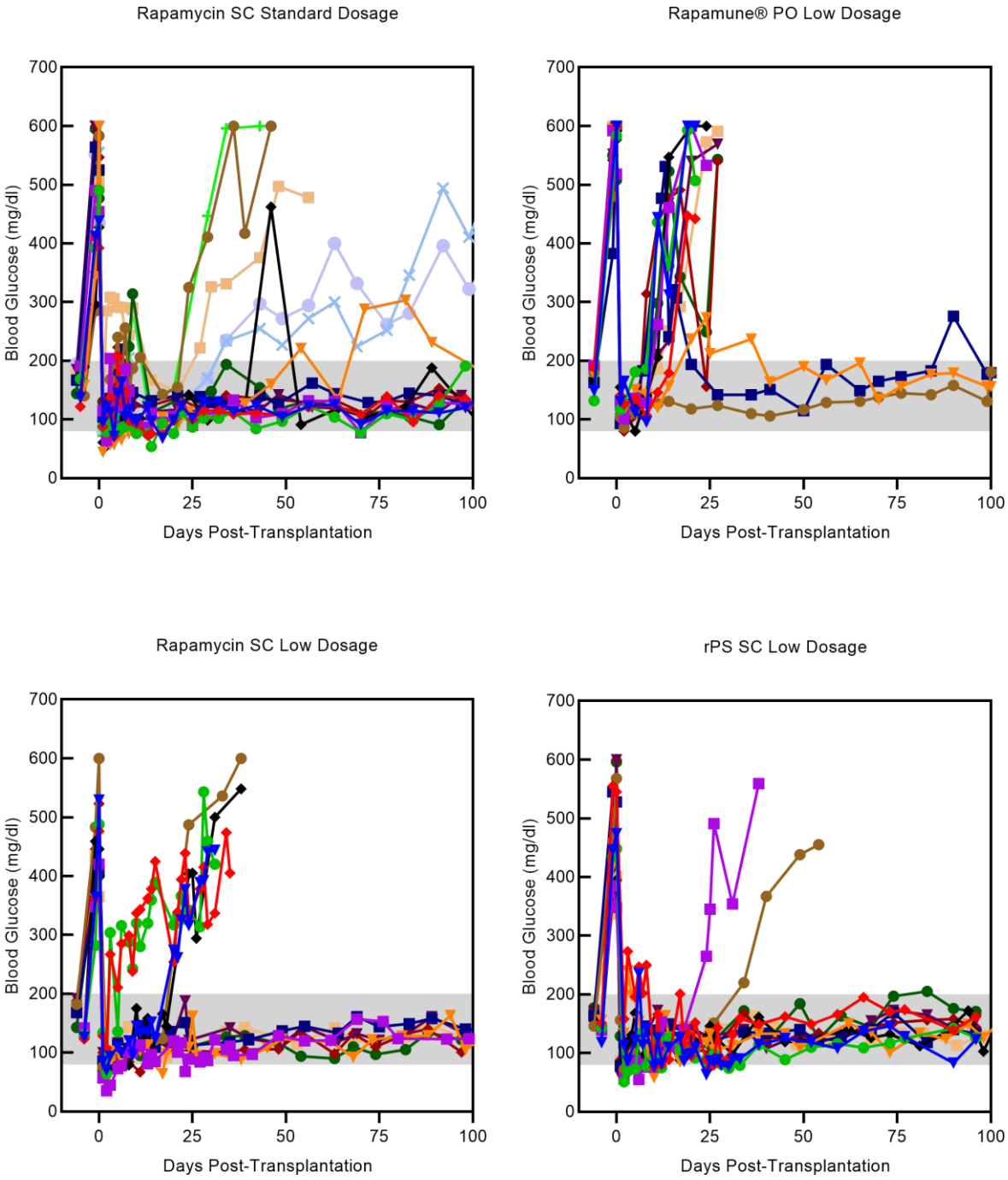

S4-7 | Islet Transplantation: Blood glucose data by treatment (continued).

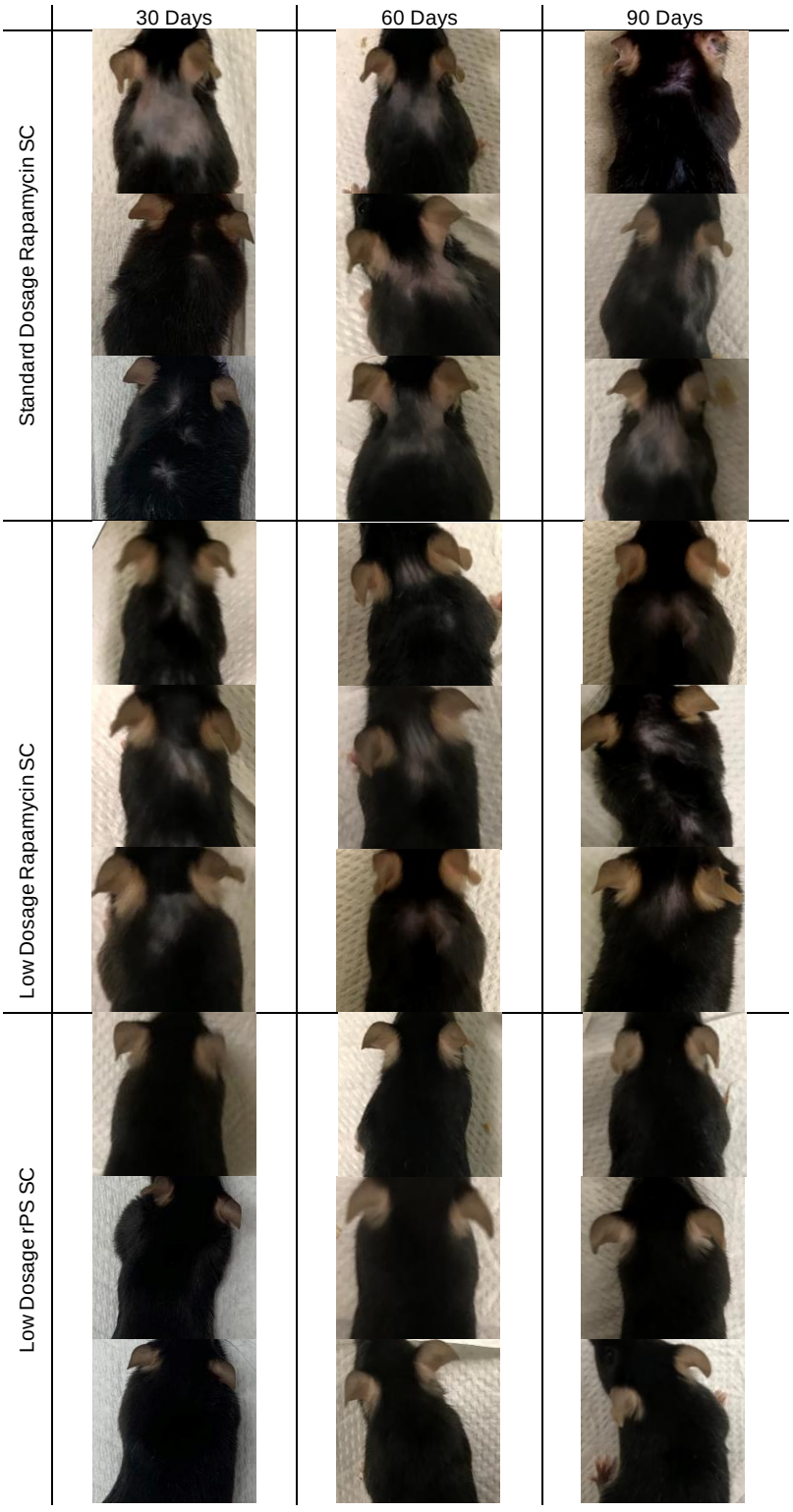

Figure S4-8 | rPS reduce injection site alopecia associated with rapamycin. Photos were taken approximately 30-, 60- or 90-days post-transplantation (n = 5-7 mice/group/timepoint; n = 3 representative images/group/timepoint shown).

Table S4-27 | Single-cell RNA sequencing analysis workflow

Workflow	Program	Command Line
Quality Control	FastQC v0.11.5	fastqc <input_path_to/untrimmed.fq.gz>
Trimming and Filtering	Trimmomatic v0.39	java -jar ./Trimmomatic-0.39/trimmomatic-0.39.jar SE -threads 16 -phred33 <input_path_to/untrimmed.fq.gz> <output_path_to/trimmed.fq.gz> ILLUMINACLIP:TruSeq3-SE.fa:2:30:10 LEADING:30 TRAILING:30 MINLEN:36 TruSeq3-PE_custom.fa: >TruSeq3_IndexedAdapter AGATCGGAAGAGCACACGTCTGAACTCCAGTCAC >TruSeq3_UniversalAdapter AGATCGGAAGAGCGTCGTGTAGGGAAAGAGTGTA
Alignment	STAR v2.7.5a	STAR --runThreadN 16 --runMode genomeGenerate --genomeDir ./ --genomeFastaFiles ../genome_fasta/GRCm39.primary_assembly.genome.fa --sjdbGTFfile ../GTF/gencode.vM27.primary_assembly.annotation.gtf --sjdbOverhang 149 --outFileNamePrefix mouse_ STAR --genomeDir ../star_index/ --readFilesCommand zcat --readFilesIn $first_read $second_read --outFilterType BySJout --runThreadN 16 --outFilterMultimapNmax 100 --alignSJoverhangMin 8 --alignSJDBoverhangMin 1 --outFilterMismatchNoverLmax 0.05 --alignIntronMin 20 --alignIntronMax 1000000 --alignMatesGapMax 1000000 --outSAMattributes NH HI NM MD --outSAMstrandField intronMotif --outSAMmapqUnique 60 --outSAMtype BAM SortedByCoordinate --limitBAMsortRAM 30000000000 --outFileNamePrefix ../star_sam/$sample_name
Quantification and Differential Expression Analysis	Cufflinks v2.2.1	cuffdiff -L NT,PS,R,RO,RPS -o ../cuffdiff_results/ -p 16 -b ../genome_fasta/GRCm39.primary_assembly.genome.fa -u ../GTF/gencode.vM27.primary_assembly.annotation.gtf NT12_S8_Aligned.bam,NT3_S3_Aligned.bam,NT1_S1_Aligned.bam, NT5_S4_Aligned.bam,NT11_S7_Aligned.bam,NT2_S2_Aligned.bam, NT8_S5_Aligned.bam,PS10_S13_Aligned.bam,PS6_S10_Aligned.bam, PS7_S11_Aligned.bam,PS9_S12_Aligned.bam,R11_S27_Aligned.bam, R2_S21_Aligned.bam,R4_S22_Aligned.bam,R5_S23_Aligned.bam, R6_S24_Aligned.bam,R8_S25_Aligned.bam,RO11_S20_Aligned.bam, RO5_S16_Aligned.bam,RO9_S19_Aligned.bam,RO6_S17_Aligned.bam, RO4_S15_Aligned.bam,RO7_S18_Aligned.bam,rPS3_S28_Aligned.bam, rPS4_S29_Aligned.bam,rPS5_S30_Aligned.bam,rPS6_S31_Aligned.bam, rPS7_S32_Aligned.bam,rPS8_S33_Aligned.bam,rPS9_S34_Aligned.bam

Table S4-28 | RNA sequencing raw data

Gene	Ensembl ID	Locus	Control vs PS SC Fold Change	Control vs Rapamune® PO Fold Change	Control vs Rapamycin SC Fold Change	Control vs rPS SC Fold Change
Ifit2	ENSMUSG00000045932.13	chr19:34528093-34553819	-0.16812	-0.449048	-0.79862	-0.34577
Slc25a37	ENSMUSG00000034248.8	chr14:69479296-69542804	-0.30591	-0.451367	0.723812	-0.15704
Pdzk1ip1	ENSMUSG00000028716.16	chr4:114945904-114951096	-0.29834	-1.58357	1.79031	0.922634
Slc43a1	ENSMUSG00000027075.17	chr2:84669193-84693938	-0.15346	-0.25095	1.03722	0.05678
Tal1	ENSMUSG00000028717.13	chr4:114913622-114928952	-0.80673	-1.01849	1.19684	0.379855
Xpo7	ENSMUSG00000022100.15	chr14:70884741-71015935	-0.31965	-0.430267	0.682542	0.040165
Ier3	ENSMUSG00000003541.7	chr17:36132575-36133815	-0.88467	-1.00099	-1.07322	-0.46079
Trib1	ENSMUSG00000032501.10	chr15:59520198-59528948	-0.46021	-0.87728	-0.60288	-0.20376

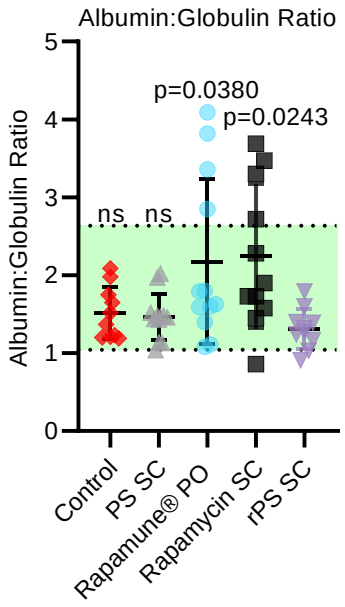

Figure S4-9 | rPS treatment does not alter the albumin: globulin ratio. Mice were treated with: polymersomes (PS; ▲) subcutaneous injection (SC), Rapamune® (●) oral gavage (PO), rapamycin (in 0.2% carboxymethyl cellulose; ■) SC, or rapamycin-loaded polymersomes (rPS; ▼) SC, using the standard dosage protocol (11 doses, over 11 days, 1 mg rapamycin per kg body weight per dose or equivalent volume (Table S4-1), formulated at 0.125 mg rapamycin per mL, PS and rPS formulations contained 6.7 mg polymer per mL). A cohort of mice were left as an untreated control (♦). Serum was analyzed for albumin via ELISA and total protein via colorimetric protein assay. The globulin concentration was determined by subtracting the albumin concertation from the total protein concentration. The albumin: globulin ratio was determined by dividing the albumin concentration (mg/mL) by the globulin concentration (mg/mL). All data are presented as mean ratio ± SD. Significant p-values relative to the rPS treatment are displayed on the graph. Statistical significance was determined by one-way ANOVA with Tukey's multiple comparisons test. (n = 10-12 mice/group).

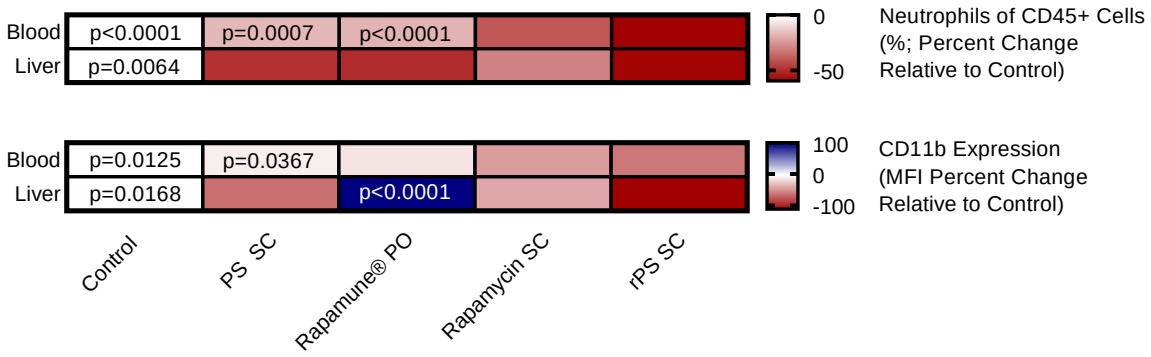

Figure S4-10 | rPS treatment mitigates neutrophils and their migration in blood and liver. Mice were treated with: polymersomes (PS) subcutaneous injection (SC), Rapamune® oral gavage (PO), rapamycin (in 0.2% carboxymethyl cellulose) SC, or rapamycin-loaded polymersomes (rPS) SC, using the standard dosage protocol (11 doses, over 11 days, 1 mg rapamycin per kg body weight per dose or equivalent volume (Table S4-1), formulated at 0.125 mg rapamycin per mL, PS and rPS formulations contained 6.7 mg polymer per mL). A cohort of mice was left as an untreated control. Cell populations were analyzed by flow cytometry. Left: Percentage of neutrophils of CD45+ cells in blood and liver. All data are presented as mean percentage change of percentage (of CD45+ cells) relative to control. **** $p<0.0001$, *** $p<0.001$, ** $p<0.01$ relative to rPS treatment. Right: CD11b expression by neutrophils in the blood and liver. All data are presented as mean percent change of mean median fluorescent intensity (211) relative to control with. **** $p<0.0001$, *** $p<0.001$, *$p<0.05$ relative to rPS treatment.

4.7 Publication Information

Sections of this chapter have been published with the following citation information:

Burke JA, Zhang X, Bobbala S, Frey MA, Furentes CB, Haddad HF, Allen SD, Richardson R, Ameer GA, Scott EA. Subcutaneous nanotherapy repurposes the immunosuppressive mechanism of rapamycin to enhance allogeneic islet graft viability. *Nat. Nanotechnol.* In Press. DOI: 10.21203/rs.3.rs-92015/v1.

CHAPTER 5: ANTI-POLY(ETHYLENE GLYCOL) ANTIBODIES AND POLY(ETHYLENE GLYCOL)-BASED THERAPEUTIC STRATEGIES

5.1 Abstract

PEG is a non-toxic, hydrophilic polymer that has become widely used in household and pharmaceutical products due to its ability to increase solubility and overcome rapid clearance by making drugs stealth to the immune system. it had been initially thought that PEG was non-immunogenic, development of anti-PEG antibodies in humans is associated with daily exposure to PEG-containing products. This has become problematic as PEG-based drugs, including the COVID-19 vaccine, are not tested on animals with αPEG antibodies, thus when these therapeutics reach the clinical stage, adverse effects can occur. Herein, we describe two mouse models for the assessment of PEG-based products. Via exposure to PEG, we stimulate adjuvant-free production of αPEG antibodies, thus mimicking native immune response. Additionally, we use a passive transfer method to create a stable and controlled model for drug assessment.

5.2 Introduction

PEG is a biocompatible polymer widely used in the food, cosmetic and pharmaceutical industries due to its low toxicity, solubility, and viscosity properties (52). Over the past forty years, a technique referred to as PEGylation has been established to covalently attach PEG chains to the surface of various materials. PEGylation has been shown to increase circulation time and therapeutic efficiency and to decrease cytotoxicity and immunogenicity (61). The technique has been applied to a variety of therapeutic agents, and currently, there are over 10 PEGylated drugs approved by the FDA (64). A notable example of a PEGylated therapeutic is Doxil®, which is a

PEGylated liposomal form of the cancer drug doxorubicin. Approved by the FDA in 1995, Doxil was the first nano-drug to come to the market in the United States. Currently, Doxil is approved for the treatment of ovarian cancer, Kaposi's

Although in early studies PEG was thought to have no immunogenicity nor antigenicity (61), there has been an increased number of reports on the correlation between the presence of αPEG antibodies and loss of therapeutic efficacy. In an open-label phase I trial of PEG-uricase (10kDa mPEG) as a treatment for patients with chronic gout, 5 out of 13 (38%) patients developed αPEG immunoglobulin G (**IgG**) and M (**IgM**) after a single subcutaneous (**SC**) injection (95). Additionally, repeated injections of PEGylated solid lipid nanoparticles (containing 5, 10, and 20%mol mPEG2kDa-DSPE) induced accelerated blood clearance in beagles and mice due to the induction of αPEG IgM (75).

Besides treatment-induced antibodies, studies have indicated potential clinical relevance of pre-existing αPEG antibodies. A recent study with Doxil®, a well-established drug that has been in the market for over 25 years, showed in vitro, pre-existing levels of αPEG antibodies contribute to complement activation by the drug (74). Additionally, another study observed a decrease in pharmacokinetics (PK) and therapeutic efficacy in mice models with pre-existing αPEG antibodies (76). Peginacovin, a modified RNA aptamer coupled to 40 kDa branched mPEG that inhibits coagulation factor IXa, caused first exposure allergic reactions in a phase 2b clinical trial linked to pre-existing levels of αPEG Antibodies (115).

Recently, it has been found that 72% of people without prior exposure to PEG-based drugs carry detectable levels of αPEG Antibodies due to the prevalence of the polymer in everyday products (72). The presence of backbone-specific αPEG antibodies, with an average IgG concentration of 52 ng/ml in the general population can jeopardize the efficacy of PEG-based

treatments, provoking hypersensitivity, rapid drug clearance, and treatment failure (64). However, the lack of a reliable and rigorous model that accurately depicts the prevalence of αPEG Antibodies in the population impacts our understanding of how these affect PEGylated therapies. In this study, we develop an ELISA to quantitatively detect the presence of αPEG IgG antibodies in mouse blood. Using this assay, we aim to understand how αPEG Antibodies are induced and how drugs respond to existing antibodies. First off, we investigate the relationship between PEG exposure and antibody specificity. Specifically, we considered antibody response to PEG exposure of various molecular weights and steric presentations (free versus bound). Additionally, we established a passive transfer mouse model with sustained αPEG IgG levels comparable to the average in the general population, and with a rigorous and clinically relevant model.

5.3 Results

5.3.1 Development of αPEG IgG ELISA

Herein, we developed an indirect ELISA to detect and quantify αPEG antibodies in the range of in mouse whole mouse blood **(Figure 5-1)**. In brief, an amine-coated plate is functionalized with mPEG-NHS and blocked with bovine serum albumin (**BSA**) to decrease non-specific binding. The primary antibody is a commercially available αPEG IgG specific to the PEG backbone, and an anti-mouse HRP secondary antibody is used in conjunction with TMB substrate to amplify and detect the absorbance of each well. A standard curve of known concentrations of αPEG IgG (0, 12.5, 25, 50, 100, and 200 ng/ml) is created with blood from naïve mice, and the absorbance of each well is measured at 450 nm in a plate reader. With linear

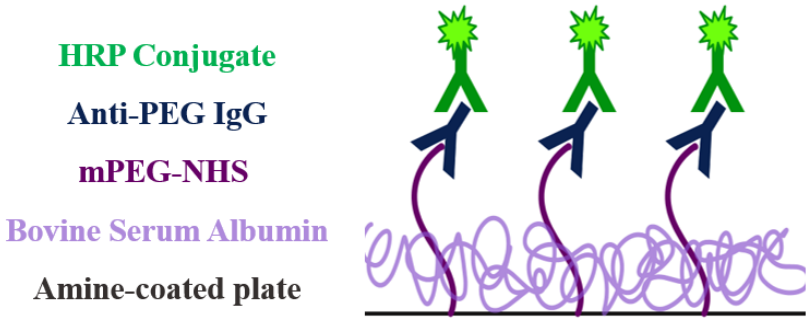

Figure 5- 1. Schematic of ELISA for detection of αPEG IgG in mouse blood.
NHS-mPEG is covalently attached to amine-functionalized 96-well plates using click chemistry. A bovine serum albumin-based blocking buffer is used to prevent nonspecific binding. Samples containing αPEG IgG are incubated an on the plate. Unbound sample is washed away. A secondary antibody reactive against mouse IgG and conjugated with HRP is incubated on the plates. Unbound secondary antibody is washed away. TMB is used to develop chromogenic signal.

regression, an equation describing the concentration in terms of sample absorbance can be found and used to calculate the antibody concentration in unknown samples. For the purposes of this study, we have determined that only curves with an R square value greater than 0.9500 were accepted.

Different iterations of the protocol have been tested to determine the most reproducible ELISA. Whole blood was chosen as the biological sample to be analyzed. The ELISA was run with a standard curve made with whole blood, plasma, and serum **(Fig. 5-2).** The calculated R square for the linear regression of each curve was 0.9468, 0.1867, and 0.5067, respectively. Moreover, the slope deviation from zero was not significant for the plasma. In addition to generating a better standard curve, the choice to use whole blood means that we need to collect less blood from each animal (50 µl per well). This makes it possible to not have to sacrifice the mice after blood collection through retro-orbital bleeding and can provide more insight on how the antibody response develops in each individual animal over time.

Although the commercially available αPEG IgG used for the standard curve and passive transfer model is specific to the backbone of PEG with molecular weights greater than 550 Da, the specificity of the induced antibodies is unknown. By varying the length of the PEG functionalized to the amine-coated plate, we can observe the specificity of the induced antibodies to several PEG lengths. Therefore, we extended the ELISA protocol to function with a variety of PEG lengths as the assay antigen. Plates were coated with 5, 10 and 20 kDa PEG, corresponding to the molecular weights of PEG used in the induction study. The assay was validated for each molecular weight, as the R square value for each standard curve was 0.9984, 0.9745, and 0.9901 for 5, 10, and 20 kDa PEG-coated plates, respectively (**Fig. 5-3**).

In summary, we have developed a quantitative ELISA to detect antibodies against the

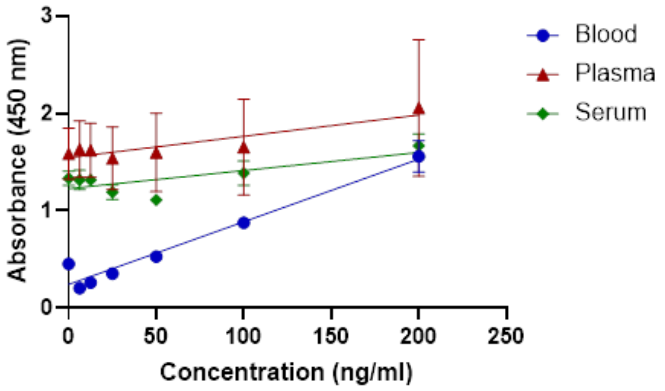

Figure 5- 2. ELISA optimization: Comparison of sample media.
Linear regression of standard curves for blood (blue), plasma (red), and serum (green) in αPEG IgG ELISA. Healthy C57BL6/J mice were bled via cardiac puncture. For whole blood, samples were used immediately to minimize clotting. For plasma, blood was collected in sodium citrate tubes and spun down. For serum, no anticoagulation was used in collection. Blood was allowed to sit for 15 minutes after collection before being spun down. All blood forms were doped with monoclonal αPEG IgG and a series dilution for performed as described in the section 5.5.5.. The concentration of αPEG IgG in the samples was determined via ELISA. (n

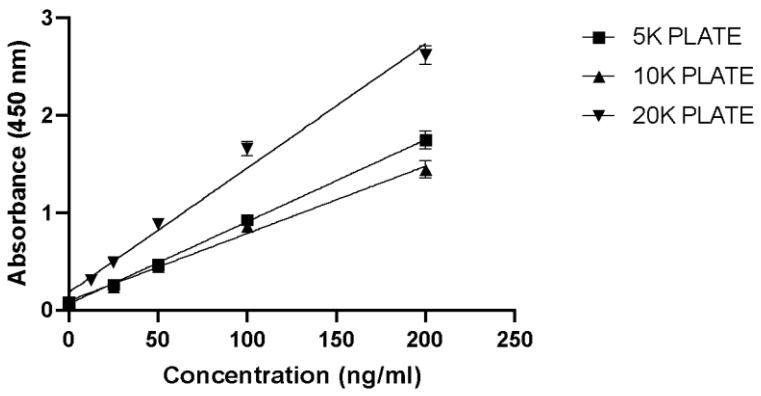

Figure 5- 3. ELISA optimization: Comparison of poly(ethylene glycol) molecular weight.
Linear regression of standard curves for amine-coated plates functionalized with 5 (black square), 10 (black upward triangle), and 20 (black downward triangle) kDa PEG in αPEG IgG ELISA. Healthy C57BL6/J mice were bled via cardiac puncture. Blood was doped with monoclonal αPEG IgG and a series dilution for performed as described in the section 5.5.5. to create a standard curve. The standard curve samples were plated on to plates coated with different molecular weights of PEG. The concentration of αPEG IgG in the samples for each plate was determined via ELISA. (n=10).

backbone of 5, 10, and 20 kDa PEG. The use of polyoxyethylene-free surfactants eliminates the possibility of cross-reactivity with αPEG Antibodies, and the use of whole blood samples decreases the sample volume necessary to run the assay. Finally, the addition of a standard curve makes it possible to translate the absorbance of unknown samples into the αPEG Antibody concentration in mouse blood.

5.3.2 Induction Mouse Model

There is a need to understand what factors influence αPEG Antibody induction. The majority of previous studies aimed at inducing αPEG Antibodies immunized animals with PEGylated proteins, including the model antigen ovalbumin, or PEGylated liposomes(61, 112). As discussed in Chapter 2, liposomes are known to act as potent adjuvants that can enhance the antibody response(105, 106, 236).

To understand the effects of PEG length and steric presentation in αPEG IgG induction, we have immunized mice (n=10) with free methoxy PEG (mPEG) or PEGylated gold nanoparticles (AuNP) of 100 nm HD, with and without a boost injection 14 days after the initial injection (**Fig. 5-4**). The molecular weights for the polymer on both mPEG and PEGylated AuNP were 2, 5, 10, and 20 kDa. Gold is known to be an inert material *in vivo*, so the nanoparticles will not enhance the immune response to PEG. Moreover, we have chosen to inject a dose of PEG comparable to what is administered in a clinical setting. In one dose of Doxil®, we have calculated that an average 70 kg adult would receive approximately 6.75 E-08 mol/kg PEG 2kDa, which is the amount used in both initial and booster doses(114). Finally, to quantify induced IgG, the blood was collected 28 days after the initial injection to ensure class switching

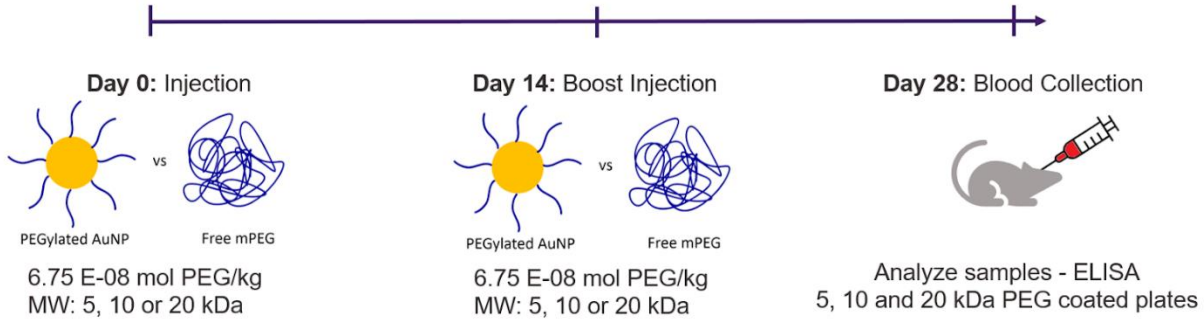

Figure 5- 4. Schematic of timeline for induction of anti-poly(ethylene glycol antibodies.
Timeline of initial injection, boost injection, and blood collection for active immunization of mice with PEGylated AuNP and free mPEG of 2, 5, 10, and 20 kDa molecular weights.

Abs specific to:

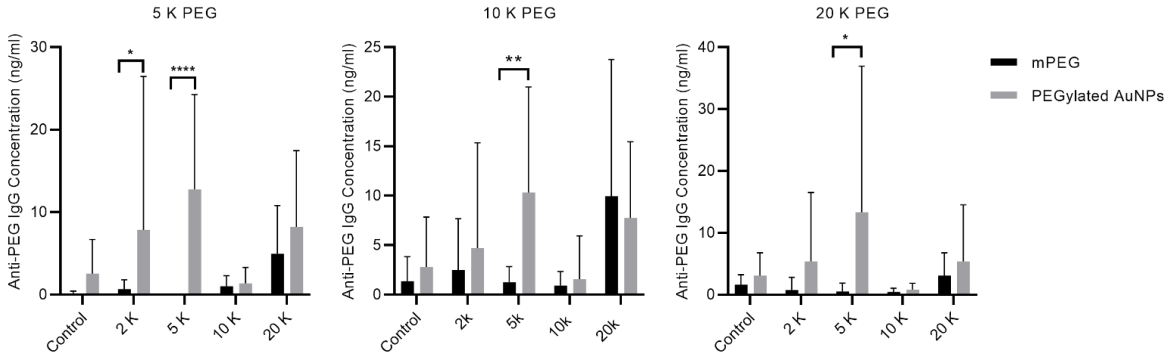

Figure 5- 5. **Following a single exposure, AuNPs induce a stronger αPEG antibody response; Steric presentation of PEG significantly alters** antibody **response against PEG MW 5 K**.
Healthy C57BL/6 mice were injected subcutaneously with methoxy poly(ethylene glycol) (mPEG) (black) or PEGylated gold nanoparticles (AuNPs) (gray) at a dose of 6.75 E-08 mol PEG/kg. PEG chains varied in molecular weight: 2, 5, 10, and 20 K. The control consisted of milliQ water was used for the mPEG-treated groups and nonPEGylated AuNPs were used as a control for the PEGylated AuNP-treated groups. A cohort of mice received a second ("booster") dose 14 days after the first injection. Blood samples were collected 28 days after the initial injection and analyzed via in-house ELISAs that detected antibodies specific to the backbone of PEG with a molecular weight of 5, 10 or 20 K. Two-way ANOVA was performed to analyze the data with *=$p<0.05$, **=$p<0.01$, ****=$p<0.0001$. (n=10 mice/group).

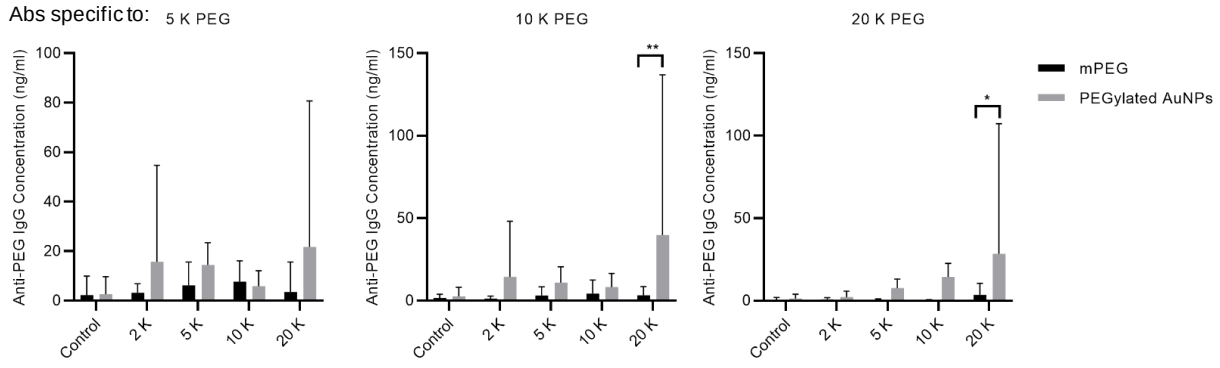

Figure 5- 6. Two PEG MW 20 K exposures increase induction relative to other PEG MW; Steric presentation of PEG significantly alters Antibody **response against PEG MW 20 K.**

Healthy C57BL/6 mice were injected subcutaneously with methoxy poly(ethylene glycol) (mPEG) (black) or PEGylated gold nanoparticles (AuNPs) (gray) at a dose of 6.75 E-08 mol PEG/kg. PEG chains varied in molecular weight: 2, 5, 10, and 20 K. A vehicle control consisting of milliQ water was used for the mPEG-treated groups and nonPEGylated AuNPs were used as a control for the PEGylated AuNP-treated groups. A cohort of mice received a second ("booster") dose 14 days after the first injection. Blood samples were collected 28 days after the initial injection and analyzed via in-house ELISAs that detected antibodies specific to the backbone of PEG with a molecular weight of 5, 10, or 20 K. (n=10 mice/group).

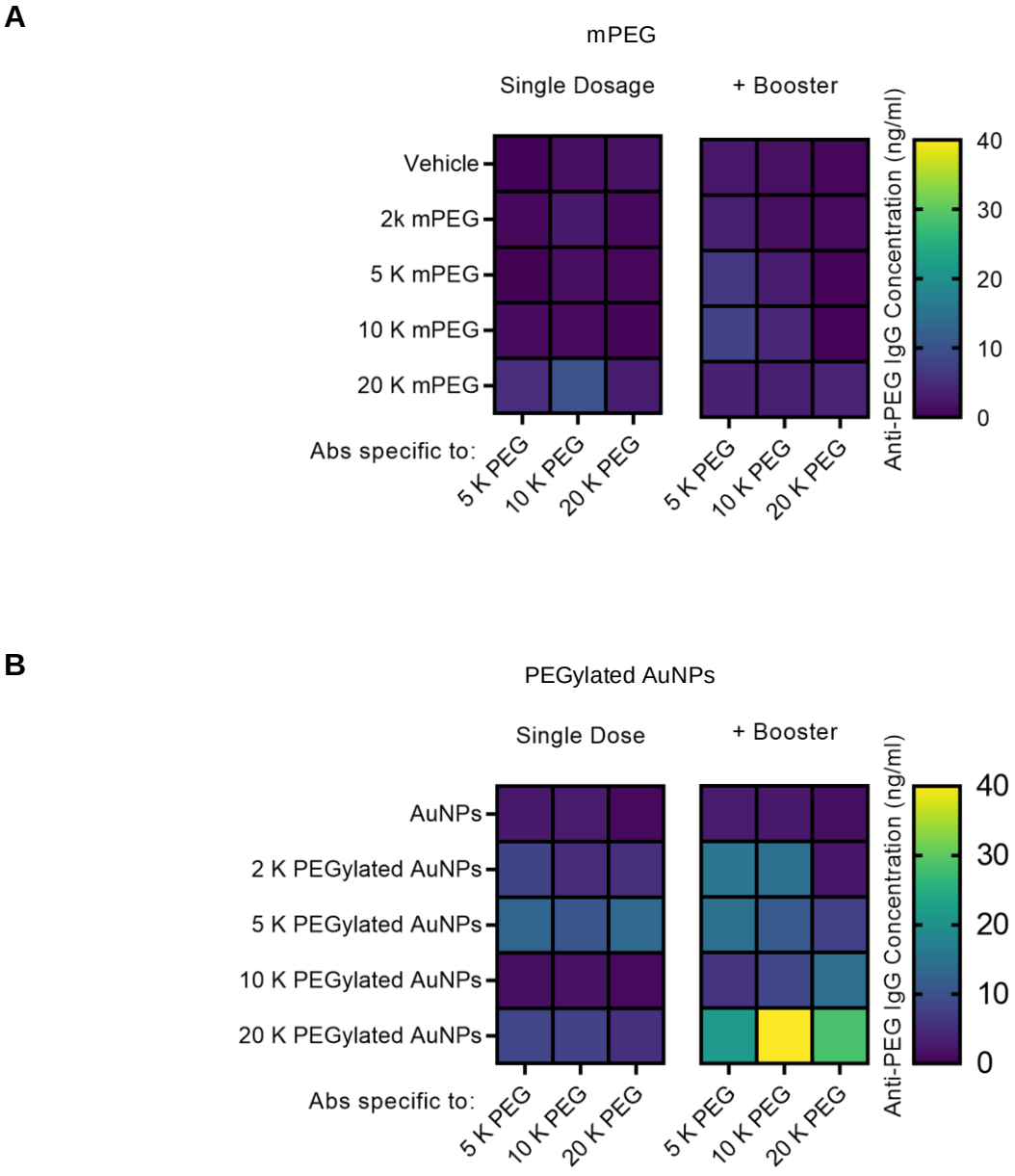

Figure 5- 7. Two doses of 20 K PEGylated AuNPs reliability induce αPEG antibodies.
Healthy C57BL/6 mice were injected subcutaneously with methoxy poly(ethylene glycol) (mPEG) (**A**) or PEGylated gold nanoparticles (AuNPs) (**B**) at a dose of 6.75 E-08 mol PEG/kg. PEG chains varied in molecular weight: 2, 5, 10, and 20 K. A vehicle control consisting of milliQ water was used for the mPEG-treated groups and nonPEGylated AuNPs were used as a control for the PEGylated AuNP-treated groups. A cohort of mice received a second ("booster") dose 14 days after the first injection. Blood samples were collected 28 days after the initial injection and analyzed via in-house ELISAs that detected antibodies specific to the backbone of PEG with a molecular weight of 5, 10 or 20 K. Heatmaps show mean αPEG immunoglobulin G (IgG) concentration. (n=10 mice/group).

has occurred(72). induced IgG, the blood was collected 28 days after the initial injection to ensure class switching has occurred(72). We first compared the αPEG IgG response after immunization with a single dose of mPEG and PEGylated AuNP (**Fig. 5-5**). In general, mPEG did not provoke a strong antibody response, with the mean concentration below 10 ng/ml for all molecular weights. A significant difference was observed between mPEG and PEGylated AuNP of 2kDa and 5kDa molecular weights in the concentration of antibodies against 5kDa PEGylated plate ($p<0.01$ and $p<0.0001$ respectively). Additionally, PEGylated AuNP with 5kDa PEG chain length induced higher titers of antibodies against 10 and 20 kDa PEGylated plate when compared to the same molecular weight of mPEG ($p<0.01$ and $p<0.001$ respectively).

Next, we investigated the effect of the addition of a boost dose 14 days after the initial injection **(Fig. 5-6)**. A significant increase in the antibody response was observed after the boost with mPEG of 2, 5, and 10 kDa ($p<0.05$, $p<0.0001$, and $p<0.0001$ respectively) against the 5 kDa PEGylated plate. No significant difference was observed for 20 kDa mPEG or for any against the 10 and 20 kDa PEGylated plates. Of notice, none of the samples had an IgG concentration above 20 ng/ml. The addition of a boost for the 20 kDa PEGylated AuNP resulted in a significant increase in IgG against the 10 and 20 PEGylated plates ($p<0.01$ and $p<0.05$ respectively). Additionally, these conditions resulted in the largest Antibody titer observed **(Fig. 5-6)**.

5.3.3 Passive Transfer Mouse Model

Without an animal model that accurately represents the presence and concentration of αPEG Antibodies found in the population, we cannot understand how PEGylated therapeutics are affected by PEG immunogenicity prior to human clinical trials. This can lead to a financial burden to drug developers as adverse reactions occur due to αPEG Antibodies, often leading to

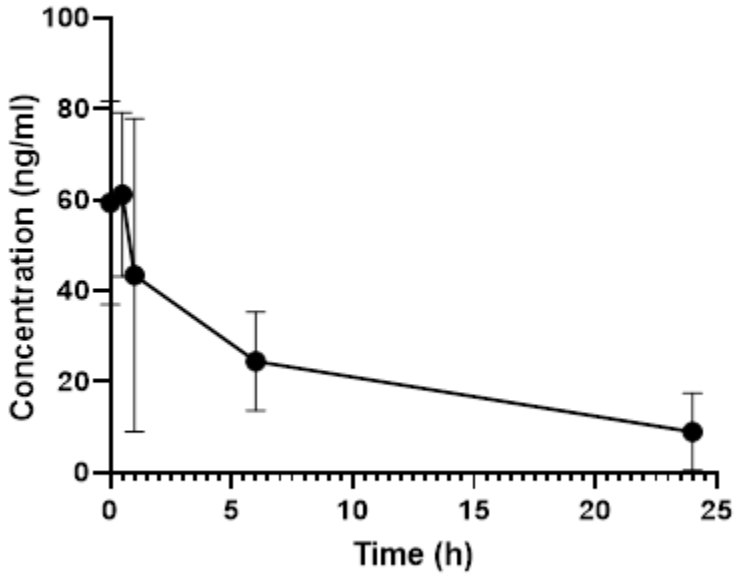

Figure 5- 8. Passive transfer of anti-poly(ethylene glycol) immunoglobulin G via intravenous injection does not provide ideal pharmacokinetics for a sustained mouse model.
Healthy C57BL6/J mice were injected intravenously with a 7.5 mg/kg dose of monoclonal αPEG IgG. Blood samples were collected via retro orbital bleed at various time points after the after injections. The concentration of αPEG IgG in the blood samples was determined via ELISA. The resulting half-life of αPEG IgG was determined to be 10.8 hours. (n=5).

the early termination of clinical trials(78). Therefore, it is of pressing need to develop an animal model to be used in the development of new PEGylated drugs and the assessment of existing therapies.

Previously, Hsieh *et al.* have attempted to inject αPEG IgG (4 mg/kg) intravenously (**IV**) in mice, at a dose of 4 mg/kg(76). Only one day after the injection, there was no more detectable αPEG IgG in circulation. We have also demonstrated rapid clearance with IV injection of αPEG IgG **(Fig. 5-8)**. The short half-life of antibodies, when administered intravenously, poses a problem for developing a mouse model with sustained concentrations of αPEG Antibodies. For a clinically significant concentration to be sustained over time, animals would have to be injected often. This is not sustainable if we aim to create a practical animal model.

With these results in mind, we have developed a strategy using a single subcutaneous αPEG IgG injection aiming to replicate in mice the average IgG concentration of 52 ng/ml found in humans(72). In addition to the ease of administration of this route, this route of administration leads to an increase in the half-life of the antibody. There are three phases to the model, the induction, experimental and extinguished phase **(Fig. 5-9)**. Users of the model need to determine the desired range for experimentation, with an upper and lower bound, as well as a target concentration. The induction phase begins right after the loading αPEG injection is given. When the blood concentration falls below the upper bound by 10% of the target value, the transition from the induction phase to the experimental phase occurs. Finally, when the blood concentration falls within 10% of the target above the lower boundary, the model enters the extinguished phase and is no longer fit for use.

By modulating the loading dose, the model can be optimized for various target concentrations. We have injected mice with a 20, 35, and 50 μg/kg dose of αPEG IgG. We then

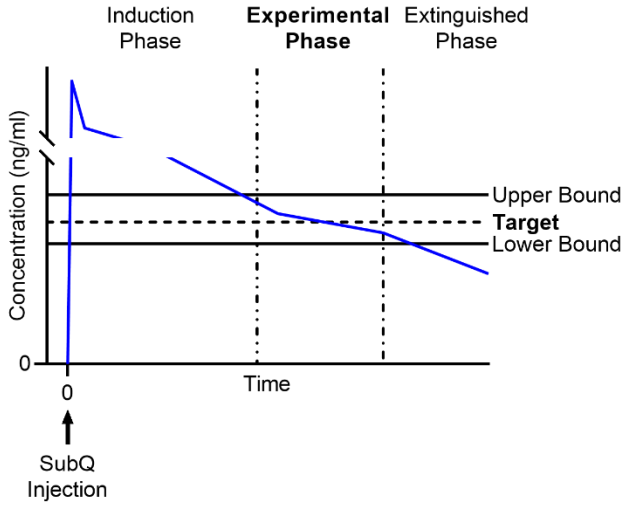

Figure 5- 9. Schematic overview of the passive transfer mouse model.
The induction phase occurs from injection until the concentration reaches the upper bound. During this period, the concentration is in excess of the upper bound. The experimental phase occurs when the concentration is between the upper bound and lower bound. The extinguished phase occurs when the concentration drops below the lower bound.

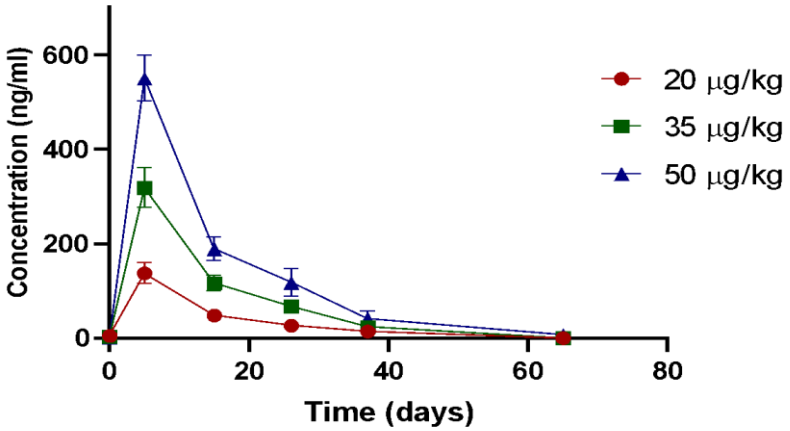

Figure 5- 10. Passive transfer model. Anti-poly(ethylene glycol) IgG concentration profile over time after subcutaneous administration.

Healthy C57BL6/J mice were injected subcutaneously with 20 (red), 35 (green), and 50 (blue) μg/kg doses of monoclonal αPEG IgG. Blood samples were collected via retro orbital bleed at various time points after the after injections. The concentration of αPEG IgG in the blood samples was determined via ELISA. (n=10).

analyzed the antibody blood concentration at different time points until no αPEG IgG was detected in blood to determine the pharmacokinetics of each dose **(Fig. 5-10)**.

The half-life of the antibody on each curve is 6.883, 7.488, and 6.848 days for the 20, 35 and 50 µg/kg, respectively. Compared to intravenous injection with a half-life of 10.8 hours (**Fig. 5-7**), we see an increase in the half-life of the antibody via this administration route. Of note, the curves decay at a similar rate regardless of the dose, with only the concentration at time zero varying significantly.

With each one of these results, we can modulate the lower and upper bounds, as well as the target concentration, to mimic the αPEG IgG concentration for different populations. To mimic the antibody concentration of only people that have circulating levels of αPEG IgG, excluding those with no antibody titer, the bounds can be modified to reflect this. Based on Yang et al.'s data, the average for αPEG-positive individuals is 67 ng/ml, with a 95% confidence interval between 47 and 98 ng/ml(72). Applying these values as the target, upper and lower bounds in the 35 µg/kg curve, the experimental window falls between 20 and 30 days after the initial injection. To mimic the antibody concentration of individuals that undergo high PEG exposure and therefore have higher levels of circulating αPEG IgG, the target concentration can be set to 150 ng/ml, and upper and lower bounds to 200 and 100 ng/ml, respectively. In the 50 µg/kg curve, that will result in an experimental window between 15 and 28 days after the initial injection **(Fig. 5-11)**.

However, for the end goal of modeling the general population's antibody titers, the 20 µg/kg curve is the best candidate. Yang et al. have determined the average of the general population is 52 ng/ml, with a 95% confidence interval between 44 and 62 ng/ml. One can use

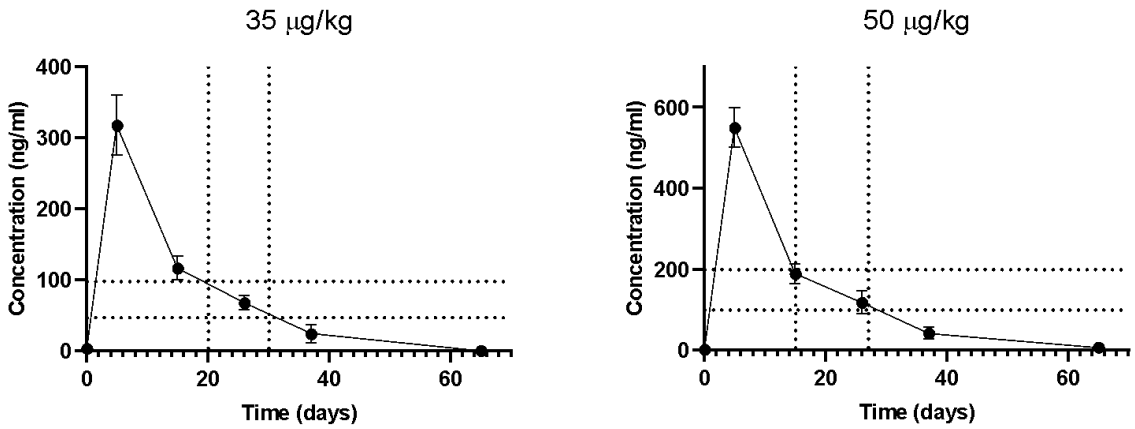

Figure 5- 11. Application of PT model to αPEG IgG concentration profile over time after subcutaneous administration of 35 and 50 μg/kg monoclonal αPEG IgG.

Healthy C57BL6/J mice were injected subcutaneously with 30 (left) or 50 (right) ug/kg monoclonal αPEG IgG. Blood samples were collected via retro orbital bleed at various time points after the after injections. The concentration of αPEG IgG in the blood samples was determined via ELISA. Data are presented as mean±standard deviation. The target concentration of 44 to 62 ng/ml is indicated by the horizontal dotted lines. The associated time frame when the concentration is within this range known as the "experimental window" is indicated by the vertical dotted lines.

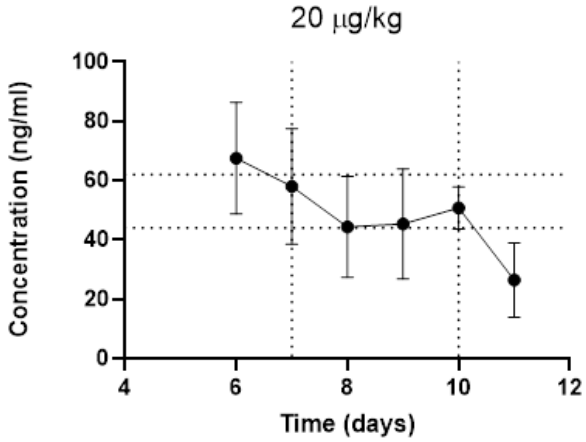

Figure 5- 12. αPEG IgG concentration profile over time after subcutaneous administration of 20 μg/kg monoclonal αPEG IgG.

Healthy C57BL6/J mice were injected subcutaneously with 20 ug/kg monoclonal αPEG IgG. Blood samples were collected via retro orbital bleed 6, 7, 8, 9, 10, and 11 days after injection. The concentration of αPEG IgG in the blood samples was determined via ELISA. Data are presented as mean±standard deviation. The target concentration of 44 to 62 ng/ml is indicated by the horizontal dotted lines. The associated time frame when the concentration is within this range known as the "experimental window" is indicated by the vertical dotted lines.

these values as the target, lower and upper bound respectively in the curve for the 20 μg/kg dose. Samples at additional time points (6, 7, 8, 9, 10, and 11 days) were collected and analyzed via ELISA to provide additional details to create the experimental window **(Fig. 5-12)**. By doing so, the experimental window will occur between days 7 and 10. The variance at each time point, as well as the slight increase that occurs on day 10, is attributed to animal-to-animal variation.

5.4 Discussion

One of the major points of criticism in the literature of αPEG Antibodies is the lack of a standardized, quantitative detection method(124). In the initial observations of PEG immunogenicity, outdated methods such as gel diffusion and hemagglutination were implemented(70, 71). This makes it difficult to compare the early data of αPEG Antibodies data to recent studies due to the gap in detection limits between old and new assays. Most pre-contemporary assays were also qualitative, so no information about the antibody concentration in blood or plasma washes has been reported for comparison. Recently, it has been common for each research group to develop their own in-house ELISA for the detection of αPEG Antibodies. However, many have used polyoxyethylene surfactants in washing and blocking steps of the assay C, that due to their cross-reactivity between these surfactants and with αPEG Antibodies invalidates these assays.

We have developed a quantitative and reproducible ELISA to determine the αPEG IgG concentration in mice whole blood. The assay protocol addresses previous points of controversy in PEG immunogenicity literature, such as the antibody cross-reactivity of polyoxyethylene surfactants and the quantification of antibody titers. We have also optimized the ELISA to detect

antibodies against the backbone of 5, 10, and 20 kDa PEG in functionalized plates. While this does not solve the issue of a standardized detection method for all, we hope our protocol can provide insight into what leads to successful detection and quantification of αPEG IgG.

Our inducted antibodies model provides methods for generating a mouse model that produces αPEG antibodies. The method does not use an adjuvant, which may influence the immune response in the model. Also provided are mice generated by said methods and methods of using these mice to screen PEG-containing products *in vivo*.

A variety of approaches to creating αPEG antibody-producing animal models have been described in literature. Mouse models are ideal due to their commonality in research, low cost, and small size[20]. However, none have successfully captured the state of pre-existing αPEG antibodies known to be present in the general population via the same immunological mechanism (PEG exposure) or at relevant concentrations. In previous models, small animals have been injected with PEGylated proteins and an adjuvant or PEGylated liposomes (which act as adjuvants) to induce antibody production[21]. Because these adjuvants also enhance the immune response[23], the immune response to the PEG therapeutic cannot be distinguished from the immune response to the adjuvant. Thus, the immune response in the human body in the absence of the adjuvant cannot be predicted from these models.

To overcome the shortcomings of previous models, we have developed a robust mouse model that produces αPEG antibodies. The primary advantage offered by the αPEG antibody-producing mouse models of the present invention is that they are adjuvant-free. As a result, the immune response generated in these mice is more representative of the immune response that is stimulated by the PEG therapeutic itself. This model can be used to screen PEG-based therapeutics for pharmacokinetics, biodistribution, effective dosing, and immunogenic responses in the

presence of αPEG antibodies. Thus, this mouse model can be used to reduce costs associated with clinical trials for drugs that would fail due to the presence of αPEG antibodies.

The results of the induction experiments show that following a single exposure of PEG MW 5 K, PEGylated AuNPs induced a stronger αPEG antibody response than mPEG (**Fig. 5-5**). This trend is nonspecific to PEG MW, such that the antibodies that are produced bind to all PEG MW that were assessed. This indicates that steric presentation of the PEG is critical to induce a response. We hypothesize that because the free form mPEG lacks the steric hindrance to prevent from interacting with itself, it effectively "balls up," preventing presentation to and recognition by cells. Alternatively, the presentation of the PEG on the AuNPs provides the steric hindrance to prevent the PEG from interacting with itself. As a result, PEGylated AuNPs allow for PEG presentation and recognition by cells. Thus, antibody production occurs.

Furthermore, a single exposure to AuNPs PEGylated with PEG 5 K induces the greatest antibody response. Again, the antibodies produced are nonspecific in regard to the MW of the PEG that they bind. Thus, the MW of the PEG used for induction is important. We hypothesis that steric hindrance may also in regard to PEG MW and αPEG antibody production. If PEG MW is too low, the length of the PEG chain is too short and a "brush-like" conformal coating occurs inhibiting interaction with cells. Alternatively, if the PEG length is too long, the PEG will interact with itself, as opposed to presenting to cells. This type of coating is known as a "mushroom" conformation. The density of the PEG grafting also plays a role in the steric presentation of the PEG.

With the two-exposure protocol, induction using AuNPs PEGylated with PEG MW 20 K resulted in increased antibody production (**Fig. 5-6**). At the 20 K PEG MW, AuNPs showed

significant increases in antibodies production reactive to 10 K and 20 K PEG. Induction with AuNPs PEGylated with PEG MW 20 K produced the highest concentration of induced antibodies over all other MW. These antibodies were specific to all assessed PEG MWs. Once more, steric presentation and PEG MW were implicated as important factors **for induction.**

Two exposures of PEG resulted in significantly higher αPEG antibody concentration as compared to a single exposure **(Fig. 5-7**). Importantly, two doses of 20 K PEGylated AuNPs most reliably induced αPEG antibodies. The produced antibodies were specific to all assessed MW of PEG, with a preference for PEG MW 10K. Given that the two-dose 20 K PEGylated AuNP protocol produced the most robust response, it is recommended that this protocol be used for antibody induction.

A final issue with existing mouse models is that they are unable to recapitulate the steady state concentration of αPEG antibodies for an extended duration of time to facilitate testing of PEG-based therapeutics[23]. Ideally, steady-state maintenance of multiple concentrations of αPEG antibodies by different cohorts of mice would be achieved. This would allow PEG-based therapeutics to be assessed in organisms with different blood concentrations of antibodies to account for variations in the general population. This would be impactful as it has been previously seen that some drugs are safe and effective for patients with low αPEG antibody concentrations but are extremely dangerous for patients with high concentrations.

The passive transfer murine model was achieved via subcutaneous injection of a commercially available monoclonal αPEG IgG. For the loading doses tested, the antibody had a half-life that ranged from 6.8 to 7.5 days *in vivo.* The model is divided into three phases, induction, experimental, and extinguished. These phases are determined by setting a target concentration as

well as an upper and lower bound. The model was applied with different bounds and target concentration modeling different populations to curves with a loading dose of 20, 35, and 50 µg/kg. To model the general population, the experimental phase occurs between 7 and 10 days after a 20 µg/kg loading dose.

5.5 Materials and Methods

5.5.1 Animals

8 to 12-week-old, male C57BL/6 mice were purchased from Jackson Labs. Mice were housed in the Center for Comparative Medicine at Northwestern University. All animal protocols were approved by Northwestern University's Institutional Animal Care and Use Committee (IACUC).

5.5.2 Enzyme-Linked Immunosorbent Assay

An in-house ELISA was developed to detect and quantify the concentration of αPEG IgG in mouse blood samples. Amine-coated 96-well plates (Life Science) were incubated with a 4 mM N-Hydroxysuccinimide-mPEG 5 kDa (Nanocs) solution for 45 minutes at 37°C. The wells were washed with PEG Wash Buffer (Life Diagnostics) and blotted three times. Solutions of known αPEG IgG concentration (0-200 ng/ml) were made by diluting APEG Monoclonal (Life Diagnostics, Inc.) in mouse blood. 50 µl of 1X PEG Blocking Buffer (Life Diagnostics, Inc.) and 50 µl of each solution were plated and incubated at room temperature for 2 hours. The wells were then washed and blotted five times. Horseradish peroxidase (HRP) secondary antibody goat X mouse IgG (H+L) HRP (Sigma) was diluted in PEG Blocking Buffer in a 1:200 dilution. 100 µl of the resulting solution was plated and incubated at room temperature for 45 minutes. The wells were then washed and blotted five times. Finally, the plate was incubated with 50 µl

tetramethylbenzidine (Sigma), and after 15 minutes, 50 µl of 0.2 M sulfuric acid was added to each well. The absorbance of each well was read at 450 nm on a Cytation 5 (BioTek). Absorbance was related to concentration to determine the concentration of an αPEG IgG of samples with unknown concentrations.

5.5.3 Induction Model

Mice (n=5) were subcutaneously injected with 2k, 5k, 10k, or 20k molecular weight mPEG, in free polymer form (Nanocs) or displayed as PEGylated AuNPs (Luna Nanotech). Non-PEGylated AuNPs and deionized water were used for controls. One set of mice was subjected to a boost at the same concentration and modality of PEG. After 28 days, the animals underwent blood collection through cardiac puncture and the samples were analyzed via ELISA on 5k, 10k, and 20k PEG-coated plates.

5.5.4 Passive Transfer Model

Mice (n=10) were subcutaneously injected with 20, 35, or 50 µg/kg of APEG Monoclonal (Life Diagnostics, Inc., Clone 1D9-6). Blood was collected retro orbitally at several different time points after the injection. The antibody concentration in each sample was analyzed via ELISA.

5.5.5 Data Analysis

Data analysis was performed in GraphPad Prism. The linear regression feature was used to generate the equation describing the relationship between concentration and absorbance of the standard curve. Non-linear regression for the pharmacokinetic curves was calculated with the one phase exponential decay feature.

5.6 Publication Information

Sections of this chapter have been published with the following citation information:

Freire Haddad H, Burke JA, Scott EA, Ameer GA. Clinical Relevance of Pre-Existing and Treatment-Induced Anti-Poly(Ethylene Glycol) Antibodies. *Regen Eng Transl Med*. 2021 Mar 25:1-11. doi: 10.1007/s40883-021-00198-y. Epub ahead of print. PMID: 33786367; PMCID: PMC7993857.

CHAPTER 6: SUMMARY & RECOMMENDATIONS FOR FUTURE WORK

6.1 Summary of thesis work

The focus of my thesis work was to utilize PEG-based biomaterials to improve outcomes for islet transplantation and to improve the understanding of αPEG antibodies to aid in the development of future PEG-based therapeutics.

CP patients suffer from highly inflammatory pancreas tissue that decreases their quality of life due to severe pain. Total pancreatectomy has the promise of reducing their pain and restoring their livelihood. However, the removal of the pancreas's insulin-producing islet cells will render these patients diabetic. Autologous islet transplantation, islets are isolated from the pancreas' inflammatory tissue and reimplanted, is a promising solution for these patients. In Chapter 3, I demonstrated the ability of a thermoresponsive, phase-changing hydrogel to protect transplanted islets from oxidative stress as a result of the material's antioxidative properties. Using this material, known as PCN, islets can be transplanted to the omentum to prevent the islets from being exposed to additional inflammation via IBMIR that is characteristic of conventional intraportal islet transplantation.

T1D patients suffer from a lifetime prescription to exogenous insulin, which does not provide the same glycemic control as native islets. Thus, these patients have a life fated with both short- and long-term complications, including seizures, amputation, and blindness. Allogeneic islet transplantation, in which cadaver islets are transplanted to the T1D patient, has the promise of restoring glycemic control. However, due to the allogeneic nature of the transplantation, patients are required to trade in their insulin prescription for a lifelong supply of immunosuppressive drugs. In their current manifestation, these immunosuppressive drugs can have worse side effects than

poorly controlled T1D. They also leave patients vulnerable to infection. Thus, islet transplantation is not the standard of care for all T1D patients. The holy grail of immunotherapy is a drug that tolerizes patients only to their transplant without immunosuppressing them. In Chapter 4, using a polymeric nanocarrier, PEG-*b*-PPS PS, and the SC route of administration, it is demonstrated that immunosuppressive drug rapamycin can be rerouted to selectively target APCs, instead of T cells. Targeting APCs induces a tolerogenic phenotype in these cells. APCs communicate this message of tolerance to T cells via a costimulation blockade. This therapeutic, known as rPS, allows for improved graph survival at a low dosage in a STZ-induced diabetic, fully-MHC mismatched, intraportal murine model of islet transplantation. *Ex vivo*, antigen-specific tolerance is demonstrated via mixed lymphocyte reaction. Furthermore, A reduced side effect profile has been shown for rPS relative to rapamycin.

The widespread distribution of a PEG-containing vacc to combat the coronavirus 2019 (**COVID-19**) pandemic has made the general public aware of adverse reactions associated with αPEG antibodies. There is a great need to study PEG-containing therapeutics in animal models that possess αPEG antibodies are par with those present in the general public. In Chapter 5, a robust ELISA assay for the detection of αPEG IgG in mice is described. Furthermore, two mouse models are developed. An adjuvant-free induction model that mimics the immunological nature by which these antibodies are developed provides insight into which types of PEG-based drugs are more likely to cause antibody formation. For example, antibodies are more readily formed when mice are exposed to PEG displayed on a nanoparticle than when in solution. Furthermore, a passive transfer model provides a rigorous platform for the assessment of PEG-based therapeutics.

6.2 Recommendations for future work

6.2.1 Omentum Autologous Islet Transplantation with an Antioxidative Citric Acid-Based Thermoresponsive Polymer in a Clinically Relevant Nonhuman Primate Model

In Chapter 3, it was shown that PPCN is highly biocompatible when implanted in the omentum of an NHP. Given that the end goal is to use PPCN for autologous islet transplantation, the next logical step towards translation is to perform autologous islet transplantation in the NHP model using PPCN. Due to size and anatomy differences, the mouse is not appropriate to evaluate the safety and efficacy of our system for eventual human clinical application: the efficient delivery of islets to the omentum in a minimally invasive manner. Furthermore, humanized small animal models do not provide reliable data pertaining to islet transplantation.[237, 238] This challenge is due to the lack of an omentum that is similar to humans in anatomy and function and the extremely high rate of rapid islet graft rejection in the first 3 weeks following transplantation, depending on the specifics of the model.[239-241] Therefore, islet transplantation to the omentum can only be evaluated in a large animal with similar anatomy and physiology to humans, namely non-human primates. The rhesus macaque is chosen due to its large size and close physiology to humans.[242]

Given that we aim to replace an autologous biomaterial source with a synthetic one to deliver and localize the islets to the omentum and we have conducted a safety study using this material, we must now conduct efficacy studies in a clinically relevant animal model. We are currently in the process of conducting these studies, however, results have been delayed due to the COVID-19 pandemic and the general difficulty of this surgical procedure.

The overarching goals of preclinical efficacy studies are to: 1) determine the efficacy of the experimental treatment relative to clinical standard in a clinically relevant animal model; 2)

aid in determining a risk/benefit assessment for the proposed clinical studies; and 3) guide in designing appropriate clinical trials. Novel route of administration is one of the FDA criteria that require additional preclinical studies prior to initiation of clinical studies. Consistent with the recommendations of the Cellular, Tissue, and Gene Therapies Advisory Committee, we must demonstrate an adequate safety profile for the delivery system and the interaction of cells with the components of the delivery system in animals prior to proceeding to clinical trials. Specifically, we will: 1) synthesize, characterize, and sterilize PPCN using good laboratory practice controls; 2) isolate islets from the rhesus monkey's pancreas, and deliver them to the omentum via laparotomy or laparoscopy, using PPCN or BS as a clinically relevant control.

The following 3 experimental groups, each consisting of 6 adult rhesus macaques (half female), will be investigated: 1) islets+PPCN in the omentum, 2) islets+BS in the omentum, and 3) islets injected in the portal vein. Group 2 is a clinically used control for a material that has been used for islet delivery to the omentum, while Group 3 is the standard location currently used for islet autotransplantation after near total or total pancreatectomy. All of the islet transplantations to the omentum will be done via laparotomy in order to observe the PPCN phase change that localizes the islets to the omentum upon application. Blood samples will be taken and assessed for C-peptide, insulin, glucose, complete blood cell count, white blood cell differential, and blood chemistry. Glucose tolerance tests will also be performed, and body weight measurements recorded. Animals will be periodically monitored for the aforementioned parameters and general behavior for at least 6 months and then euthanized. Prior to euthanasia, a survival surgery will be performed to confirm that euglycemia, if achieved, is due to the transplanted islets. Animals will be euthanized once the blood glucose levels exceed 250 mg/dL for two consecutive days or 3 days after excising the targeted omentum tissue. The explanted omentum tissue that contains the islets

will be fixed and subjected to histology, histomorphometry, and immunofluorescence to assess the foreign body response (fibrosis via MT for collagen), PPCN degradation, insulin production (via immunofluorescence for insulin), vascularization (via α-SMA, CD31, and endothelial nitric oxide synthase (**eNOS**) immunofluorescence), inflammation (via CD68 immunofluorescence), and oxidative tissue damage (via 8-OHdG). A Tukey test will be performed between groups with significant differences to correct for the multiple pair-wise comparisons. A value of $P \leq 0.05$ will be considered to be statistically significant. The Kaplan-Meier test will be used for graft survival analyses. If successful, an additional two islet transplantations will be performed in one male and one female adult rhesus macaque using laparoscopic surgery, the intended delivery mechanism for humans.

6.2.2 Subcutaneous Nanotherapy Repurposes the Immunosuppressive Mechanism of Rapamycin to Enhance Allogeneic Kidney Graft Viability

Given that the market for islet transplantation in the United States is extremely small, as this therapy is currently not reimbursed by insurance, it makes sense to assess rPS for a transplantation application with a larger market. Chronic kidney disease impacts over 8 million Americans.(243) ESKF patients undergo dialysis, wait for transplantation, or die. While transplants are on the rise, the rates of graft loss and immunosuppressive (**IS**) mortality remain high.(34, 244) Only 54% of grafts are still functional 10 years post-transplant, resulting in an increase of $1.38 billion in medical spending and a loss of 29,289 quality-adjusted life years.(244) Most graft rejections are due to complications or failures of IS drugs.(34) Specifically, the drugs fail to prevent rejection or side effects and lead to non-compliance.(34) Ironically, one of the most

common side effects of immunosuppressive therapy for kidney transplant is nephrotoxicity.(34) Other common side effects include recurrent hepatitis, cancer, infection, hypertension, hyperlipidemia, diabetes, and anemia.(34) There is a tremendous need for selective drugs that have targeted effects to prevent graft rejection and reduce toxicity.(34)

Furthermore, kidney transplantation is a great platform to assess rPS as, unlike islet transplantation where immunomodulatory drugs have to protect the graft against both autoimmune and allogeneic responses, which kidney transplant only allogeneic protection is needed. Furthermore, the mouse model for fully MHC-mismatched kidney transplantation is the same one where rPS has been successful for islet transplantation (Balb/c to C57BL/6).

To assess rPS for kidney transplantation, we will perform fully MHC-mismatched allogeneic Balb/c to B6 kidney transplantation. The donor kidney will be excised from a Balb/c mouse, the left kidney will be removed from the recipient mouse, and the donor kidney will be attached by connecting arteries, veins, and ureters. Rapamycin or rPS will be administered SC according to low dosage or standard dosage protocol (see Chapter 4) (N=10 per group). PBS and blank PS will be given in equivalent volumes and/or masses of polymer, as vehicle controls (N=5 per group). Animals will be monitored daily 2 weeks post-op, and then weekly; body weight and survival will be recorded. At baseline and weekly post-op, we will assess kidney functions by measuring mean arterial pressure (tail-cuff blood pressure), sampling urine, and collecting blood. Urine will be assayed for protein and creatine (colorimetric assay). Blood will be assessed for creatine (LC-MS/MS), blood kidney injury molecule-1, and gelatinase-associated lipocalin (ELISA).(245) At baseline and every 2 weeks, glomerular filtration rate (**GFR**) will be assessed via clearance of injected fluorescently tagged sinistrin.(245) At 100 days post-transplant, mice will be sacrificed; exsanguination and urine collection will be performed for final analysis. The kidney

will be excised and histology will be performed to assess for morphology (H&E), fibrosis (MT), mononuclear cell infiltration (periodic acid-Schiff), and specific inflammatory cells (CD3+, CD4+, CD8+, CD25+, FoxP3+, CD19+).(245, 246) The size and weight of the kidney will be measured.(245) The spleen will be used for a mixed lymphocyte reaction.(25) Non-transplanted, non-treated mice will be used as controls. T cells from recipient C57BL/6 splenocytes and labeled with cell trace violet proliferation stain. In parallel, splenocytes will be isolated from Balb/c spleens and undergo T cell depletion and mitomycin-c treatment. Donor Balb/c or non-donor C3H splenocytes "stimulators" and C57BL/6 "responders" will be cultured together for 4 days and then analyzed via flow cytometry. The proliferation of C57BL/6 "responders" will be assessed to determine if recipient C57BL/6 mice were tolerized to Balb/c antigens. If antigen-specific tolerance is conferred, results will be similar to those described for rPS in islet transplantation in Chapter 4.

To further probe tolerance, a secondary, dual-antigen skin transplantation will be performed. Kidney transplant and drug dosing will be performed as described previously. At 50-days post-transplant, mice will undergo skin transplants. Mice will receive two dorsal 10 mm x 10 mm full-thickness skin grafts taken from Balb/c and C3H tails.(247) 100-days post kidney transplant, mice will be sacrificed. Both kidney and skin grafts will be excised for histology. As for the skin transplantation, for any rapamycin-treated groups, we expect to see acceptance of either type of graft, as rapamycin confers immunosuppression, not antigen tolerance. If the rPS induce antigen-specific tolerance, we expect to see Balb/c skin graft survival, but C3H skin graft failure. If this does not occur, we will know that rPS immunomodulation is not antigen specific.

REFERENCES

1. Hering BJ, Clarke WR, Bridges ND, Eggerman TL, Alejandro R, Bellin MD, Chaloner K, Czarniecki CW, Goldstein JS, Hunsicker LG. Phase 3 trial of transplantation of human islets in type 1 diabetes complicated by severe hypoglycemia. Diabetes care. 2016;39(7):1230-40.

2. Alman AC, Talton JW, Wadwa RP, Urbina EM, Dolan LM, Daniels SR, Hamman RF, D'Agostino RB, Marcovina SM, Mayer-Davis EJ, Dabelea DM. Cardiovascular health in adolescents with type 1 diabetes: the SEARCH CVD study. Pediatr Diabetes. 2014;15(7):502-10. Epub 2014/01/24. doi: 10.1111/pedi.12120. PubMed PMID: 24450411; PMCID: PMC4107203.

3. Dabelea D, Rewers A, Stafford JM, Standiford DA, Lawrence JM, Saydah S, Imperatore G, D'Agostino RB, Jr., Mayer-Davis EJ, Pihoker C, Group SfDiYS. Trends in the prevalence of ketoacidosis at diabetes diagnosis: the SEARCH for diabetes in youth study. Pediatrics. 2014;133(4):e938-45. Epub 2014/04/02. doi: 10.1542/peds.2013-2795. PubMed PMID: 24685959; PMCID: PMC4074618.

4. Atkinson MA, Eisenbarth GS, Michels AW. Type 1 diabetes. The Lancet. 2014;383(9911):69-82.

5. Rother KI, Harlan DM. Challenges facing islet transplantation for the treatment of type 1 diabetes mellitus. The Journal of clinical investigation. 2004;114(7):877-83.

6. Robertson RP. Chronic oxidative stress as a central mechanism for glucose toxicity in pancreatic islet beta cells in diabetes. Journal of Biological Chemistry. 2004;279(41):42351-4.

7. Robertson RP, Harmon JS. Pancreatic islet beta-cell and oxidative stress: The importance of glutathione peroxidase. Febs Lett. 2007;581(19):3743-8. PubMed PMID: WOS:000248787000022.

8. Bennet W, Groth C-G, Larsson R, Nilsson B, Korsgren O. Isolated human islets trigger an instant blood mediated inflammatory reaction: implications for intraportal islet transplantation as a treatment for patients with type 1 diabetes. Upsala journal of medical sciences. 2000;105(2):125-33.

9. Schmidt C. Pancreatic islets find a new transplant home in the omentum. Nat Biotech. 2017;35(1):8-. doi: 10.1038/nbt0117-8.

10. Baidal DA, Ricordi C, Berman DM, Alvarez A, Padilla N, Ciancio G, Linetsky E, Pileggi A, Alejandro R. Bioengineering of an Intraabdominal Endocrine Pancreas. New England Journal of Medicine. 2017;376(19):1887-9. doi: 10.1056/NEJMc1613959. PubMed PMID: 28489987.

11. Esposito K, Nappo F, Marfella R, Giugliano G, Giugliano F, Ciotola M, Quagliaro L, Ceriello A, Giugliano D. Inflammatory Cytokine Concentrations Are Acutely Increased by Hyperglycemia in Humans. Role of Oxidative Stress. 2002;106(16):2067-72. doi: 10.1161/01.cir.0000034509.14906.ae.

12. Dantal J, Hourmant M, Cantarovich D, Giral M, Blancho G, Dreno B, Soulilou J-P. Effect of long-term immunosuppression in kidney-graft recipients on cancer incidence: Randomised comparison of two cyclosporin regimens. Lancet. 1998;351(9103):623. PubMed PMID: 294074.

13. Etemad B, Whitcomb DC. Chronic pancreatitis: diagnosis, classification, and new genetic developments. Gastroenterology. 2001;120(3):682-707.

14. Yadav D, Lowenfels AB. The epidemiology of pancreatitis and pancreatic cancer. Gastroenterology. 2013;144(6):1252-61.

15. Rilo HLR, Ahmad SA, D'alessio D, Iwanaga Y, Kim J, Choe KA, Moulton JS, Martin J, Pennington LJ, Soldano DA. Total pancreatectomy and autologous islet cell transplantation as a means to treat severe chronic pancreatitis. Journal of gastrointestinal surgery. 2003;7(8):978-89.

16. Chinnakotla S, Bellin MD, Schwarzenberg SJ, Radosevich DM, Cook M, Dunn TB, Beilman GJ, Freeman ML, Balamurugan A, Wilhelm J. Total pancreatectomy and islet auto-transplantation in children for chronic pancreatitis. indication, surgical techniques, post operative management and long-term outcomes. Annals of surgery. 2014;260(1):56.

17. Sutherland DE, Radosevich DM, Bellin MD, Hering BJ, Beilman GJ, Dunn TB, Chinnakotla S, Vickers SM, Bland B, Balamurugan A. Total pancreatectomy and islet autotransplantation for chronic pancreatitis. Journal of the American College of Surgeons. 2012;214(4):409-24.

18. Au - Bötticher G, Au - Sturm D, Au - Ehehalt F, Au - Knoch KP, Au - Kersting S, Au - Grützmann R, Au - Baretton GB, Au - Solimena M, Au - Saeger HD. Isolation of Human Islets from Partially Pancreatectomized Patients. JoVE. 2011(53):e2962. doi: doi:10.3791/2962.

19. Kemp CB, Knight MJ, Scharp DW, Ballinger WF, Lacy PE. Effect of transplantation site on the results of pancreatic islet isografts in diabetic rats. Diabetologia. 1973;9(6):486-91. doi: 10.1007/bf00461694.

20. Korsgren O, Jansson L, Andersson A. Effects of Hyperglycemia on Function of Isolated Mouse Pancreatic Islets Transplanted Under Kidney Capsule. Diabetes. 1989;38(4):510-5. doi: 10.2337/diab.38.4.510.

21. Christoffersson G, Henriksnäs J, Johansson L, Rolny C, Ahlström H, Caballero-Corbalan J, Segersvärd R, Permert J, Korsgren O, Carlsson P-O, Phillipson M. Clinical and Experimental Pancreatic Islet Transplantation to Striated Muscle. Establishment of a Vascular System Similar to That in Native Islets. 2010;59(10):2569-78. doi: 10.2337/db10-0205.

22. Merani S, Toso C, Emamaullee J, Shapiro AMJ. Optimal implantation site for pancreatic islet transplantation. British Journal of Surgery. 2008;95(12):1449-61. doi: 10.1002/bjs.6391.

23. Habtezion A. Inflammation in acute and chronic pancreatitis. Curr Opin Gastroenterol. 2015;31(5):395-9. Epub 2015/06/25. doi: 10.1097/MOG.0000000000000195. PubMed PMID: 26107390; PMCID: PMC4618697.

24. Cantarelli E, Citro A, Marzorati S, Melzi R, Scavini M, Piemonti L. Murine animal models for preclinical islet transplantation No model fits all (research purposes). Islets. 2013;5(2):79-86. PubMed PMID: WOS:000327609000003.

25. Manzoli V, Villa C, Bayer AL, Morales LC, Molano RD, Torrente Y, Ricordi C, Hubbell JA, Tomei AA. Immunoisolation of murine islet allografts in vascularized sites through conformal coating with polyethylene glycol. Am J Transplant. 2018;18(3):590-603. Epub 2017/10/27. doi: 10.1111/ajt.14547. PubMed PMID: 29068143; PMCID: PMC5820142.

26. Giraldo JA, Molano RD, Rengifo HR, Fotino C, Gattas-Asfura KM, Pileggi A, Stabler CL. The impact of cell surface PEGylation and short-course immunotherapy on islet graft survival in an allogeneic murine model. Acta Biomater. 2017;49:272-83. Epub 2016/12/05. doi: 10.1016/j.actbio.2016.11.060. PubMed PMID: 27915019; PMCID: PMC5253093.

27. Ali MK, Bullard KM, Saaddine JB, Cowie CC, Imperatore G, Gregg EW. Achievement of goals in US diabetes care, 1999–2010. New England Journal of Medicine. 2013;368(17):1613-24.

28. Dabelea D, Mayer-Davis EJ, Saydah S, Imperatore G, Linder B, Divers J, Bell R, Badaru A, Talton JW, Crume T, Liese AD, Merchant AT, Lawrence JM, Reynolds K, Dolan L, Liu LL, Hamman RF, Study SfDiY. Prevalence of type 1 and type 2 diabetes among children and adolescents from 2001 to 2009. JAMA. 2014;311(17):1778-86. Epub 2014/05/06. doi: 10.1001/jama.2014.3201. PubMed PMID: 24794371; PMCID: PMC4368900.

29. Tao B, Pietropaolo M, Atkinson M, Schatz D, Taylor D. Estimating the cost of type 1 diabetes in the U.S.: a propensity score matching method. Plos One. 2010;5(7):e11501. Epub

2010/07/17. doi: 10.1371/journal.pone.0011501. PubMed PMID: 20634976; PMCID: PMC2901386.

30. Tao BT, Taylor DG. Economics of type 1 diabetes. Endocrinol Metab Clin North Am. 2010;39(3):499-512. Epub 2010/08/21. doi: 10.1016/j.ecl.2010.05.004. PubMed PMID: 20723816.

31. Shapiro AM, Pokrywczynska M, Ricordi C. Clinical pancreatic islet transplantation. Nat Rev Endocrinol. 2017;13(5):268-77. Epub 2016/11/12. doi: 10.1038/nrendo.2016.178. PubMed PMID: 27834384.

32. Stock PG, Bluestone JA. Beta-cell replacement for type I diabetes. Annu Rev Med. 2004;55:133-56. Epub 2004/01/30. doi: 10.1146/annurev.med.55.091902.103539. PubMed PMID: 14746513.

33. Ryan EA, Paty BW, Senior PA, Bigam D, Alfadhli E, Kneteman NM, Lakey JR, Shapiro AJ. Five-year follow-up after clinical islet transplantation. Diabetes. 2005;54(7):2060-9.

34. Halloran PF. Immunosuppressive drugs for kidney transplantation. N Engl J Med. 2004;351(26):2715-29. Epub 2004/12/24. doi: 10.1056/NEJMra033540. PubMed PMID: 15616206.

35. Kory L. Nonadherence to immunosuppressive medications: a pilot survey of members of the transplant recipients international organization. Transplant Proc. 1999;31(4A):14S-5S. Epub 1999/06/18. doi: 10.1016/s0041-1345(99)00114-1. PubMed PMID: 10372034.

36. Wiseman AC. Immunosuppressive Medications. Clin J Am Soc Nephrol. 2016;11(2):332-43. Epub 2015/07/15. doi: 10.2215/CJN.08570814. PubMed PMID: 26170177; PMCID: PMC4741049.

37. Berney T, Secchi A. Rapamycin in islet transplantation: friend or foe? Transpl Int. 2009;22(2):153-61. Epub 2008/08/21. doi: 10.1111/j.1432-2277.2008.00743.x. PubMed PMID: 18713146.

38. Trepanier DJ, Gallant H, Legatt DF, Yatscoff RW. Rapamycin: distribution, pharmacokinetics and therapeutic range investigations: an update. Clin Biochem. 1998;31(5):345-51. Epub 1998/08/29. PubMed PMID: 9721433.

39. Yatscoff RW, Wang P, Chan K, Hicks D, Zimmerman J. Rapamycin: distribution, pharmacokinetics, and therapeutic range investigations. Ther Drug Monit. 1995;17(6):666-71. Epub 1995/12/01. PubMed PMID: 8588238.

40. Napoli KL, Wang ME, Stepkowski SM, Kahan BD. Distribution of sirolimus in rat tissue. Clin Biochem. 1997;30(2):135-42. Epub 1997/03/01. PubMed PMID: 9127695.

41. Ferron GM, Mishina EV, Zimmerman JJ, Jusko WJ. Population pharmacokinetics of sirolimus in kidney transplant patients. Clin Pharmacol Ther. 1997;61(4):416-28. Epub 1997/04/01. doi: 10.1016/S0009-9236(97)90192-2. PubMed PMID: 9129559.

42. Meier-Kriesche HU, Kaplan B. Toxicity and efficacy of sirolimus: relationship to whole-blood concentrations. Clin Ther. 2000;22 Suppl B:B93-100. Epub 2000/05/24. PubMed PMID: 10823377.

43. Hafiz MM, Faradji RN, Froud T, Pileggi A, Baidal DA, Cure P, Ponte G, Poggioli R, Cornejo A, Messinger S, Ricordi C, Alejandro R. Immunosuppression and procedure-related complications in 26 patients with type 1 diabetes mellitus receiving allogeneic islet cell transplantation. Transplantation. 2005;80(12):1718-28. Epub 2005/12/27. PubMed PMID: 16378067.

44. Ventola CL. Progress in Nanomedicine: Approved and Investigational Nanodrugs. P T. 2017;42(12):742-55. Epub 2017/12/14. PubMed PMID: 29234213; PMCID: PMC5720487.

45. Kang SY, Sohn KH, Lee JO, Kim SH, Cho SH, Chang YS. Intravenous tacrolimus and cyclosporine induced anaphylaxis: what is next? Asia Pac Allergy. 2015;5(3):181-6. Epub 2015/08/05. doi: 10.5415/apallergy.2015.5.3.181. PubMed PMID: 26240796; PMCID: PMC4521168.

46. Inc) WPLP. Rapamune® (sirolimus). US Food and Drug Administration. 2020.

47. Haeri A, Osouli M, Bayat F, Alavi S, Dadashzadeh S. Nanomedicine approaches for sirolimus delivery: a review of pharmaceutical properties and preclinical studies. Artif Cells Nanomed Biotechnol. 2018;46(sup1):1-14. Epub 2017/12/01. doi: 10.1080/21691401.2017.1408123. PubMed PMID: 29186990.

48. Alexis F, Pridgen E, Molnar LK, Farokhzad OC. Factors affecting the clearance and biodistribution of polymeric nanoparticles. Mol Pharm. 2008;5(4):505-15. Epub 2008/08/05. doi: 10.1021/mp800051m. PubMed PMID: 18672949; PMCID: PMC2663893.

49. Dowling DJ, Scott EA, Scheid A, Bergelson I, Joshi S, Pietrasanta C, Brightman S, Sanchez-Schmitz G, Van Haren SD, Ninkovic J, Kats D, Guiducci C, de Titta A, Bonner DK, Hirosue S, Swartz MA, Hubbell JA, Levy O. Toll-like receptor 8 agonist nanoparticles mimic immunomodulating effects of the live BCG vaccine and enhance neonatal innate and adaptive immune responses. J Allergy Clin Immunol. 2017;140(5):1339-50. Epub 2017/03/28. doi: 10.1016/j.jaci.2016.12.985. PubMed PMID: 28343701; PMCID: PMC5667586.

50. Allen S, Osorio O, Liu YG, Scott E. Facile assembly and loading of theranostic polymersomes via multi-impingement flash nanoprecipitation. J Control Release. 2017;262:91-

103. Epub 2017/07/25. doi: 10.1016/j.jconrel.2017.07.026. PubMed PMID: 28736263; PMCID: PMC5603398.

51. Yi S, Allen SD, Liu YG, Ouyang BZ, Li X, Augsornworawat P, Thorp EB, Scott EA. Tailoring Nanostructure Morphology for Enhanced Targeting of Dendritic Cells in Atherosclerosis. ACS Nano. 2016;10(12):11290-303. doi: 10.1021/acsnano.6b06451. PubMed PMID: 27935698.

52. Fruijtier-Polloth C. Safety assessment on polyethylene glycols (PEGs) and their derivatives as used in cosmetic products. Toxicology. 2005;214(1-2):1-38. Epub 2005/07/14. doi: 10.1016/j.tox.2005.06.001. PubMed PMID: 16011869.

53. Final Report on the Safety Assessment of Polyethylene Glycols (PEGs)-6,-8,-32,-75,-150,-14M,-20M. J Am Coll Toxicol. 1993;12(5):429–57. doi: 10.3109/10915819309141598.

54. C. Delgado GEF, and D. Fisher. The uses and properties of PEG-linked proteins. Crit Rev Ther Drug Carrier Syst. 1992;9(3-4):249-304.

55. Berthold PBaW. Polyethylene glycol-conjugated pharmaceutical proteins. Pharm Sci Technol Today. 1998;1(8):352-6.

56. Harris JM, Chess RB. Effect of pegylation on pharmaceuticals. Nat Rev Drug Discov. 2003;2(3):214-21. Epub 2003/03/04. doi: 10.1038/nrd1033. PubMed PMID: 12612647.

57. Harris JM, Martin NE, Modi M. Pegylation: a novel process for modifying pharmacokinetics. Clin Pharmacokinet. 2001;40(7):539-51. Epub 2001/08/21. doi: 10.2165/00003088-200140070-00005. PubMed PMID: 11510630.

58. Bazile D, Prud'homme C, Bassoullet MT, Marlard M, Spenlehauer G, Veillard M. Stealth Me.PEG-PLA nanoparticles avoid uptake by the mononuclear phagocytes system. J Pharm Sci. 1995;84(4):493-8. Epub 1995/04/01. doi: 10.1002/jps.2600840420. PubMed PMID: 7629743.

59. Deen WM, Lazzara MJ, Myers BD. Structural determinants of glomerular permeability. Am J Physiol Renal Physiol. 2001;281(4):F579-96. Epub 2001/09/13. doi: 10.1152/ajprenal.2001.281.4.F579. PubMed PMID: 11553505.

60. Longmire M, Choyke PL, Kobayashi H. Clearance properties of nano-sized particles and molecules as imaging agents: considerations and caveats. Nanomedicine (Lond). 2008;3(5):703-17. Epub 2008/09/27. doi: 10.2217/17435889.3.5.703. PubMed PMID: 18817471; PMCID: PMC3407669.

61. Abuchowski A, van Es T, Palczuk NC, Davis FF. Alteration of immunological properties of bovine serum albumin by covalent attachment of polyethylene glycol. J Biol Chem. 1977;252(11):3578-81. Epub 1977/06/10. PubMed PMID: 405385.

62. Hoang Thi TT, Pilkington EH, Nguyen DH, Lee JS, Park KD, Truong NP. The Importance of Poly(ethylene glycol) Alternatives for Overcoming PEG Immunogenicity in Drug Delivery and Bioconjugation. Polymers (Basel). 2020;12(2). Epub 2020/02/07. doi: 10.3390/polym12020298. PubMed PMID: 32024289; PMCID: PMC7077443.

63. Aguilar AMR-d-l-PaO. Progress and Challenges in PEGylated Proteins Downstream Processing: A Review of the Last 8 Years. Int J Pept Res Ther. 2020;26(1):333-48. doi: 10.1007/s10989-019-09840-4.

64. Swierczewska M, Lee KC, Lee S. What is the future of PEGylated therapies? Expert Opin Emerg Drugs. 2015;20(4):531-6. Epub 2015/11/20. doi: 10.1517/14728214.2015.1113254. PubMed PMID: 26583759; PMCID: PMC4908577.

65. Pfizer I. FACT SHEET FOR HEALTHCARE PROVIDERS ADMINISTERING VACCINE (VACCINATION PROVIDERS)2020.

66. Moderna US I. FACT SHEET FOR RECIPIENTS AND CAREGIVERS, EMERGENCY USE AUTHORIZATION (EUA) OF THE MODERNA COVID-19 VACCINE TO PREVENT CORONAVIRUS DISEASE 2019 (COVID-19) IN INDIVIDUALS 18 YEARS OF AGE AND OLDER2021.

67. Moderna US I. FACT SHEET FOR HEALTHCARE PROVIDERS ADMINISTERING VACCINE (VACCINATION PROVIDERS), EMERGENCY USE AUTHORIZATION (EUA) OF THE MODERNA COVID-19 VACCINE TO PREVENT CORONAVIRUS DISEASE 2019 (COVID-19)2021.

68. Jang HJ, Shin CY, Kim KB. Safety Evaluation of Polyethylene Glycol (PEG) Compounds for Cosmetic Use. Toxicol Res. 2015;31(2):105-36. Epub 2015/07/21. doi: 10.5487/TR.2015.31.2.105. PubMed PMID: 26191379; PMCID: PMC4505343.

69. J. M. Nikitakis MMR, G. T. Hewitt, and T. and F. A. Cosmetic. CTFA cosmetic ingredient handbook. Cosmetic, Toiletry, and Fragrance Association. 1988.

70. Richter AW, Akerblom E. Antibodies against polyethylene glycol produced in animals by immunization with monomethoxy polyethylene glycol modified proteins. Int Arch Allergy Appl Immunol. 1983;70(2):124-31. Epub 1983/01/01. doi: 10.1159/000233309. PubMed PMID: 6401699.

71. Richter AW, Akerblom E. Polyethylene glycol reactive antibodies in man: titer distribution in allergic patients treated with monomethoxy polyethylene glycol modified allergens or placebo, and in healthy blood donors. Int Arch Allergy Appl Immunol. 1984;74(1):36-9. Epub 1984/01/01. doi: 10.1159/000233512. PubMed PMID: 6706424.

72. Yang Q, Jacobs TM, McCallen JD, Moore DT, Huckaby JT, Edelstein JN, Lai SK. Analysis of Pre-existing IgG and IgM Antibodies against Polyethylene Glycol (PEG) in the

General Population. Anal Chem. 2016;88(23):11804-12. Epub 2016/11/03. doi: 10.1021/acs.analchem.6b03437. PubMed PMID: 27804292; PMCID: PMC6512330.

73. Bandilla KK, McDuffie FC, Gleich GJ. Immunoglobulin classes of antibodies produced in the primary and secondary responses in man. Clin Exp Immunol. 1969;5(6):627-41. Epub 1969/12/01. PubMed PMID: 4189127; PMCID: PMC1579156.

74. Ganson NJ, Povsic TJ, Sullenger BA, Alexander JH, Zelenkofske SL, Sailstad JM, Rusconi CP, Hershfield MS. Pre-existing anti-polyethylene glycol antibody linked to first-exposure allergic reactions to pegnivacogin, a PEGylated RNA aptamer. J Allergy Clin Immunol. 2016;137(5):1610-3 e7. Epub 2015/12/22. doi: 10.1016/j.jaci.2015.10.034. PubMed PMID: 26688515; PMCID: PMC5819876.

75. Zhao Y, Wang L, Yan M, Ma Y, Zang G, She Z, Deng Y. Repeated injection of PEGylated solid lipid nanoparticles induces accelerated blood clearance in mice and beagles. Int J Nanomedicine. 2012;7:2891-900. Epub 2012/06/30. doi: 10.2147/IJN.S30943. PubMed PMID: 22745552; PMCID: PMC3383289.

76. Hsieh YC, Wang HE, Lin WW, Roffler SR, Cheng TC, Su YC, Li JJ, Chen CC, Huang CH, Chen BM, Wang JY, Cheng TL, Chen FM. Pre-existing anti-polyethylene glycol antibody reduces the therapeutic efficacy and pharmacokinetics of PEGylated liposomes. Theranostics. 2018;8(11):3164-75. Epub 2018/06/14. doi: 10.7150/thno.22164. PubMed PMID: 29896310; PMCID: PMC5996368.

77. Aksu F, Topacoglu H, Arman C, Atac A, Tetik S, Hasanovic A, Kulenovic A, Mornjakovic Z, Pikula B, Sarac-Hadzihalilovic A, Voljevica A, Bamac B, Colak T, Alemdar M, Dundar G, Selekler M, Dincer O, Colak E, Ozbek A, Kilic C, Kamburoglu K, Ozen T, Kavak V, Kirici Y, Oztas E, Soysal HA, Unur E, Ekinci N, Karaca O, Malakhova O, Kocaoglu M, Toker S, Taser F,

Kilincoglu V, Yurtgun MF, Dalcik C, Zeybek A, Baroncini M, Peltier J, Jissendi P, Pruvo JP, Francke JP, Prevot V, Kosif R, Arifoglu Y, Diramali M, Sarsilmaz M, Kose E, Ogeturk M, Akpinar B, Kus I, Meydan S, Kara A, Kurtoglu Z, Tekdemir I, Elhan A, Bas O, Odaci E, Mollaoglu H, Ucok K, Kaplan S, Senoglu M, Nacitarhan V, Kurutas EB, Senoglu N, Altun I, Atli Y, Ozbag D, Karakas S, Bilgin MD, Tellioglu AM, Ozlem S, Akcanal B, Yildiz Y, Gunes H, Kose H, Uzum I, Gundogmus UN, Caglayan C, Pavlova V, Dimitrova M, Georgieva L, Nikolova E, Uzmansel D, Ozturk NC, Saylam CY, Ozgiray E, Orhan M, Cagli S, Zileli M, Ozkan D, Akkaya T, Comert A, Balikci N, Ozdemir E, Gumus H, Ergul Z, Kaya O, Altun S, Unlu RE, Orbay H, Kim DI, Han SH, Kim YS, Kim HJ, Lee KS, Elcioglu O, Ozden H, Guven G, Imre N, Yalcin B, Ozan H, Akyer P, Guvencer M, Karatosun V, Sagoo MG, Aland RC, Ustuner D, Ustuner MC, Ai J, Ghazi SR, Mansouri SH, Tuncer MC, Aluclu MU, Karabulut O, Hatipoglu ES, Nazaroglu H, Icke C, Akbay E, Gunay T, Icke S, Yildiz S, Yazar F, Barlas BO, Zahoi DE, Kavakli A, Tas U, Dabak DO, Sapmaz HI, Kocabiyik N, Ozer CM, Ozcan A, Elevli L, Desdicioglu K, Alanbay I, Govsa F, Saylam CY, Akdogan I, Kiroglu Y, Onur S, Evcil EH, Cankara N, Malas MA, Kalcioglu MT, Duman S, Ulcay T, Uzun A, Karabulut Z, Barut C, Sevinc O, Yurdakan G, Kacar D, Erdogan AR, Kurt H, Demir B, Saltan M, Burukoglu D, Ustuner MC, Degirmenci I, Erdogan A, Damar O, Is M, Bayramoglu G, Kabay S, Uysal O, Senturk H, Bayramoglu A, Ozbayar C, Kutlu A, Canbek M, Cevli SC, Hancerlioglu O, Koplay M, Aksakalli E, Dikici F, Kale A, Gayretli O, Gurses IA, Ozdemir ST, Ercan I, Baskan EB, Yilmaz M, Ozkaya G, Saricaoglu H, Erturk M, Kayalioglu G, Uzel M, Kahraman G, Tanyeli E, Soyluoglu AI, Tacar O, Demirant A, Bilgin M, Karadede A, Aktas A, Evcil EH, Koyuncu E, Sulak O, Albay S, Ozguner G, Ozbek A, Ozbek E, Ozturk AH, Demirci T, Ciftcioglu E, Demir MT, Kopuz C, Eroglu E, Gedikli S, Ozyurek H, Nural MS, Incesu L, Ogur G, Kara E, Celebi B, Yildiz A, Altunkaynak BZ, Kuvat SV, Tagil SM, Ertekin C, Uysal

H, Bademkiran F, Albayrak N, Esmer AF, Coskun NK, Sindel M, Kizilay F, Yalin S, Karapinar N, Tokdemir M, Karakurt L, Tumkaya L, Korkmaz A, Ayas B, Ciftci N, Terzi Y, Baran O, Nergiz Y, Akkus M, Aluclu U, Topal AE, Yuksel D, Acar HI, Kendir S, Hekimoglu E, Basman D, Duman S, Ozener B, Pelin C, Zagyapan R, Kurkcuoglu A, Koc M, Erdinc M, Erdinc L, Kelle I, Sancakdar E, Cetin N, Tunik S, Yildirim A, Kaplanoglu I, Ayaz E, Ilhan N, Okumus M, Yuksel KZ, Ciralik H, Yilmaz Z, Gumusalan Y, Gamsizkan M, Kazkayasi M, Unver Dogan N, Uysal, II, Karalezli A, Fazliogullari Z, Buyukmumcu M, Bozkurt MC, Cicekcibasi AE, Demiryurek D, Ozsoy MH, Bayramoglu A, Tuccar E, Baran OP, Soker S, Bahceci S, Nasir Y, Yilmaz MT, Cicekcibasi EA, Ulusoy M, Gunaslan P, Bilge N, Akkaya M, Genc A, Akcer S, Gonul Y, Cosar E, Koken G, Ari I, Bakirci S, Kafa IM, Uysal M, Karabulut AK, Keles B, Emlik D, Uyar Y, Ozturk K, Yilmaz NA, Salbacak A, Kacira BK, Arazi M, Demirci S, Kiresi D, Gumus S, Seker M, Uyar M, Astaneh ME, Khorshid A, Uygur R, Songur A, Sonmez OF, Dogan KH, Kolcu G, Iliescu M, Bordei P, Iliescu D, Ciobotaru C, Lucescu V, Covaleov A, Ionescu C, Guirao M, Paramo E, Mutuberria R, Sanchez-Montesinos I, Roda O, Giron F, Lopez-Soler M, Roda O, Campos-Lopez R, Guirao-Pineiro M, Pascual-Morenilla MT, Sanchez-Montesinos I, Pascual MT, Garzon I, Serrato D, Nieto-Aguilar R, Sanchez-Montesinos I, Sanchez-Quevedo M, Ozdemir MB, Ozean RH, Bagdatli D, Adiguzel E, Dogan Z, Aycan O, Vardi N, Erkal HS, Ozturk H, Mocanu S, Stefanescu C, Ionescu A, Talpes R, Sapte E, Dina C, Surdu L, Bulbuc I, Medina MT, Medina J, Lopez-Soler M, Martin-Oviedo C, Lowy-Benoliel A, Maranillo E, Martinez-Guirado T, Sanudo J, Scola B, Vazquez T, Arraez-Aybar LA, Conejo-Menor JL, Gonzales-Gomez CC, Torres-Garcia AJ, Nasu H, Chiba S, Gutierrez-Semillera M, Paksoy Y, Kalaycioglu A, Yildirim M, Ozyasar A, Ozdogmus O, Cakmak YO, Verimli U, Cavdar S, Yildizhan B, Aktan Ikiz ZA, Ucerler H, Ozgur Z, Yilmaz S, Demirtas A, Mavili E, Hacialiogullari M, Susar H, Arslan S, Aycan K, Ozkaya V, Pilmane M, Boka S, Ortug

G, Ramirez C, Pascual-Font A, Valderrama-Canales F, Kucukalic A, Kapur E, Talovic E, Baca V, Grill R, Horak Z, Kachlik D, Dzupa V, Konarik M, Knize J, Veleminsky P, Smrzova T, Otcenasek M, Chmelova J, Kheck M, Kheck M, Sr., Cupka T, Hnatek L, van der Meijs F, Cech P, Musil V, Ozkan HM, Muratli SK, Tayefi H, Ergur I, Kiray A, Toktas M, Alkoc O, Acar T, Uzun I, Ozen OA, Aycicek A, Alkoc OA, Unlu M, Corumlu U, Ikiz IC, Oygucu IH, Sendemir E, Kaner T, Caglar V, Eser O, Demir MT, Iyigun O, Pirzirenli G, Kaya AH, Aydin ME, Celik F, True H, Ozkaya S, Ergur BU, Zeybek G, Bacakoglu K, Tadjalli M, Poostpasand A, Mansouiri SH, Allahvaisi O, Soleimanirad J, Nikkhoo B, Nagato Y, Haruki Y, Yazawa K, Okazaki T, Haida M, Imai Y, Peirouvi T, Mahzad-Sadaghiani M, Noroozinia F, Siamak S, Farjah G, Mola S, Biegaj E, Skadorwa T, Pawlewicz K, Kapolka R, Chachulska A, Zabicka J, Krasowska A, Prusik A, Jaczewski G, Kolesnik A, Taghavi MM, Alavi SH, Moallem SA, Safikhani Z, Panahi M, Dabiri S, Shekaari MA, Latorre R, Soria F, Lopez-Albors O, Sarria R, Ayala I, Serrano I, Perez-Cuadrado E, Musienko V, Tkachenko D, Colakoglu N, Kus MA, Jalali M, Nikravesh MR, Moeen AA, Karimfar MH, Rafighdoost H, Mohammadi S, Korneeva M, Rafighdoust H, Lovasova K, Bolekova A, Kluchova D, Sulla I, Kapitonova MY, Syed Ahmad Fuad SB, Jayakaran F, Shams AR, Aghaee F, Baqer Z, Faroki M, Das S, Kassim N, Latiff A, Suhaimi F, Ghafar N, Hlaing KP, Maatoq I, Othman F, Kiray M, Bagriyanik HA, Pekcetin C, Ozogul C, Fidan M, Suhaimi F, Sun F, Sanchez-Margallo F, Gil F, Crisostomo V, Uson J, Ramirez G, Turamanlar O, Kirpiko O, Haktanir A, Climent S, Losilla S, Climent M, Sarikcioglu L, Senol Y, Yildirim FB, Utuk A, Kunicki J, Pasbakhsh P, Omidi N, Omidi H, Nazhvani FD, Ghalebi SR, Javan N, Mohagery A, Bideskan AR, Taheri MM, Fazel AR, Tiengo C, Macchi V, Stecco C, Porzionato A, Mazzoleni F, De Caro R, Clemente A, Morra A, Greco P, Pavan P, Natali A, Demir M, Dokur M, Acer N, Mavi A, Matveeva N, Lazarova D, Korneti K, Jovevska S, Jurkovik D, Papazova M, Havasi M,

Alboghobeish N, Savari A, Salamat N, Sharifi M, Kwak HH, Hu KS, Kim GC, Park BS, Kim HJ, Sinav A, Gulati AK, Gulati NK, Alshammary H, Nazhvani SD, Vafafar A, Esmaeilpour T, Bahmanpour S, Elyasi L, Monabbati A, Ghanadi M, Paryani MR, Gilanpour H, Amirsam B, Omana RE, Lopez SG, De la Garza Castro O, Vega EU, Lopez SG, Talebpour F, Golmohammadi R, Dashti G, Atlasi MA, Mehdizadeh M, Bahadori MH, Joghataei MT, Hatami L, Boroujeni MB, Estakhr J, Esfandiary E, Marzban M, Bakhtiary M, Modiry N, Jafarpur M, Mofidpur H, Alavi SH, Mahmoudian A, Taghavi MM, Jafarpour M, Mahmoudian AR, Sanjarmousavi N, Doassans I, Sorrenti N, Decuadro G, Saibene A, Poumayrac M, Laza S, Almiron C, Vergara ME, Soria V, Lasa S, Perez A, Castro G, Maria AS, Soleimani M, Katebi M, Bakhshayesh M, Oner M, Halici M, Yikilmaz A, Guney A, Turk Y, Edizer M, Beden U, Icten N, Afshar M, Hasanzadeh Taheri MM, Moalem A, Golalipour MJ, Tamizi A, Ahi M, Mohammadpour S, Maiery A, Acikel C, Ulkur E, Karagoz H, Celikoz B, Bedi K, Ginus P, Golalipoor MJ, Mohammadi MR, Jhand P, Mansourian AR, Hosseinpoor K, Keshtkar AA, Alsaffar R, Balajadeh BK, Ghafari S, Azarhosh R, Fazeli SA, Jahanshahi M, Gharravi AM, Alicioglu B, Karakas HM, Harma A, Yang HM, Won SY, Lee JG, Lee JY, Lee JY, Kim YR, Song WC, Koh KS, Hwang EN, Choi HG, Kim SH, Kim SY, Hur MS, Ulucam E, Celbis O, Kim DH, Hong HS, Kim HJ, Choi JH, Park JT, Kim HC, Abbasi H, Hosseinipanah SM, Hosseini M, Amani A, Ashrafi HR, Sadeghimehr M, Kim HJ, Sheverdin V, Amani Z, Ashrafi A, Ashrafi AR, Javad H, Kachap MJ, Laza S, Poumayrac MC, Doassans I, Vergara ME, Almiron C, Soria V, Rivara A, Sirilo A, Freire D, Cirillo A, Veragara ME, Krmek V, Krmek N, Jo-Osvatic A, Nikolic V, Radic R, Tubbs RS, Loukas M, Fogg Q, Ashwood N, Cilingiroglu S, Ozbakir C, Mazoochi T, Sabanciogullari V, Gumus C, Erdil FH, Cimen M, Moodi H, Ghiasi F, Akbari A, Hami J, Khazei M, Haghparast E, Mitsakis I, Anastasiou A, Mitsakis M, Sianou K, Hainoglou R, Francisco M, Mitsaki C, Konstantinidi M, Prapa S, Leksan I, Mrcela T,

Selthofer R, Kermanian F, Mahmoudian A, Ahmadpoor ME, Dalili N, Elian AH, Moaiery A, Jamalpour Z, Nourani MR, Asgari A, Hassanzadeh Taheri MM, Ebrahimzadeh A, Eftekharvaghefi SH, Mohammadi A, Sheibani V, Nematollahi-Mahani SN, Latifpour M, Deilami M, Soroure-Azimzadeh B, Nabipour F, Najafipour H, Nakhaee N, Yaghoobi M, Eftekharvaghefi R, Salehinejad P, Azizi H, Riasi HR, Nobakht M, Asalgoo S, Rahbar R, Najafzadeh N, Moosavizadeh K, Ezzatabadypour M, Majidi M, Malekpor-Afshar R, Karimzade F, Hoseini M, Bayat M, Gorgi A, Nezhadi A, Bakhtiari M, Jazi HR, Jafaryan M, Haghir H, Hosseini M, Rahimi S, Rassouli FB, Gorji A, Habibi A, Pouya F, Dabiri S, Mousavi A, Rajabalian S, Abolidokht A, Khanlarkhani N, Naderian H, Berjis N, Namavar MR, Talaei T, Mazaheri Z, Monabati A, Kosar MI, Karacan K, Chegini H, Nikzad H, Ayhan E, Ustundag S, Akkin SM, Ogut T, Rayegan P, Meibodi MA, Ghaem RM, Zargarpoor R, Eftekhar Vaghefi SH, Moshkdanian G, Poya F, Kohestani H, Abarghoeai RR, Abarghoeai PR, Eftekhar Vaghefi SH, Mahmodi AA, Poraboli A, Kohestani HR, Vaghefi RE, Eftekhar Vaghefy SH, Vaghefy RE, Abarghoeai PR, Saba M, Gharravi AM, Javadnia F, Zhaleh M, Nezhad DB, Gholami MR, Piagkou M, Aikaterini VK, Piagkos G, Douvetzemis S, Skandalakis P, Anagnostopoulou S, Papadopoulos N, Celik HH, Tatar I, Tatar EC, Mocan BO, Sargon MF, Denk CC, Rasoolijazi H, Joghataie MT, Roghani M, Akkin SM, Dinc G, Kurklu M, Ozboluk S, Komurcu M, Koebke J, Balioglu MB, Kaygusuz MA, Bozkus FS, Korkmaz O, Bayram SB, Can MA, Nasiri E, Jafar-Kazemi K, Hosseini M, Maghoul S, Soleimani M, Amini A, Hassanzade MM, Davari MH, Van Hoof T, Gomes GT, Audenaert E, Verstraete K, Kerckaert I, D'Herde K, Benninger B, Hedley G, Filipoiu FM, Tarta E, Enyedi M, Pantu C, Stanciulescu R, Skobowiat C, Calka J, Majewski M, Rezaian M, Yaghoobfar A, Hamedi S, Shomali T. Poster presentations. Surg Radiol Anat. 2009;31 Suppl 1:95-229. Epub 2009/09/01. doi: 10.1007/BF03371486. PubMed PMID: 27392492.

78. Povsic TJ, Vavalle JP, Aberle LH, Kasprzak JD, Cohen MG, Mehran R, Bode C, Buller CE, Montalescot G, Cornel JH, Rynkiewicz A, Ring ME, Zeymer U, Natarajan M, Delarche N, Zelenkofske SL, Becker RC, Alexander JH, Investigators R. A Phase 2, randomized, partially blinded, active-controlled study assessing the efficacy and safety of variable anticoagulation reversal using the REG1 system in patients with acute coronary syndromes: results of the RADAR trial. Eur Heart J. 2013;34(31):2481-9. Epub 2012/08/04. doi: 10.1093/eurheartj/ehs232. PubMed PMID: 22859796; PMCID: PMC3895957.

79. Hershfield MS, Ganson NJ, Kelly SJ, Scarlett EL, Jaggers DA, Sundy JS. Induced and pre-existing anti-polyethylene glycol antibody in a trial of every 3-week dosing of pegloticase for refractory gout, including in organ transplant recipients. Arthritis Res Ther. 2014;16(2):R63. Epub 2014/03/08. doi: 10.1186/ar4500. PubMed PMID: 24602182; PMCID: PMC4060462.

80. Fogel DB. Factors associated with clinical trials that fail and opportunities for improving the likelihood of success: A review. Contemp Clin Trials Commun. 2018;11:156-64. Epub 2018/08/17. doi: 10.1016/j.conctc.2018.08.001. PubMed PMID: 30112460; PMCID: PMC6092479.

81. Mima Y, Hashimoto Y, Shimizu T, Kiwada H, Ishida T. Anti-PEG IgM Is a Major Contributor to the Accelerated Blood Clearance of Polyethylene Glycol-Conjugated Protein. Mol Pharm. 2015;12(7):2429-35. Epub 2015/06/14. doi: 10.1021/acs.molpharmaceut.5b00144. PubMed PMID: 26070445.

82. Ichihara M, Shimizu T, Imoto A, Hashiguchi Y, Uehara Y, Ishida T, Kiwada H. Anti-PEG IgM Response against PEGylated Liposomes in Mice and Rats. Pharmaceutics. 2010;3(1):1-11. Epub 2010/01/01. doi: 10.3390/pharmaceutics3010001. PubMed PMID: 24310423; PMCID: PMC3857034.

83. Shimizu T, Mima Y, Hashimoto Y, Ukawa M, Ando H, Kiwada H, Ishida T. Anti-PEG IgM and complement system are required for the association of second doses of PEGylated liposomes with splenic marginal zone B cells. Immunobiology. 2015;220(10):1151-60. Epub 2015/06/23. doi: 10.1016/j.imbio.2015.06.005. PubMed PMID: 26095176.

84. Ishida T, Wang X, Shimizu T, Nawata K, Kiwada H. PEGylated liposomes elicit an anti-PEG IgM response in a T cell-independent manner. J Control Release. 2007;122(3):349-55. Epub 2007/07/06. doi: 10.1016/j.jconrel.2007.05.015. PubMed PMID: 17610982.

85. Abu Lila AS, Ichihara M, Shimizu T, Ishida T, Kiwada H. Ex-vivo/in-vitro anti-polyethylene glycol (PEG) immunoglobulin M production from murine splenic B cells stimulated by PEGylated liposome. Biol Pharm Bull. 2013;36(11):1842-8. Epub 2013/11/06. doi: 10.1248/bpb.b13-00562. PubMed PMID: 24189428.

86. Sherman MR, Williams LD, Sobczyk MA, Michaels SJ, Saifer MG. Role of the methoxy group in immune responses to mPEG-protein conjugates. Bioconjug Chem. 2012;23(3):485-99. Epub 2012/02/16. doi: 10.1021/bc200551b. PubMed PMID: 22332808; PMCID: PMC3309606.

87. Ishida T, Ichihara M, Wang X, Kiwada H. Spleen plays an important role in the induction of accelerated blood clearance of PEGylated liposomes. J Control Release. 2006;115(3):243-50. Epub 2006/10/03. doi: 10.1016/j.jconrel.2006.08.001. PubMed PMID: 17011060.

88. Defrance T, Taillardet M, Genestier L. T cell-independent B cell memory. Curr Opin Immunol. 2011;23(3):330-6. Epub 2011/04/13. doi: 10.1016/j.coi.2011.03.004. PubMed PMID: 21482090.

89. Saifer MG, Williams LD, Sobczyk MA, Michaels SJ, Sherman MR. Selectivity of binding of PEGs and PEG-like oligomers to anti-PEG antibodies induced by methoxyPEG-proteins. Mol

Immunol. 2014;57(2):236-46. Epub 2013/11/10. doi: 10.1016/j.molimm.2013.07.014. PubMed PMID: 24200843.

90. Sundy JS, Ganson NJ, Kelly SJ, Scarlett EL, Rehrig CD, Huang W, Hershfield MS. Pharmacokinetics and pharmacodynamics of intravenous PEGylated recombinant mammalian urate oxidase in patients with refractory gout. Arthritis Rheum. 2007;56(3):1021-8. Epub 2007/03/01. doi: 10.1002/art.22403. PubMed PMID: 17328081.

91. Xu L, Yang J, Xue B, Zhang C, Shi L, Wu C, Su Y, Jin X, Liu Y, Zhu X. Molecular insights for the biological interactions between polyethylene glycol and cells. Biomaterials. 2017;147:1-13. Epub 2017/09/20. doi: 10.1016/j.biomaterials.2017.09.002. PubMed PMID: 28923681.

92. Kozma GT, Meszaros T, Vashegyi I, Fulop T, Orfi E, Dezsi L, Rosivall L, Bavli Y, Urbanics R, Mollnes TE, Barenholz Y, Szebeni J. Pseudo-anaphylaxis to Polyethylene Glycol (PEG)-Coated Liposomes: Roles of Anti-PEG IgM and Complement Activation in a Porcine Model of Human Infusion Reactions. ACS Nano. 2019;13(8):9315-24. Epub 2019/07/28. doi: 10.1021/acsnano.9b03942. PubMed PMID: 31348638.

93. Elsadek NE, Emam SE, Abu Lila AS, Shimizu T, Ando H, Ishima Y, Ishida T. Pegfilgrastim (PEG-G-CSF) Induces Anti-polyethylene Glycol (PEG) IgM via a T Cell-Dependent Mechanism. Biol Pharm Bull. 2020;43(9):1393-7. Epub 2020/09/04. doi: 10.1248/bpb.b20-00345. PubMed PMID: 32879214.

94. Karl S, Ring J. Pro and contra of specific hyposensitization. Eur J Dermatol. 1999;9(4):325-31. Epub 1999/08/28. PubMed PMID: 10356415.

95. Ganson NJ, Kelly SJ, Scarlett E, Sundy JS, Hershfield MS. Control of hyperuricemia in subjects with refractory gout, and induction of antibody against poly(ethylene glycol) (PEG), in a

phase I trial of subcutaneous PEGylated urate oxidase. Arthritis Res Ther. 2006;8(1):R12. Epub 2005/12/17. doi: 10.1186/ar1861. PubMed PMID: 16356199; PMCID: PMC1526556.

96. Boos HJMaJ. Use of L-asparaginase in childhood ALL. Crit Rev Oncol Hematol. 1998;28(2):97-113.

97. Amylon MD, Shuster J, Pullen J, Berard C, Link MP, Wharam M, Katz J, Yu A, Laver J, Ravindranath Y, Kurtzberg J, Desai S, Camitta B, Murphy SB. Intensive high-dose asparaginase consolidation improves survival for pediatric patients with T cell acute lymphoblastic leukemia and advanced stage lymphoblastic lymphoma: a Pediatric Oncology Group study. Leukemia. 1999;13(3):335-42. Epub 1999/03/23. doi: 10.1038/sj.leu.2401310. PubMed PMID: 10086723.

98. Henriksen LT, Harila-Saari A, Ruud E, Abrahamsson J, Pruunsild K, Vaitkeviciene G, Jonsson OG, Schmiegelow K, Heyman M, Schroder H, Albertsen BK, Nordic Society of Paediatric H, Oncology g. PEG-asparaginase allergy in children with acute lymphoblastic leukemia in the NOPHO ALL2008 protocol. Pediatr Blood Cancer. 2015;62(3):427-33. Epub 2014/11/25. doi: 10.1002/pbc.25319. PubMed PMID: 25418987.

99. Tong WH, Pieters R, Kaspers GJ, te Loo DM, Bierings MB, van den Bos C, Kollen WJ, Hop WC, Lanvers-Kaminsky C, Relling MV, Tissing WJ, van der Sluis IM. A prospective study on drug monitoring of PEGasparaginase and Erwinia asparaginase and asparaginase antibodies in pediatric acute lymphoblastic leukemia. Blood. 2014;123(13):2026-33. Epub 2014/01/23. doi: 10.1182/blood-2013-10-534347. PubMed PMID: 24449211; PMCID: PMC3968389.

100. Armstrong JK, Hempel G, Koling S, Chan LS, Fisher T, Meiselman HJ, Garratty G. Antibody against poly(ethylene glycol) adversely affects PEG-asparaginase therapy in acute lymphoblastic leukemia patients. Cancer. 2007;110(1):103-11. Epub 2007/05/23. doi: 10.1002/cncr.22739. PubMed PMID: 17516438.

101. Kloos R, van der Sluis IM, Mastrobattista E, Hennink W, Pieters R, Verhoef JJ. Acute lymphoblastic leukaemia patients treated with PEGasparaginase develop antibodies to PEG and the succinate linker. Br J Haematol. 2020;189(3):442-51. Epub 2019/12/29. doi: 10.1111/bjh.16254. PubMed PMID: 31883112.

102. Silverman LB, Gelber RD, Dalton VK, Asselin BL, Barr RD, Clavell LA, Hurwitz CA, Moghrabi A, Samson Y, Schorin MA, Arkin S, Declerck L, Cohen HJ, Sallan SE. Improved outcome for children with acute lymphoblastic leukemia: results of Dana-Farber Consortium Protocol 91-01. Blood. 2001;97(5):1211-8. Epub 2001/02/27. doi: 10.1182/blood.v97.5.1211. PubMed PMID: 11222362.

103. van der Sluis IM, de Groot-Kruseman H, Te Loo M, Tissing WJE, van den Bos C, Kaspers GJL, Bierings M, Kollen WJW, Konig T, Pichlmeier U, Kuhnel HJ, Pieters R. Efficacy and safety of recombinant E. coli asparaginase in children with previously untreated acute lymphoblastic leukemia: A randomized multicenter study of the Dutch Childhood Oncology Group. Pediatr Blood Cancer. 2018;65(8):e27083. Epub 2018/05/05. doi: 10.1002/pbc.27083. PubMed PMID: 29727043.

104. Barenholz Y. Doxil(R)--the first FDA-approved nano-drug: lessons learned. J Control Release. 2012;160(2):117-34. Epub 2012/04/10. doi: 10.1016/j.jconrel.2012.03.020. PubMed PMID: 22484195.

105. O'Hagan DT, Singh M. Microparticles as vaccine adjuvants and delivery systems. Expert Rev Vaccines. 2003;2(2):269-83. Epub 2003/08/06. doi: 10.1586/14760584.2.2.269. PubMed PMID: 12899577.

106. W. M. Li MBB, and M. P. Schutze-Redelmeier. Enhanced immune response to T-independent antigen by using CpG oligodeoxynucleotides encapsulated in liposomes. Vaccine. 2001;20(1-2):148-57.

107. Dams ETM. Accelerated Blood Clearance and Altered Biodistribution of Repeated Injections of Sterically Stabilized Liposomes. J Pharmacol Exp Ther. 2000;292(3):1071-9.

108. Ishida T, Atobe K, Wang X, Kiwada H. Accelerated blood clearance of PEGylated liposomes upon repeated injections: effect of doxorubicin-encapsulation and high-dose first injection. J Control Release. 2006;115(3):251-8. Epub 2006/10/19. doi: 10.1016/j.jconrel.2006.08.017. PubMed PMID: 17045355.

109. Ishida T, Kiwada H. Accelerated blood clearance (ABC) phenomenon upon repeated injection of PEGylated liposomes. Int J Pharm. 2008;354(1-2):56-62. Epub 2007/12/18. doi: 10.1016/j.ijpharm.2007.11.005. PubMed PMID: 18083313.

110. Ishida T, Maeda R, Ichihara M, Irimura K, Kiwada H. Accelerated clearance of PEGylated liposomes in rats after repeated injections. J Control Release. 2003;88(1):35-42. Epub 2003/02/15. doi: 10.1016/s0168-3659(02)00462-5. PubMed PMID: 12586501.

111. Judge A, McClintock K, Phelps JR, Maclachlan I. Hypersensitivity and loss of disease site targeting caused by antibody responses to PEGylated liposomes. Mol Ther. 2006;13(2):328-37. Epub 2005/11/09. doi: 10.1016/j.ymthe.2005.09.014. PubMed PMID: 16275098.

112. K. Sroda JR, M. Langner, A. Kozubek, M. Grzybek, and A. F. Sikorski. Repeated injections of PEG-PE liposomes generate anti-PEG antibodies. Cell Mol Biol Lett. 2005;10(1):37-47.

113. Semple SC, Harasym TO, Clow KA, Ansell SM, Klimuk SK, Hope MJ. Immunogenicity and rapid blood clearance of liposomes containing polyethylene glycol-lipid conjugates and

nucleic Acid. J Pharmacol Exp Ther. 2005;312(3):1020-6. Epub 2004/11/05. doi: 10.1124/jpet.104.078113. PubMed PMID: 15525796.

114. Doxil Package Insert. Baxter Healthcare Corproation. 2019.

115. Neun BW, Barenholz Y, Szebeni J, Dobrovolskaia MA. Understanding the Role of Anti-PEG Antibodies in the Complement Activation by Doxil in Vitro. Molecules. 2018;23(7). Epub 2018/07/14. doi: 10.3390/molecules23071700. PubMed PMID: 30002298; PMCID: PMC6100003.

116. Szebeni J. The Interaction of Liposomes with the Complement System. Crit Rev Ther Drug Carr Syst. 1998;216(2):106-21.

117. Chanan-Khan A, Szebeni J, Savay S, Liebes L, Rafique NM, Alving CR, Muggia FM. Complement activation following first exposure to pegylated liposomal doxorubicin (Doxil): possible role in hypersensitivity reactions. Ann Oncol. 2003;14(9):1430-7. Epub 2003/09/05. doi: 10.1093/annonc/mdg374. PubMed PMID: 12954584.

118. Szebeni J. Complement activation-related pseudoallergy: a new class of drug-induced acute immune toxicity. Toxicology. 2005;216(2-3):106-21. Epub 2005/09/06. doi: 10.1016/j.tox.2005.07.023. PubMed PMID: 16140450.

119. Control CfD. ACIP December 19 and 20, 2020 Presentation Slides | Immunization Practices2020.

120. Vrieze Jd. Suspicions grow that nanoparticles in Pfizer's COVID-19 vaccine trigger rare allergic reactions. Science. 2020.

121. C. Zimmer JC, and S.-L. Wee. Coronavirus Vaccine Tracker. New York Times. 2020.

122. Wonodi MDKaC. Oxford–AstraZeneca COVID-19 vaccine efficacy. Lancet. 2020.

123. Zhang Y. Safety, tolerability, and immunogenicity of an inactivated SARS-CoV-2 vaccine in healthy adults aged 18–59 years: a randomised, double-blind, placebo-controlled, phase 1/2 clinical trial. Lancet Infect Dis. 2020.

124. Schellekens H, Hennink WE, Brinks V. The immunogenicity of polyethylene glycol: facts and fiction. Pharm Res. 2013;30(7):1729-34. Epub 2013/05/16. doi: 10.1007/s11095-013-1067-7. PubMed PMID: 23673554.

125. Huckaby JT. Structure of an anti-PEG antibody reveals an open ring that captures highly flexible PEG polymers. Commun Chem. 2020;3(1).

126. Kim SU, De Vellis J. Stem cell-based cell therapy in neurological diseases: a review. Journal of neuroscience research. 2009;87(10):2183-200.

127. Jeevanantham V, Butler M, Saad A, Abdel-Latif A, Zuba-Surma EK, Dawn B. Adult bone marrow cell therapy improves survival and induces long-term improvement in cardiac parameters: a systematic review and meta-analysis. Circulation. 2012:CIRCULATIONAHA. 111.086074.

128. Wobma H, Vunjak-Novakovic G. Tissue engineering and regenerative medicine 2015: a year in review. Tissue Engineering Part B: Reviews. 2016;22(2):101-13.

129. Antonioli B, Galuzzi M. Islet transplantation 30 years after the first transplants. European review for medical and pharmacological sciences. 2018;22:1463-8.

130. Shapiro AJ, Pokrywczynska M, Ricordi C. Clinical pancreatic islet transplantation. Nature Reviews Endocrinology. 2017;13(5):268.

131. Kesseli SJ, Wagar M, Jung MK, Smith KD, Lin YK, Walsh RM, Hatipoglu B, Freeman ML, Pruett TL, Beilman GJ. Long-term glycemic control in adult patients undergoing remote vs. local total pancreatectomy with islet autotransplantation. The American journal of gastroenterology. 2017;112(4):643.

132. Sutherland DE, Gruessner AC, Carlson AM, Blondet JJ, Balamurugan AN, Reigstad KF, Beilman GJ, Bellin MD, Hering BJ. Islet autotransplant outcomes after total pancreatectomy: a contrast to islet allograft outcomes. Transplantation. 2008;86(12):1799-802.

133. Lundberg R, Beilman GJ, Dunn TB, Pruett TL, Chinnakotla SC, Radosevich DM, Robertson RP, Ptacek P, Balamurugan A, Wilhelm JJ. Metabolic assessment prior to total pancreatectomy and islet autotransplant: utility, limitations and potential. American Journal of Transplantation. 2013;13(10):2664-71.

134. Barton FB, Rickels MR, Alejandro R, Hering BJ, Wease S, Naziruddin B, Oberholzer J, Odorico JS, Garfinkel MR, Levy M. Improvement in outcomes of clinical islet transplantation: 1999–2010. Diabetes care. 2012;35(7):1436-45.

135. Paty BW, Ryan EA, Shapiro AJ, Lakey JR, Robertson RP. Intrahepatic islet transplantation in type 1 diabetic patients does not restore hypoglycemic hormonal counterregulation or symptom recognition after insulin independence. Diabetes. 2002;51(12):3428-34.

136. Papas KK, Pisania A, Wu H, Weir GC, Colton CK. A stirred microchamber for oxygen consumption rate measurements with pancreatic islets. Biotechnology and bioengineering. 2007;98(5):1071-82.

137. Sener A, Malaisse W. Nutrient metabolism in islet cells. Experientia. 1984;40(10):1026-35.

138. Szot GL, Koudria P, Bluestone JA. Transplantation of Pancreatic Islets Into the Kidney Capsule of Diabetic Mice. Journal of Visualized Experiments : JoVE. 2007(9):404. doi: 10.3791/404. PubMed PMID: PMC2566322.

139. Carlsson P-O, Palm F, Andersson A, Liss P. Markedly decreased oxygen tension in transplanted rat pancreatic islets irrespective of the implantation site. Diabetes. 2001;50(3):489-95.

140. Merani S, Toso C, Emamaullee J, Shapiro A. Optimal implantation site for pancreatic islet transplantation. British Journal of Surgery. 2008;95(12):1449-61.

141. Blomeier H, Zhang X, Rives C, Brissova M, Hughes E, Baker M, Powers AC, Kaufman DB, Shea LD, Lowe Jr WL. Polymer scaffolds as synthetic microenvironments for extrahepatic islet transplantation. Transplantation. 2006;82(4):452.

142. Dufour JM, Rajotte RV, Zimmerman M, Rezania A, Kin T, Dixon DE, Korbutt GS. Development of an ectopic site for islet transplantation, using biodegradable scaffolds. Tissue engineering. 2005;11(9-10):1323-31.

143. Hernández R, Pedraz J, Desai T, Calafiore R, de Vos P. Engineering a Clinically Translatable Bioartificial Pancreas to Treat Type I Diabetes2018.

144. Zhu Y, Hoshi R, Chen S, Yi J, Duan C, Galiano RD, Zhang HF, Ameer GA. Sustained release of stromal cell derived factor-1 from an antioxidant thermoresponsive hydrogel enhances dermal wound healing in diabetes. Journal of Controlled Release. 2016;238(Supplement C):114-22. doi: https://doi.org/10.1016/j.jconrel.2016.07.043.

145. Morochnik S, Zhu Y, Duan C, Cai M, Reid RR, He TC, Koh J, Szleifer I, Ameer GA. A thermoresponsive, citrate-based macromolecule for bone regenerative engineering. Journal of Biomedical Materials Research Part A. 2018.

146. Yang J, Van Lith R, Baler K, Hoshi RA, Ameer GA. A thermoresponsive biodegradable polymer with intrinsic antioxidant properties. Biomacromolecules. 2014;15(11):3942-52.

147. Dumanian ZP, Tollemar V, Ye J, Lu M, Zhu Y, Liao J, Ameer GA, He T-C, Reid RR. Repair of critical sized cranial defects with BMP9-transduced calvarial cells delivered in a thermoresponsive scaffold. PloS one. 2017;12(3):e0172327.

148. Xiong Y, Yuan L, Chen L, Zhu Y, Zhang S, Liu X, Xiao Y, Wang X. Identifying a Novel Biomarker TOP2A of Clear Cell Renal Cell Carcinoma (ccRCC) Associated with Smoking by Co-Expression Network Analysis. J Cancer. 2018;9(21):3912-22. Epub 2018/11/10. doi: 10.7150/jca.25900. PubMed PMID: 30410595; PMCID: PMC6218786.

149. Kumar S, Wong PF, Melling AC, Leaper DJ. Effects of perioperative hypothermia and warming in surgical practice. International Wound Journal. 2005;2(3):193-204.

150. Todd MM, Hindman BJ, Clarke WR, Torner JC. Mild intraoperative hypothermia during surgery for intracranial aneurysm. New England Journal of Medicine. 2005;352(2):135-45.

151. Toledano MB, Leonard WJ. Modulation of transcription factor NF-kappa B binding activity by oxidation-reduction in vitro. Proceedings of the National Academy of Sciences. 1991;88(10):4328-32.

152. Schreck R, Albermann K, Baeuerle PA. Nuclear factor kB: an oxidative stress-responsive transcription factor of eukaryotic cells (a review). Free radical research communications. 1992;17(4):221-37.

153. Biswas SK. Does the interdependence between oxidative stress and inflammation explain the antioxidant paradox? Oxidative medicine and cellular longevity. 2016;2016.

154. Baeuerle PA, Baichwal VR. NF-kB as a frequent target for immunosuppressive and anti-inflammatory molecules. Advances in immunology. 1997;65:111-38.

155. Ryan EA, Lakey JR, Rajotte RV, Korbutt GS, Kin T, Imes S, Rabinovitch A, Elliott JF, Bigam D, Kneteman NM. Clinical outcomes and insulin secretion after islet transplantation with the Edmonton protocol. Diabetes. 2001;50(4):710-9.

156. Wierer S, Peter S, Elgass K, Mack H-G, Bieker S, Meixner AJ, Zentgraf U, Schleifenbaum F. Determination of the in vivo redox potential by one-wavelength spectro-microscopy of roGFP. Analytical and bioanalytical chemistry. 2012;403(3):737-44.

157. Rosenwasser S, Rot I, Meyer AJ, Feldman L, Jiang K, Friedman H. A fluorometer-based method for monitoring oxidation of redox-sensitive GFP (roGFP) during development and extended dark stress. Physiologia Plantarum. 2010;138(4):493-502.

158. Takasu N, Komiya I, Asawa T, Nagasawa Y, Yamada T. Streptozocin-and alloxan-induced H2O2 generation and DNA fragmentation in pancreatic islets: H2O2 as mediator for DNA fragmentation. Diabetes. 1991;40(9):1141-5.

159. Miceli V, Pampalone M, Frazziano G, Grasso G, Rizzarelli E, Ricordi C, Casu A, Iannolo G, Conaldi PG. Carnosine protects pancreatic beta cells and islets against oxidative stress damage. Molecular and cellular endocrinology. 2018.

160. Neal A, Rountree A, Kernan K, Van Yserloo B, Zhang H, Reed BJ, Osborne W, Wang W, Sweet IR. Real-time imaging of intracellular hydrogen peroxide in pancreatic islets. Biochemical Journal. 2016;473(23):4443-56.

161. Yasunami Y, Lacy PE, Finke EH. A new site for islet transplantation--a peritoneal-omental pouch. Transplantation. 1983;36(2):181-2.

162. DeWolfe D, Gandhi J, Mackenzie MR, Broge TA, Jr., Bord E, Babwah A, Mandelbrot DA, Pavlakis M, Cardarelli F, Viscidi R, Chandraker A, Tan CS. Pre-transplant immune factors may be associated with BK polyomavirus reactivation in kidney transplant recipients. Plos One.

2017;12(5):e0177339. Epub 2017/06/01. doi: 10.1371/journal.pone.0177339. PubMed PMID: 28562595; PMCID: PMC5451008.

163. Berman DM, Molano RD, Fotino C, Ulissi U, Gimeno J, Mendez AJ, Kenyon NM, Kenyon NS, Andrews DM, Ricordi C. Bioengineering the endocrine pancreas: intraomental islet transplantation within a biologic resorbable scaffold. Diabetes. 2016;65(5):1350-61.

164. Wain LV, Verwoert GC, O'Reilly PF, Shi G, Johnson T, Johnson AD, Bochud M, Rice KM, Henneman P, Smith AV, Ehret GB, Amin N, Larson MG, Mooser V, Hadley D, Dorr M, Bis JC, Aspelund T, Esko T, Janssens AC, Zhao JH, Heath S, Laan M, Fu J, Pistis G, Luan J, Arora P, Lucas G, Pirastu N, Pichler I, Jackson AU, Webster RJ, Zhang F, Peden JF, Schmidt H, Tanaka T, Campbell H, Igl W, Milaneschi Y, Hottenga JJ, Vitart V, Chasman DI, Trompet S, Bragg-Gresham JL, Alizadeh BZ, Chambers JC, Guo X, Lehtimaki T, Kuhnel B, Lopez LM, Polasek O, Boban M, Nelson CP, Morrison AC, Pihur V, Ganesh SK, Hofman A, Kundu S, Mattace-Raso FU, Rivadeneira F, Sijbrands EJ, Uitterlinden AG, Hwang SJ, Vasan RS, Wang TJ, Bergmann S, Vollenweider P, Waeber G, Laitinen J, Pouta A, Zitting P, McArdle WL, Kroemer HK, Volker U, Volzke H, Glazer NL, Taylor KD, Harris TB, Alavere H, Haller T, Keis A, Tammesoo ML, Aulchenko Y, Barroso I, Khaw KT, Galan P, Hercberg S, Lathrop M, Eyheramendy S, Org E, Sober S, Lu X, Nolte IM, Penninx BW, Corre T, Masciullo C, Sala C, Groop L, Voight BF, Melander O, O'Donnell CJ, Salomaa V, d'Adamo AP, Fabretto A, Faletra F, Ulivi S, Del Greco F, Facheris M, Collins FS, Bergman RN, Beilby JP, Hung J, Musk AW, Mangino M, Shin SY, Soranzo N, Watkins H, Goel A, Hamsten A, Gider P, Loitfelder M, Zeginigg M, Hernandez D, Najjar SS, Navarro P, Wild SH, Corsi AM, Singleton A, de Geus EJ, Willemsen G, Parker AN, Rose LM, Buckley B, Stott D, Orru M, Uda M, LifeLines Cohort S, van der Klauw MM, Zhang W, Li X, Scott J, Chen YD, Burke GL, Kahonen M, Viikari J, Doring A, Meitinger T, Davies G,

Starr JM, Emilsson V, Plump A, Lindeman JH, Hoen PA, Konig IR, EchoGen c, Felix JF, Clarke R, Hopewell JC, Ongen H, Breteler M, Debette S, Destefano AL, Fornage M, AortaGen C, Mitchell GF, Group CCHFW, Smith NL, KidneyGen c, Holm H, Stefansson K, Thorleifsson G, Thorsteinsdottir U, consortium CK, Cardiogenics c, CardioGram, Samani NJ, Preuss M, Rudan I, Hayward C, Deary IJ, Wichmann HE, Raitakari OT, Palmas W, Kooner JS, Stolk RP, Jukema JW, Wright AF, Boomsma DI, Bandinelli S, Gyllensten UB, Wilson JF, Ferrucci L, Schmidt R, Farrall M, Spector TD, Palmer LJ, Tuomilehto J, Pfeufer A, Gasparini P, Siscovick D, Altshuler D, Loos RJ, Toniolo D, Snieder H, Gieger C, Meneton P, Wareham NJ, Oostra BA, Metspalu A, Launer L, Rettig R, Strachan DP, Beckmann JS, Witteman JC, Erdmann J, van Dijk KW, Boerwinkle E, Boehnke M, Ridker PM, Jarvelin MR, Chakravarti A, Abecasis GR, Gudnason V, Newton-Cheh C, Levy D, Munroe PB, Psaty BM, Caulfield MJ, Rao DC, Tobin MD, Elliott P, van Duijn CM. Genome-wide association study identifies six new loci influencing pulse pressure and mean arterial pressure. Nat Genet. 2011;43(10):1005-11. Epub 2011/09/13. doi: 10.1038/ng.922. PubMed PMID: 21909110; PMCID: PMC3445021.

165. Collins D, Hogan AM, O'Shea D, Winter DC. The omentum: anatomical, metabolic, and surgical aspects. Journal of Gastrointestinal Surgery. 2009;13(6):1138-46.

166. Cabrera O, Berman DM, Kenyon NS, Ricordi C, Berggren P-O, Caicedo A. The unique cytoarchitecture of human pancreatic islets has implications for islet cell function. P Natl Acad Sci USA. 2006;103(7):2334-9.

167. Farney AC, Sutherland DE, Opara EC. Evolution of islet transplantation for the last 30 years. Pancreas. 2016;45(1):8-20.

168. Strand BL, Coron AE, Skjak-Braek G. Current and future perspectives on alginate encapsulated pancreatic islet. Stem cells translational medicine. 2017;6(4):1053-8.

169. Salvay DM, Rives CB, Zhang X, Chen F, Kaufman DB, Lowe Jr WL, Shea LD. Extracellular matrix protein-coated scaffolds promote the reversal of diabetes after extrahepatic islet transplantation. Transplantation. 2008;85(10):1456.

170. Beattie GM, Montgomery AM, Lopez AD, Hao E, Perez B, Just ML, Lakey JR, Hart ME, Hayek A. A novel approach to increase human islet cell mass while preserving β-cell function. Diabetes. 2002;51(12):3435-9.

171. Pedraza E, Brady A-C, Fraker CA, Molano RD, Sukert S, Berman DM, Kenyon NS, Pileggi A, Ricordi C, Stabler CL. Macroporous three-dimensional PDMS scaffolds for extrahepatic islet transplantation. Cell transplantation. 2013;22(7):1123-35.

172. Brady A-C, Martino MM, Pedraza E, Sukert S, Pileggi A, Ricordi C, Hubbell JA, Stabler CL. Proangiogenic hydrogels within macroporous scaffolds enhance islet engraftment in an extrahepatic site. Tissue engineering Part A. 2013;19(23-24):2544-52.

173. Berman DM, O'Neil JJ, Coffey LC, Chaffanjon PC, Kenyon NM, Ruiz P, Pileggi A, Ricordi C, Kenyon NS. Long-term survival of nonhuman primate islets implanted in an omental pouch on a biodegradable scaffold. American Journal of Transplantation. 2009;9(1):91-104.

174. Stendahl JC, Wang L-J, Chow LW, Kaufman DB, Stupp SI. Growth factor delivery from self-assembling nanofibers to facilitate islet transplantation. Transplantation. 2008;86(3):478.

175. Weaver JD, Headen DM, Hunckler MD, Coronel MM, Stabler CL, García AJ. Design of a vascularized synthetic poly (ethylene glycol) macroencapsulation device for islet transplantation. Biomaterials. 2018;172:54-65.

176. Devaraj S, Glaser N, Griffen S, Wang-Polagruto J, Miguelino E, Jialal I. Increased monocytic activity and biomarkers of inflammation in patients with type 1 diabetes. Diabetes. 2006;55(3):774-9.

177. Targher G, Bertolini L, Zoppini G, Zenari L, Falezza G. Increased plasma markers of inflammation and endothelial dysfunction and their association with microvascular complications in Type 1 diabetic patients without clinically manifest macroangiopathy. Diabetic Medicine. 2005;22(8):999-1004.

178. Pepper AR, Gala-Lopez B, Pawlick R, Merani S, Kin T, Shapiro AJ. A prevascularized subcutaneous device-less site for islet and cellular transplantation. Nature biotechnology. 2015;33(5):518.

179. Liu JM, Zhang J, Zhang X, Hlavaty KA, Ricci CF, Leonard JN, Shea LD, Gower RM. Transforming growth factor-beta 1 delivery from microporous scaffolds decreases inflammation post-implant and enhances function of transplanted islets. Biomaterials. 2016;80:11-9.

180. Jiang K, Weaver JD, Li Y, Chen X, Liang J, Stabler CL. Local release of dexamethasone from macroporous scaffolds accelerates islet transplant engraftment by promotion of anti-inflammatory M2 macrophages. Biomaterials. 2017;114:71-81.

181. Halliwell B. Oxidative stress in cell culture: an under-appreciated problem? FEBS letters. 2003;540(1-3):3-6.

182. Bottino R, Balamurugan A, Tse H, Thirunavukkarasu C, Ge X, Profozich J, Milton M, Ziegenfuss A, Trucco M, Piganelli JD. Response of human islets to isolation stress and the effect of antioxidant treatment. Diabetes. 2004;53(10):2559-68.

183. Monfared SSMS, Larijani B, Abdollahi M. Islet transplantation and antioxidant management: a comprehensive review. World journal of gastroenterology: WJG. 2009;15(10):1153.

184. Amoli MM, Moosavizadeh R, Larijani B. Optimizing conditions for rat pancreatic islets isolation. Cytotechnology. 2005;48(1-3):75-8.

185. Ricordi C, Lacy PE, Finke EH, Olack BJ, Scharp DW. Automated method for isolation of human pancreatic islets. Diabetes. 1988;37(4):413-20.

186. Pedraza E, Coronel MM, Fraker CA, Ricordi C, Stabler CL. Preventing hypoxia-induced cell death in beta cells and islets via hydrolytically activated, oxygen-generating biomaterials. Proceedings of the National Academy of Sciences. 2012;109(11):4245-50.

187. Gholipourmalekabadi M, Zhao S, Harrison BS, Mozafari M, Seifalian AM. Oxygen-generating biomaterials: a new, viable paradigm for tissue engineering? Trends in biotechnology. 2016;34(12):1010-21.

188. Roma LP, Pascal SM, Duprez J, Jonas J-C. Mitochondrial oxidative stress contributes differently to rat pancreatic islet cell apoptosis and insulin secretory defects after prolonged culture in a low non-stimulating glucose concentration. Diabetologia. 2012;55(8):2226-37.

189. Kahancová A, Sklenář F, Ježek P, Dlasková A. Regulation of glucose-stimulated insulin secretion by ATP ase Inhibitory Factor 1 (IF 1). FEBS letters. 2018;592(6):999-1009.

190. Shoichet MS. Polymer scaffolds for biomaterials applications. Macromolecules. 2009;43(2):581-91.

191. Diken AI, Alemdaroglu U, Ozyalcin S, Hafez I, Tunel HA, Yalcinkaya A, Ecevit AN. Adjuvant radiofrequency thermocoagulation improves the outcome of liquid sclerotherapy in the treatment of spider veins of the leg: A pilot study. Phlebology. 2021;36(8):620-6. Epub 2021/04/06. doi: 10.1177/02683555211006534. PubMed PMID: 33813962.

192. Molano RD, Pileggi A, Berney T, Poggioli R, Zahr E, Oliver R, Malek TR, Ricordi C, Inverardi L. Long-term islet allograft survival in nonobese diabetic mice treated with tacrolimus, rapamycin, and anti-interleukin-2 antibody. Transplantation. 2003;75(11):1812-9. PubMed PMID: WOS:000183684900007.

193. Shapiro AM, Lakey JR, Ryan EA, Korbutt GS, Toth E, Warnock GL, Kneteman NM, Rajotte RV. Islet transplantation in seven patients with type 1 diabetes mellitus using a glucocorticoid-free immunosuppressive regimen. N Engl J Med. 2000;343(4):230-8. Epub 2000/07/27. doi: 10.1056/NEJM200007273430401. PubMed PMID: 10911004.

194. Rapamune (sirolimus) [Package Insert]. Collegeville P, Wyeth Pharmaceuticals (2011).

195. Lombardi G, Vasquez Y. Dendritic cells. Preface. Handb Exp Pharmacol. 2009(188):v-ix. Epub 2009/02/07. PubMed PMID: 19195126.

196. Stabler CL, Li Y, Stewart JM, Keselowsky BC. Engineering immunomodulatory biomaterials for type 1 diabetes. Nat Rev Mater. 2019;4(6):429-50. PubMed PMID: WOS:000470655400009.

197. Emoto C, Fukuda T, Cox S, Christians U, Vinks AA. Development of a Physiologically-Based Pharmacokinetic Model for Sirolimus: Predicting Bioavailability Based on Intestinal CYP3A Content. CPT Pharmacometrics Syst Pharmacol. 2013;2:e59. Epub 2013/07/26. doi: 10.1038/psp.2013.33. PubMed PMID: 23884207; PMCID: PMC3731827.

198. Alemdar AY, Baker KA, Sadi D, McAlister VC, Mendez I. Liposomal tacrolimus administered systemically and within the donor cell suspension improves xenograft survival in hemiparkinsonian rats. Exp Neurol. 2001;172(2):416-24. Epub 2001/11/22. doi: 10.1006/exnr.2001.7801. PubMed PMID: 11716565.

199. Haeri A, Sadeghian S, Rabbani S, Anvari MS, Boroumand MA, Dadashzadeh S. Use of remote film loading methodology to entrap sirolimus into liposomes: preparation, characterization and in vivo efficacy for treatment of restenosis. Int J Pharm. 2011;414(1-2):16-27. Epub 2011/05/11. doi: 10.1016/j.ijpharm.2011.04.055. PubMed PMID: 21554939.

200. Allen SD LY, Bobbala S, Cai L, Hecker PI, Temel R, Scott EA. Polymersomes scalably fabricated via flash nanoprecipitation are non-toxic in non-human primates and associate with leukocytes in the spleen and kidney following intravenous administration. Nano Research. 2018. Epub 28 April 2018. doi: 10.1007/s12274-018-2069-x.

201. Stano A, Scott EA, Dane KY, Swartz MA, Hubbell JA. Tunable T cell immunity towards a protein antigen using polymersomes vs. solid-core nanoparticles. Biomaterials. 2013;34(17):4339-46. doi: 10.1016/j.biomaterials.2013.02.024. PubMed PMID: 23478034.

202. Scott EA, Stano A, Gillard M, Maio-Liu AC, Swartz MA, Hubbell JA. Dendritic cell activation and T cell priming with adjuvant- and antigen-loaded oxidation-sensitive polymersomes. Biomaterials. 2012;33(26):6211-9. doi: 10.1016/j.biomaterials.2012.04.060. PubMed PMID: 22658634.

203. Yi S, Allen SD, Liu Y-G, Ouyang BZ, Li X, Augsornworawat P, Thorp EB, Scott EA. Tailoring Nanostructure Morphology for Enhanced Targeting of Dendritic Cells in Atherosclerosis. ACS Nano. 2016;10(12):11290-303. doi: 10.1021/acsnano.6b06451.

204. Bracho-Sanchez E, Hassanzadeh A, Brusko MA, Wallet MA, Keselowsky BG. Dendritic Cells Treated with Exogenous Indoleamine 2,3-Dioxygenase Maintain an Immature Phenotype and Suppress Antigen-specific T cell Proliferation. J Immunol Regen Med. 2019;5. Epub 2019/12/04. doi: 10.1016/j.regen.2019.100015. PubMed PMID: 31788580; PMCID: PMC6884339.

205. Peng Y, Latchman Y, Elkon KB. Ly6C(low) monocytes differentiate into dendritic cells and cross-tolerize T cells through PDL-1. J Immunol. 2009;182(5):2777-85. Epub 2009/02/24. doi: 10.4049/jimmunol.0803172. PubMed PMID: 19234172; PMCID: PMC2704574.

206. Allen RP, Bolandparvaz A, Ma JA, Manickam VA, Lewis JS. Latent, Immunosuppressive Nature of Poly(lactic-co-glycolic acid) Microparticles. ACS Biomater Sci Eng. 2018;4(3):900-18. Epub 2018/12/18. doi: 10.1021/acsbiomaterials.7b00831. PubMed PMID: 30555893; PMCID: PMC6290919.

207. Zhang N, Su D, Qu S, Tse T, Bottino R, Balamurugan AN, Xu J, Bromberg JS, Dong HH. Sirolimus is associated with reduced islet engraftment and impaired beta-cell function. Diabetes. 2006;55(9):2429-36. Epub 2006/08/29. doi: 10.2337/db06-0173. PubMed PMID: 16936190.

208. Rosborough BR, Raich-Regue D, Liu Q, Venkataramanan R, Turnquist HR, Thomson AW. Adenosine triphosphate-competitive mTOR inhibitors: a new class of immunosuppressive agents that inhibit allograft rejection. Am J Transplant. 2014;14(9):2173-80. Epub 2014/10/14. doi: 10.1111/ajt.12799. PubMed PMID: 25307040; PMCID: PMC4196715.

209. van den Bosch TP, Kannegieter NM, Hesselink DA, Baan CC, Rowshani AT. Targeting the Monocyte-Macrophage Lineage in Solid Organ Transplantation. Front Immunol. 2017;8:153. Epub 2017/03/07. doi: 10.3389/fimmu.2017.00153. PubMed PMID: 28261211; PMCID: PMC5312419.

210. Abbas AK, Lichtman AH. Basic immunology : functions and disorders of the immune system. 2nd ed. Philadelphia: Saunders; 2004. ix, 322 p. p.

211. Gupta PK, Reid RC, Liu LG, Lucke AJ, Broomfield SA, Andrews MR, Sweet MJ, Fairlie DP. Inhibitors selective for HDAC6 in enzymes and cells. Bioorg Med Chem Lett. 2010;20(23):7067-70. doi: 10.1016/j.bmcl.2010.09.100. PubMed PMID: WOS:000283801400041.

212. Mahe E, Morelon E, Lechaton S, Sang KH, Mansouri R, Ducasse MF, Mamzer-Bruneel MF, de Prost Y, Kreis H, Bodemer C. Cutaneous adverse events in renal transplant recipients

receiving sirolimus-based therapy. Transplantation. 2005;79(4):476-82. Epub 2005/02/25. PubMed PMID: 15729175.

213. Burrack AL, Martinov T, Fife BT. T Cell-Mediated Beta Cell Destruction: Autoimmunity and Alloimmunity in the Context of Type 1 Diabetes. Front Endocrinol (Lausanne). 2017;8:343. Epub 2017/12/21. doi: 10.3389/fendo.2017.00343. PubMed PMID: 29259578; PMCID: PMC5723426.

214. Bouhdoud L, Villain P, Merzouki A, Arella M, Couture C. T-cell receptor-mediated anergy of a human immunodeficiency virus (HIV) gp120-specific CD4(+) cytotoxic T-cell clone, induced by a natural HIV type 1 variant peptide. J Virol. 2000;74(5):2121-30. Epub 2000/02/09. doi: 10.1128/jvi.74.5.2121-2130.2000. PubMed PMID: 10666241; PMCID: PMC111692.

215. Vieyra-Lobato MR, Vela-Ojeda J, Montiel-Cervantes L, Lopez-Santiago R, Moreno-Lafont MC. Description of CD8(+) Regulatory T Lymphocytes and Their Specific Intervention in Graft-versus-Host and Infectious Diseases, Autoimmunity, and Cancer. J Immunol Res. 2018;2018:3758713. Epub 2018/08/30. doi: 10.1155/2018/3758713. PubMed PMID: 30155493; PMCID: PMC6098849.

216. Fu C, Peng P, Loschko J, Feng L, Pham P, Cui W, Lee KP, Krug AB, Jiang A. Plasmacytoid dendritic cells cross-prime naive CD8 T cells by transferring antigen to conventional dendritic cells through exosomes. Proc Natl Acad Sci U S A. 2020;117(38):23730-41. Epub 2020/09/04. doi: 10.1073/pnas.2002345117. PubMed PMID: 32879009.

217. Thomas HE, Darwiche R, Corbett JA, Kay TW. Interleukin-1 plus gamma-interferon-induced pancreatic beta-cell dysfunction is mediated by beta-cell nitric oxide production. Diabetes. 2002;51(2):311-6. Epub 2002/01/29. doi: 10.2337/diabetes.51.2.311. PubMed PMID: 11812737.

218. Kawamura S, Ohteki T. Monopoiesis in humans and mice. Int Immunol. 2018;30(11):503-9. Epub 2018/09/25. doi: 10.1093/intimm/dxy063. PubMed PMID: 30247712.

219. Zhu J, Chen H, Huang X, Jiang S, Yang Y. Ly6C(hi) monocytes regulate T cell responses in viral hepatitis. JCI Insight. 2016;1(17):e89880. Epub 2016/10/26. doi: 10.1172/jci.insight.89880. PubMed PMID: 27777980; PMCID: PMC5070953.

220. Parrot T, Oger R, Allard M, Desfrancois J, Raingeard de la Bletiere D, Coutolleau A, Preisser L, Khammari A, Dreno B, Delneste Y, Guardiola P, Fradin D, Gervois N. Transcriptomic features of tumour-infiltrating CD4(low)CD8(high) double positive alphabeta T cells in melanoma. Sci Rep. 2020;10(1):5900. Epub 2020/04/05. doi: 10.1038/s41598-020-62664-x. PubMed PMID: 32246006; PMCID: PMC7125144.

221. Parel Y, Aurrand-Lions M, Scheja A, Dayer JM, Roosnek E, Chizzolini C. Presence of CD4+CD8+ double-positive T cells with very high interleukin-4 production potential in lesional skin of patients with systemic sclerosis. Arthritis Rheum. 2007;56(10):3459-67. Epub 2007/10/02. doi: 10.1002/art.22927. PubMed PMID: 17907151.

222. Overgaard NH, Jung JW, Steptoe RJ, Wells JW. CD4+/CD8+ double-positive T cells: more than just a developmental stage? J Leukoc Biol. 2015;97(1):31-8. Epub 2014/11/02. doi: 10.1189/jlb.1RU0814-382. PubMed PMID: 25360000.

223. Dew MA, DiMartini AF, De Vito Dabbs A, Myaskovsky L, Steel J, Unruh M, Switzer GE, Zomak R, Kormos RL, Greenhouse JB. Rates and risk factors for nonadherence to the medical regimen after adult solid organ transplantation. Transplantation. 2007;83(7):858-73. Epub 2007/04/27. doi: 10.1097/01.tp.0000258599.65257.a6. PubMed PMID: 17460556.

224. Nulojix (belatacept) [Package Insert]. Princeton N. Bristol-Myer Squibb2011.

225. O'Hare FM, Watson W, O'Neill A, Grant T, Onwuneme C, Donoghue V, Mooney E, Downey P, Murphy J, Twomey A, Molloy EJ. Neutrophil and monocyte toll-like receptor 4, CD11b and reactive oxygen intermediates, and neuroimaging outcomes in preterm infants. Pediatr Res. 2015;78(1):82-90. Epub 2015/04/01. doi: 10.1038/pr.2015.66. PubMed PMID: 25826119.

226. Yasunami Y, Kojo S, Kitamura H, Toyofuku A, Satoh M, Nakano M, Nabeyama K, Nakamura Y, Matsuoka N, Ikeda S, Tanaka M, Ono J, Nagata N, Ohara O, Taniguchi M. Valpha14 NK T cell-triggered IFN-gamma production by Gr-1+CD11b+ cells mediates early graft loss of syngeneic transplanted islets. J Exp Med. 2005;202(7):913-8. Epub 2005/09/28. doi: 10.1084/jem.20050448. PubMed PMID: 16186183; PMCID: PMC2213168.

227. Allen SD, Bobbala S, Karabin NB, Modak M, Scott EA. Benchmarking Bicontinuous Nanospheres against Polymersomes for in Vivo Biodistribution and Dual Intracellular Delivery of Lipophilic and Water-Soluble Payloads. ACS Appl Mater Interfaces. 2018;10(40):33857-66. Epub 2018/09/15. doi: 10.1021/acsami.8b09906. PubMed PMID: 30213189.

228. Yu YR, O'Koren EG, Hotten DF, Kan MJ, Kopin D, Nelson ER, Que L, Gunn MD. A Protocol for the Comprehensive Flow Cytometric Analysis of Immune Cells in Normal and Inflamed Murine Non-Lymphoid Tissues. Plos One. 2016;11(3):e0150606. Epub 2016/03/05. doi: 10.1371/journal.pone.0150606. PubMed PMID: 26938654; PMCID: PMC4777539.

229. Belkina AC, Ciccolella CO, Anno R, Halpert R, Spidlen J, Snyder-Cappione JE. Automated optimized parameters for T-distributed stochastic neighbor embedding improve visualization and analysis of large datasets. Nat Commun. 2019;10(1):5415. Epub 2019/11/30. doi: 10.1038/s41467-019-13055-y. PubMed PMID: 31780669; PMCID: PMC6882880.

230. Andrews S. FastQC: a quality control tool for high throughput sequence data. Available online at: http://wwwbioinformaticsbabrahamacuk/projects/fastqc. 2010.

231. Bolger AM, Lohse M, Usadel B. Trimmomatic: a flexible trimmer for Illumina sequence data. Bioinformatics. 2014;30(15):2114-20. Epub 2014/04/04. doi: 10.1093/bioinformatics/btu170. PubMed PMID: 24695404; PMCID: PMC4103590.

232. Dobin A, Davis CA, Schlesinger F, Drenkow J, Zaleski C, Jha S, Batut P, Chaisson M, Gingeras TR. STAR: ultrafast universal RNA-seq aligner. Bioinformatics. 2013;29(1):15-21. Epub 2012/10/30. doi: 10.1093/bioinformatics/bts635. PubMed PMID: 23104886; PMCID: PMC3530905.

233. Trapnell C, Williams BA, Pertea G, Mortazavi A, Kwan G, van Baren MJ, Salzberg SL, Wold BJ, Pachter L. Transcript assembly and quantification by RNA-Seq reveals unannotated transcripts and isoform switching during cell differentiation. Nat Biotechnol. 2010;28(5):511-5. Epub 2010/05/04. doi: 10.1038/nbt.1621. PubMed PMID: 20436464; PMCID: PMC3146043.

234. Trapnell C, Hendrickson DG, Sauvageau M, Goff L, Rinn JL, Pachter L. Differential analysis of gene regulation at transcript resolution with RNA-seq. Nat Biotechnol. 2013;31(1):46-53. Epub 2012/12/12. doi: 10.1038/nbt.2450. PubMed PMID: 23222703; PMCID: PMC3869392.

235. Roberts A, Trapnell C, Donaghey J, Rinn JL, Pachter L. Improving RNA-Seq expression estimates by correcting for fragment bias. Genome Biol. 2011;12(3):R22. Epub 2011/03/18. doi: 10.1186/gb-2011-12-3-r22. PubMed PMID: 21410973; PMCID: PMC3129672.

236. Boeckler C. Design of highly immunogenic liposomal constructs combining structurally independent B cell and T helper cell peptide epitopes. Eur J Immunol. 1999;29(7):2297-308.

237. King M, Pearson T, Rossini AA, Shultz LD, Greiner DL. Humanized mice for the study of type 1 diabetes and beta cell function. Ann N Y Acad Sci. 2008;1150:46-53. doi: 10.1196/annals.1447.009. PubMed PMID: 19120266; PMCID: PMC2620029.

238. Brehm MA, Shultz LD, Greiner DL. Humanized mouse models to study human diseases. Curr Opin Endocrinol Diabetes Obes. 2010;17(2):120-5. doi: 10.1097/MED.0b013e328337282f. PubMed PMID: 20150806; PMCID: PMC2892284.

239. King M, Pearson T, Shultz LD, Leif J, Bottino R, Trucco M, Atkinson MA, Wasserfall C, Herold KC, Woodland RT, Schmidt MR, Woda BA, Thompson MJ, Rossini AA, Greiner DL. A new Hu-PBL model for the study of human islet alloreactivity based on NOD-scid mice bearing a targeted mutation in the IL-2 receptor gamma chain gene. Clin Immunol. 2008;126(3):303-14. doi: 10.1016/j.clim.2007.11.001. PubMed PMID: 18096436.

240. Jacobson S, Heuts F, Juarez J, Hultcrantz M, Korsgren O, Svensson M, Rottenberg M, Flodstrom-Tullberg M. Alloreactivity but failure to reject human islet transplants by humanized Balb/c/Rag2gc mice. Scand J Immunol. 2010;71(2):83-90. doi: 10.1111/j.1365-3083.2009.02356.x. PubMed PMID: 20384859.

241. Xiao F, Ma L, Zhao M, Huang G, Mirenda V, Dorling A, Lechler R, Lombardi G. Ex vivo expanded human regulatory T cells delay islet allograft rejection via inhibiting islet-derived monocyte chemoattractant protein-1 production in CD34+ stem cells-reconstituted NOD-scid IL2rgammanull mice. Plos One. 2014;9(3):e90387. doi: 10.1371/journal.pone.0090387. PubMed PMID: 24594640; PMCID: PMC3940883.

242. Gaur LK. Nonhuman primate models for islet transplantation in type 1 diabetes research. ILAR J. 2004;45(3):324-33. PubMed PMID: 15229379.

243. Saran R, Li Y, Robinson B, Abbott KC, Agodoa LY, Ayanian J, Bragg-Gresham J, Balkrishnan R, Chen JL, Cope E, Eggers PW, Gillen D, Gipson D, Hailpern SM, Hall YN, He K, Herman W, Heung M, Hirth RA, Hutton D, Jacobsen SJ, Kalantar-Zadeh K, Kovesdy CP, Lu Y, Molnar MZ, Morgenstern H, Nallamothu B, Nguyen DV, O'Hare AM, Plattner B, Pisoni R, Port

FK, Rao P, Rhee CM, Sakhuja A, Schaubel DE, Selewski DT, Shahinian V, Sim JJ, Song P, Streja E, Kurella Tamura M, Tentori F, White S, Woodside K, Hirth RA. US Renal Data System 2015 Annual Data Report: Epidemiology of Kidney Disease in the United States. Am J Kidney Dis. 2016;67(3 Suppl 1):Svii, S1-305. Epub 2016/03/02. doi: 10.1053/j.ajkd.2015.12.014. PubMed PMID: 26925525; PMCID: PMC6643990.

244. Sussell J, Silverstein AR, Goutam P, Incerti D, Kee R, Chen CX, Batty DS, Jr., Jansen JP, Kasiske BL. The economic burden of kidney graft failure in the United States. Am J Transplant. 2020. Epub 2020/02/06. doi: 10.1111/ajt.15750. PubMed PMID: 32020739.

245. Wang L, Wang X, Jiang S, Wei J, Buggs J, Fu L, Zhang J, Liu R. Graft function assessment in mouse models of single- and dual-kidney transplantation. Am J Physiol Renal Physiol. 2018;315(3):F628-F36. Epub 2018/05/24. doi: 10.1152/ajprenal.00068.2018. PubMed PMID: 29790388; PMCID: PMC6172578.

246. Tse GH, Hughes J, Marson LP. Systematic review of mouse kidney transplantation. Transpl Int. 2013;26(12):1149-60. Epub 2013/06/22. doi: 10.1111/tri.12129. PubMed PMID: 23786597.

247. Zhao D, Liao T, Li S, Zhang Y, Zheng H, Zhou J, Han F, Dong Y, Sun Q. Mouse Model Established by Early Renal Transplantation After Skin Allograft Sensitization Mimics Clinical Antibody-Mediated Rejection. Front Immunol. 2018;9:1356. Epub 2018/07/20. doi: 10.3389/fimmu.2018.01356. PubMed PMID: 30022978; PMCID: PMC6039569.